Technical Report Documentation Page

1. Report No. SSRP-2001/23	2. Government Accession No.	3. Recipient's Catalog No.
4. Title and Subtitle Seismic Response of Sacrificial Shear Keys in Bridge Abutments		5. Report Date May 2002 6. Performing Organization Code
7. Author(s) Sami Hanna Megally, Pedro F. Silva, Frieder Seible		8. Performing Organization Report No. UCSD / SSRP-2001/23
9. Performing Organization Name and Address Department of Structural Engineering School of Engineering University of California, San Diego La Jolla, California 92093-0085		10. Work Unit No. (TRAIS) 11. Contract or Grant No. 59A0051
12. Sponsoring Agency Name and Address California Department of Transportation Division of Engineering Services 1801 30th St., West Building MS-9 Sacramento, California 95807		13. Type of Report and Period Covered Final Report – July 1997 / December 2001 14. Sponsoring Agency Code
15. Supplementary Notes Prepared in cooperation with the State of California Department of Transportation.		

16. Abstract

Sacrificial shear keys are used at abutments to provide transverse support for bridge superstructures under seismic loads. In addition, sacrificial shear keys serve as structural fuses to control damage in abutments and the supporting piles under transverse seismic loads. Sacrificial shear keys may be interior or exterior. Exterior shear keys are usually recommended for new construction because they are easier to inspect and repair. One of the important issues addressed in this report is the post-earthquake inspection and repair of abutments with shear keys.

This report presents the results of an experimental program that was performed at the University of California-San Diego (UCSD) to study the seismic response of interior and exterior sacrificial shear keys. The experimental program consisted of seven interior and six exterior shear keys experiments. Variables investigated during testing of the interior keys were: (1) loading protocol (monotonic, quasi-static reversed cyclic, and dynamic reversed cyclic), (2) geometric aspect ratio of the shear key, and (3) reinforcement ratio of the shear key. Variables investigated during testing of the exterior keys were: (1) inclusion of back and wing walls, (2) adoption of different key details such as the use of sacrificial flexural keys and construction joints between the abutment stem wall and the shear keys, and (3) post-tensioning of the abutment stem wall just below the shear keys. The experiments provided useful results to develop analytical models that will serve as means to evaluate the capacity of shear keys as well as their post-peak performance under cyclic loads.

It was found that the shear friction model, with the coefficient of friction values given in the Caltrans Design Specifications, significantly underestimates the capacity of the interior and exterior sacrificial shear keys. This is non-conservative in the design of sacrificial shear keys, because it may lead to overloading of the abutments and the supporting piles. As a result of this, the piles may suffer severe damage before failure of the sacrificial shear keys.

It was also found that without post-tensioning of the abutments, extensive damage is likely to occur in the stem wall during a major earthquake. These experiments have shown that post-tensioning of the abutment stem wall can: (1) minimize damage to the abutments, and (2) post-earthquake inspection and repair can be accomplished with minimum resources. Based on the experimental results, recommendations for the design of interior and exterior sacrificial shear keys and future research are made in this report.

17. Key Words Abutments, sacrificial, shear keys, structural fuse, seismic		18. Distribution Statement Unlimited	
19. Security Classification (of this report) Unclassified	20. Security Classification (of this page) Unclassified	21. No. of Pages 198	22. Price

Form DOT F 1700.7 (8-72) Reproduction of completed page authorized

DISCLAIMER

The contents of this report reflect the views of the authors who are responsible for the facts and accuracy of the data presented herein. The contents do not necessarily reflect the official views or policies of the California Department of Transportation or the Federal Highway Administration. This report does not constitute a standard, specification or regulation.

ACKNOWLEDGEMENTS

This study was made possible by funding from the California Department of Transportation under contract No. 59A0051.

As in any other research program there are several people that made this work possible. We would like to thank Dr. Charles Sikorsky from Caltrans for his technical participation during the design and testing phases of this research program.

The experiments presented in this report were tested at the Charles Lee Powell Laboratory of the University of California-San Diego (UCSD). A number of technical personnel at UCSD assisted in the experimental investigation. Among them Mr. Lawrence Berman and Dr. Christopher Latham deserve special mention for their contribution in construction and testing of the shear key units. Thanks are also due to Mr. Charles Stearns and Alex Sherman for their invaluable assistance.

Headed reinforcement and mechanical couplers incorporated in the last two exterior shear key test units were donated by the Headed Reinforcement Corporation, California, which is gratefully acknowledged.

LIST OF SYMBOLS

A_b	Cross sectional area of a bar.
A_{cv}	Area of the shear key-abutment wall interface.
A_g	Gross section area.
A_{vf}	Area of vertical reinforcement crossing the shear key-abutment wall interface.
b	Shear key width.
C_c	Concrete compression force.
C_sN	Reinforcing steel compression force.
d_b	Diameter of reinforcement bar.
d	Depth of shear key
E_c	Young's modulus of concrete or tangent modulus of elasticity of concrete.
E_s	Young's modulus of reinforcing steel.
f_y	Yield strength of the steel.
f_{sp}	Concrete cylinder splitting strength.
f_cN	Concrete compressive strength.
f_y	Yield strength of steel reinforcement.
$f^o{}_y$	Reinforcement yield strength at over-strength.
h	Height of stem wall
l_d	Development length of reinforcing steel.
NA	Section neutral axis.
T_s	Reinforcing steel tension force.
V	Applied shear force.
V_C	Concrete contribution to capacity of the shear key.
V_N	Shear key nominal shear capacity.
V_S	Contribution of mild steel reinforcement to capacity of the shear key.
VN_y	Lateral load at first yielding.
V_y	Lateral load at yielding.
V_I	Lateral load at ideal flexural strength.
α	Shear key height-to–depth ratio.
β	Shear key width-to–depth ratio.
$)$	Shear key top lateral deflection.
$)_y{}^N$	Lateral displacement at first yielding.
$)_y$	Yield displacement.
$)_U$	Ultimate displacement.
N	Section curvature.

N_{ave}	Experimentally determined average curvature.
η_s	Total number of rows crossing the shear key interface
$\mu_)$	Displacement ductility.
μ	Coefficient of friction, taken as 1.4λ for concrete cast monolithically.
ρ	Shear key reinforcement ratio.

TABLE OF CONTENTS

DISCLAIMER ii
ACKNOWLEDGEMENTS iii
LIST OF SYMBOLS iv
TABLE OF CONTENTS vi
LIST OF FIGURES xi
LIST OF TABLES xv
ABSTRACT xvi
1 INTRODUCTION 1
1.1 Development of Experimental program 1
1.2 Literature Review 3
1.3 Report Layout 4
2 EXPERIMENTAL PROGRAM OF SACRIFICIAL INTERIOR SHEAR KEYS 6
2.1 Test Matrix 8
2.2 Capacity Evaluation of Interior Shear Keys 8
2.2.1 Sliding Shear Friction Model 9
2.2.2 Strut-and-Tie Model 9
2.2.3 Moment Resistance Model 11
2.3 Overall Test Setup and Design of the Test Units 12
2.3.1 Design of the Test Units – Test Series I 13
2.3.2 Design of the Test Units – Test Series II 13
2.4 Instrumentation of the Test Units 16
2.4.1 Test Series I 16
2.4.1.1 Strain Gages 16
2.4.1.2 Displacement Transducers 17
2.4.2 Test Series II 18
2.4.2.1 Strain Gages 18
2.4.2.2 Displacement Transducers 20
2.5 Loading Protocol 20
2.5.1 Test Series I 20
2.5.1.1 Monotonic Loading 20
2.5.1.2 Quasi-Static Reversed Cyclic Loading 20
2.5.1.3 Dynamic Reversed Cyclic Loading 21
2.5.2 Test Series II 22
2.6 Material Properties 23
2.6.1 Test Series I 23
2.6.2 Test Series II 24
3 EXPERIMENTAL RESULTS OF SACRIFICIAL INTERIOR SHEAR KEYS 25
3.1 Description of Damage Levels 25
3.1.1 LEVEL I 25
3.1.2 LEVEL II 25
3.1.3 LEVEL III 26
3.1.4 LEVEL IV 26
3.1.5 LEVEL V 26

3.2 Test Series I – Test Unit 1A 26
3.2.1 General Test Observations 26
3.2.2 Load versus Displacement Curve 28
3.2.3 Horizontal Strain Profiles 30
3.2.4 Vertical Strain Profiles 31
3.2.5 Vertical Shear Key Movement 32
3.3 Test Series I – Test Unit 1B 34
3.3.1 General Test Observations 34
3.3.2 Load versus Displacement Curve 35
3.3.3 Horizontal Strain Profiles 36
3.3.4 Vertical Shear Key Movement 37
3.4 Test Series I – Test Unit 1C 38
3.4.1 General Test Observations 38
3.4.2 Load versus Displacement Curve 38
3.4.3 Horizontal Strain Profiles 38
3.4.4 Vertical Shear Key Movement 39
3.5 Test Series II – Test Unit 2A 41
3.5.1 General Test Observations 41
3.5.2 Load versus Displacement Curve 41
3.5.3 Horizontal Strain Profiles 43
3.5.4 Vertical Shear Key Movement 43
3.6 Test Series II – Test Unit 2B 46
3.6.1 General Test Observations 46
3.6.2 Load versus Displacement Curve 47
3.6.3 Horizontal Strain Profiles 48
3.6.4 Vertical Shear Key Movement 49
3.7 Test Series II – Test Unit 2C 51
3.7.1 General Test Observations 51
3.7.2 Load versus Displacement Curve 52
3.7.3 Horizontal Strain Profiles 53
3.7.4 Vertical Shear Key Movement 54
3.8 Test Series II – Test Unit 2D 56
3.8.1 General Test Observations 56
3.8.2 Load versus Displacement Curve 58
3.8.3 Horizontal Strain Profiles 59
3.8.4 Vertical Shear Key Movement 61
4 ANALYTICAL MODELS FOR SACRIFICIAL INTERIOR SHEAR KEYS 62
4.1 Discussion of Experimental Results 62
4.1.1 Test Series I 62
4.1.1.1 Development of Strut-and-Tie Mechanism 64
4.1.1.2 Development of Sliding Shear Friction Mechanism 66
4.1.2 Test Series II 66
4.1.2.1 Development of Strut-and-Tie Mechanism 69
4.1.2.2 Development of Shear Friction Mechanism 72
4.2 Development of Analytical Model 72
4.2.1 Calculation of Shear Key Capacity 72

4.2.1.1 Cracking Strength Concrete Approach For Deep Beams 72
4.2.1.2 Sliding Shear Friction Model 73
4.2.1.3 Strut-and-Tie Mechanism 73
4.2.1.4 Maximum Shear Stress of 800 psi (5.52 MPa) 73
4.2.2 Discussion of Analytical Models 75
4.2.3 Sacrificial Shear Keys Peak Capacity 76
4.2.4 Calculation of Force versus Displacement Envelopes 77
4.2.5 Calculation of Effective Damping and Effective Stiffness 79
5 EXPERIMENTAL PROGRAM OF SACRIFICIAL EXTERIOR SHEAR KEYS 83
5.1 Test Matrix 83
5.2 Capacity Evaluation of Exterior Shear Keys 85
5.2.1 Sliding Shear Friction Model 85
5.2.2 Strut-and-Tie Analogous Model 86
5.2.3 Moment-Curvature Analysis 88
5.3 Overall Test Setup and Design of Test Units 90
5.3.1 Design of the Test Units – Test Series I 90
5.3.1.1 Reinforcement Layout 92
5.3.2 Design of Test Units – Test Series II 95
5.3.2.1 Reinforcement Layout 97
5.3.3 Design of Test Units – Test Series III 101
5.3.3.1 Reinforcement Layout 103
5.4 Instrumentation of the Test Units 108
5.4.1 Test Series I 108
5.4.1.1 Strain Gages 108
5.4.1.2 Displacement Transducers 109
5.4.2 Test Series II 112
5.4.2.1 Strain Gages 112
5.4.2.2 Displacement Transducers 112
5.4.3 Test Series III 113
5.4.3.1 Strain Gages 113
5.4.3.2 Displacement Transducers 113
5.4.3.3 Load Cells 113
5.5 Loading Protocol 114
5.5.1 Test Series I 114
5.5.2 Test Series II 115
5.5.2.1 Test Unit 2A 115
5.5.2.2 Test Unit 2B 115
5.5.3 Test Series III 116
5.6 Material Properties 116
5.6.1 Test Series I 117
5.6.2 Test Series II 117
5.6.3 Test Series III 117
6 EXPERIMENTAL RESULTS OF SACRIFICIAL EXTERIOR SHEAR KEYS 119
6.1 Test Unit 1A 119
6.1.1 General Test Observations 119
6.1.2 Lateral Load vs. Displacement Curve 121

6.1.3 Shear Key Reinforcement Strain Profiles 122
6.1.4 Horizontal Reinforcement Strain Profiles 123
6.1.5 Vertical Reinforcement Strain Profiles 124
6.2 Test Unit 1B 125
6.2.1 General Test Observations 125
6.2.2 Lateral Load vs. Displacement Curve 127
6.2.3 Shear Key Reinforcement Strain Profiles 128
6.2.4 Horizontal Reinforcement Strain Profiles 129
6.2.5 Vertical Reinforcement Strain Profiles 130
6.3 Test Unit 2A 131
6.3.1 General Test Observations 131
6.3.2 Lateral Load vs. Displacement Curve 133
6.3.3 Shear Key Reinforcement Strain Profiles 134
6.3.4 Horizontal Reinforcement Strain Profiles 136
6.4 Test Unit 2B 137
6.4.1 General Test Observations 137
6.4.2 Lateral Load vs. Displacement Curve 139
6.4.3 Strain Profiles in Vertical Bars of the Flexural Key 140
6.4.4 Horizontal Strain Profiles in the Side Reinforcement of the Abutment Wall 140
6.5 Test Unit 3A 142
6.5.1 General Test Observations 142
6.5.2 Lateral Load vs. Displacement Curve 144
6.5.3 Shear Key Reinforcement Strain Profiles 146
6.5.4 Strains in Side Vertical Reinforcement in the Abutment Wall 147
6.5.5 Horizontal Reinforcement Strain Profiles 148
6.5.6 Variation of Prestressing Force in the Abutment 150
6.6 Test Unit 3B 151
6.6.1 General Test Observations 151
6.6.2 Lateral Load vs. Displacement Curve 153
6.6.3 Shear Key Reinforcement Strain Profiles 155
6.6.4 Horizontal Reinforcement Strain Profiles 155
6.6.5 Variation of Prestressing Force in the Abutment 155
7 DISCUSSION OF EXPERIMENTAL RESULTS OF SACRIFICIAL EXTERIOR SHEAR KEYS 160
7.1 Comparison of Cracking Patterns at Different Damage Levels 160
7.2 Maximum Load Carrying Capacity 165
7.3 Post-Peak Performance 166
7.4 Post-Earthquake Repair 169
7.5 Analytical Models for Sacrificial Exterior Shear Keys 171
7.5.1 Sliding Shear Friction Model 171
7.5.2 Strut-and-Tie Analogous Model Type I 172
7.5.3 Strut-and-Tie Analogous Model Type II 173
7.5.4 Strut-and-Tie Analogous Model Type III 174
7.5.5 Moment-Curvature Analysis 175
8 ANALYTICAL MODELS OF EXTERIOR SHEAR KEYS 177
8.1 Development of Strut-and-Tie Mechanism and Hysteretic Model 178

8.1.1 LEVEL I 180
8.1.2 LEVEL II 182
8.1.3 LEVEL III 184
8.1.4 LEVEL IV 185
8.1.5 LEVEL V 186
8.2 Time History Analysis 187
9 CONLUSIONS AND RECOMMENDATIONS 189
9.1 Interior Sacrificial Shear Keys 189
9.2 Exterior Sacrificial Shear Keys 191
9.3 Recommendations for Future Research 194
10 REFERENCES 196

LIST OF FIGURES

Figure 1.1 Schematic of Typical Bridge Abutments……...2

Figure 2.1 Typical Interior Shear Key Schematic Drawing 6
Figure 2.2 Strut-and-Tie Model 10
Figure 2.3 Capacity Based on Moment Resistance 11
Figure 2.4 Sacrificial Interior Shear Key Test Unit and the Loading Arm 12
Figure 2.5 Overall Test Setup 13
Figure 2.6 Reinforcement Layout – Test Series I 14
Figure 2.7 Effect of Aspect Ratio on Shear Key Capacity 14
Figure 2.8 Effect of Reinforcement Ratio on Shear Key Capacity 15
Figure 2.9 Reinforcement Layout – Test Series II 16
Figure 2.10 Strain Gage Locations – Test Series I 17
Figure 2.11 Linear Potentiometer Locations 18
Figure 2.12 Strain Gage Locations - Test Series II 19
Figure 2.13 Quasi-Static Reversed Cyclic Load History 21
Figure 2.14 Dynamic Reversed Cyclic Load History 22
Figure 2.15 Loading History - Test Series II 23

Figure 3.1 Test Observations – Test Unit 1A 27
Figure 3.2 Load vs. Displacement – Test Unit 1A 29
Figure 3.3 Horizontal Strain Profiles – Test Unit 1A 31
Figure 3.4 Vertical Strain Profiles – Test Unit 1A 33
Figure 3.5 Vertical Key Movement – Test Unit 1A 34
Figure 3.6 Load vs. Displacement – Test Unit 1B 35
Figure 3.7 Horizontal Strain Profiles – Test Unit 1B 36
Figure 3.8 Vertical Key Movement – Test Unit 1B 37
Figure 3.9 Load vs. Displacement – Test Unit 1C 39
Figure 3.10 Horizontal Strain Profiles – Test Unit 1C 40
Figure 3.11 Test Observations – Test Unit 2A 42
Figure 3.12 Load vs. Displacement – Test Unit 2A 44
Figure 3.13 Horizontal Strain Profiles – Test Unit 2A 45
Figure 3.14 Vertical Key Movement – Test Unit 2A 46
Figure 3.15 Test Observations – Test Unit 2B 47
Figure 3.16 Load vs. Displacement – Test Unit 2B 48
Figure 3.17 Horizontal Strain Profiles – Test Unit 2B 50
Figure 3.18 Vertical Key Movement – Test Unit 2B 51
Figure 3.19 Test Observations – Test Unit 2C 52
Figure 3.20 Load vs. Displacement – Test Unit 2C 53
Figure 3.21 Horizontal Strain Profiles – Test Unit 2C 55
Figure 3.22 Vertical Key Movement – Test Unit 2C 56
Figure 3.23 Test Observations – Test Unit 2D 57
Figure 3.24 Load vs. Displacement – Test Unit 2D 58
Figure 3.25 Horizontal Strain Profiles – Test Unit 2D 60

Figure 3.26 Vertical Key Movement – Test Unit 2D 61

Figure 4.1 Load vs. Displacement - Test Series I 62
Figure 4.2 Envelopes of Load vs. Displacement Curves – Test Series I 63
Figure 4.3 Horizontal Profiles of Strains in Vertical Reinforcement of the Shear Key at Peak Load – Test Series I 65
Figure 4.4 Typical Crack Pattern in Interior Shear Keys 66
Figure 4.5 Load vs. Displacement – Varying Aspect Ratio 67
Figure 4.6 Load vs. Displacement Envelopes – Varying Aspect Ratio 67
Figure 4.7 Load vs. Displacement – Varying Reinforcement Ratio 68
Figure 4.8 Load vs. Displacement Envelopes – Varying Reinforcement Ratio 68
Figure 4.9 Test Observations at Onset of Cracking (LEVEL I) – Test Series II 69
Figure 4.10 Test Observations at Peak Load (LEVEL III) – Test Series II 70
Figure 4.11 Comparison of Experimental and Calculated Capacities of Exterior Shear Keys 74
Figure 4.12 Comparison of Experimental Results versus Predicted Capacity 75
Figure 4.13 Load vs. Displacement Envelopes 78
Figure 4.14 Calculated Load vs. Displacement Envelopes 81
Figure 4.15 Experimental vs. Calculated Equivalent Viscous Damping 82
Figure 4.16 Cyclic Friction Hysteretic Behavior of Interior Shear Keys 82

Figure 5.1 Test Units – Series I 84
Figure 5.2 Test Units – Series II 84
Figure 5.3 Test Units – Series III 85
Figure 5.4 Exterior Shear Keys – Strut-and-Tie Analogous Model 87
Figure 5.5 Stress Block Design Parameters 88
Figure 5.6 Overall Test Setup for Exterior Shear keys 90
Figure 5.7 Plan View of the Test Setup of Exterior Shear Keys – Test Series I 91
Figure 5.8 Elevation View of the Test Setup of Exterior Shear Keys – Test Series I 91
Figure 5.9 Plan View of the Reinforcement Layout – Test Series I 92
Figure 5.10 Elevation View of the Reinforcement Layout (Section C-C) –Test Series I 93
Figure 5.11 Reinforcement Layout (Section D-D) –Test Series I 94
Figure 5.12 Reinforcement Layout (Section E-E) –Test Series I 94
Figure 5.13 Reinforcement Layout (Section F-F) – Test Series I 95
Figure 5.14 Plan View of the Test Setup of Exterior Shear Keys – Test Series II 96
Figure 5.15 Elevation View of the Test Setup of Exterior Shear Keys – Test Series II 96
Figure 5.16 Elevation View of the Reinforcement Layout (Section C-C) – Test Series II 97
Figure 5.17 Plan View of the Reinforcement Layout – Test Series II 98
Figure 5.18 Reinforcement Layout (Section D-D) – Test Series II 98
Figure 5.19 Reinforcement Layout (Section E-E) –Test Series II 99
Figure 5.20 Reinforcement Layout (Section F-F) – Test Series II 99
Figure 5.21 Reinforcement Layout (Section G-G) – Test Series II 100
Figure 5.22 Details of Loading Arm of Test Unit 2B 101
Figure 5.23 Concrete Dimensions of Test Series III Units – Elevation View 102
Figure 5.24 Concrete Dimensions of Test Series III Abutment Stem Wall – Plan View 102
Figure 5.25 Schematic Drawing of the Shear Key Reinforcement of Units 3A and 3B 104
Figure 5.26 Elevation View of the Reinforcement Layout – Test Series III 105

Figure 5.27 Reinforcement Layout (Section A-A) – Test Series III 105
Figure 5.28 Reinforcement Layout (Section B-B) –Test Series III 106
Figure 5.29 Reinforcement Layout (Section C-C) – Test Series III 106
Figure 5.30 Layout of Vertical Reinforcement of the Shear Keys – Test Series III 107
Figure 5.31 Reinforcement Layout (Section F-F) – Test Series III 107
Figure 5.32 Reinforcement Layout (Section G-G) – Test Series III 108
Figure 5.33 Locations of Strain Gages in Shear Key Reinforcement – Test Series I 109
Figure 5.34 Locations of Strain Gages in Vertical Bars of Wing Wall and Back Wall – Test Series I 110
Figure 5.35 Locations of Strain Gages in Horizontal Reinforcement of the Abutment Stem Wall – Test Series I 111
Figure 5.36 Layout of Displacement Transducers – Test Series I 111
Figure 5.37 Labels of Displacement Transducers – Test Series I 112
Figure 5.38 Labels of Displacement Transducers – Test Series II 113
Figure 5.39 Labels of Displacement Transducers – Test Series III 114
Figure 5.40 Loading Protocol of Test Series I, Series III and Test Unit 2A 115
Figure 5.41 Loading Protocol of Test Unit 2B 116

Figure 6.1 Observations at Relevant Limit States of Test Unit 1A 120
Figure 6.2 Load-Deformation Response of Test Unit 1A 122
Figure 6.3 Horizontal Profiles of Strains in Shear Key Reinforcement of Unit 1A 123
Figure 6.4 Horizontal Profiles of Strains in Horizontal Side Reinforcement of Unit 1A 124
Figure 6.5 Vertical Profiles of Strains in Vertical Bars of the Abutment Wall of Unit 1A 124
Figure 6.6 Observations at Relevant Limit States of Test Unit 1B 126
Figure 6.7 Load Deformation Response of Test Unit 1B 127
Figure 6.8 Horizontal Profiles of Strains in Shear Key Reinforcement of Unit 1B 129
Figure 6.9 Horizontal Profiles of Strains in Horizontal Side Reinforcement of Unit 1B 130
Figure 6.10 Horizontal Profiles of Strains in Vertical Reinforcement of Abutment Back Wall and Wing Wall of Test Unit 1B 130
Figure 6.11 Observations at Relevant Limit States of Test Unit 2A 132
Figure 6.12 Load Deformation Response of Test Unit 2A 134
Figure 6.13 Horizontal Profiles of Strains in Shear Key Reinforcement of Unit 2A (at Level of Shear Key-Abutment Wall Interface) 135
Figure 6.14 Horizontal Profiles of Strains in Shear Key Reinforcement of Unit 2A (at 4 inches Below the Shear Key-Abutment Wall Interface) 135
Figure 6.15 Horizontal Profiles of Strains in Shear Key Reinforcement of Unit 2A (at 8 inches Below the Shear Key-Abutment Wall Interface) 136
Figure 6.16 Horizontal Profiles of Strains in Horizontal Side Reinforcement of Unit 2A 136
Figure 6.17 Observation at Relevant Limit States of Test Unit 2B 138
Figure 6.18 Load Deformation Response of Test Unit 2B 139
Figure 6.19 Horizontal Profiles of Strains in Flexural Key Reinforcement of Unit 2B 140
Figure 6.20 Horizontal Strain Profiles in Abutment Horizontal Reinforcement in Unit 2B 141
Figure 6.21 Observations at Relevant Limit States of Test Unit 3A 143
Figure 6.22 Load Deformation Response of Test Unit 3A 145
Figure 6.23 Top Surface of the Abutment Stem Wall After Removal of the Shear Key of Test Unit 3A 146

Figure 6.24 Horizontal Profiles of Strains in Shear Key Vertical Reinforcement of Test Unit 3A 147
Figure 6.25 Strain in Side Vertical Reinforcement of the Abutment Stem Wall in Unit 3A..... 148
Figure 6.26 Horizontal Profiles of Strains in Horizontal Reinforcement of the Abutment Wall in Unit 3A (#3 bars)..... 148
Figure 6.27 Horizontal Profiles of Strains in Horizontal Reinforcement of the Abutment Wall in Unit 3A (#5 bars)..... 149
Figure 6.28 Variation of Prestressing Force in the Abutment Stem Wall During Testing of Unit 3A 150
Figure 6.29 Observations at Relevant Limit States of Test Unit 3B..... 152
Figure 6.30 Load Deformation Response of Test Unit 3B 154
Figure 6.31 Horizontal Profiles of Strains in Shear Key Vertical Reinforcement of Unit 3B.... 156
Figure 6.32 Horizontal Profiles of Strains in Horizontal Reinforcement of the Abutment Wall in Unit 3B (#3 bars)..... 157
Figure 6.33 Horizontal Profiles of Strains in Horizontal Reinforcement of the Abutment Wall in Unit 3B (#5 bars)..... 158
Figure 6.34 Variation of Prestressing Force in the Abutment Stem Wall During Testing of Unit 3B 159

Figure 7.1 Cracking Patterns at Level II 161
Figure 7.2 Cracking Patterns at Level III..... 162
Figure 7.3 Cracking Patterns at Level IV..... 163
Figure 7.4 Cracking Patterns at End of Testing 164
Figure 7.5 Load versus Deformation for Exterior Shear Key Test Units 167
Figure 7.6 Load-Deformation Response of Unit 2B with Flexural Key..... 168
Figure 7.7 Abutment Stem Wall of Test Unit 3A after Removal of the Exterior Shear Key 170
Figure 7.8 Shear Key Reinforcement with Mechanical Couplers in Test Unit 3B..... 171
Figure 7.9 Strut-and-Tie Analogous Model Type I..... 172
Figure 7.10 Strut-and-Tie Analogous Model Type II 173
Figure 7.11 Strut-and-Tie Analogous Model Type III..... 174

Figure 8.1 Load vs. Displacement – Exterior Shear Keys 177
Figure 8.2 Envelope of Load vs. Displacement Curves..... 178
Figure 8.3 Hysteresis Rule for Exterior Shear Keys 179
Figure 8.4 Concrete Component Model..... 179
Figure 8.5 Steel Component Model 180
Figure 8.6 Finite Element Analysis Results..... 180
Figure 8.7 Shear Keys Response Mechanism 183
Figure 8.8 Crack Width Opening at Interface with Shear Key 183
Figure 8.9 Top Displacement..... 184
Figure 8.10 Simulated Ground Motion 188
Figure 8.11 Experimental vs. Time History Results of Exterior Shear Keys 188

LIST OF TABLES

Table 2.1 Bridge Designation 7
Table 2.2 Values of Typical Shear Key Parameters 7
Table 2.3 Sacrificial Interior Shear Keys Research Program Test Matrix 8
Table 2.4 Calculated Capacity of Interior Shear Key Test Units 12
Table 2.5 Parameter Data 15
Table 2.6 Concrete Properties – Test Series I 23
Table 2.7 Concrete Properties - Test Series II 24

Table 3.1 Damage Levels Definition 25

Table 4.1 Strut Angle - θ 64
Table 4. 2 Experimental and Calculated Capacities 74
Table 4.3 Summary of Experimental $f'_c{}^{1/2}$ Factors 75
Table 4.4 Experimental Equivalent Viscous Damping 80

Table 5.1 Sacrificial Exterior Shear Keys Research Program Test Matrix 83
Table 5.2 Calculated Capacity of Exterior Shear Key Test Units 89
Table 5.3 Concrete Properties – Test Series I 117
Table 5.4 Concrete Properties – Test Series II 117
Table 5.5 Concrete Properties – Test Series III 118

Table 7.1 Loads and Modes of Failure of Sacrificial Exterior Shear Key Test Units 165
Table 7.2 Experimental and Calculated Maximum Load Carrying Capacities of Exterior Sacrificial Shear Keys 175

Table 8.1 Experimental vs. Theoretical Loads - Level I 181
Table 8.2 Experimental versus Theoretical Loads and Displacements- Level II 184
Table 8.3 Experimental vs. Theoretical Loads and Displacements - Level III 185
Table 8.4 Experimental vs. Theoretical Displacements - Level IV 186
Table 8.5 Experimental vs. Theoretical Displacements - Level V 187

ABSTRACT

Sacrificial shear keys are used at abutments to provide transverse support for bridge superstructures under seismic loads. In addition, sacrificial shear keys serve as structural fuses to control damage in abutments and the supporting piles under transverse seismic loads. Sacrificial shear keys may be interior or exterior. Exterior shear keys are usually recommended for new construction because they are easier to inspect and repair. One of the important issues addressed in this report is the post-earthquake inspection and repair of abutments with shear keys.

This report presents the results of an experimental program that was performed at the University of California-San Diego (UCSD) to study the seismic response of interior and exterior sacrificial shear keys. The experimental program consisted of seven interior and six exterior shear keys experiments. Variables investigated during testing of the interior keys were: (1) loading protocol (monotonic, quasi-static reversed cyclic, and dynamic reversed cyclic), (2) geometric aspect ratio of the shear key, and (3) reinforcement ratio of the shear key. Variables investigated during testing of the exterior keys were: (1) inclusion of back and wing walls, (2) adoption of different key details such as the use of sacrificial flexural keys and construction joints between the abutment stem wall and the shear keys, and (3) post-tensioning of the abutment stem wall just below the shear keys. The experiments provided useful results to develop analytical models that will serve as means to evaluate the capacity of shear keys as well as their post-peak performance under cyclic loads.

It was found that the shear friction model, with the coefficient of friction values given in the Caltrans Design Specifications, significantly underestimates the capacity of the interior and exterior sacrificial shear keys. This is non-conservative in the design of sacrificial shear keys, because it may lead to overloading of the abutments and the supporting piles. As a result of this, the piles may suffer severe damage before failure of the sacrificial shear keys.

It was also found that without post-tensioning of the abutments, extensive damage is likely to occur in the stem wall during a major earthquake. These experiments have shown that post-tensioning of the abutment stem wall can: (1) minimize damage to the abutments, and (2) post-earthquake inspection and repair can be accomplished with minimum resources. Based on the experimental results, recommendations for the design of interior and exterior sacrificial shear keys and future research are made in this report.

1 INTRODUCTION

Shear keys are commonly used at the abutments of small to medium span bridges to provide transverse support for the bridge superstructure under lateral loads. They do not carry gravity loads, but in the event of an earthquake are required to transfer the lateral reactions of the superstructure to the abutment or across movement joints. From the abutment these forces are then transferred to the ground through shear in the piles and wing-walls. It is also assumed that shear keys provide no further support for the superstructure once their capacity has been exceeded []. The bridge columns or bents must, therefore, be designed to provide full transverse support for the entire length of the bridge superstructure once the shear keys have failed.

Caltrans bridge design specifications [2] state that damage to the abutments under a major seismic event is admissible providing that any damage in the abutments will not result in collapse of the bridge or unseating of the superstructure. In addition, Caltrans bridge design specifications state that seismic loads cannot control the number of piles in the abutments [2]. Thus, in order to control damage to the abutments and piles the transverse seismic input force is limited by constructing sacrificial interior and/or exterior shear keys at the abutments.

Transverse seismic input forces are controlled by designing shear keys such that, the ultimate capacity of the keys does not exceed the sum of 75% of the piles shear capacity and one of the wing-walls shear capacity []. Two types of shear keys are constructed at the abutments. Interior shear keys are constructed within the abutment, and exterior shear keys are provided at sides of the superstructure. Interior keys, which act in both directions, are used within the width of the superstructure and because interior keys are not as accessible as exterior keys, it is recommended that interior keys be avoided for new construction projects. This design recommendation has been recently adopted, and many existing structures that utilize internal shear keys are currently in use. Both types of shear keys are shown schematically in Figure 1.1.

1.1 Development of Experimental program

The experimental program adopted by UCSD, in collaboration with Caltrans, seeks to determine the response of interior and exterior shear keys to transverse seismic loading. The results of the experimental program can be used to make realistic assumptions regarding the performance of shear keys in bridge abutments. This is particularly important for bridge assessment. The main objectives of this research program were to develop recommendations for the design of sacrificial shear keys with the intent of determining their peak as well as post-peak response, and to develop design details to reduce damage in the abutment stem walls and to enable both easy visual inspection and repair of the abutments following a major seismic event

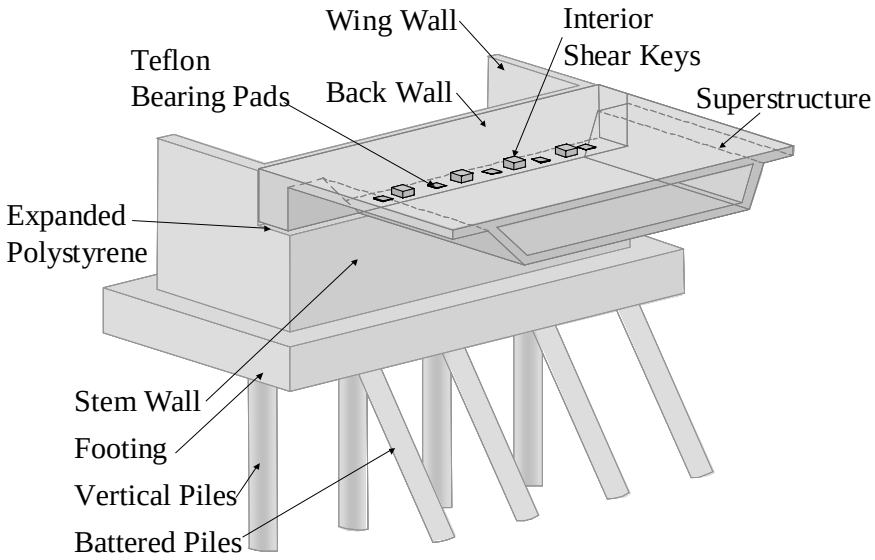

(a) Interior Shear Keys

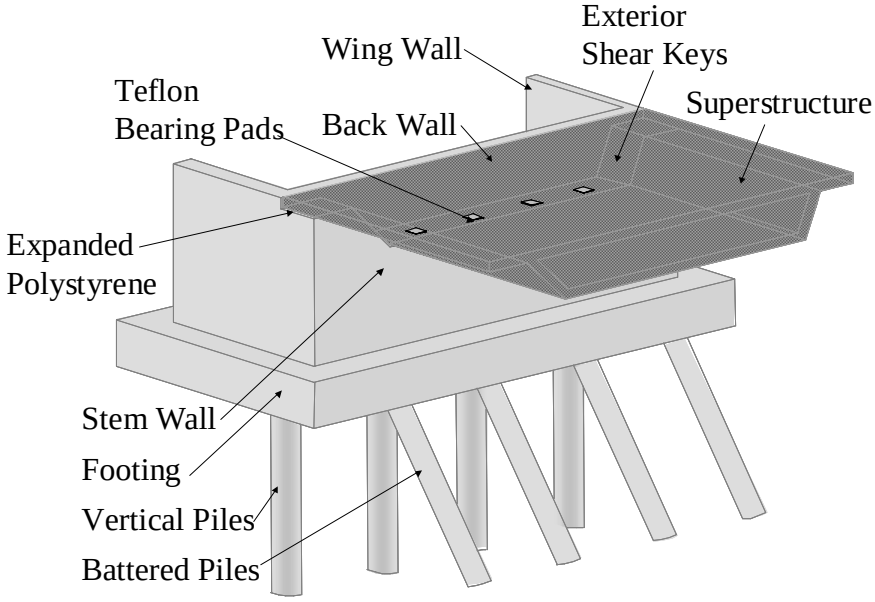

(b) Exterior Shear Keys

Figure 1.1 Schematic of Typical Bridge Abutments

The tests discussed in this report deal with three critical aspects of shear key design. The first is the determination of their peak capacity. Because shear keys are designed as sacrificial elements, it is of principle importance that realistic assumptions be made in determining their required proportions and reinforcement. In addition, assumptions, which are regarded as conservative for the design of non-sacrificial elements, are actually non-conservative for the design of elements that act as a structural fuse.

The second aspect of shear key performance is their behavior under cyclic load, both before and after reaching their peak load. The assumption that the shear keys provide no further support after reaching their peak capacity will be investigated experimentally, along with their damping and energy absorbing properties.

Finally, because the shear keys investigated in this report are used as structural fuses, it is expected that significant damage will occur in some parts of the abutments. However, alternatives to shear keys design details should be investigated in order to provide details that are both easy to inspect and repair following an earthquake. In this research program, these three aspects of sacrificial shear key design are addressed in terms of experimental and analytical studies.

1.2 Literature Review

There has been considerable research performed up-to-date to investigate the failure of plain and reinforced concrete shear keys. Analyses of shear keys are mainly based on two distinct types of cracking mechanisms. One model describes the response of shear keys by a single horizontal crack that develops at the shear key-abutment seat interface, and another model that takes into account the formation of multiple inclined cracks along the direction of predominant principal compressive stresses. The first approach has led to the development of simplified sliding shear friction based models, and the second to the development of simplified strut-and-tie based models. These analytical approaches are based on fracture mechanics and make use of a wedge crack model or rotating smeared crack model to predict their capacity [3]-[5].

There has also been extensive research to investigate the behavior of reinforced concrete brackets and corbels that can be idealized as strut and tie mechanisms, which are similar to the response of shear keys. Analytical tools such as strut-and-tie mechanisms assume that equilibrium is achieved through the reinforcing acting as tension ties, and the concrete acting as compressive struts. A number of possible strut-and-tie models have been developed, each based on different assumptions regarding the behavior of the bracket or corbel. The capacity of the bracket is then controlled by either the tensile capacity of the reinforcement or the compressive capacity of the concrete struts [6]-[11].

The concept of modeling the behavior of reinforced concrete using strut and tie models has also been researched extensively. The rational for its development was to determine the reinforcement required in discontinuity regions. Discontinuity regions are those in which the assumptions of traditional reinforced concrete design are not valid. The discontinuity regions include joints and areas of concentrated applied loads. Prior to cracking, the stress field in these

regions may be determined using simplified elastic analyses, however, after cracking significant disturbances occur in the stress field and the elastic approach is no longer valid. A widely used approach for the design of the reinforcement in discontinuity regions can be determined using a strut-and-tie model. Again, the concept is to assume that the concrete acts as a compression strut, with the reinforcement behaving as a tie [12]-[13].

The mechanism used to carry shear across an interface between members connected with reinforcing bars is known as sliding shear friction. Extensive tests have been performed on pre-cracked or non-cracked sections to determine the performance of reinforced concrete sections using this mechanism [14]. The aggregate interlock along the interface provides friction, with a passive normal force provided by the reinforcing. For slip along the interface to occur, the distance across the interface must increase, which activates the reinforcing. Research shows that the coefficient of friction for monolithic construction using normal weight concrete is 1.4 [14]-[15].

Other valuable research work includes the testing of deep beams. It can be rationalized that a shear key is similar to a deep, cantilever beam. Research in this area have shown that the determination of the shear strength of deep beams is generally empirical, with the contributions of various parameters to the shear strength measured and calibrated over a given range [16]-[24].

1.3 Report Layout

This chapter introduces some of the main objectives of this research program, which deal with the seismic performance of sacrificial shear keys. Important aspects in the design of shear keys were obtained based on a detailed literature search, and a brief description of literature findings are outlined in Chapter 1.

Chapter 2 describes the experimental program for sacrificial interior shear keys, in which detailed information regarding the design of test units is presented. Chapter 3 presents key experimental results for the interior shear keys, which were tested under three different loading protocols, such as monotonic, quasi-static reversed cyclic, and dynamic reversed cyclic. In Chapter 3 damage levels that were used to establish the performance of shear keys are also discussed. The experimental results are compared to determine the effects of the load history and the rate of the applied load on the performance of shear keys. The effect of varying the aspect ratio and the reinforcing ratio on performance of interior shear keys is also discussed in Chapter 3. The results are compared to determine how the parameters investigated influence the response of shear keys. In Chapter 4, a method of analysis was developed to assess the response of interior shear keys, based on realistic, rather than overly conservative, assumptions. Finally, Chapter 4

concludes with recommendations for determining the key response characteristics for interior shear keys based on the research presented.

Chapter 5 presents the experimental program for sacrificial exterior shear keys. The variables investigated in the exterior shear key tests are inclusion of abutment back wall and wing-wall, adoption of smooth construction joint at the interface between the abutment and the shear key, use of different details for shear keys such as use of flexural shear keys, and transverse post-tensioning of the abutments. The experimental results of sacrificial exterior shear keys are presented in Chapter 6. Experimental results are presented with the main intent of describing the response of the test units at their peak capacity, post-peak capacity and levels of damage in the abutment stem walls, which are critical aspects in shear key design as they relate to post-earthquake inspections and repair. In Chapter 7 detailed discussion of the experimental results of the exterior shear keys is presented along with simplified analytical models. Chapter 8 describes a hysteretic model used in assessing the seismic performance of exterior shear keys. The model is based on the experimental results presented in this report.

Finally, Chapter 9 presents a summary of this research project, along with conclusions based on the experimental results, and recommendations for design of sacrificial interior and exterior shear keys. An outline of future research needs is also presented in this chapter.

2 EXPERIMENTAL PROGRAM OF SACRIFICIAL INTERIOR SHEAR KEYS

This chapter presents some key aspects used in the design of the interior shear keys test units. The test units accurately reflected typical proportions of keys commonly used in practice. Caltrans provided information for a number of projects that used interior shear keys, both for new construction and retrofitting (see Table 2.1). Table 2.2 summarizes the dimensions and reinforcement of sacrificial shear keys of these selected projects. In Table 2.2, *h* is the height of the shear key; *b* is the shear key width; *d* is the shear key depth (see Figure 2.1). Also in Table 2.2, A_{cv} is area of the shear key-abutment wall interface; A_{vf} is area of vertical reinforcing bars crossing the shear key-abutment wall interface; α is the height-to-depth ratio or the aspect ratio; β is the shear key width-to-depth ratio and ρ is the reinforcement ratio.

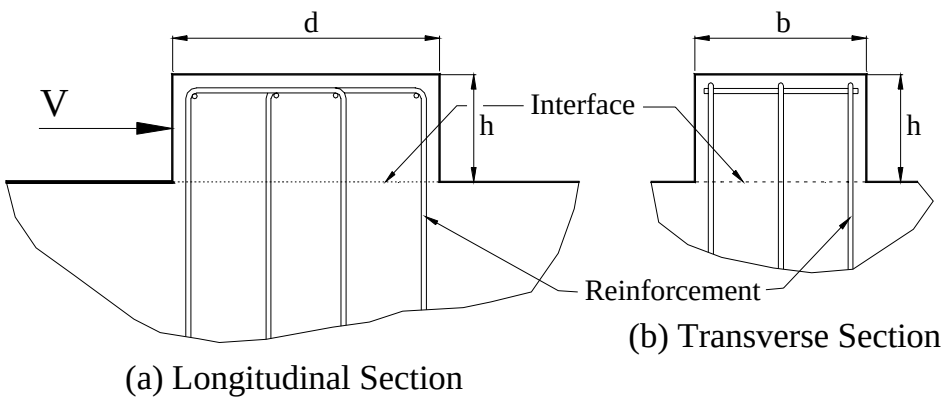

Figure 2.1 Typical Interior Shear Key Schematic Drawing

Proportions of interior shear keys can be expressed in terms of the aspect ratio, α (which is equal to *h/d*), β (which is equal to *b/d*) and ratio of the shear key vertical reinforcement, ρ (which is equal to A_{vf} / A_{cv}). The average values of these ratios were $\alpha = 0.32$, $\beta = 0.72$ and $\rho = 0.49\%$.

The next step was to proportion the shear keys with dimensions that were representative of those tabulated in Table 2.2, and with predicted capacities that were within the limits of the actuator used, which was 220 kips (979 kN). The predicted capacities of the test units were obtained from three different models, which were: (1) sliding shear friction model, (2) strut-and-tie model, and (3) a third model, which considered the flexural capacity of the shear key. These three models are described in Section 2.2.

Table 2.1 Bridge Designation

Project	Bridge Location	Caltrans Bridge Number
1	Taylor Street	Bridge No. 37-0583 New Construction
2	Taylor Street	Bridge No. 37-0583 New Construction
3	South Avenue	Bridge No. 39-0146 New Construction
4	State Street Overcrossing Ramp	Bridge No. 53-1350K Earthquake Retrofit Project No. 54
5	Elysian Viaduct	Bridge No. 53-1424 Earthquake Retrofit Phase II
6	Alemany Circle Undercrossing	Bridge No. 34-33 Earthquake Retrofit Project No. 305
7	Ballona Creek Bridge	Bridge No. 53-1256 Earthquake Retrofit Project No. 197
8	Capitol Expressway Overcrossing	Bridge No. 37-0101 Earthquake Retrofit Project No. 101
9	Northwest Connector Overcrossing	Bridge No. 56-687G Earthquake Project No. 445
10	Susan River Bridge	Bridge No. 07-0046 Earthquake Project No. 348

Table 2.2 Values of Typical Shear Key Parameters

Project	Type of Construction	h (in.)	d (in.)	b (in.)	A_{cv} (in.^{2})	A_{vf} (in.^{2})	α	β	ρ (%)
1	New	18	42	42	1764	8.80	0.43	1.00	0.50
2	New	18	74	42	3108	13.9	0.24	0.57	0.45
3	New	21	47	42	1990	8.72	0.44	0.89	0.44
4	Rehabilitation	18	110	22	2420	16.0	0.16	0.20	0.66
5	Rehabilitation	8.5	30	21	6360	4.34	0.28	0.70	0.69
6	Rehabilitation	10	72	27	1944	9.00	0.14	0.38	0.46
7	Rehabilitation	29	60	36	2160	9.30	0.48	0.60	0.43
8	Rehabilitation	18	79	15	1185	3.52	0.23	0.19	0.30

2.1 Test Matrix

The sacrificial interior shear key research program was divided in two series. As shown in Table 2.3, Test Series I consisted of three test specimens with the same height-to–depth ratio, α, width-to–depth ratio, β, and reinforcement ratio, ρ. In all of the interior shear keys the width of the key, *b*, was 14 in. (356 mm). In this test series the three test units were loaded with a different loading protocol (see Table 2.3).

Table 2.3 Sacrificial Interior Shear Keys Research Program Test Matrix

Test Series	Test Unit Designation	h in. (mm)	d in. (mm)	α	ρ (%)	Loading Protocol
I	1A	8 (203)	20 (508)	0.40	0.47	Monotonic
	1B	8 (203)	20 (508)	0.40	0.47	Quasi-Static Reversed Cyclic
	1C	8 (203)	20 (508)	0.40	0.47	Dynamic Reversed Cyclic
II	2A	6 (152)	20 (508)	0.30	0.47	Quasi-Static Reversed Cyclic
	2B	10 (254)	20 (508)	0.50	0.47	Quasi-Static Reversed Cyclic
	2C	8 (203)	20 (508)	0.40	0.32	Quasi-Static Reversed Cyclic
	2D	8 (203)	20 (508)	0.40	0.63	Quasi-Static Reversed Cyclic

The first test series showed that the shear keys response was essentially independent of the history and speed of the applied load. Because of the large variations in design parameters found in the shear keys presented in Table 2.2, it was decided that the second series would explore the effects of varying the aspect and reinforcement ratio on the performance of interior shear keys under cyclic loading. The second test series or Test Series II consisted of four specimens, two with different aspect ratios, and two with different reinforcement ratios

2.2 Capacity Evaluation of Interior Shear Keys

It has been proposed that shear keys be categorized based on their aspect ratio [2]. The capacity of a shear key would be calculated based on its category. These categories are:

$$\begin{aligned} &\alpha < 0.5 && \text{Shear friction} \\ &0.5 < \alpha < 1.0 && \text{Bracket and corbel} \\ &\alpha > 1.0 && \text{Flexural (cantilever beam)} \end{aligned} \qquad \textbf{(2.1)}$$

Three analytical models were used in evaluating the capacity of interior shear keys, namely: (1) sliding shear friction model, (2) strut-and-tie model, and (3) moment resistance model. These three models are described next.

2.2.1 Sliding Shear Friction Model

Based on the information presented in Table 2.2, most of interior shear keys currently in place fall within the first category, or the sliding shear friction model, with capacities calculated using the ACI [15] sliding shear friction approach. The capacity of a shear key was given by [1]:

$$V_N = \mu\ A_{vf}\ f_y \qquad \textbf{(2.2)}$$

Where A_{vf} is the area of vertical reinforcing bars crossing the shear key-abutment interface, f_y is the yield strength of the steel, μ is the coefficient of friction, taken as 1.4λ for concrete cast monolithically, and λ is taken as 1.0 for normal weight concrete. This model is based on the assumption that a continuous crack develops along the full length of the shear key-abutment seat interface. Caltrans bridge design specifications also state that the nominal capacity should not exceed []:

$$V_N < 800\ A_c\,(psi); \quad [5.52 A_c\,(MPa)] \qquad \textbf{(2.3)}$$

and

$$V_N < 0.2\ A_c\ f_c^{'} \qquad \textbf{(2.4)}$$

Where A_c is the concrete gross area at the interface. Equation (2.3) gives the upper limit of the shear stress capacity that may be developed at the shear key interface, and Eq. (2.4) gives an upper limit for V_N if the capacity of the diagonal compression strut is reached.

2.2.2 Strut-and-Tie Model

In this approach the shear key capacity is calculated according to a strut-and-tie mechanism. The reinforcement is assumed to act as a tension member, or tie, with the concrete acting as compressive struts [12],[25]. This is shown schematically in Figure 2.2. The nominal capacity of the key was calculated as:

$$V_N = T_s \cot\theta \qquad \textbf{(2.5)}$$

Percentage of number of reinforcement rows that cross the shear key-abutment interface and contribute to the tension tie capacity can be calculated by:

$$\frac{(\eta_s - 1)}{\eta_s} \qquad \textbf{(2.6)}$$

The tension T_s, is calculated as:

$$T_s = \frac{(\eta_s - 1)}{\eta_s} A_s f_y \qquad \textbf{(2.7)}$$

Where η_s is the total number of rows of reinforcement crossing the shear key interface. Only four rows of reinforcement are shown in Figure 2.2, but additional rows can be found in interior shear keys in other bridge structures. The number of reinforcement rows that contribute to the tension tie shown in Figure 2.2 may also be determined by any rational method of analysis. The tension tie was assumed to act at the location of the center of the total tensile force. The horizontal distance from the tie to the compression toe was:

$$d_s = \frac{\eta_s}{(\eta_s - 1)} \frac{d}{2} \qquad \textbf{(2.8)}$$

In addition, the diagonal compression strut, $C_{c,1}$, was assumed to extend from the intersection of the tension tie and the centroid of the horizontal compression strut, $C_{c,2}$, to the toe of the shear key, as shown in Figure 2.2. This is based on the assumption that the neutral axis depth, c, is small relative to the depth of the key. With the centroid of the applied load assumed to act at $h/2$, the resulting angle of inclination, θ, of the diagonal compression strut , $C_{c,1}$, is:

$$\theta = ATAN\left(\frac{h}{2d_s} \right) = ATAN\left[\frac{(\eta_s - 1)}{\eta_s} \alpha \right] \qquad \textbf{(2.9)}$$

Substituting Eqs. (2.7) and (2.9) into Eq. (2.5) gives:

$$V_N = \frac{A_s f_y}{\alpha} \qquad \textbf{(2.10)}$$

In Eq. (2.10) it is important to recognize that the nominal capacity of the shear key is inversely proportional to the shear key height-to-depth aspect ratio, α.

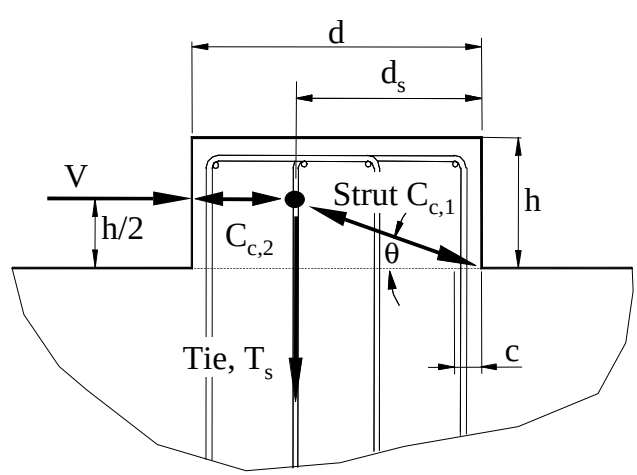

Figure 2.2 Strut-and-Tie Model

2.2.3 Moment Resistance Model

This model is based on the flexural-moment resistance capacity of the shear key section at the interface. The shear capacity can then be expressed as [2],[25]:

$$V_N = \frac{2M_N}{h} \tag{2.11}$$

Where the applied load was assumed at the mid-height of the key (h/2), as in the strut-and-tie model (as seen in Figure 2.3), and M_N is the nominal moment capacity calculated as [2],[25]:

$$M_N = \frac{(\eta_s - 1)}{\eta_s} A_s f_y \; j\, d_s \tag{2.12}$$

Where *jd/2* represents the distance from the centroid of the tension force to the centroid of the compression force, and one of the rows of reinforcement was assumed within the compression zone. Combining Eqs. (2.8), (2.11) and (2.12) results in:

$$V_N = \frac{jA_s f_y}{\alpha} \tag{2.13}$$

As in the strut-and-tie model, in Eq. (2.13) the capacity is also inversely proportional to the shear key aspect ratio. In the capacity evaluation of the shear key j was assumed equal to 0.90.

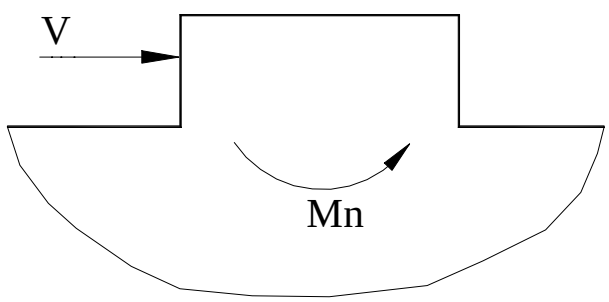

Figure 2.3 Capacity Based on Moment Resistance

The three methods of shear key capacity assessment were used in capacity assessment of the test units. The computed capacities of the test units based on each of the approaches outlined above are presented in Table 2.4. In preparation of Table 2.4, it was assumed that the yield strength of the bars, f_y, was 60 ksi (414 MPa).

Table 2.4 Calculated Capacity of Interior Shear Key Test Units

Test Series	Test Unit Designation	A_{vf} in^2 (mm^2)	V_N Shear Friction kips (kN) Eq. (2.2)	V_N Strut-and-Tie kips (kN) Eq. (2.10)	V_N , Moment Resistance kips (kN) Eq. (2.13)
I	1A	1.32 (852)	111 (494)	198 (881)	178 (792)
	1B	1.32 (852)	111 (494)	198 (881)	178 (792)
	1C	1.32 (852)	111 (494)	198 (881)	178 (792)
II	2A	1.32 (852)	111 (494)	264 (1174)	238 (1,059)
	2B	1.32 (852)	111 (494)	158 (703)	143 (636)
	2C	0.88 (568)	74 (329)	132 (587)	119 (529)
	2D	1.76 (1136)	148 (658)	264 (1174)	238 (1,059)

2.3 Overall Test Setup and Design of the Test Units

The test setup was approximately the same for the two test series. The test setup was designed to realistically model the various bridge components that interact with the shear key. The abutment itself was replicated by the specimen base, which was post-tensioned to the laboratory strong floor. As shown in Figure 2.4 and Figure 2.5, the load was applied to the key by a loading arm, which in turn was connected to the actuator. A hold-down frame was used to prevent any upward movement of the loading arm, which would be prevented in actual bridge abutments by the self-weight of the superstructure.

Figure 2.4 Sacrificial Interior Shear Key Test Unit and the Loading Arm

Figure 2.5 Overall Test Setup

2.3.1 Design of the Test Units – Test Series I

The base of the specimen was square with a side length of 5 ft-6 in. (1.68 m), enabling the base to be post-tensioned to the strong floor using a total of six 1 3/8 in. (35 mm) diameter bars. The base reinforcement consisted of #5 bars spaced at 6 in. (152 mm) for both longitudinal and transverse reinforcement, and the concrete base shear reinforcement consisted of #4 bars placed at each intersection between the #5 longitudinal and transverse bars. The shear key itself was reinforced with three rows of reinforcement formed by 2-#3 U-shaped bars, as shown in Figure 2.6. These were extended 9 in. (229 mm) beyond the development length and into the reinforced concrete base.

2.3.2 Design of the Test Units – Test Series II

In order to establish the parameters of each test unit in Test Series II, a study of the influence of these parameters on shear key performance was required. To do this, the capacity of the key was plotted as a function of both the aspect ratio and the reinforcement ratio, with all other parameters held constant; the results are shown in Figure 2.7 and Figure 2.8, respectively. The shear key capacity is shown for the three analytical evaluation procedures previously described. From the first series of tests, it was found that the strut-and-tie model best approximated the ultimate capacity of the key. The shear friction analytical method best approximates the post-peak load strength. The curves in Figure 2.7 and Figure 2.8 can be used to predict both levels of response.

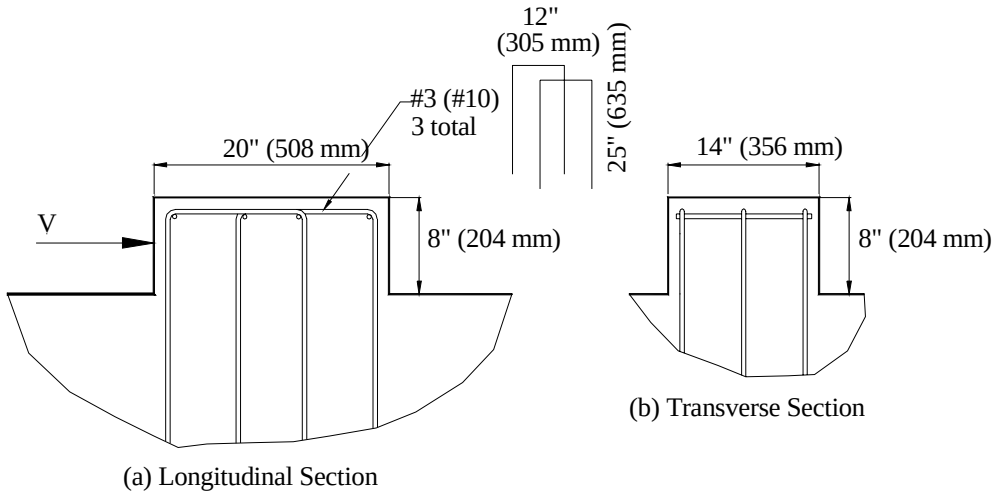

Figure 2.6 Reinforcement Layout – Test Series I

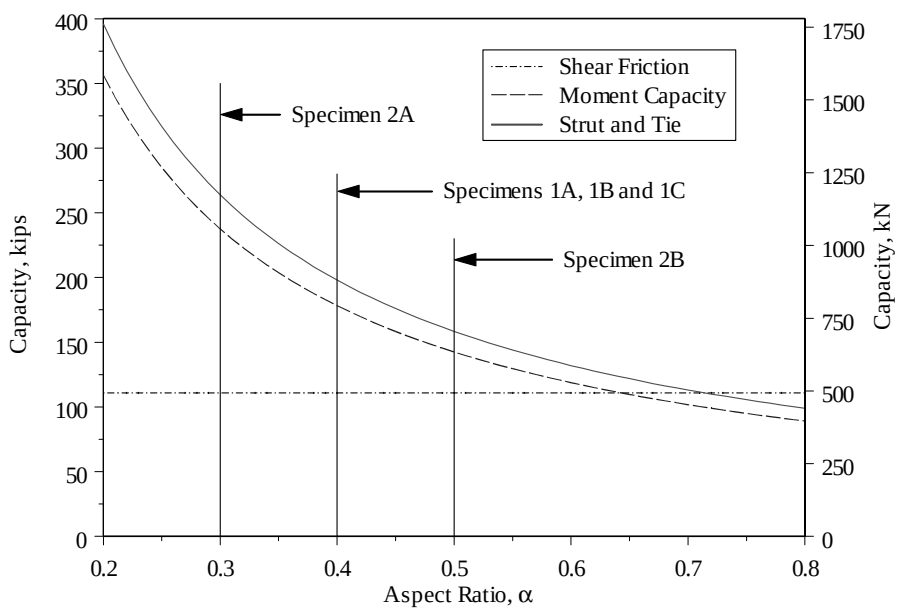

Figure 2.7 Effect of Aspect Ratio on Shear Key Capacity

Curves based on the strut-and-tie model and moment capacity in Figure 2.7 show that for low aspect ratios the shear key capacity approaches infinity, because the shear key capacity is inversely proportional to the shear key aspect ratio, as defined in Eqs. (2.10) and (2.13). However, it is reasonable to expect that this curve will reach a maximum value that is controlled by the capacity of the compressive struts. The reinforcement ratio has a more linear effect on the capacity of the key, as seen in Figure 2.8. Unlike the aspect ratio, however, it affects both the

peak and post peak capacity. To determine the effects of these parameters on the performance of the shear key, it was decided to perform a series of four tests, according to the test matrix shown in Table 2.3. Each parameter was varied twice, raising it for one specimen and lowering it for the other. All other parameters were held constant. As for the first series of tests, the specific details were decided using the information provided by Caltrans.

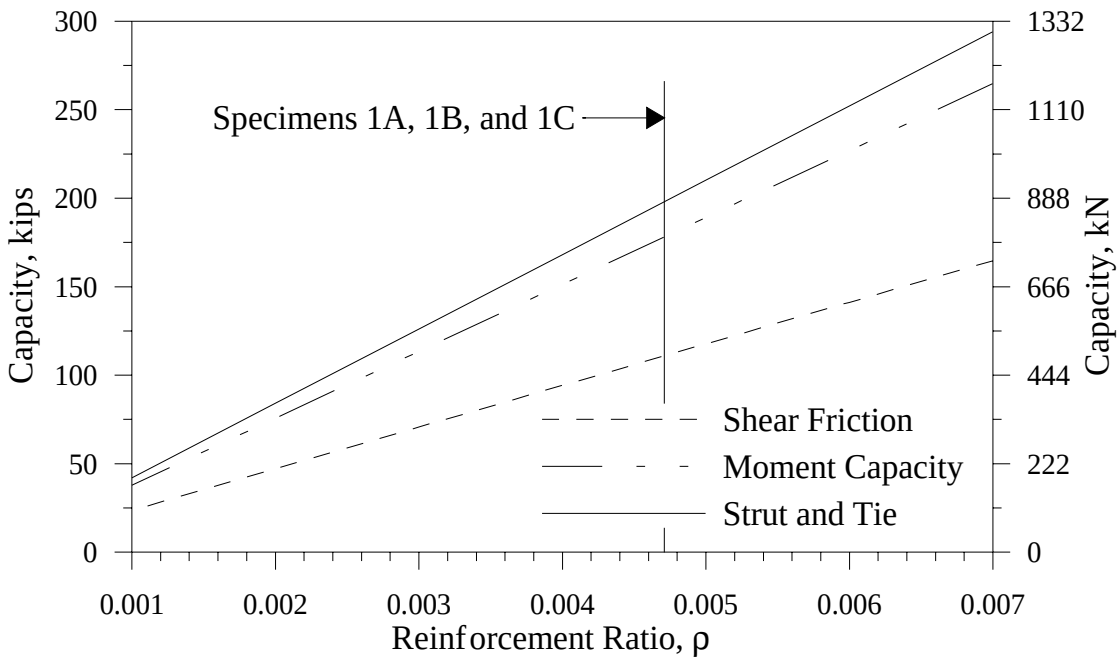

Figure 2.8 Effect of Reinforcement Ratio on Shear Key Capacity

For Test Series II, a range of values was required to determine limits for varying the test parameters. The standard deviation of the parameters under consideration was calculated and added to, or subtracted from the mean. The results are shown in Table 2.5.

Figure 2.9 shows the details of the test units of Test Series II. A practical limit in the aspect ratio was reached with a key height of six inches. Any decrease in the key height below this would make it impossible to develop yield strength of the reinforcement above the interface. Table 2.3 describes the dimensions and reinforcement amounts of each test unit.

Table 2.5 Parameter Data

	α	ρ
Maximum	0.48	0.69
Average+1xStd. Deviation	0.44	0.62
Average	0.32	0.49
Average-1xStd. Deviation	0.20	0.36
Minimum	0.14	0.06

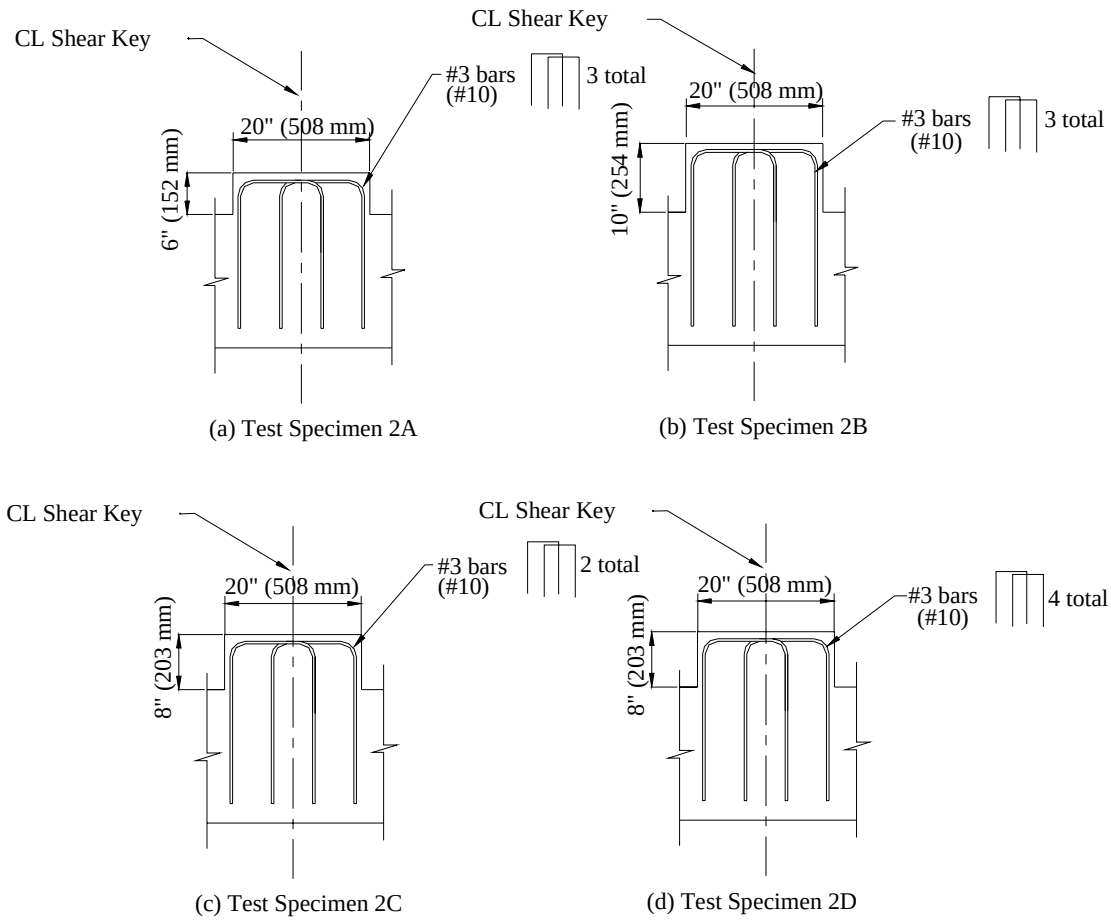

Figure 2.9 Reinforcement Layout – Test Series II

2.4 Instrumentation of the Test Units

2.4.1 Test Series I

In Test Series I, each test unit was instrumented with 13 linear potentiometers and 26 strain gages. All instrumentation was connected to a high-speed data acquisition system. The data acquisition system was used to record data triggered at a predetermined displacement or force interval.

2.4.1.1 Strain Gages

Electrical resistance strain gages were attached to the shear key reinforcement at the locations shown in Figure 2.10. Gages were placed on all the outer legs of the shear key reinforcement. Additional gages were placed on the inner legs of the middle line only. Gages were placed on all of these legs at the following three locations: (1) shear key-abutment wall interface, (2) nominal

development length of the reinforcement bars, 9 in. (229 mm) below the interface, and (3) at a location halfway the previous two gages. This gives a total of three gages per leg, which was adequate in evaluating the force transfer between the shear key reinforcement and the reinforced concrete base. In addition, two additional gages were placed on two of the reinforcement bars of the middle leg of reinforcement. These were placed to measure additional transfer beyond the development length of the bar.

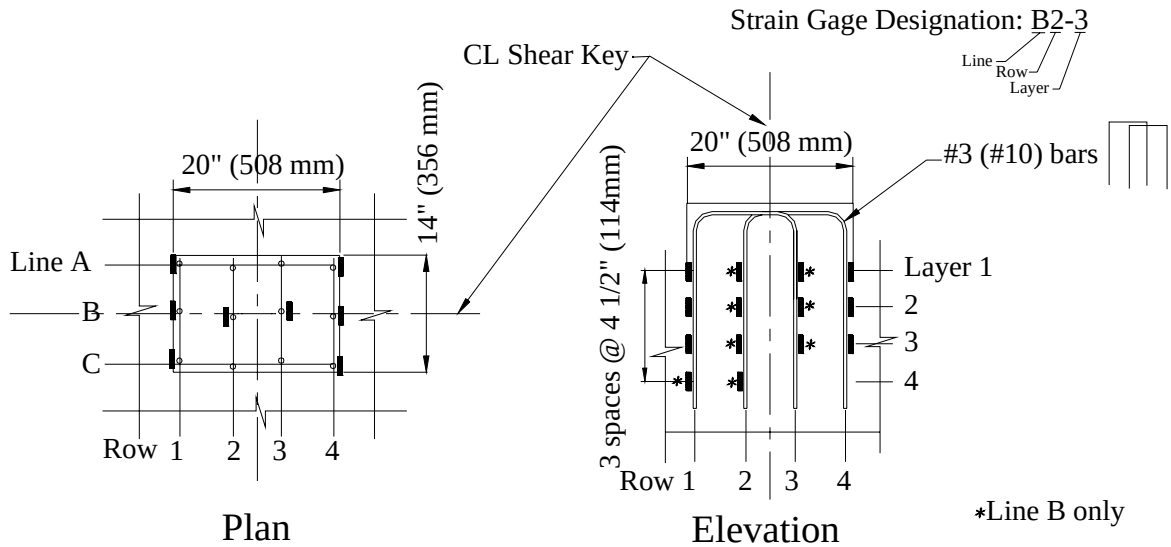

Figure 2.10 Strain Gage Locations – Test Series I

2.4.1.2 Displacement Transducers

The longitudinal movement of the loading arm was measured by a single potentiometer with a stroke of 66 inches (152 mm), labeled AN in Figure 2.11. This potentiometer was also used to control the testing procedure.

In addition to AN, two more potentiometers were used to measure any lateral movement of the loading arm, one on each end of the shear key. These were labeled ANE and ASW. There were a total of six potentiometers placed to measure movement of the key. Two potentiometers, one on each side of the key, were used to measure longitudinal movement. These were labeled KEH and KWH. In addition, four potentiometers were placed vertically at the corners of the key to measure vertical movement of the key at each face, labeled KNE, KSE, KSW and KNW.

Four additional potentiometers were used to measure any movement of the base of the specimen relative to strong floor. Two were placed at each end of the specimen base, in the direction of the applied load. One of each pair was placed horizontally to measure any sliding of the key along

the strong floor and the other was placed vertically to measure any uplift or rotation. These potentiometers were labeled BSV, BSH, BNV, and BNH.

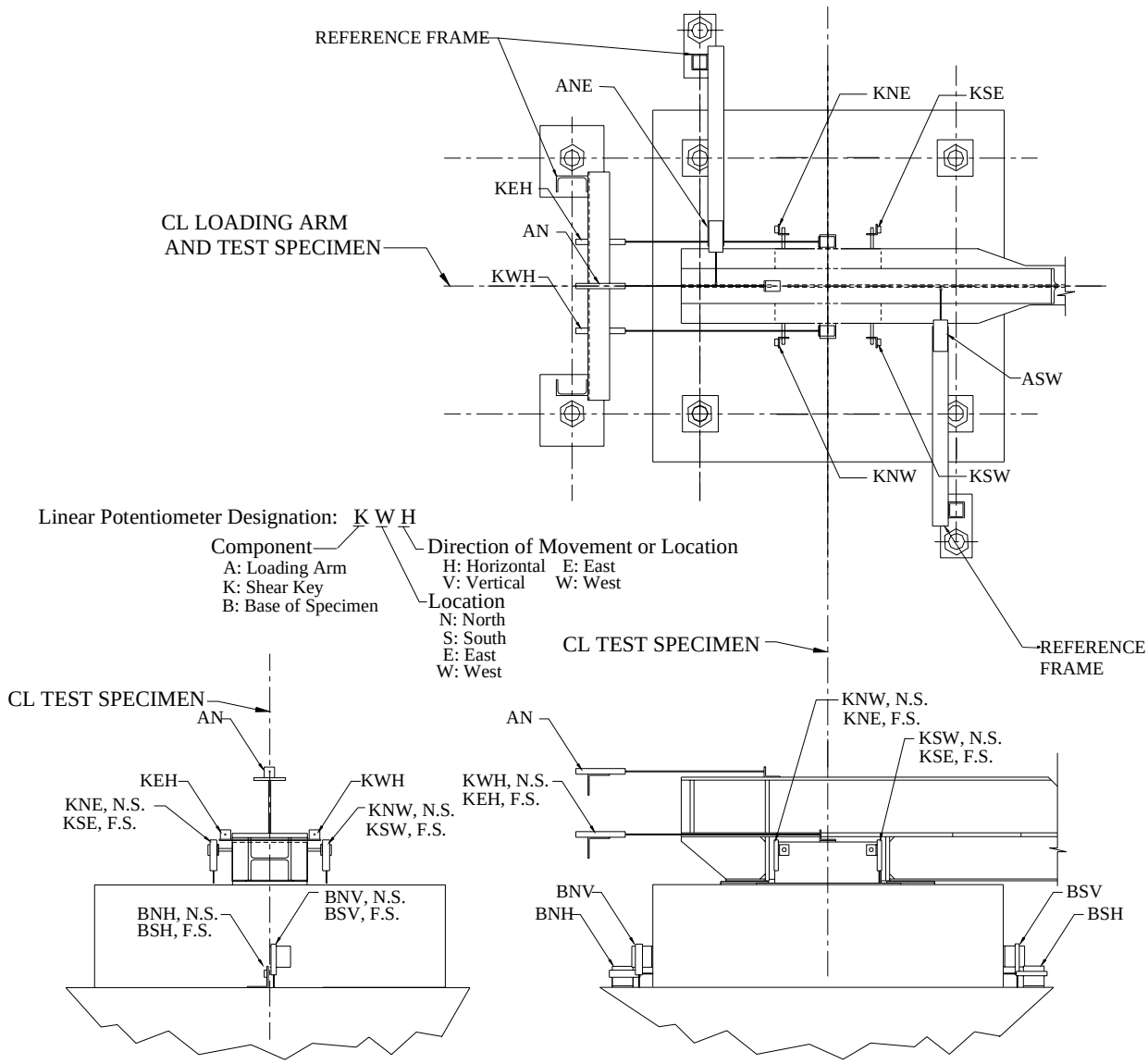

Figure 2.11 Linear Potentiometer Locations

2.4.2 Test Series II

2.4.2.1 Strain Gages

There were some modifications in the placement of the strain gages compared to those of Test Series I. In the instrumentation of Test Series II, it was decided to place strain gages at the interface for all reinforcement bars in order to evaluate properly the development of the strut-

and-tie load transfer mechanism. This is also the most heavily damaged location, and by placing extra gages in this region would ensure description of reliable strain profiles in the horizontal direction and along the shear key-abutment wall interface.

The results from Test Series I showed that the transfer of force along the length of the reinforcement was essentially identical at all locations. It was, therefore, decided to place strain gages along the length of the reinforcement only for one line of reinforcing bars, and only on the outer legs, which have the highest strains, as indicated by results of the first series of tests. It was also decided to eliminate the fourth strain gage used at locations B1-4, and B2-4 (see Figure 2.10), which showed essentially no strain during the first series of tests. Two additional gages were placed on the inner legs of one line of reinforcement. This would enable full determination of strain profiles 4½ in. (114 mm) into the base from the interface at one location. The resulting strain gage patterns are shown in Figure 2.12.

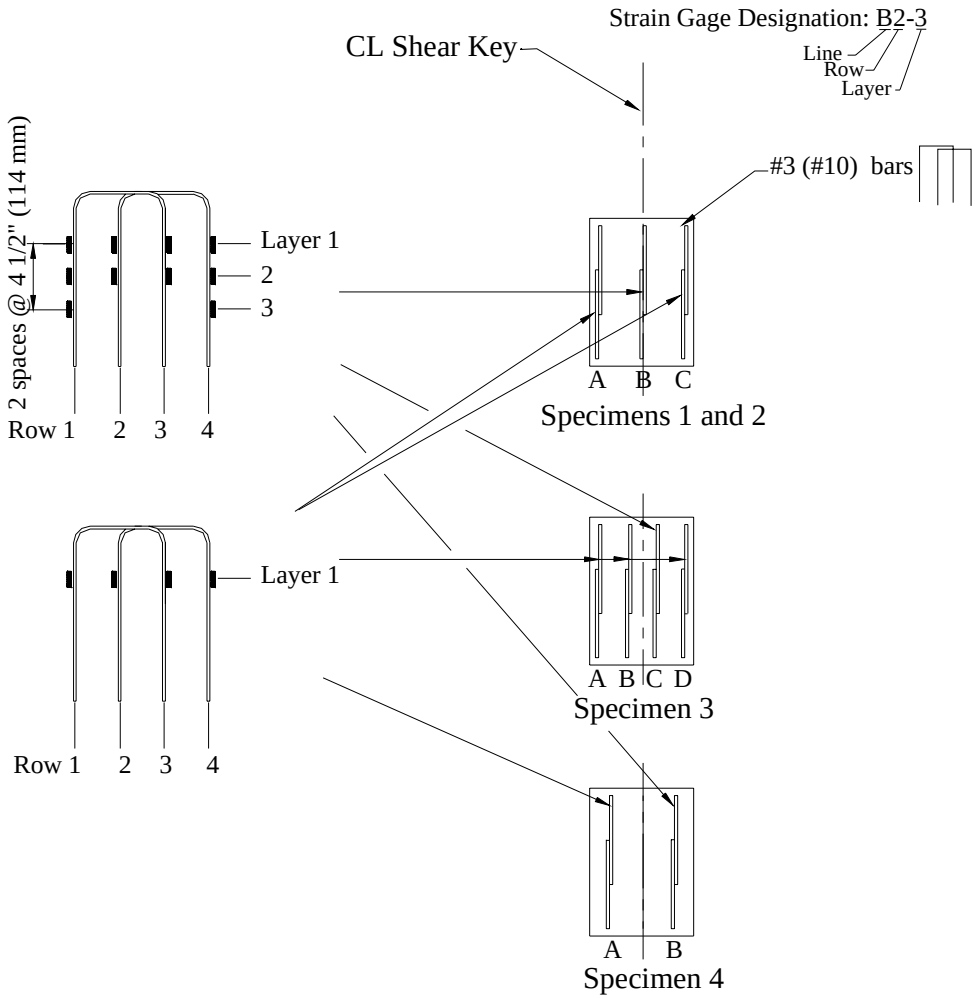

Figure 2.12 Strain Gage Locations - Test Series II

2.4.2.2 Displacement Transducers

As in Test Series I, Test Series II units were also instrumented with linear potentiometers. Redundancy was eliminated however, by eliminating KWH, KSW, and KNW in Figure 2.11. Potentiometers BSV, BSH, and BNV at the base were also eliminated since they have recorded no movement during the first series tests. Potentiometer BNH was left to measure any unanticipated sliding of the specimen along the floor.

2.5 Loading Protocol

2.5.1 Test Series I

The objective of Test Series I was to determine the shear key response under three different loading protocols. The monotonic loading protocol was used to characterize the monotonic load versus displacement relationship of the shear key. The quasi-static reversed cyclic loading protocol was then performed to establish the response of the shear key under reversed cyclic loading. The final loading protocol was dynamic reversed cyclic to investigate the effects of the loading rate on the cyclic behavior of the shear key.

2.5.1.1 Monotonic Loading

The loading protocol described in this section was used in the test of Unit 1A. For the monotonic loading protocol, it was decided to push the key until the peak capacity was reached, after which the capacity of the key was expected to degrade. After a significant amount of degradation had occurred, the shape of the force-displacement curve had been established, and the load was cycled to determine the performance of the key under further cyclic loading. The key was pushed to a displacement of about 2.4 in. (61mm), and then pulled in the other direction to a displacement of –2.8 in. (-71 mm). The loading was then cycled twice at 3 in. (76 mm) and once at 3.75 in. (95 mm).

2.5.1.2 Quasi-Static Reversed Cyclic Loading

The loading protocol described in this section was used in the test of Unit 1B. For the quasi-static reversed cyclic load application, it was decided to test the shear key under increasing force levels in load control until the peak load was reached, and then switch the tests to displacement control. There was a 1 in. (25 mm) gap between the loading arm and the face of the key. This gap resulted in a region of essentially zero stiffness, which made it impossible to perform the tests in this early stage in load control. There was an attempt to overcome this condition, by running the

actuator in displacement control through this zero stiffness region, and then switch the test to load control after the gap was closed. This approach was not very effective because of the sharp increase in the shear key stiffness and the delay in the actuator switching from displacement to load control. As a result, the test was performed completely in displacement control.

In terms of displacements, the key was loaded to 3 fully reversed cycles at 1 in. (25mm), 2 in. (51mm), and 3 in. (76 mm), and one cycle at 3.75 in. (95 mm), as shown in Figure 2.13.

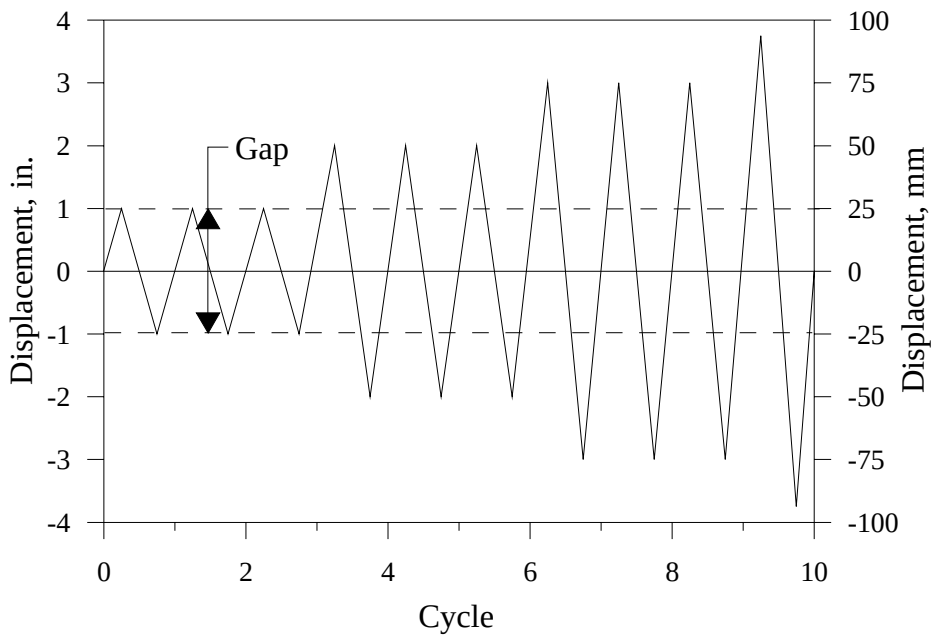

Figure 2.13 Quasi-Static Reversed Cyclic Load History

2.5.1.3 Dynamic Reversed Cyclic Loading

The loading protocol described in this section was used in the test of Unit 1C. The displacement history of the quasi-static test was also used in the dynamic reversed cyclic loading test. The load was cycled with the maximum velocity of the actuator, at 13 in./sec (330 mm/sec.). To reduce noise in the system caused by the infinite accelerations experienced at the direction reversals of triangular load input, the load was applied in the form of a sine wave, as shown in Figure 2.14.

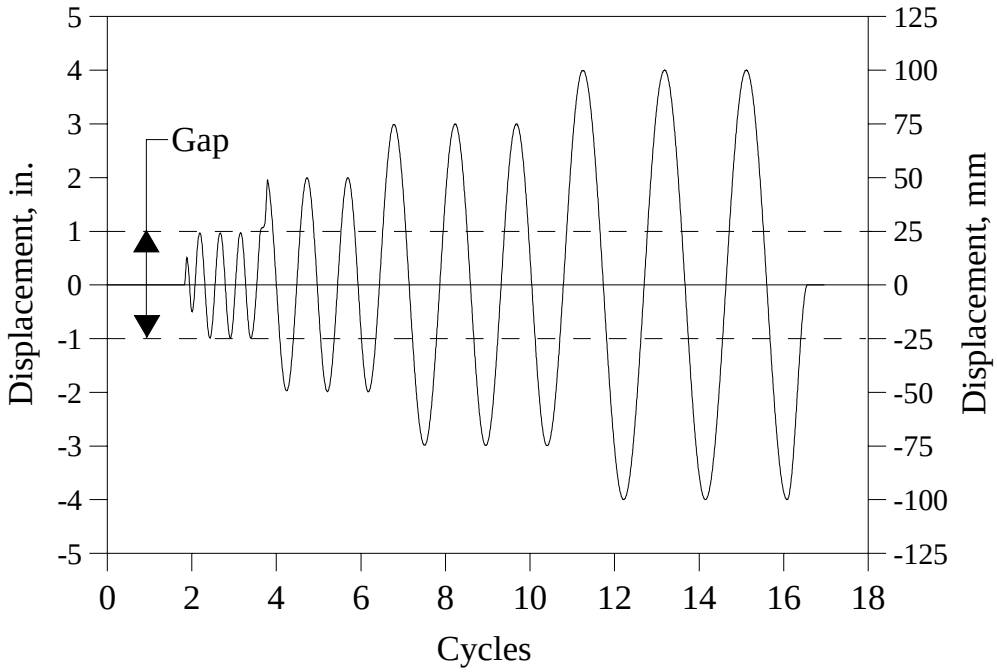

Figure 2.14 Dynamic Reversed Cyclic Load History

2.5.2 Test Series II

The first series of tests showed that the performance of the shear key was essentially independent of the history and speed of the applied load. As a result in Test Series II, it was decided to apply the load using a quasi-static reversed cyclic load history. This enabled loading of the key cyclically at a slower rate, which made it easier to observe the key performance at different stages of testing. The load history was identical to that of test Unit 1B, and is shown in Figure 2.15.

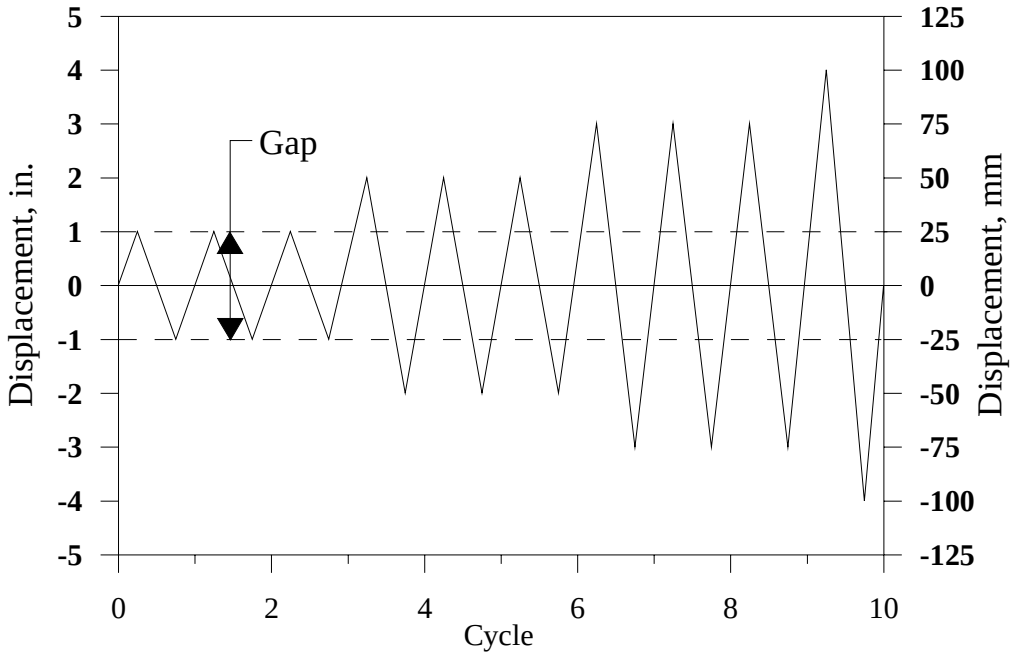

Figure 2.15 Loading History - Test Series II

2.6 Material Properties

2.6.1 Test Series I

The concrete used in the construction of the first test series was specified to have a minimum 28 day compressive strength f'_c = 3,250 psi (22.4 MPa). Maximum aggregate size was ½ in. (13mm). Test cylinders were cast with the specimens and tested at 28 days and on the day of test for Unit 1C. The cylinder test results are presented in Table 2.6. The day of test strengths for Units 1A and 1B were found by interpolation. The actual 28 day compressive strength was 4,090 psi (28.2 MPa).

The reinforcement used was Grade 60 (f_y = 60 ksi = 414 MPa) deformed mild steel bars. Tensile tests were performed on three bars to determine their properties. The yield strength was found to be 63 ksi (434 MPa) and the ultimate strength, 100 ksi (690 MPa).

Table 2.6 Concrete Properties – Test Series I

Test Unit Designation	Day of Test Strength psi (MPa)
1A	4230 (29.2)
1B	4570 (31.5)
1C	5070 (35.0)

2.6.2 Test Series II

The concrete mix used in Test Series II units was the same as for Series I test units, with a nominal 28 day compressive strength of f'_c = 3,250 psi (22.4 MPa). Cylinders were cast as for the first series and the results are shown in Table 2.7. Cylinders were tested on day of test of each unit. Test Units 2A, 2B and 2D were poured on a single day, and Unit 2C was cast on a different day. The same grade of reinforcement was used as in the first series. Again, tensile tests were performed on three bars and the yield and ultimate strengths were 63 ksi (434 MPa) and 100 ksi (690 MPa), respectively.

Table 2.7 Concrete Properties - Test Series II

Test Unit Designation	Day of Test psi (MPa)	28 day psi (MPa)
2A	4600 (31.7)	4280 (29.5)
2B	4490 (31.0)	4280 (29.5)
2C	3820 (26.3)	3920 (27.0)
2D	4250 (29.3)	4280 (29.5)

3 EXPERIMENTAL RESULTS OF SACRIFICIAL INTERIOR SHEAR KEYS

Experimental results of the sacrificial interior shear key test units will be presented in this chapter. Analytical models for interior shear keys will be discussed in Chapter 4.

3.1 Description of Damage Levels

Observations recorded during testing were used to characterize the load deformation response, and establish damage levels for shear keys subjected to seismic loads. Description of five damage levels is presented in Table 3.1 and these levels are described next.

Table 3.1 Damage Levels Definition

LEVEL	Damage Evaluation	Performance Evaluation
I	NO REPAIR	CRACKING
II	POSSIBLE REPAIR	YIELDING
III	MINIMUM REPAIR	INITIATION OF LOCAL MECHANISM
IV	REPAIR	FULL DEVELOPMENT OF LOCAL MECHANISM
V	REPLACEMENT	STRENGTH DEGRADATION

3.1.1 LEVEL I

This damage level was characterized by onset of cracking, which is qualitatively evaluated by cracks that are barely visible and close after load removal. At this damage level no repair should be required [26].

3.1.2 LEVEL II

This damage was defined when the reinforcement has yielded, and was quantified visually by cracks that were clearly visible but most likely would not require repair [26].

3.1.3 LEVEL III

This damage level was characterized by the onset of concrete spalling or large open cracks, which are typically good indicators of local damage, and would require minimum repair [26].

3.1.4 LEVEL IV

Qualitatively, this level was evaluated when cracks and spalling extended over the full region of the shear keys. Depending on the prevalent failure mechanism, damage at this level would require some form of major repair [26].

3.1.5 LEVEL V

This damage level was defined when the load carrying capacity of the shear key is compromised due primarily to fracture of the reinforcement, and would require replacement or major repair of the bridge abutments shear keys [26].

These damage levels were set as target in describing the response of the shear keys. Next is a description of key experimental results for the sacrificial interior shear keys.

3.2 Test Series I – Test Unit 1A

The experimental results for Test Unit 1A will be presented in this section. This test unit was subjected to the monotonic loading protocol described in Section 2.5.1.1.

3.2.1 General Test Observations

Level I: The first observation was the closing of the 1 in. (25 mm) gap between the face of the key and the loading arm, during which only the expanded polystyrene resisted the applied load. With the polystyrene compressed, the applied load increased rapidly, and the test was paused at about 120 kips (534 kN) corresponding to the onset of cracking. These consisted of a horizontal crack at the interface and extending approximately halfway the depth of the key. Smaller horizontal cracks were also visible on the sides of the key, as shown in Figure 3.1(b).

Level II: As the test continued, the cracks began to propagate further into the key and some began to incline towards the compression toe, as shown in Figure 3.1(c). These observations indicate formation of diagonal compression struts, which are representative of the strut-and-tie mechanism previously described in Section 2.2.2.

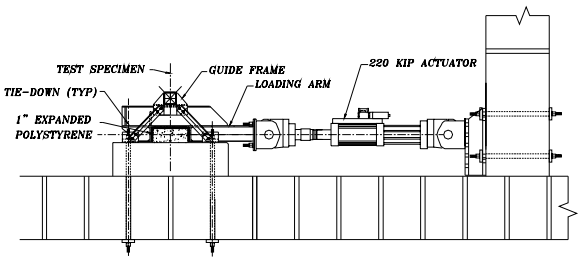

(a) Test Unit Layout

(b) LEVEL I

(c) LEVEL II

(d) LEVEL III

(e) LEVEL IV

(f) LEVEL V

Figure 3.1 Test Observations – Test Unit 1A

Level III: The peak load was reached at about 210 kips (934 kN). At this level the horizontal crack was almost running the full length of the shear key, and wide-open cracks were observed on the sides of the key, as shown in Figure 3.1(d).

Level IV: After the peak load was reached, the lateral load stabilized at about 110 kips (490 kN). This value is very close to the computed capacity using the sliding shear friction model, given by Eq. (2.2). At this level the horizontal crack at the interface propagated the full length of the key,

basically separating the concrete of the key from that of the base. This crack was accompanied by a large crack developing on the side of the key, which was formed when one of the horizontal cracks at mid-height of the key intersected an inclined crack, as shown in Figure 3.1(e).

After a peak displacement of about 2.4 in. (61 mm) was reached, and the monotonic profile of the force displacement curve was established, the load was reversed. The load immediately dropped to essentially zero as the key remained in place while the loading arm lost contact with the face of the key. The arm continued to move with very little resistance until the gap was once again closed on the opposite face of the shear key. The resistance was then increased very slowly until a deflection of about 1.3 in. (33 mm) was reached. The load began to increase until a maximum load of about 65 kips (289 kN) was reached, this capacity was maintained with minor degradation until the load was cycled at a displacement of about 3 in. (76 mm).

Level V: With continued cycling, the damage to the key became increasingly severe, exposing the outer lines of reinforcement, rendering them ineffective, as shown in Figure 3.1(f). This severe damage in addition to fracture of the reinforcement resulted in the continued degradation of the strength and stiffness of the key.

3.2.2 Load versus Displacement Curve

Figure 3.2 shows the load versus displacement relationship, which depicts both the movement of the loading arm and the movement of the shear key itself during the monotonic portion of the test. The 1 in. (25 mm) layer of expanded polystyrene causes an offset in the two profiles, which have the same overall shape.

Performance of the shear key during the test can be described as follows:

i. Closure of the initial gap: This zone is the initial region of very low stiffness up to about ¾ in. (19 mm) displacement, over which the applied load was resisted only by the expanded polystyrene.

ii. Resistance of the key through a strut-and-tie load transfer mechanism: This region is characterized by its high stiffness, beginning at the closure of the gap and terminating when the peak capacity of the strut–and-tie is reached, at about 1 in. (25 mm) displacement. Figure 3.2 shows the following locations in this region: first cracking, yielding of the first row of reinforcement (Row 1 in Figure 2.10) nearest to the location of the applied load, and yielding of the second row (Row 2 in Figure 2.10).

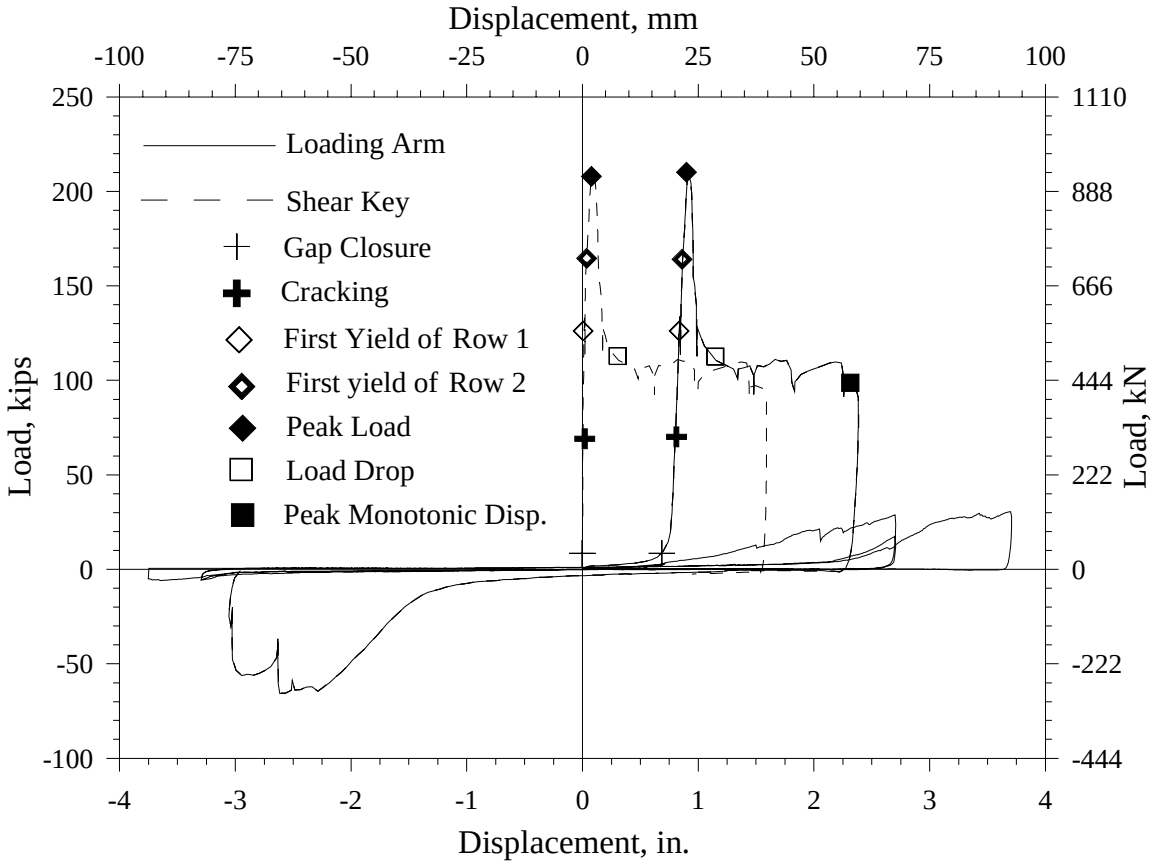

Figure 3.2 Load vs. Displacement – Test Unit 1A

iii. Resistance through a shear friction mechanism: This region began when the crack at the interface propagated completely through the key, effectively separating the concrete of the key from that of the base. This resulted in a significant decrease in the load as the load transfer mechanism switched to sliding shear friction, with the key itself behaving as a rigid body connected to the base by the reinforcement. The friction was provided in the crack developed at the interface. This region is characterized by a constant load level, which was maintained until the load was reversed.

iv. Cyclic shear friction: As the shear key was further displaced, the load increased, but at much lower stiffness than that of the strut-and-tie mechanism. This stiffness was maintained through the target displacement, barring any fracture of the reinforcement. As the load was cycled at this displacement, the damage of the concrete at the interface resulted in substantial stiffness degradation. When the target displacement was increased, the stiffness observed during the last cycle at the previous displacement was maintained until the new target displacement was reached, again barring any fracture of the reinforcement. The sides of the keys also showed substantial spalling, rendering the outer lines of reinforcing bars ineffective.

The resulting load displacement curve shows an extremely pinched hysteresis, with extremely limited energy absorbing potential and a rapid degradation under cyclic loading. Based on the analyses previously described, the peak load of 210 kips (934 kN) was most accurately calculated using the strut-and-tie model, with predicted shear key capacity, V_N = 198 kips (881 kN) as shown in Table 2.4. The sliding shear friction approach, which has been proposed for shear keys with aspect ratios less than 0.5, resulted in a calculated capacity of 110 kips (489 kN). This agrees with the resistance of the shear key after failure of the strut-and-tie, and after the crack propagated along the interface.

3.2.3 Horizontal Strain Profiles

Figure 3.3 shows the strain profile through the key section at different load levels, beginning with the closure of the 1 in. (25 mm) gap and ending with the peak monotonic displacement. The horizontal dashed line shown in the figure represents the yield strain of the shear key reinforcement, ε_y. This clearly shows the development of the tie formed by the reinforcement at locations A, B, and C shown in the figure. As the load increased, the force in the reinforcement contributing to the tie also increased. The reinforcement at location D remained at relatively low strain levels until the crack at the interface propagated completely through the section, and the sliding shear friction transfer mechanism was activated.

From Figure 3.3, the development of the tie is apparent from observation of the specimen as it was loaded, by the formation of a crack forming along the interface horizontally nearest the loaded face of the key. As the applied load was increased, this crack propagated along the interface through the key section, with an increasing amount of reinforcement contributing to the tie.

The strain profile at a depth of 4 ½ in. (114 mm) from the interface shows that the strains at locations E, F, and G are nearly similar, with small compressive strains recorded at location H. This verifies the data from the gages at the interface, also showing the reinforcement effective in forming the tie.

After reaching the peak load the capacity of the key dropped to the shear friction capacity level, the strains increased at location H resulting in a more uniform distribution over the length of the key. This shows that the load is no longer being resisted through a strut-and-tie mechanism.

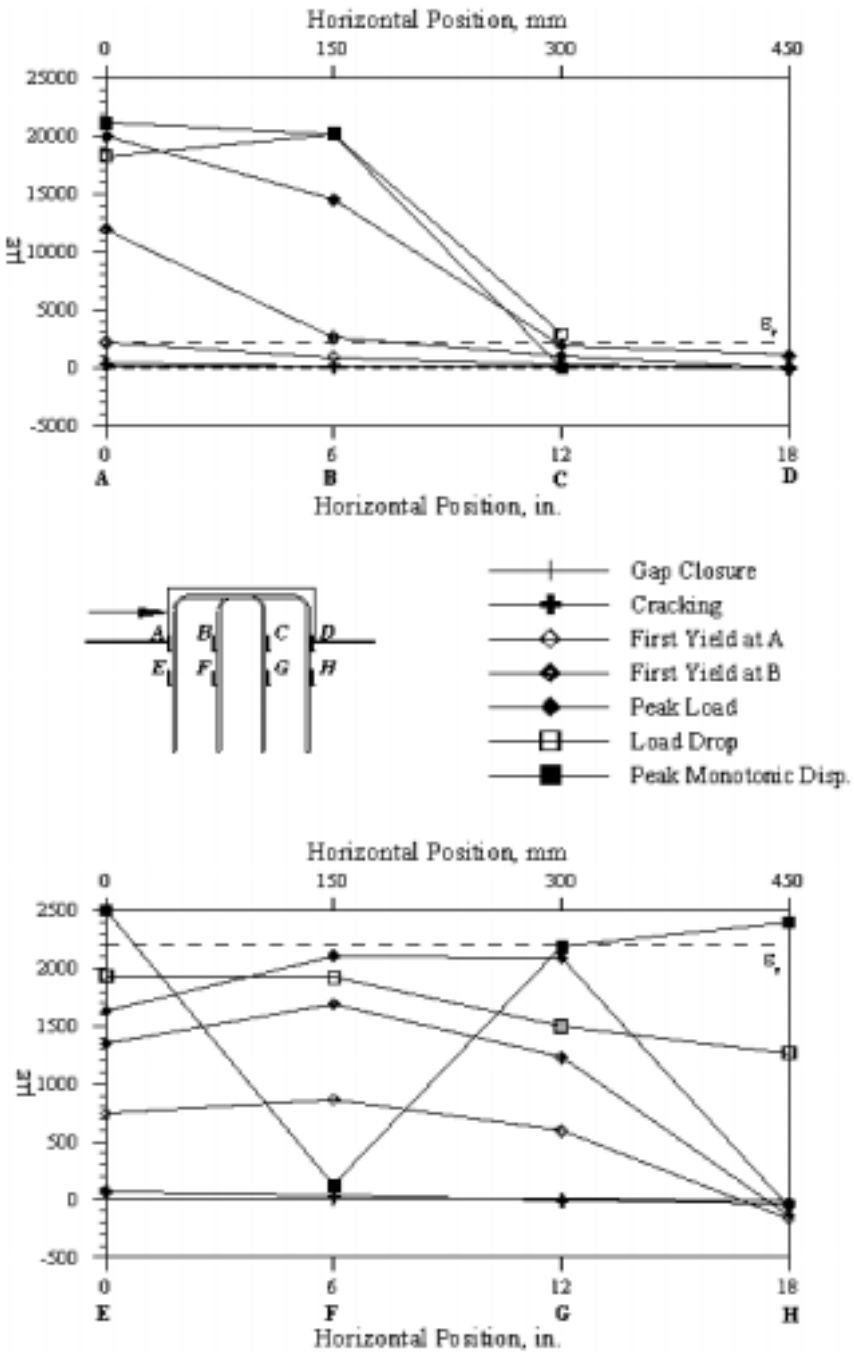

Figure 3.3 Horizontal Strain Profiles – Test Unit 1A

3.2.4 Vertical Strain Profiles

The strain profiles along the length of the reinforcement bars are shown in Figure 3.4. As mentioned in Section 2.4, the spacing of the gages along the reinforcement is 4½ in. (114 mm).

The vertical dashed line shown in Figure 3.4 represents the yield strain of the shear key reinforcement, ε_y. The highest strains were measured at the shear key-abutment interface in the two reinforcement rows nearest the applied load (locations 1 and 5 in Figure 3.4). The strains decreased rapidly as the force in the reinforcement was transferred to the reinforced concrete base. At the nominal development length of the reinforcement, 9 in. (229 mm), at locations 3 and 7, essentially all of the force has been transferred to the concrete. This shows that the assumed development length of the reinforcement was reasonable.

The third row of reinforcement shows higher strains at location 10, 4 ½ in. (114 mm) below the interface, than at the interface itself. This indicates that some forces were transferred into the reinforcement below the interface. The profile for the fourth line shows the same behavior, but in compression.

3.2.5 Vertical Shear Key Movement

The vertical movement of the key is shown in Figure 3.5. The movement shown agrees with the horizontal strain profiles. The upward movement at the loaded face of the key corresponds to the high tensile strains in the adjacent reinforcement, due to the tension in the tie. At the opposite face of the key, the very small downward movements correspond to the small compressive strain in the adjacent reinforcement at this location. This is the location of the toe of the strut, at which very little vertical movement was expected.

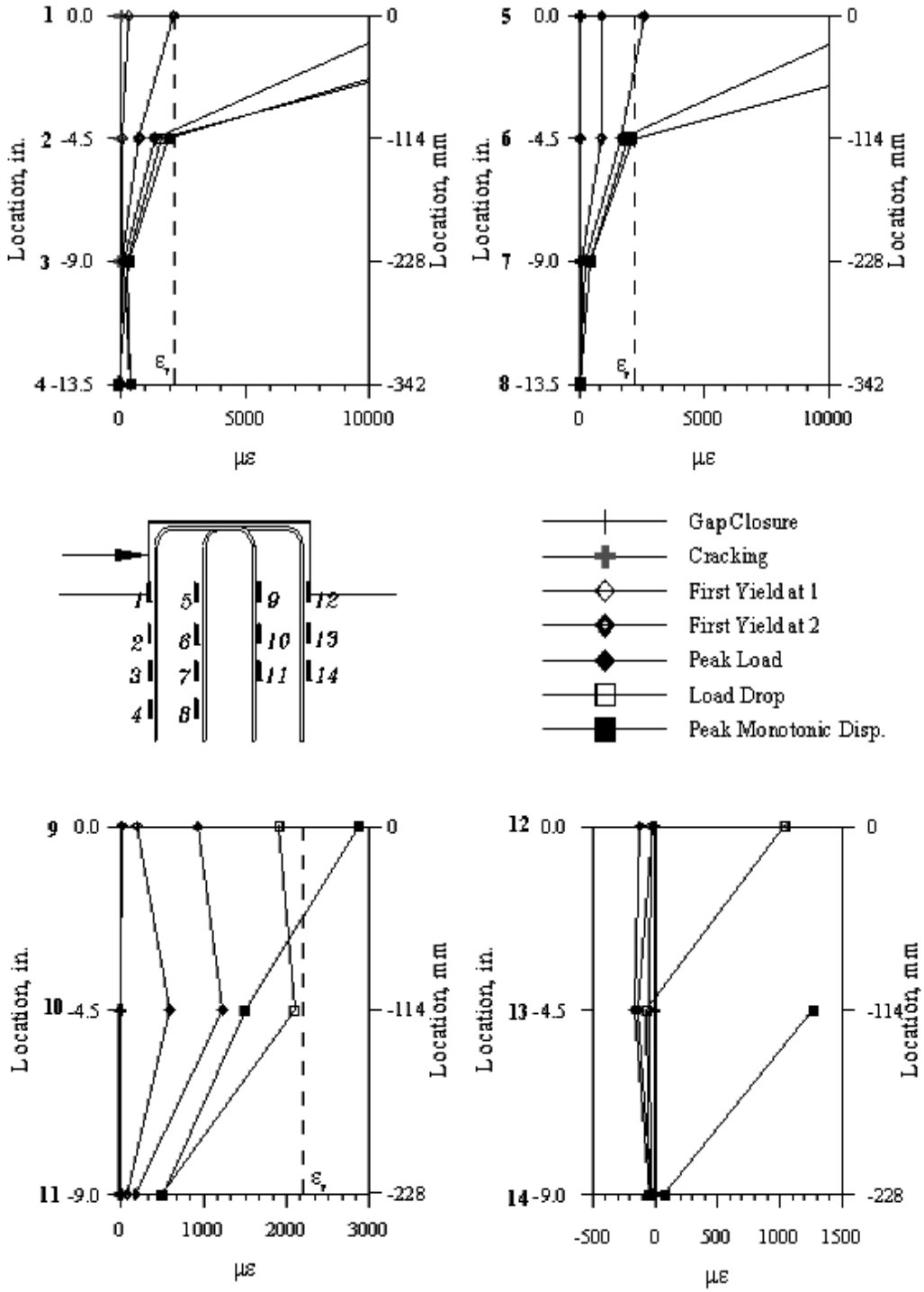

Figure 3.4 Vertical Strain Profiles – Test Unit 1A

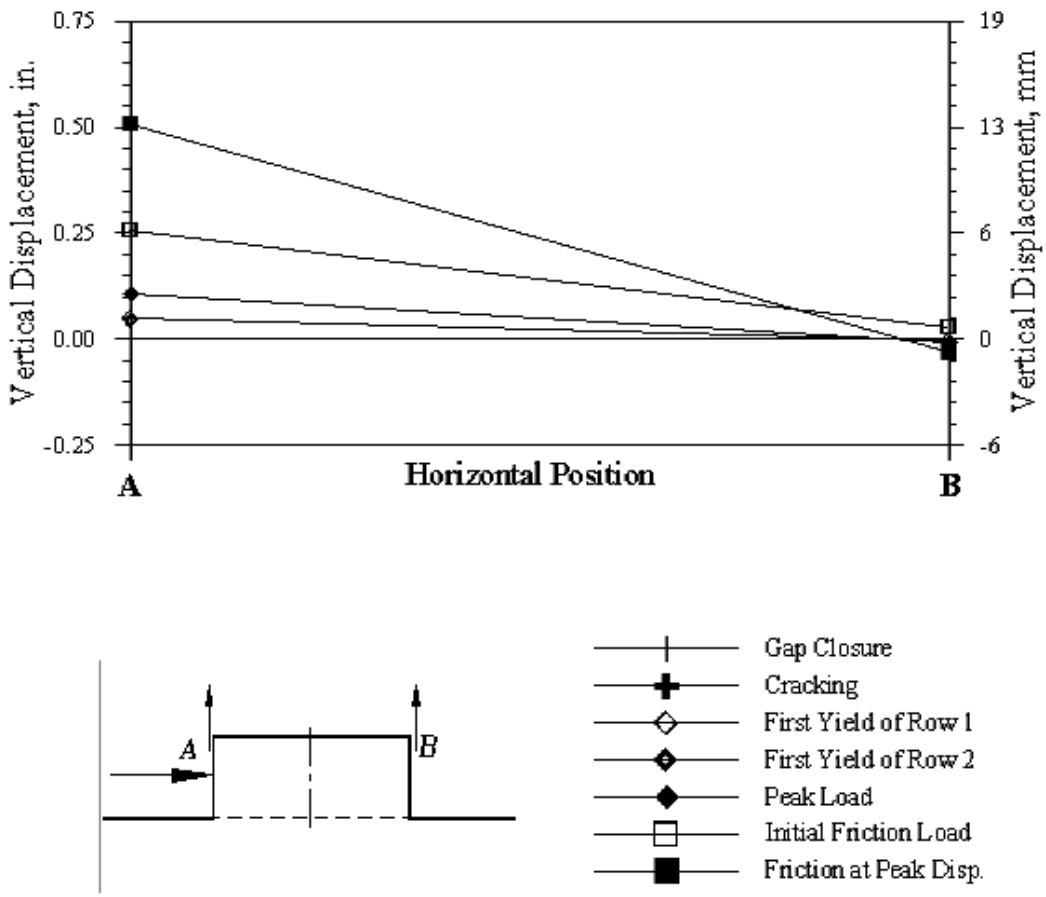

Figure 3.5 Vertical Key Movement – Test Unit 1A

3.3 Test Series I – Test Unit 1B

The experimental results for Test Unit 1B will be presented in this section. This test unit was subjected to the quasi-static loading protocol shown in Figure 2.13.

3.3.1 General Test Observations

Test Unit 1B, which was subjected to quasi-static reversed cyclic loading, behaved essentially as Unit 1A, which was subjected to monotonic loading. However, There were some important observations made during the test. The initial stiffness of the key after gap closure was the same in both directions. As the load was cycled, a crack pattern similar to that of Test Unit 1A developed in both loading directions. The key behaved in this manner until the load was cycled near peak capacity in both directions. Beyond the peak load, the key responded to subsequent loading with the same initial stiffness, but upon reaching a load of 150 kips (667 kN), it began to slide along the base, maintaining this load level with essentially no stiffness increase.

With further reversed cyclic loading, the capacity of the key degraded rapidly. Fracturing of the reinforcement began at the cycles of 2 in. (51 mm) displacement amplitude with the spalling of the sides of the key occurring during the 3 in. (76 mm) displacement cycles. The observations agreed well with those made during the monotonic test, with similar degradation of the strength and stiffness of the shear key.

3.3.2 Load versus Displacement Curve

The load versus displacement curve is shown in Figure 3.6. The figure clearly shows that the initial stiffness of the shear key is maintained during cyclic loading until the load reaches levels comparable to the peak load of the monotonic test. After this point the key responds with the same stiffness after the closing of the gap, but switches to a sliding shear friction mechanism prior to attaining the peak load. The strength and stiffness degradation is virtually identical in both directions, with a linear decrease in capacity from the peak load, which was reached at a displacement near 1 in. (25 mm).

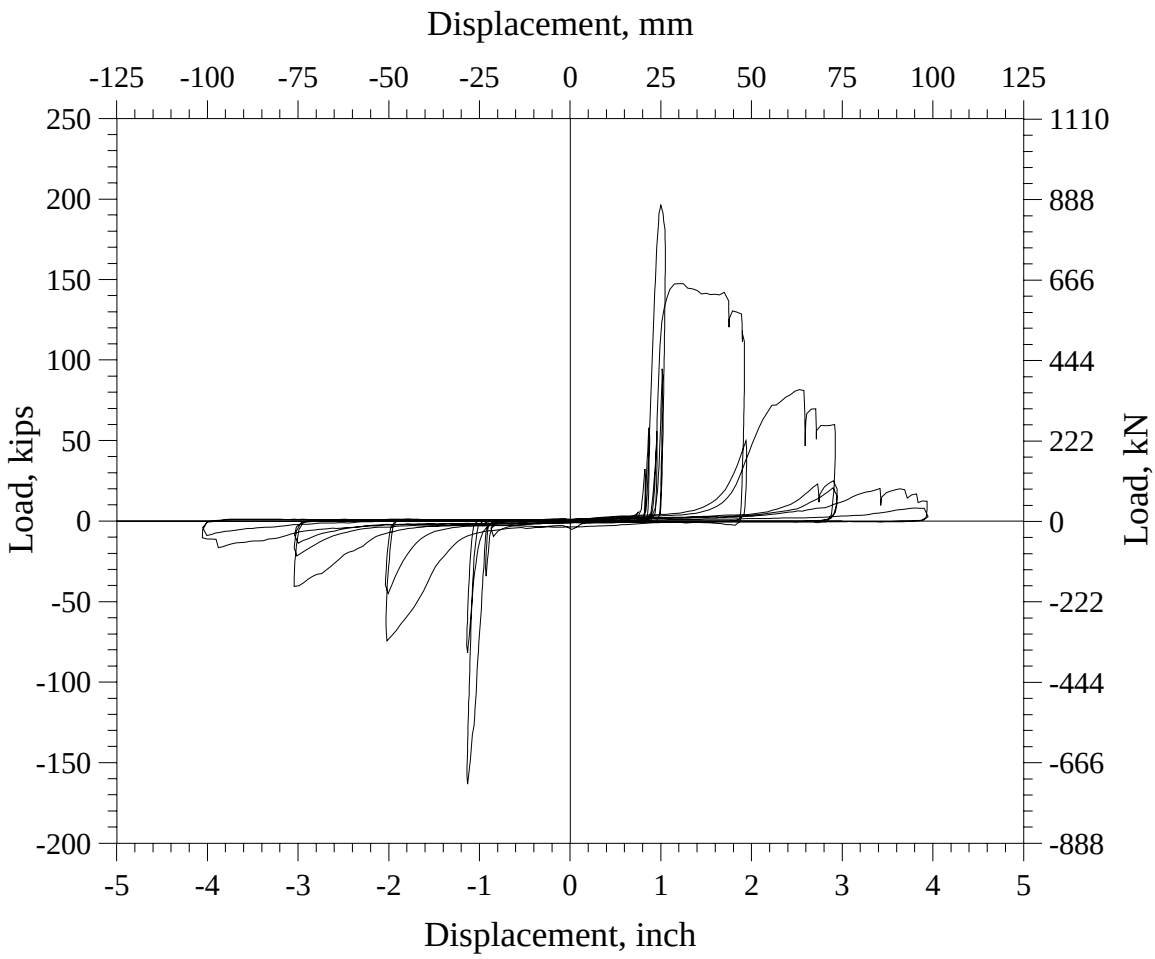

Figure 3.6 Load vs. Displacement – Test Unit 1B

3.3.3 Horizontal Strain Profiles

Figure 3.7 shows the horizontal strain profiles through the key section. For the first three cycles, in which the maximum load was less than 100 kips (445kN), the strains in the reinforcement remained small. The strains did not become significant until the pull portion of the third cycle, when the load reached a maximum value of about 160 kips (712kN). At this time the reinforcement at locations B, C, and D had yielded, with location D experiencing very high strains. Because of this, the strains at location D remained above yield during the subsequent push cycles, without contributing to the formation of the tie.

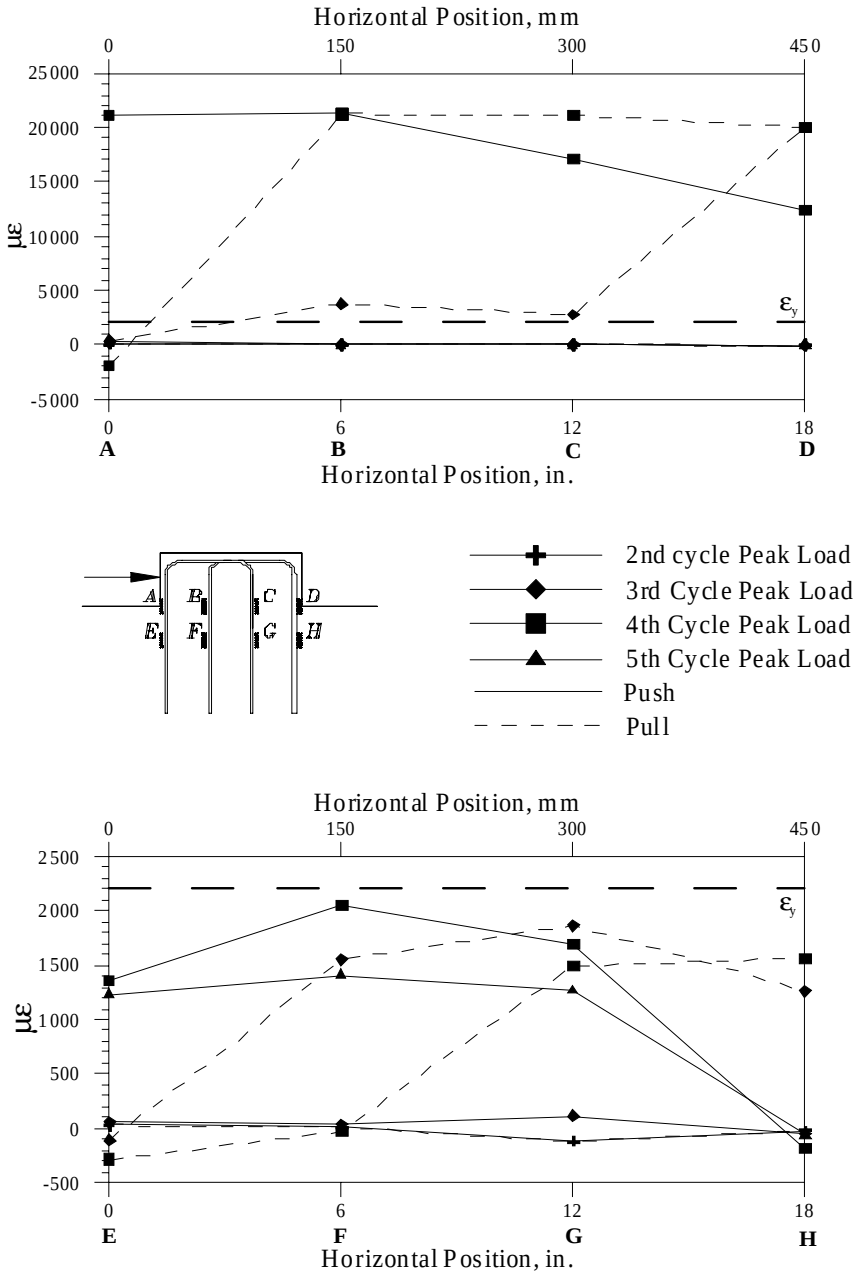

Figure 3.7 Horizontal Strain Profiles – Test Unit 1B

The same distribution of strains is also evident at 4½ in. (114mm) below the interface, as shown in Figure 3.7, which clearly shows that the three locations of high strain are reversed as the load is cycled. This shows that the location of the tie switches from one end of the key to the other as the load is cycled. The three rows shown to be effective in forming the tie agree with the results of Test Unit 1A.

3.3.4 Vertical Shear Key Movement

The vertical movement of the key is shown in Figure 3.8, which shows the upward movement experienced at the face of the key during different displacement cycles. This shows how the strut-and-tie changes direction with the applied load. This behavior is similar to that of Test Unit 1A.

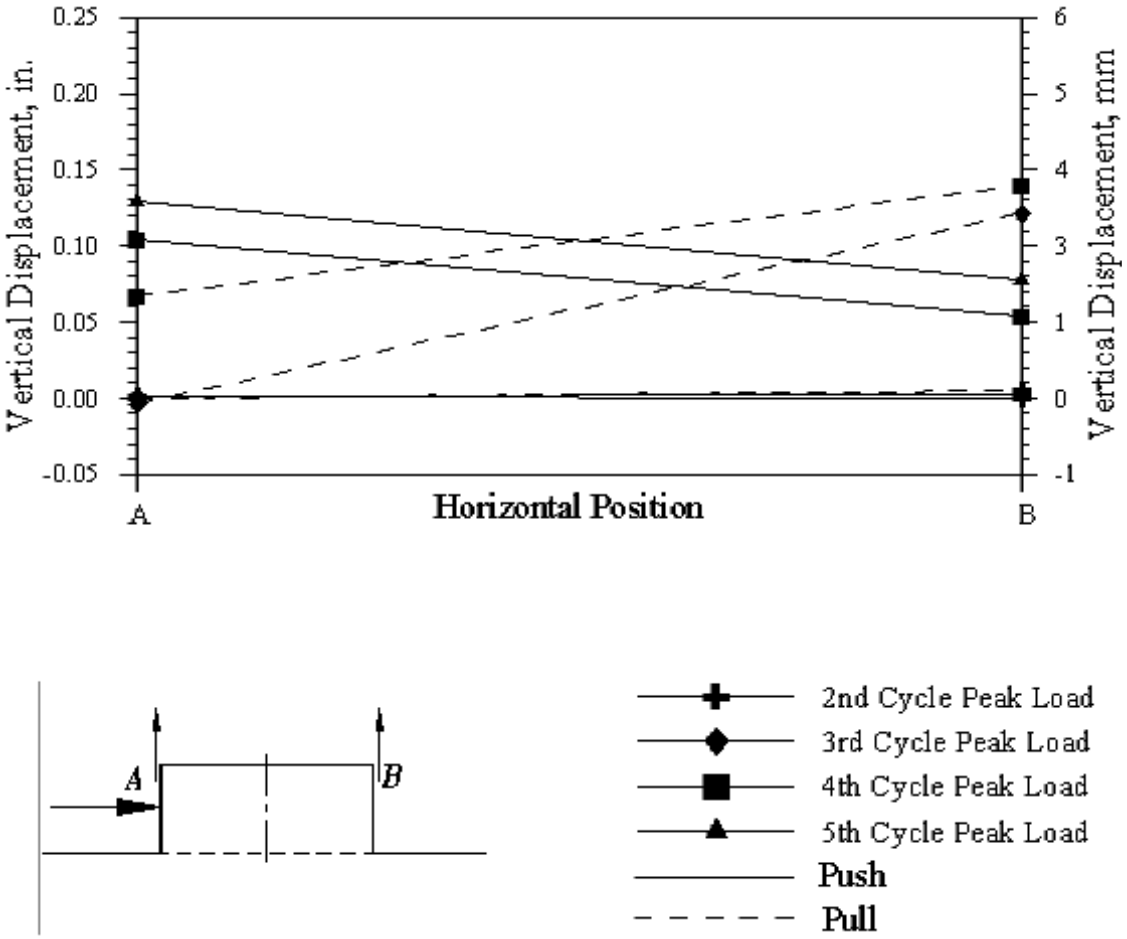

Figure 3.8 Vertical Key Movement – Test Unit 1B

3.4 Test Series I – Test Unit 1C

The experimental results for Test Unit 1C will be presented in this section. This test unit was subjected to the dynamic loading protocol shown in Figure 2.14.

3.4.1 General Test Observations

Cracking of the shear key occurred during the 1 in. (25 mm) displacement cycles. The peak load was reached as the displacement was increased to 2 in. (51 mm). After surpassing this deflection, it was obvious that the stiffness of the key reduced dramatically with all movement occurring at the interface. The key essentially experienced sliding in both loading directions at the shear key-abutment interface. The overall behavior was very similar to that of Test Units 1A and 1B.

3.4.2 Load versus Displacement Curve

Figure 3.9 shows that the load versus deflection curve of Test Unit 1C under dynamic reversed cyclic loading is similar to that of the quasi-static test. The differences in the magnitudes of the maximum load during the cycles at 1 in. (25 mm) are due to a small offset in the starting position of the test. Figure 3.9 shows that the initial stiffness of the key after gap closure is maintained as the load is cycled until the capacity of the key is reached. After this level, the shear key experienced rapid degradation under further cyclic loading. This is very similar to the behavior observed in the previous two tests (Units 1A and 1B).

3.4.3 Horizontal Strain Profiles

The horizontal strain profiles, shown in Figure 3.10, agree well with those obtained from the previous two tests. They show that strains in the reinforcement at the interface remained below yield while the load was cycled at 1 in. (25 mm), with the maximum force at around 120 kips (534 kN). At peak load, three of the four rows of reinforcement have yielded, while strains in the fourth row remained small. This was the same behavior observed in Test Units 1A and 1B.

After reaching the peak load, the inelastic strains at location D increased and the strains became more uniform through the depth of the section. The strains at a depth of 4½ in. (114 mm) agree well with those at the interface, and are indicative of strain penetration to this depth.

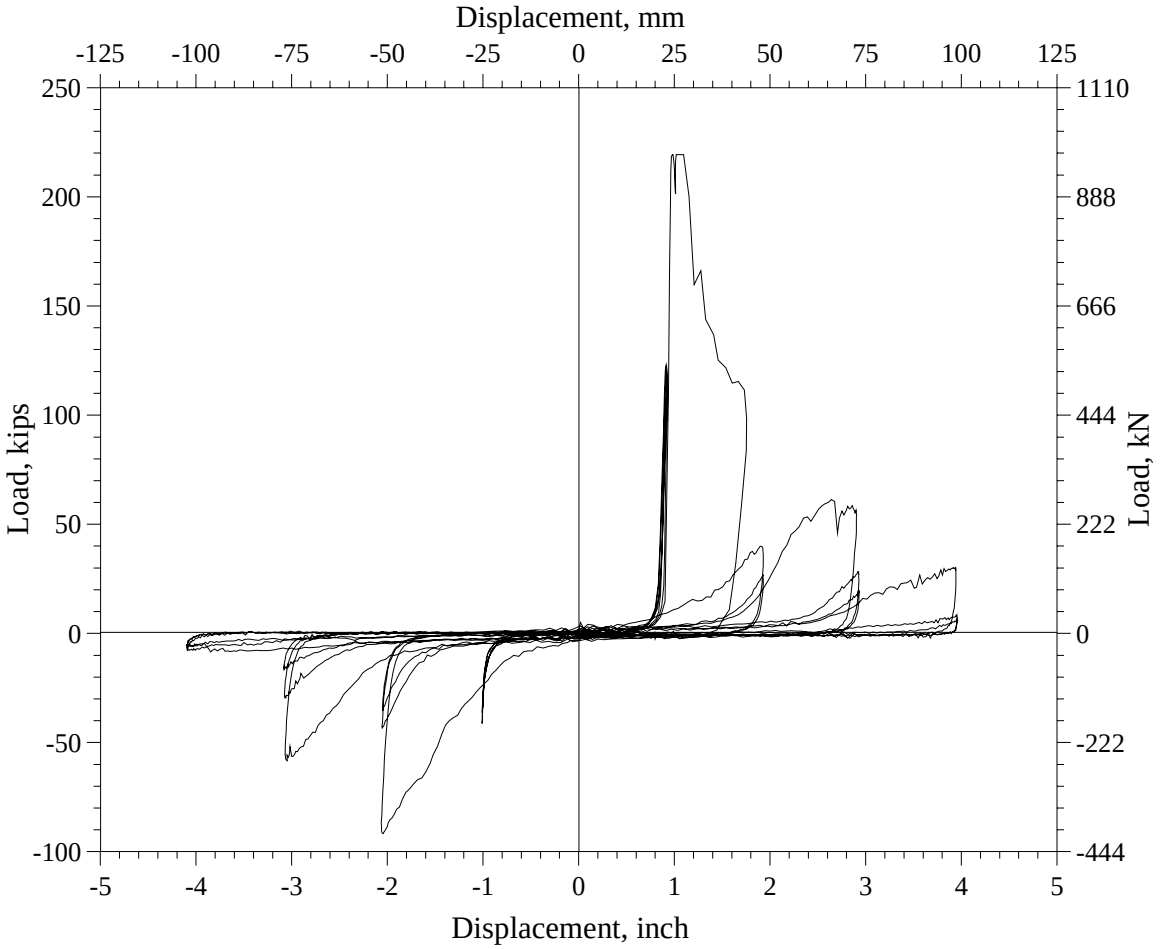

Figure 3.9 Load vs. Displacement – Test Unit 1C

3.4.4 Vertical Shear Key Movement

The vertical movement of Specimen 1C is not shown, due to the poor performance of the potentiometers due to the dynamic nature of the loading.

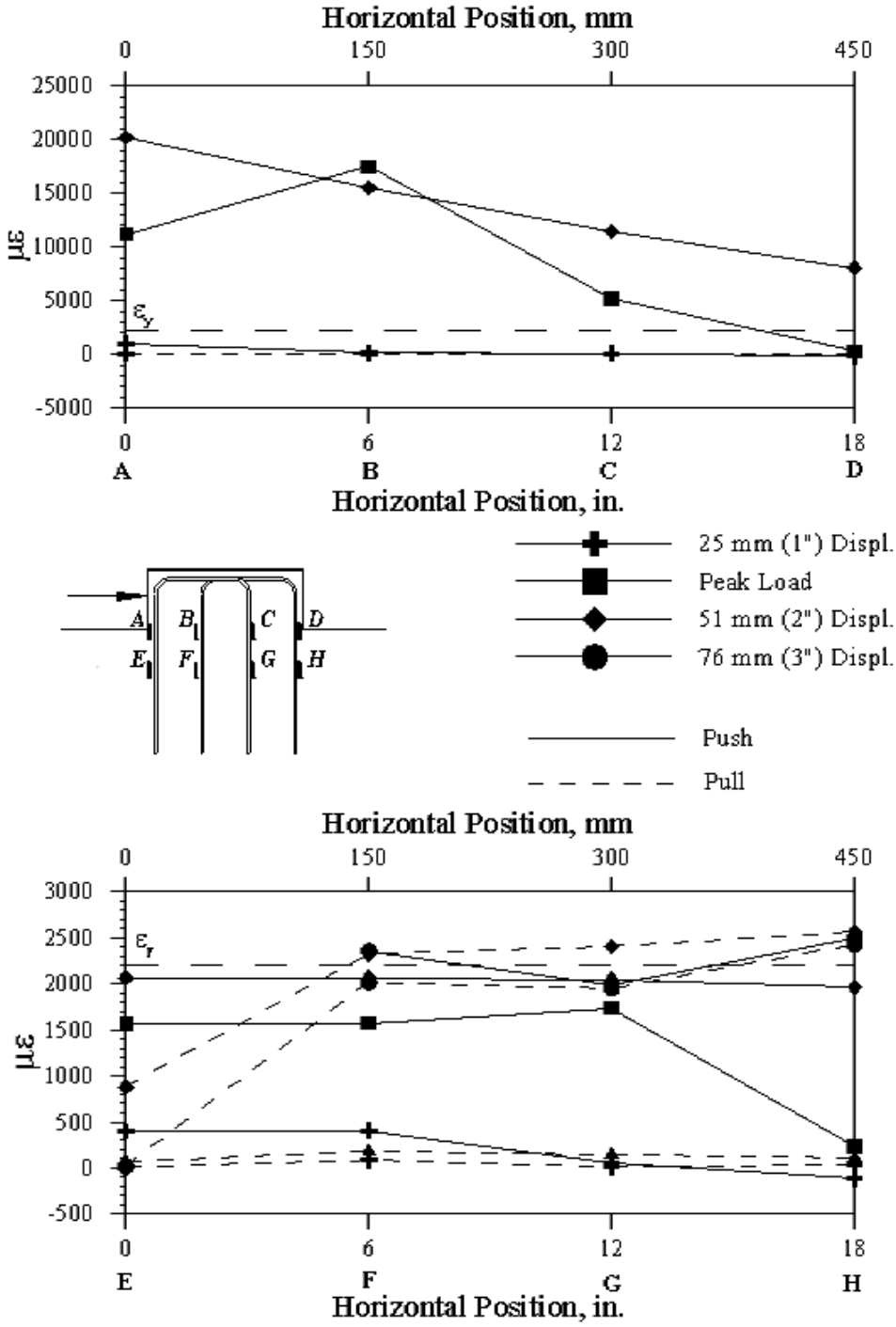

Figure 3.10 Horizontal Strain Profiles – Test Unit 1C

3.5 Test Series II – Test Unit 2A

The experimental results for Test Unit 2A will be presented in this section. This test unit was subjected to the quasi-static loading protocol shown in Figure 2.15.

3.5.1 General Test Observations

Level I: First cracking was observed during the first cycle to the displacement of about 1 in. (25 mm). After cracking during the push portion of the cycle, the load was reversed in the opposite direction to a displacement of about –1 in. (-25 mm) corresponding roughly to cracking in the opposite direction. The first cracks observed in the shear key were horizontal cracks at the interface, extending from the face of the key at which the load was applied, as shown in Figure 3.11(b).

Level II: The initial horizontal cracks were followed by horizontal cracks extending from the location of the applied load, where the loading arm was in contact with the key, as shown in Figure 3.11(c). The first cracks were noted at a load of about 60 kips (267 kN). The same types of cracking were noted with the load reversed, at a similar load magnitude.

Level III: As the load was increased beyond cracking, the horizontal cracks at the location of the applied load increased in size and number. They propagated across the side of the key, culminating at the interface opposite to the applied load, forming an arc. At the peak load of 200 kips (890 kN), there was severe cracking of the concrete at the applied load location, as shown in Figure 3.11(d). This was accompanied by the propagation of the crack at the interface.

Level IV: After reaching the maximum load carrying capacity, the load immediately dropped to about 100 kips (445 kN). At this level damage of the key is best exemplified by Figure 3.11(e).

Level V: As the load was cycled, the degradation of the concrete of the key became more severe. There was substantial damage on the sides of the key, which exposed the outer lines of reinforcing, rendering them ineffective. Concrete spalling, shown in Figure 3.11(f), in addition to fracture of reinforcement, beginning at the 2 in. (51 mm) displacement cycles, resulted in a substantial degradation of capacity.

3.5.2 Load versus Displacement Curve

The load versus displacement curve is shown in Figure 3.12. The figure shows that the stiffness and strength of the shear key were maintained during the first three cycles at 1 in. (25 mm)

displacement. The shape of the curve shows a sudden decrease in capacity after reaching the peak load, decreasing to 100 kips (445 kN) at a displacement of 2 in. (51 mm). It also shows the rapid decrease in capacity corresponding to the observed degradation of the concrete and fracturing of the reinforcement.

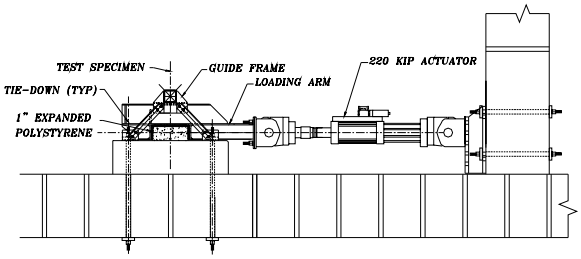

(a) Test Unit Layout

(b) LEVEL I

(c) LEVEL II

(d) LEVEL III

(e) LEVEL IV

(f) LEVEL V

Figure 3.11 Test Observations – Test Unit 2A

3.5.3 Horizontal Strain Profiles

The horizontal strain profiles are shown in Figure 3.13. The strains at first cracking show an inclined distribution, similar to that observed in the first test series, with the reinforcement nearest the applied load having the highest strains, at location A. The distribution is essentially linear, with the maximum strains well below yielding.

At the peak load, the strains in the row of reinforcement opposite to the applied load, at location D, remained insignificant, while those on the other three rows of reinforcement, locations A, B, and C, increased well beyond yielding. The highest strains at this load level are at location B, rather than location A, depicting high strains at cracking.

After reaching the peak load, the strains remained essentially constant until the load was reversed. This resulted in small compressive strains being developed at location A. The strains at locations B and C decreased significantly, with those at location C decreasing below yielding. The strains at location D, however, were very small during the "push" cycle and increased beyond yielding. After this level, the gages located at the interface were damaged, and provided no further useful information.

The strains below the interface, at locations E, F, G, and H, resembled those at the interface, but at a lower level, remaining for the most part below yielding. However after cycling beyond 2 in. (51 mm), the rapid degradation of the concrete and fracture of reinforcement resulted in a lack of useful information beyond this point.

3.5.4 Vertical Shear Key Movement

The vertical movement of the shear key is shown in Figure 3.14. The movement shown corresponds well with the strains in the reinforcement, with the greatest vertical movement at the face of the key nearest the applied load. This corresponds to location A for the push portion of the cycle and location B for the pull portion of the cycle. These movements remained small during the cycles at 1 in. (25 mm), but increased dramatically at the peak load. After reaching the peak load, the vertical displacement at location A, nearest the applied load decreased, while that at location B increased, resulting in a decrease in the rotation of the shear key. The displacements at -2 in. (–51 mm) show a small increase in the displacement at A, with a substantial increase in those at location B, nearest the applied load.

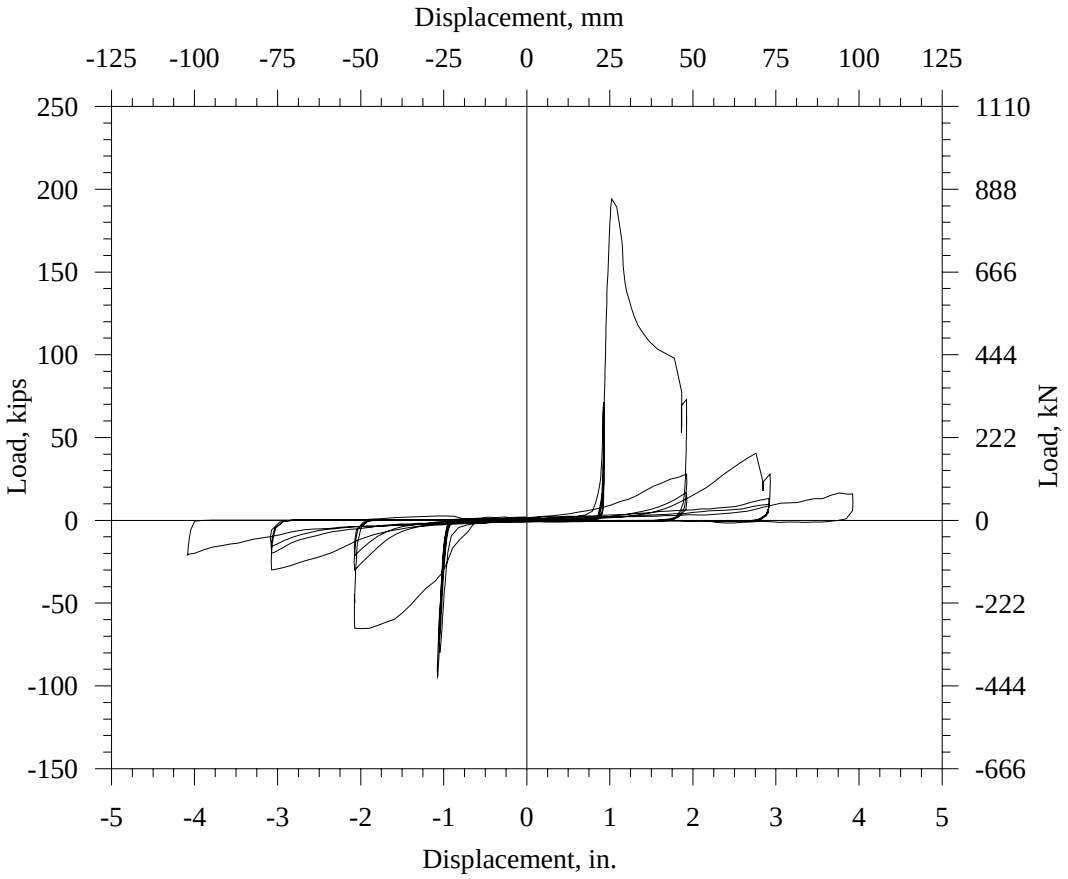

Figure 3.12 Load vs. Displacement – Test Unit 2A

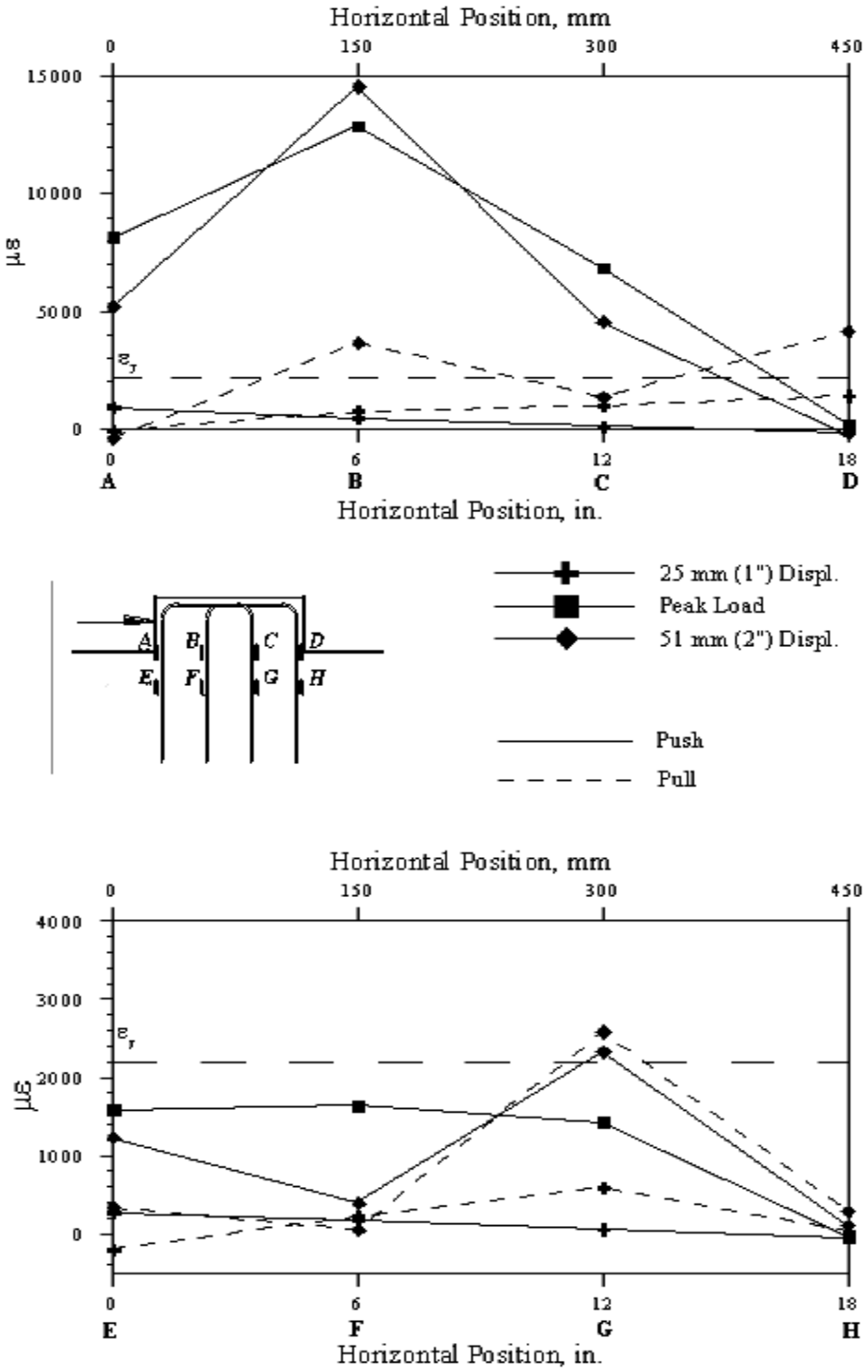

Figure 3.13 Horizontal Strain Profiles – Test Unit 2A

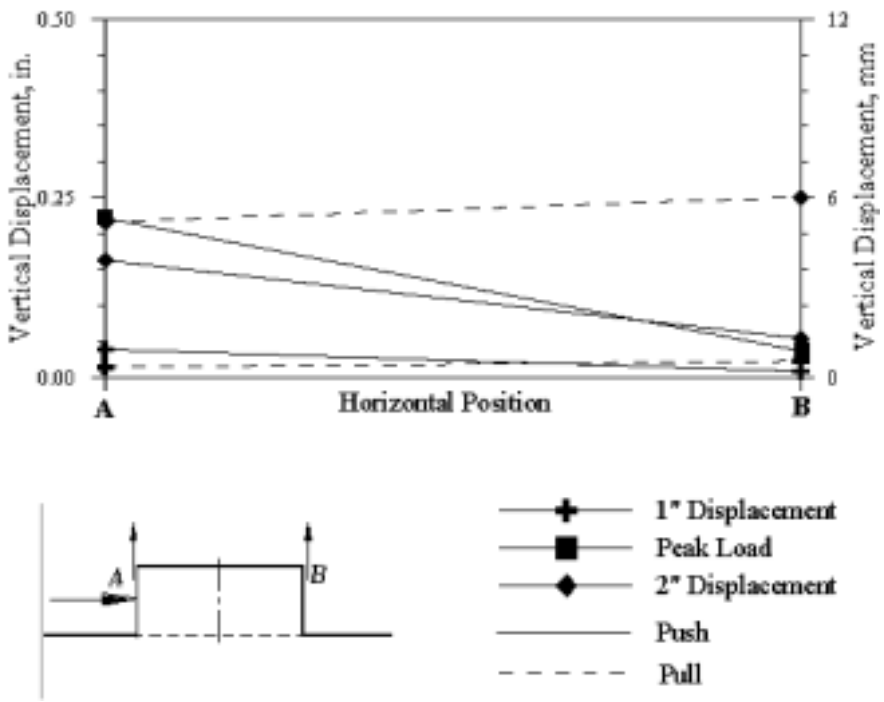

Figure 3.14 Vertical Key Movement – Test Unit 2A

3.6 Test Series II – Test Unit 2B

The experimental results for Test Unit 2B will be presented in this section. As before, this test unit was subjected to the quasi-static loading protocol shown in Figure 2.15.

3.6.1 General Test Observations

Level I: First cracking was observed at a displacement of about 1 in. (25 mm). After reaching cracking during the "push" portion of the cycle, the load was reversed in the opposite direction to a total displacement of about -1 in. (-25 mm) corresponding roughly to cracking in the opposite direction. The first cracks observed in the key were horizontal at the interface, extending from the face of the key at which the load was applied, as shown in Figure 3.15(b). The same type of cracking developed with load reversal.

Level III: As the load was increased beyond cracking, the horizontal cracks at the interface grew wider and propagated along the length of the interface. This was accompanied by some relatively minor inclined cracking adjacent to the applied load, shown in Figure 3.15(b). The test unit had a peak load capacity of 215 kips (956 kN). Figure 3.15(c) shows the shear key at the peak load.

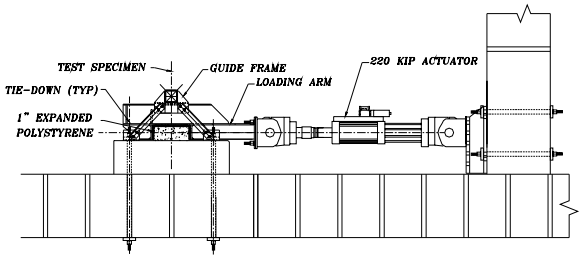

(a) Test Unit Layout

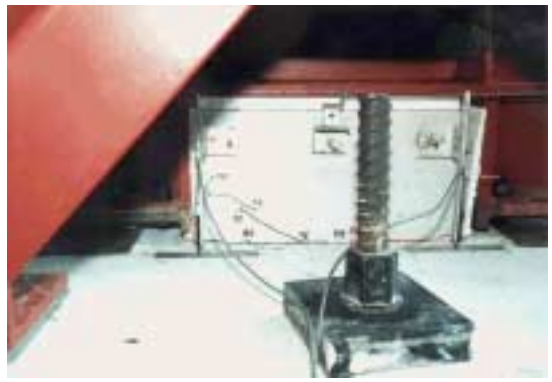

(b) LEVEL I

(c) LEVEL III

(d) LEVEL V

Figure 3.15 Test Observations – Test Unit 2B

Level V: After reaching the peak, the load dropped to about 180 kips (801 kN). The fracture of one of the reinforcement bars was noted prior to reaching the first cycle at 2 in. (51 mm). As the load was cycled, the degradation of the concrete of the key became increasingly severe, with spalling of the cover occurring in the locations of the inclined cracks. The outer lines of reinforcement were exposed during the cycles at 3 in. (76 mm), as shown in Figure 3.15(d). This decreased the effectiveness of the reinforcing bars in resisting the applied load. This condition in combination with fracture of the reinforcement resulted in a substantial degradation in the shear key capacity.

3.6.2 Load versus Displacement Curve

The load versus displacement curve is shown in Figure 3.16. It shows that the stiffness and strength of the shear key were maintained during the first three cycles at 1 in. (25 mm) displacement. The rounded peak resulted from the greater aspect ratio, which tends to increase the more ductile flexural influence on the shear key response. After reaching the peak load there was a gradual decrease in capacity to 180 kips (801 kN) at 2 in. (51 mm). Figure 3.16 also shows

the decrease in capacity associated with the observed degradation of the concrete and the fracture of reinforcement.

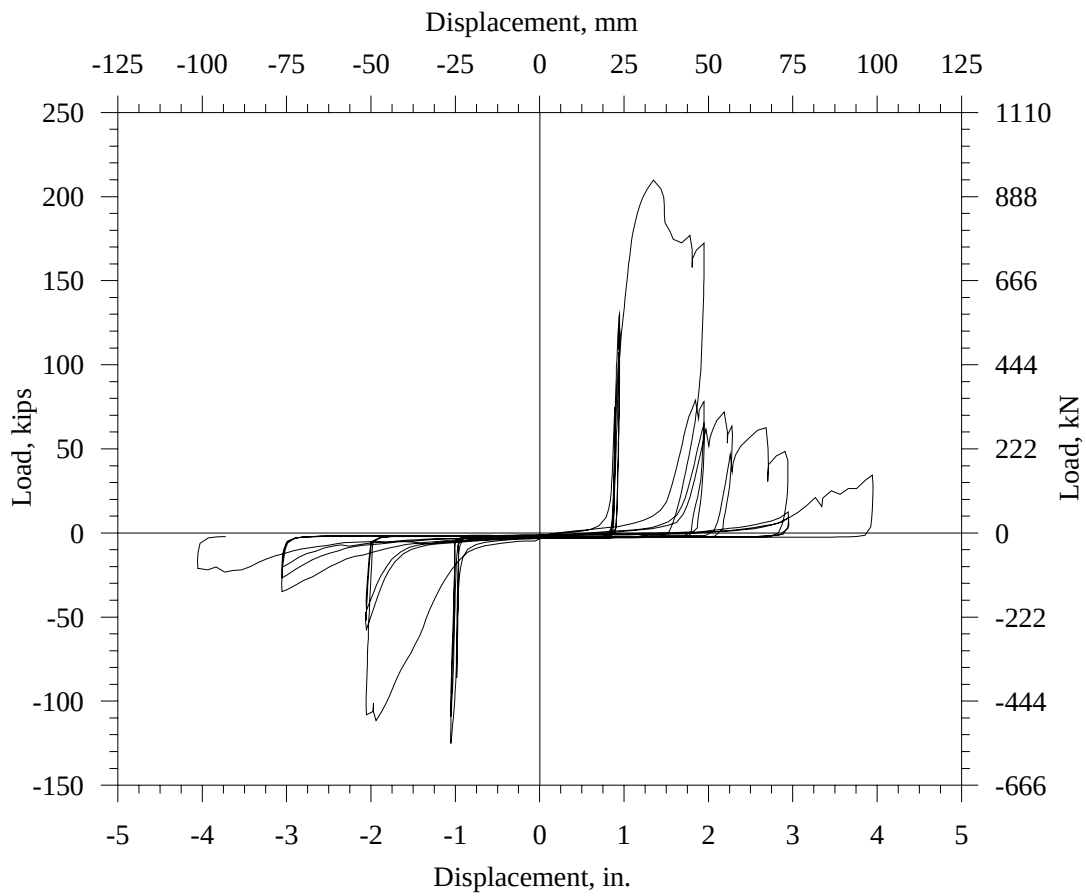

Figure 3.16 Load vs. Displacement – Test Unit 2B

3.6.3 Horizontal Strain Profiles

The horizontal strain profiles are shown in Figure 3.17. The strains at first cracking show an inclined distribution, with the reinforcement nearest the applied load showing the highest strains, at location A during the push portion of the cycle and location D during the pull portion. The distribution is essentially linear, with the maximum strains well below yield.

At the peak load, the strains at locations A, B, and C increased significantly, while those opposite the applied load, at location D, increased with a smaller amount, but still exceeding yield. After reaching the peak load, the strains at locations A, B, and C remained essentially constant, while those at D increased substantially. All gages at the interface were damaged at this level resulting in no further useful information.

The strains below the interface, at locations E, F, G, and H, resembled those at the interface, but at lower strain levels, exceeding yield at 2 in. (51 mm) displacement. The strains recorded at the maximum displacement of the pull portion of the first cycle at 2 in. (51 mm) showed a profile, which was a mirror image of that obtained during the push portion of the cycle. After cycling beyond 2 in. (51 mm) displacement the rapid degradation of the concrete and fracture of reinforcement resulted in a lack of useful information.

3.6.4 Vertical Shear Key Movement

The vertical movement of the shear key is shown in Figure 3.18. The movement shown corresponds well with the strains in the reinforcement, with the greatest vertical movement at the face of the key nearest to the applied load. This corresponds to location A for the push portion of the cycle and location B for the pull portion of the cycle. These movements remained small during the 1 in. (25 mm) displacement cycles. The shear key vertical movement increased up to the peak load, but remained relatively small. The negative displacement was greater at this point than the positive displacement at the face of the shear key. The potentiometer nearest to the applied load was disturbed at this point by localized spalling of the concrete, and did not provide any further useful information.

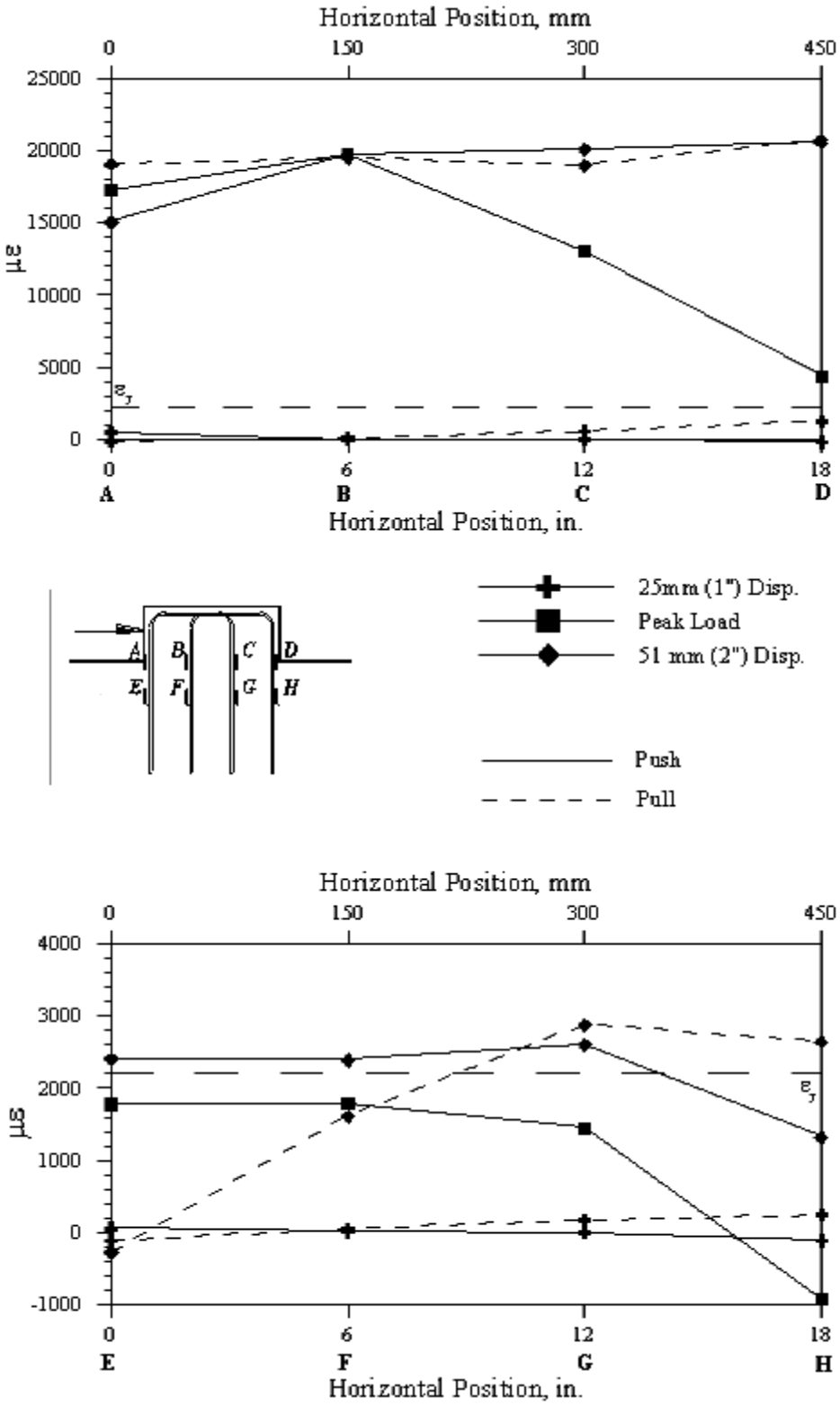

Figure 3.17 Horizontal Strain Profiles – Test Unit 2B

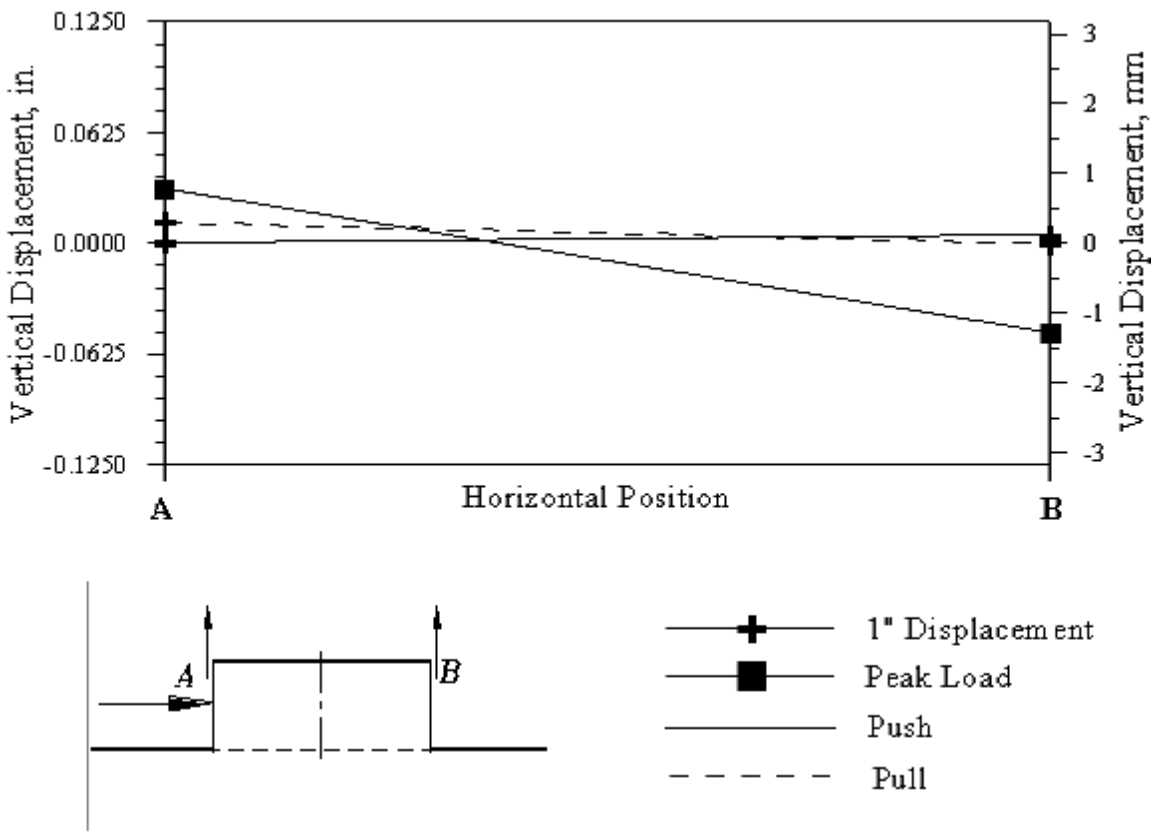

Figure 3.18 Vertical Key Movement – Test Unit 2B

3.7 Test Series II – Test Unit 2C

The experimental results for Test Unit 2C will be presented in this section. This test unit was subjected to the quasi-static loading protocol shown in Figure 2.15.

3.7.1 General Test Observations

Level I: As in the previous test units, onset of cracking was observed during the first cycles to the displacement of about 1 in. (25 mm), as shown in Figure 3.19(b). The first cracks were noted at a load of about 75 kips (334 kN). Similar cracks were observed with the load reversal at a load level of about 85 kips (378 kN).

Level III: The key reached a peak capacity of about 185 kips (823 kN). As the load increased beyond cracking, the width of the horizontal cracks at the interface increased dramatically, with only minor development of cracking in the key, as shown in Figure 3.19(c). The key maintained the peak load over a displacement of about 2 in. (51 mm).

Level V: After reaching the maximum load carrying capacity, the load dropped gradually to about 150 kips (667 kN). As the load was cycled, there was some degradation of the concrete, mostly at the shear key-abutment interface, with fracture of reinforcement beginning during the 2 in. (51 mm) displacement cycles. At the completion of the test the sides of the key still showed no inclined cracking, with severe degradation at the interface region as shown in Figure 3.19(d).

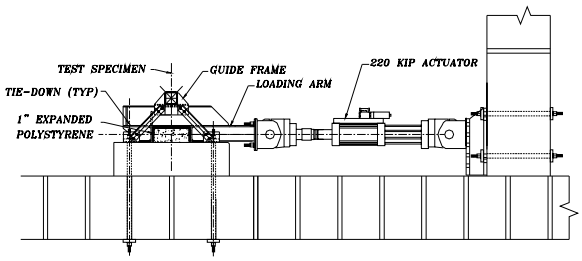

(a) Test Unit Layout

(b) LEVEL I

(c) LEVEL III

(d) LEVEL V

Figure 3.19 Test Observations – Test Unit 2C

3.7.2 Load versus Displacement Curve

The load versus displacement curve is shown in Figure 3.20. It shows that the stiffness and strength of the shear key were maintained during the three cycles at 1 in. (25 mm) displacement. The rounded peak characterizes the load-displacement curve; the curve shows the increased ductility. The more ductile response characterized by this rounded peak is caused by the yielding of the shear key reinforcement at lower load levels, resulting from the lower reinforcing ratio. After reaching the peak load, there was a gradual drop in load to about 150 kips (667 kN) at 2 in. (51 mm) displacement.

Cycling loading caused a rapid reduction in capacity as a result of fracture of the reinforcing bars.

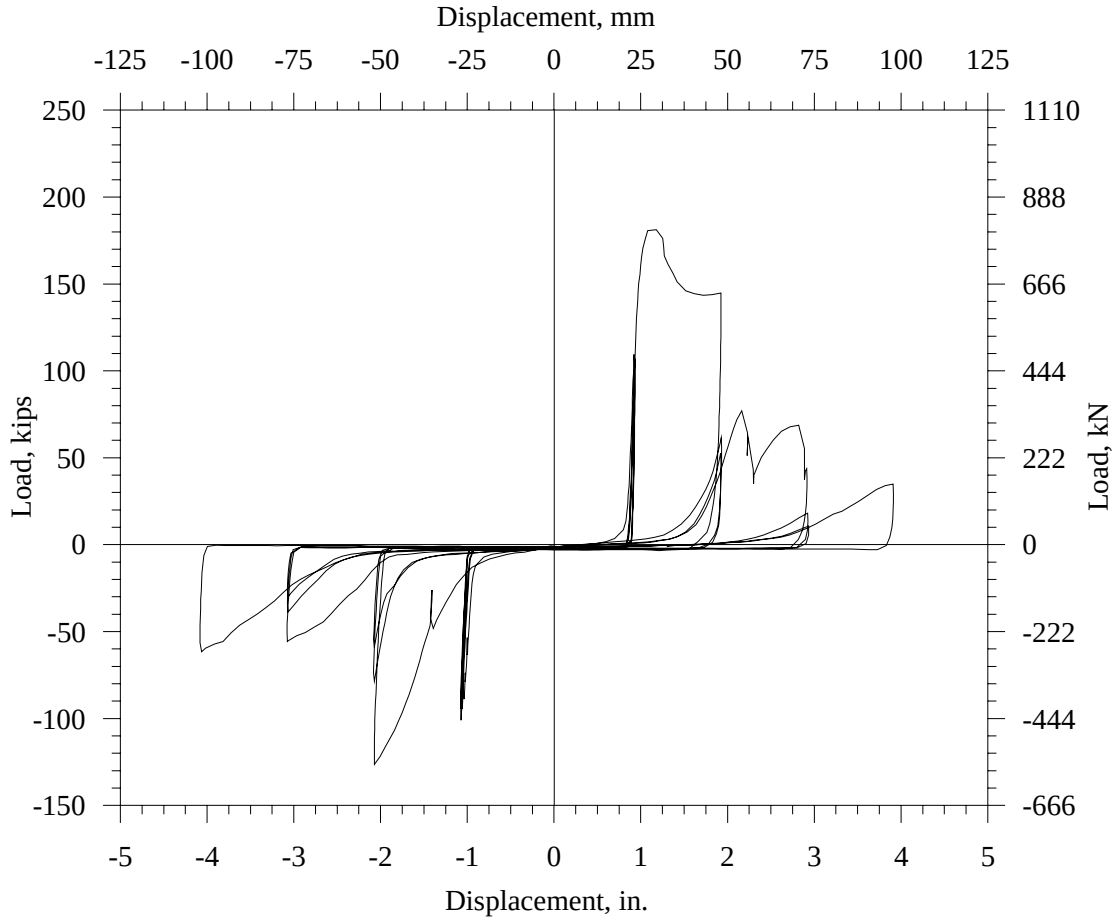

Figure 3.20 Load vs. Displacement – Test Unit 2C

3.7.3 Horizontal Strain Profiles

The horizontal strain profiles are shown in Figure 3.21. The strains at first cracking show an inclined distribution of strains, with the reinforcement nearest the applied load showing the highest strains at location A. The distribution of strains is essentially linear. The bars at location D yielded during the pull portion of the cycles at 1 in. (25 mm) displacement.

At the peak load, the strains at the interface were well beyond yielding for all rows of reinforcement. The strains at location A were the highest, with those at locations B, C, and D essentially the same. It was noted that the strains at location D exceeded yielding during the previous cycles. After reaching the peak load, the strains remained essentially the same at

location A, while increasing significantly at locations B, C, and D, resulting in an essentially uniform strain distribution through the shear key-base interface.

At a displacement of -2 in. (–51 mm), the strains at location A decreased to near yielding, while the strains at B, C, and D remained essentially constant. After this level, the gages located at the interface were damaged, and provided no further useful information. The strains below the interface, at locations E, F, G, and H, resembled those at the interface, but at lower strain levels, remaining for the most part below yielding. However, after cycling beyond 2 in. (51 mm), the fracture of the reinforcement resulted in lack of any further useful information.

3.7.4 Vertical Shear Key Movement

The vertical movement of the key is shown in Figure 3.22. The movements shown corresponded well with the strains in the reinforcement, with the greatest vertical movement at the face of the key nearest the applied load. This corresponds to location A for the push portion of the cycle and location B for the pull portion of the cycle. These movements remained small during the cycles at 1 in. (25 mm) displacement, but increased at the peak load. After reaching the peak load, the vertical displacements increased by the same amount at both locations. Vertical movement profile of the shear key at the peak displacement of the pull portion of the cycle was a mirror image of that of the push portion of the cycle, with similar magnitudes of vertical movement.

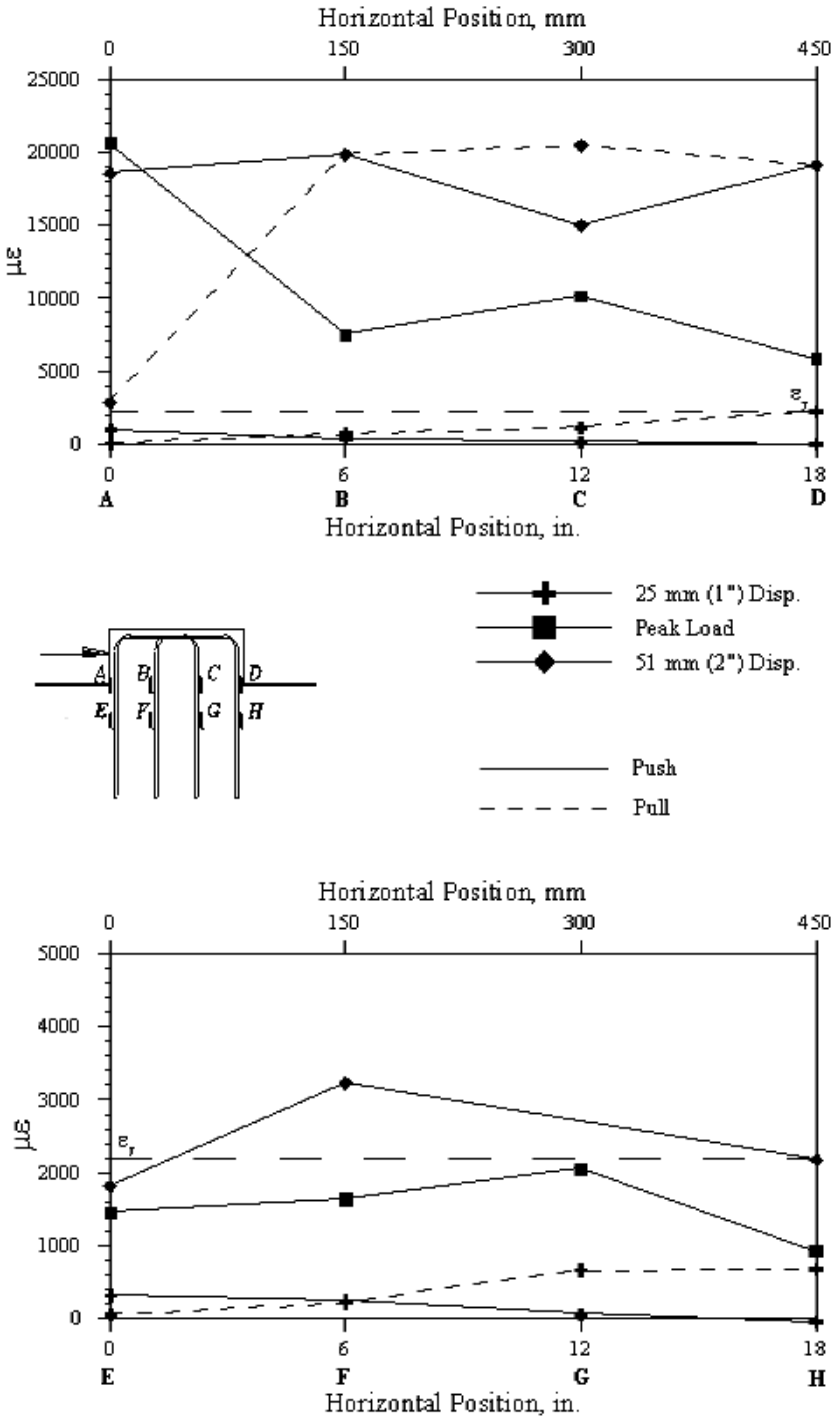

Figure 3.21 Horizontal Strain Profiles – Test Unit 2C

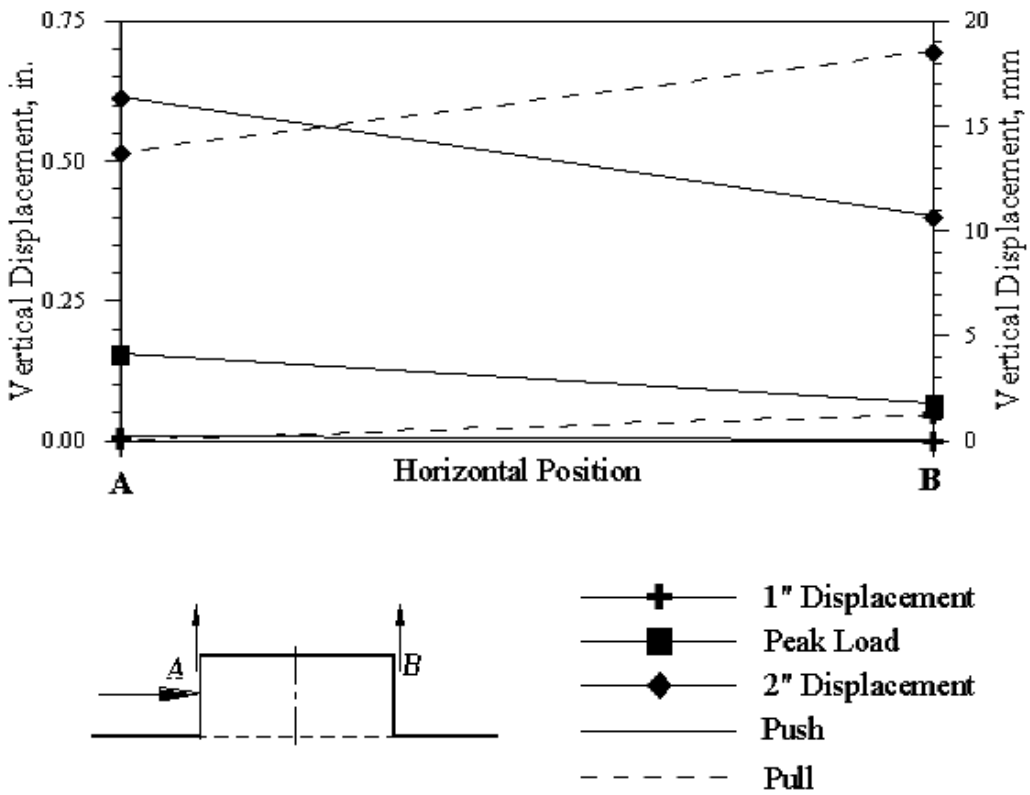

Figure 3.22 Vertical Key Movement – Test Unit 2C

3.8 Test Series II – Test Unit 2D

The experimental results for Test Unit 2D will be presented in this section. This test unit was subjected to the quasi-static loading protocol shown in Figure 2.15.

3.8.1 General Test Observations

Level I: First cracking was noted at a load of 200 kips (890 kN). These were inclined cracks, as shown in Figure 3.23(b). There was limited cracking at the interface. The load at -1 in. (-25 mm) displacement was much less than that at 1 in. (25 mm) displacement due to a small initial offset in the starting position of the load. This was associated with only minor cracking. The key reached essentially the same load during each of the three 1 in. (25 mm) displacement cycles.

Level II: The cracking at the interface was mainly caused by the inclined cracks in the sides of the shear key, which propagated down at the sides of the shear key and along the interface. Prior to the peak load significant increase in the number of horizontal and inclined cracks were observed on the sides of the shear keys, as depicted in Figure 3.23(c).

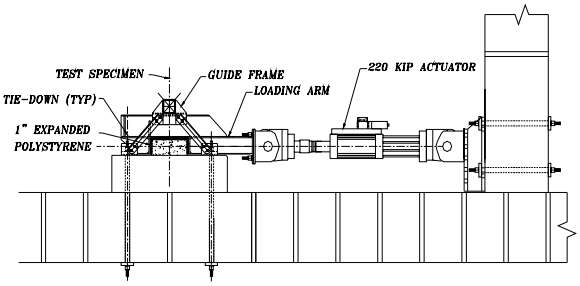

(a) Test Unit Layout

(b) LEVEL I

(c) LEVEL II

(d) LEVEL III

(e) LEVEL IV

(f) LEVEL V

Figure 3.23 Test Observations – Test Unit 2D

Level III: The key reached a peak load of 232 kips (1032 kN) at slightly over than 1 in. (25 mm) displacement. Increasing the load caused a rapid development of both horizontal and inclined cracks on the sides of the key and some concrete spalling, as shown in Figure 3.23(d).

Level IV: The test was basically over once the inclined concrete strut failed in compression. Significant spalling of sides of the shear key occurred at this load level, as shown in Figure 3.23(e). This was apparent by substantial cracking at the sides of the key, culminating with the sides expanding outward beyond the peak load, as shown in Figure 3.23(e). After reaching the

peak load carrying capacity, the load immediately dropped to a value of about 160 kips (712 kN). This was maintained with minor degradation to about 150 kips (667 kN) at a displacement of 2 in. (51 mm).

Level V: Further cyclic loading caused severe damage to the sides of the key, especially at the interface region, as shown in Figure 3.23(f). This damage combined with fracture of the reinforcement, resulting in substantial degradation in strength and stiffness of the shear key as observed during testing of other test units.

3.8.2 Load versus Displacement Curve

The load versus displacement curve is shown in Figure 3.24. It shows that the strength and stiffness were maintained during the three cycles at 1 in. (25 mm) displacement. After reaching the peak load the capacity immediately dropped to the shear friction mechanism level. Further cyclic loading resulted in a substantial degradation of the strength and stiffness of the shear key similar to that of the other test units.

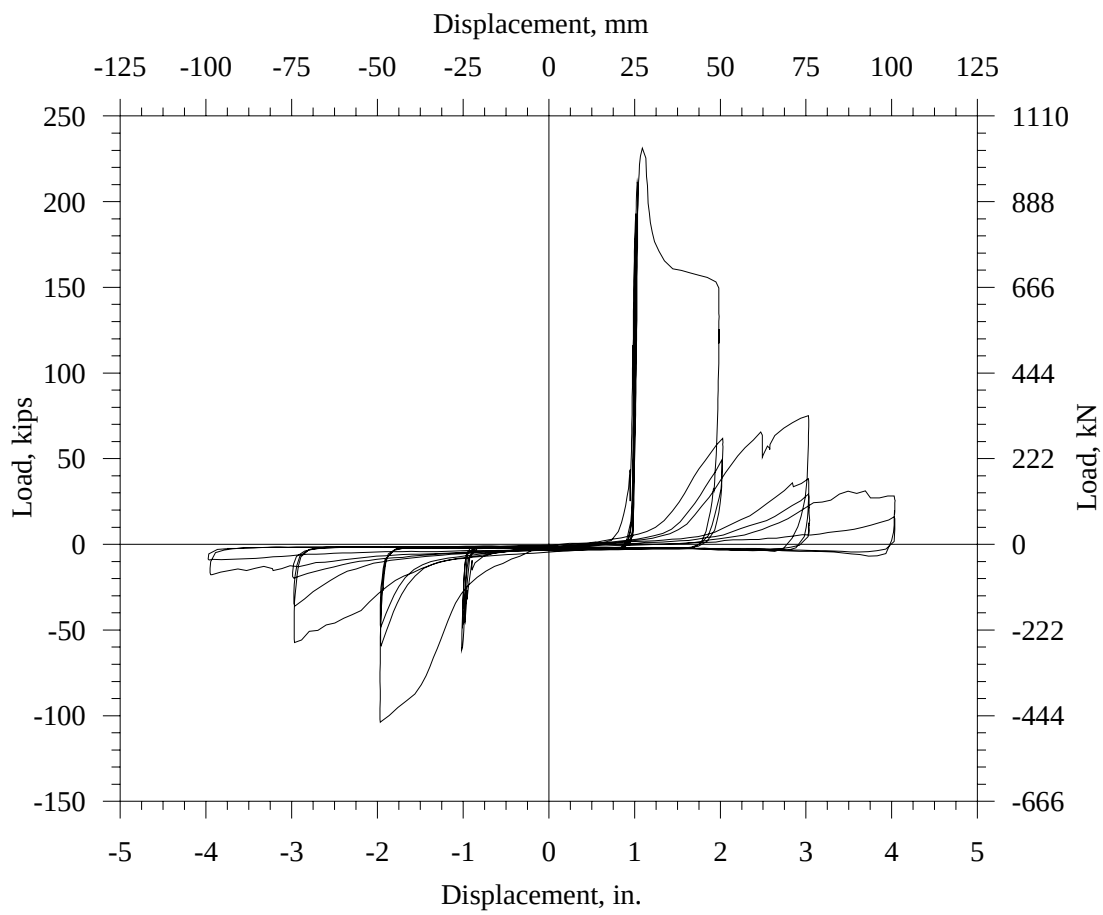

Figure 3.24 Load vs. Displacement – Test Unit 2D

3.8.3 Horizontal Strain Profiles

The horizontal strain profiles are shown in Figure 3.25. The figure shows that the strains at location A were above yielding at first cracking during the push portion of the cycle, whereas strains at locations B and C were within yielding. Strains at location D were very small. The strain distribution was nonlinear, as expected once the strains surpassed the yield level. At the peak displacement of the subsequent pull portion, the strains at location D increased, while remaining below yielding. Strains at other locations decreased with increased loading in the pull direction.

At the peak load, the strains at locations A and B increased substantially, while those at locations C and D remained essentially constant. The peak strain at this level was at location B. Beyond the peak load, the strains at location B remained constant, while those at location A increased substantially. The strains at locations C and D decreased, while those at location D reached the maximum limit of the strain gage, probably due to localized bending in the reinforcement.

The strain profiles at the peak displacement of the pull portion of the cycle was a mirror image of those of the push portion, with the strains at location A below yield. The maximum strain was at location D. All gages at the interface were damaged at this level, resulting in no further useful information.

The strains below the interface, at locations E, F, G, and H, resembled those at the interface, but at a lower level, remaining below yield. The strains recorded at the maximum displacement of the pull portion of the first cycle at 2 in. (51 mm) showed a profile that was a mirror image of that obtained during the push portion of the cycle. After cycling beyond 2 in. (51 mm) displacement the rapid degradation of the concrete and fracture of reinforcement resulted in lack of useful information.

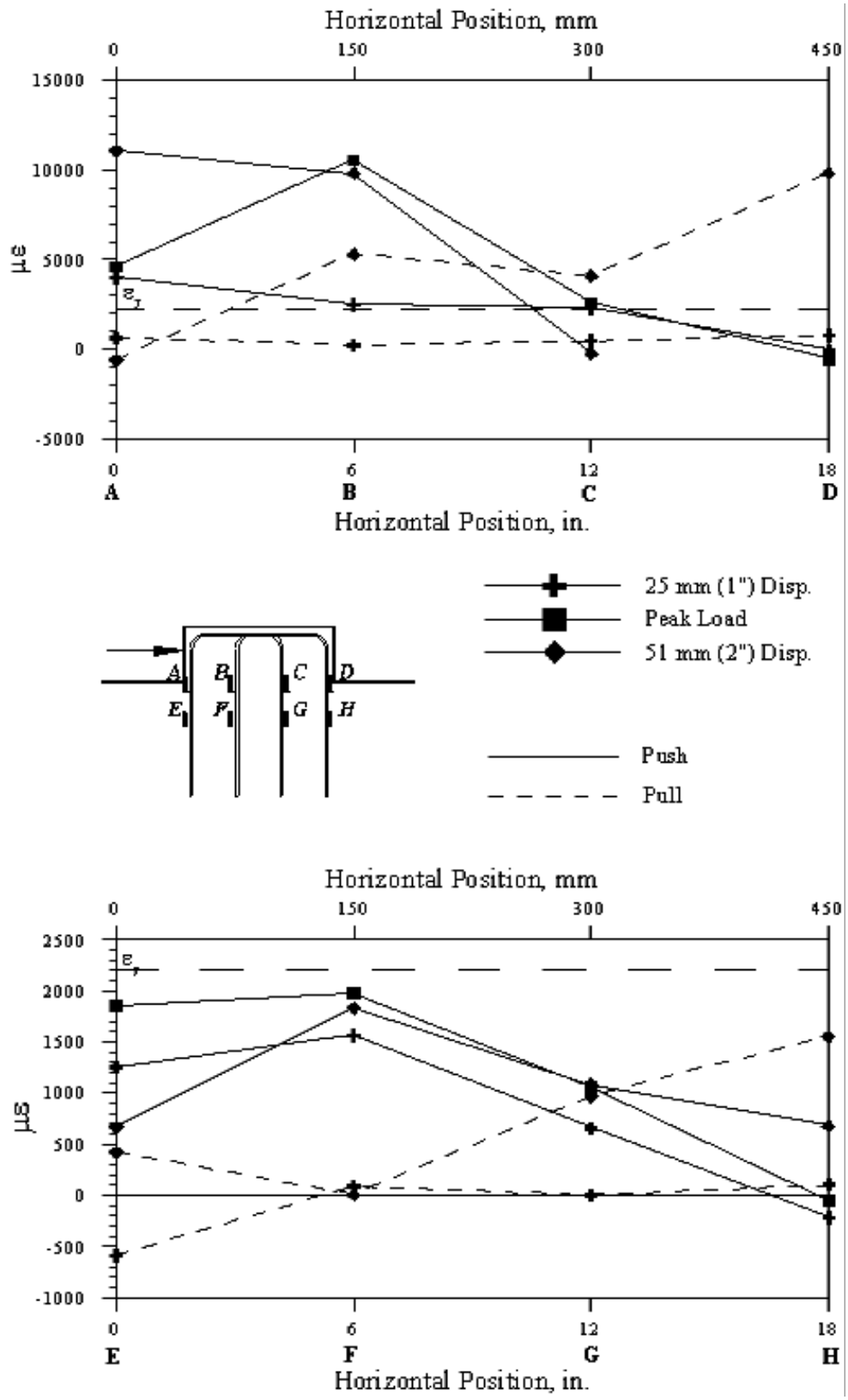

Figure 3.25 Horizontal Strain Profiles – Test Unit 2D

3.8.4 Vertical Shear Key Movement

The vertical movement of the key is shown in Figure 3.26. The movements shown corresponded well with the strains in the reinforcement, with the greatest vertical movement at the face of the key nearest the applied load. This corresponds to location A for the push portion of the cycle and location B for the pull portion of the cycle. These movements remained small during the 1 in. (25 mm) displacement cycles, but they increased at the peak load. After reaching the peak load, the vertical displacements increased markedly at location A, but slightly decreased at location B.

The movements during the push and pull portions of each cycle are both inclined, but in opposite directions. During the push cycle, the vertical movement at location B decreased substantially, past their original value. During the pull portion the vertical movement of location A decreased, but by a much smaller amount, remaining above its original position. With continued cycling, the magnitudes of the vertical displacement increased at both locations during the pull portions of each cycle, while increasing at location A and decreasing at location B during the push portions.

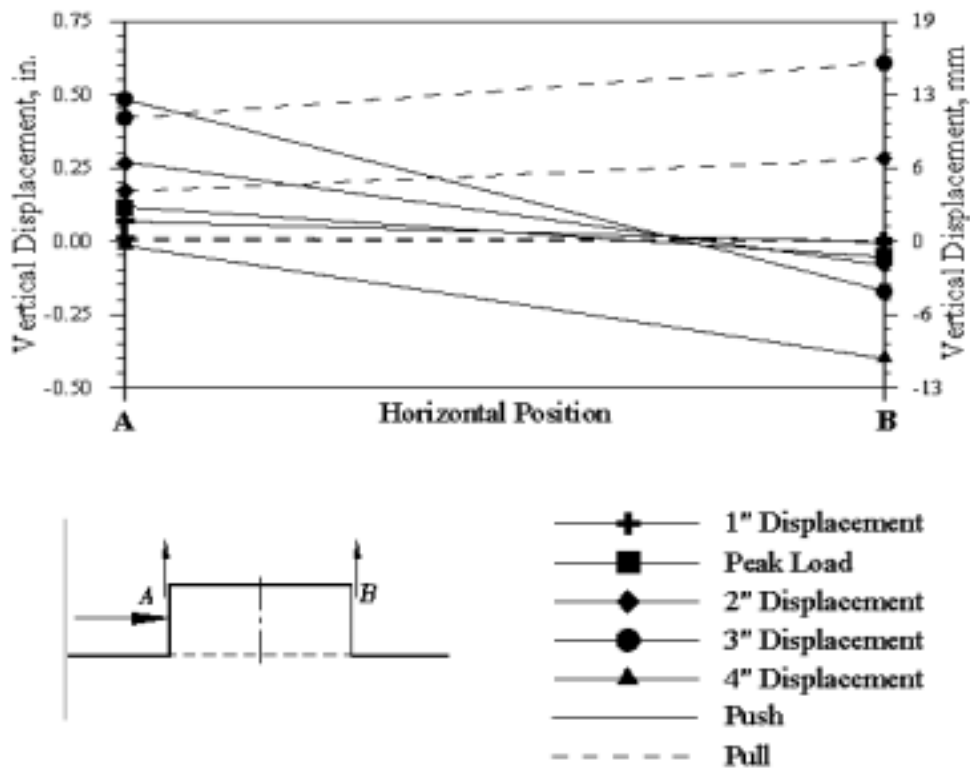

Figure 3.26 Vertical Key Movement – Test Unit 2D

4 ANALYTICAL MODELS FOR SACRIFICIAL INTERIOR SHEAR KEYS

4.1 Discussion of Experimental Results

4.1.1 Test Series I

The load versus displacement curves for Units 1A, 1B, and 1C are shown in Figure 4.1, and their envelopes in Figure 4.2. Figure 4.1 and Figure 4.2 show remarkable similarities in the performance of the test units under the various load applications. All test units showed the same gap closure behavior, resulting from the 1 in. (25 mm) gap between the key and the loading arm, filled with expanded polystyrene. This resulted in a region of zero stiffness and resistance, at a displacement in both directions equivalent to about 95% of the thickness of the polystyrene. All test units showed the same stiffness after the closure of the gap. This stiffness was the same in both directions for cyclic loading, and was maintained as the load was cycled.

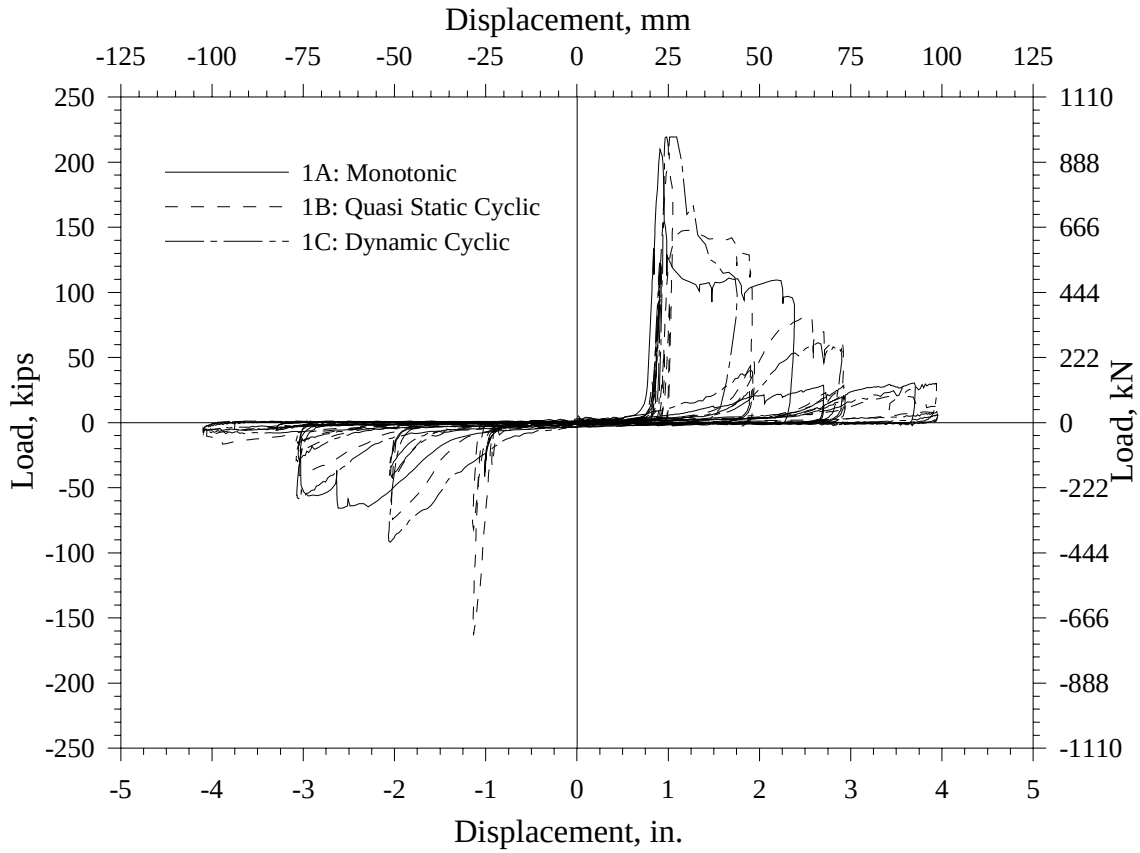

Figure 4.1 Load vs. Displacement - Test Series I

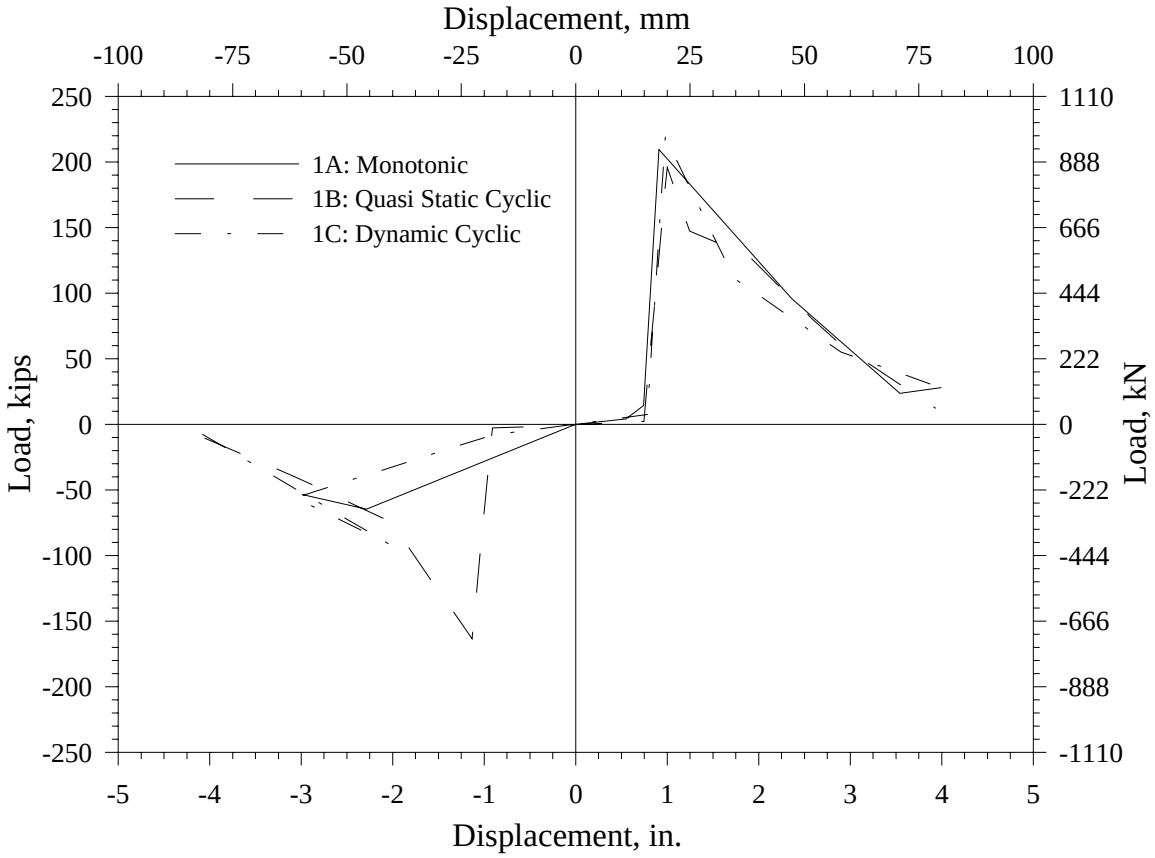

Figure 4.2 Envelopes of Load vs. Displacement Curves – Test Series I

All test units showed essentially the same peak load, with very little variation from one test unit to the next. The strut-and-tie model most accurately predicted the magnitude of the peak load, with the sliding shear friction approach resulting in a calculated capacity of about 50% of the experimental capacity. The capacity based on the moment resistance of the test units also underestimated the peak load. A drop in load was observed after reaching the peak value. The decrease was in the order of 50% for Units 1A and 1C, with a remaining capacity of about 110 kips (489 kN), equivalent to that calculated using the sliding shear friction approach. This drop in capacity was not as dramatic for Unit 1B, in which the load dropped to about 145 kips (645 kN) after reaching the maximum load carrying capacity of the shear key.

The degradation under cyclic loading was also essentially the same for all test units. This was caused by degradation of the concrete aggregate interlock and resulting friction at the crack formed along the interface, the fracture of the reinforcement, and the damage to the concrete on the sides of the shear key. Damage of the shear key side faces resulted in exposure of the outer lines of reinforcement, rendering them ineffective in resisting the applied load.

4.1.1.1 Development of Strut-and-Tie Mechanism

The development of the strut-and-tie load transfer mechanism began with the closure of the gap and ended with the peak load. This was reached when the crack developed along the interface had propagated completely through the length of the key.

The test results show that the assumptions made in the strut-and-tie model are reasonable. The first assumption was that three rows of reinforcement are effective in contributing to the tie, as shown in Figure 4.3. The observations made during the test also reflect this behavior; these observations include the crack at the interface that corresponded to the development of the tie, and the cracks in the sides of the key formed parallel to the assumed strut location. The resulting crack pattern consists of horizontal cracks nearest the applied load, where the applied load was transferred to the intersection of the resultant tie force with the strut. Inclined cracks developed in the region of the strut itself, which extended to the compression toe of the key. The resulting crack pattern is shown in Figure 4.4.

The actual angle of inclination was calculated by first finding the actual force in the tie from the strains in the reinforcement. The tangent of this angle is the ratio of the tie force to the applied load. This angle was found to be constant from the time of the yielding of the row of reinforcement nearest the applied load to the peak load. Table 4.1 shows that this angle was very close to the value of 17.1^{o} found using the methods presented earlier.

The forces in the tie and strut increased in proportion to the applied load, with the tie activating more and more of the available reinforcement. The location of the resultant tie force was found by summing the moments of the individual rows of reinforcement about the toe of the strut and dividing by the total tie force. This number was verified by summing the moments of the resultant tie force with that of the applied load. The location of the resultant tie force agreed with that originally assumed at the middle row of the three rows of reinforcement contributing to the tie.

Table 4.1 Strut Angle - θ

Limit State	V Kips (kN)	T kips (kN)	θ = atan(T/V) deg.
Yield of First Row	129 (574)	39 (173)	16.7
Yield of Second Row	164 (730)	51 (227)	17.3
Peak Load	210 (934)	64 (285)	16.9

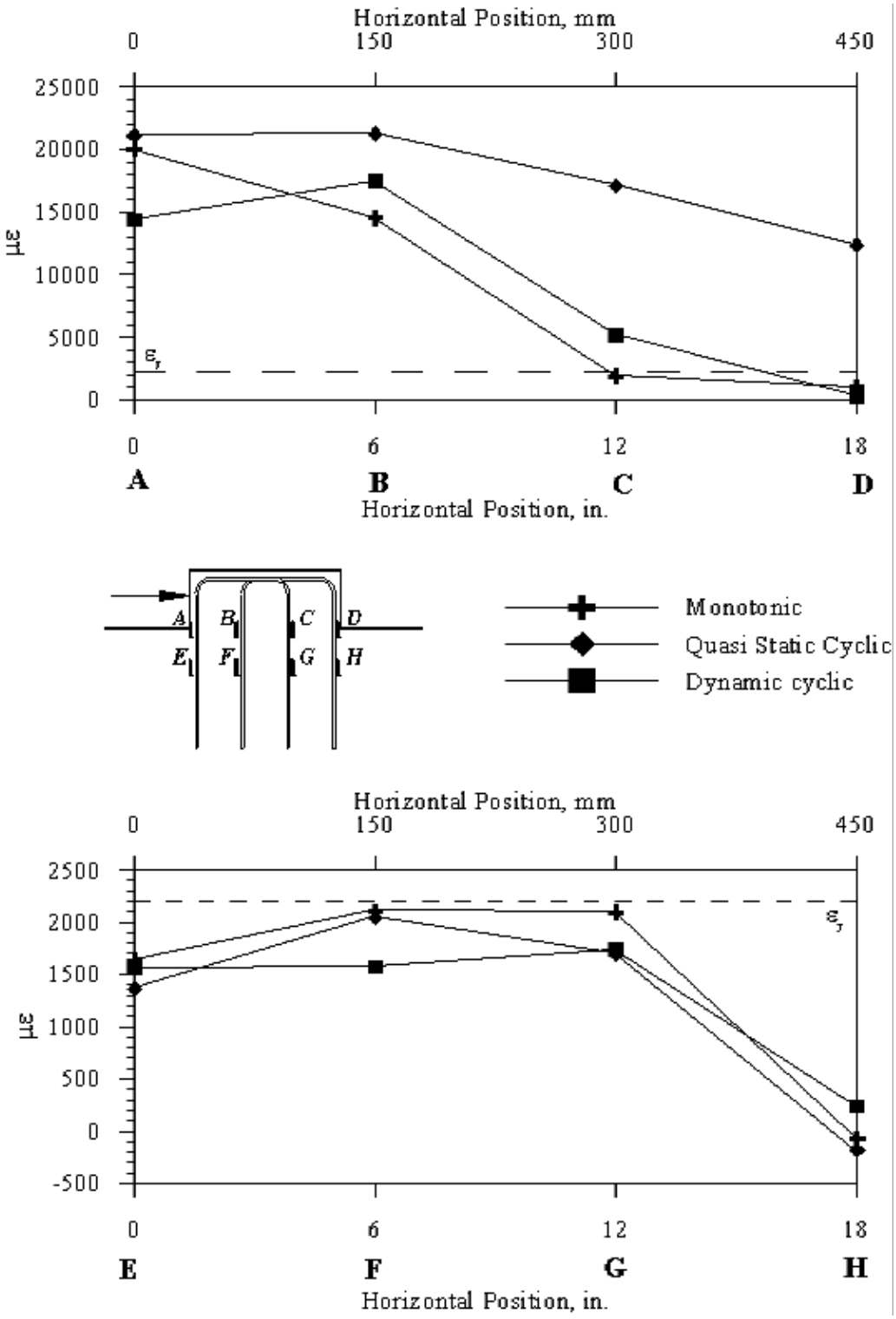

Figure 4.3 Horizontal Profiles of Strains in Vertical Reinforcement of the Shear Key at Peak Load – Test Series I

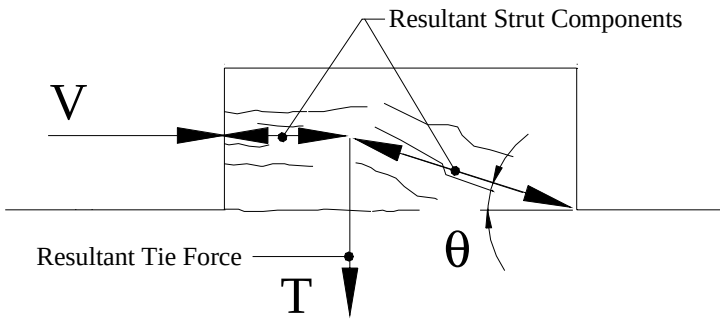

Figure 4.4 Typical Crack Pattern in Interior Shear Keys

4.1.1.2 Development of Sliding Shear Friction Mechanism

After reaching the peak load, the resistance dropped to that best predicted by the sliding shear friction model. The shear friction model is based on the assumption that the section is cracked. The transition from a strut-and-tie mechanism to that of sliding shear friction occurred when a horizontal crack propagated at the entire surface of the shear key-abutment interface. After this level, the key behaved essentially as a rigid body, transferring the applied load to the base (the abutment stem wall) through shear friction. The reinforcement provided a passive normal force activated by the opening of the crack at the interface providing a jagged surface due to aggregate interlock and resulting in a substantial coefficient of friction.

As the load was cycled, widening of the crack and the associated degradation of the aggregate interlock at the interface resulted in a decrease of the friction coefficient and a rapid decrease of resistance of the shear key. This also affected the ability of the key to activate the reinforcement to provide a normal force. This was accompanied by fracture of the reinforcement and spalling of the sides of the key, resulting in a loss of the available reinforcement.

4.1.2 Test Series II

The load versus displacement curves for the test units with varying aspect ratios are shown in Figure 4.5, and the envelope of these curves are superimposed in Figure 4.6. Similarly, The load versus displacement curves for the test units with varying reinforcement ratio are shown in Figure 4.7, and the envelope of these curve are superimposed in Figure 4.8. These curves show that the load versus displacement relationship is very similar among the test units tested. They all shared the same characteristics in terms of gap closure, initial stiffness, peak load, and cyclic degradation. As well as sharing these same performance characteristics, the test units also shared very similar magnitudes of these characteristics. They all had the same initial stiffness, approximate peak load, and very similar degradations in strength and stiffness under cyclic load.

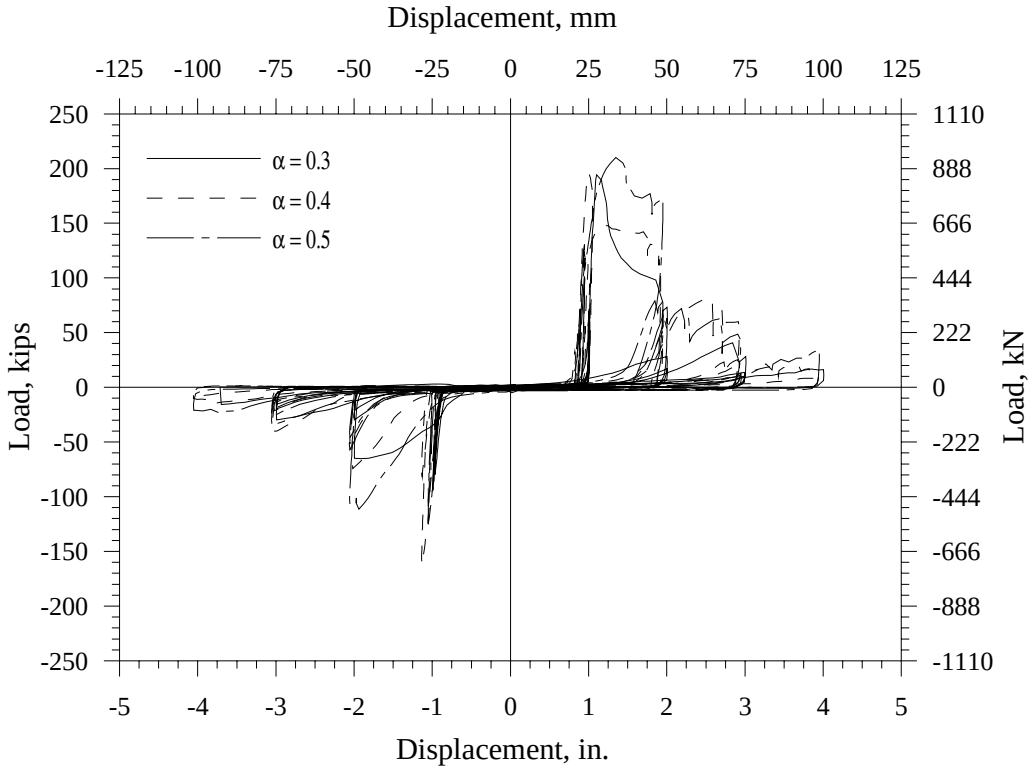

Figure 4.5 Load vs. Displacement – Varying Aspect Ratio

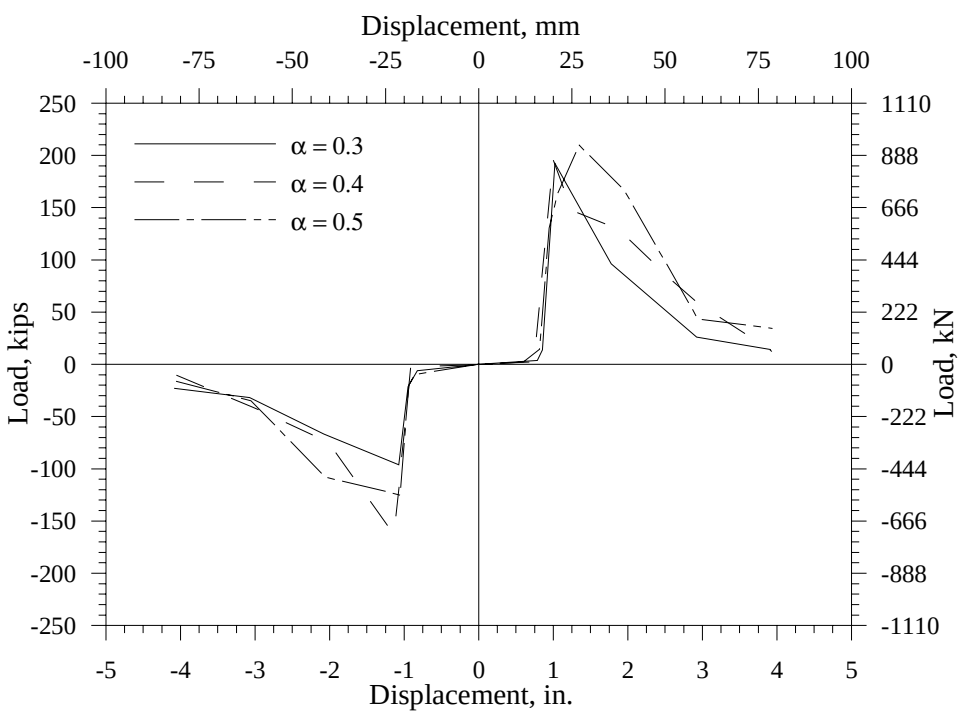

Figure 4.6 Load vs. Displacement Envelopes – Varying Aspect Ratio

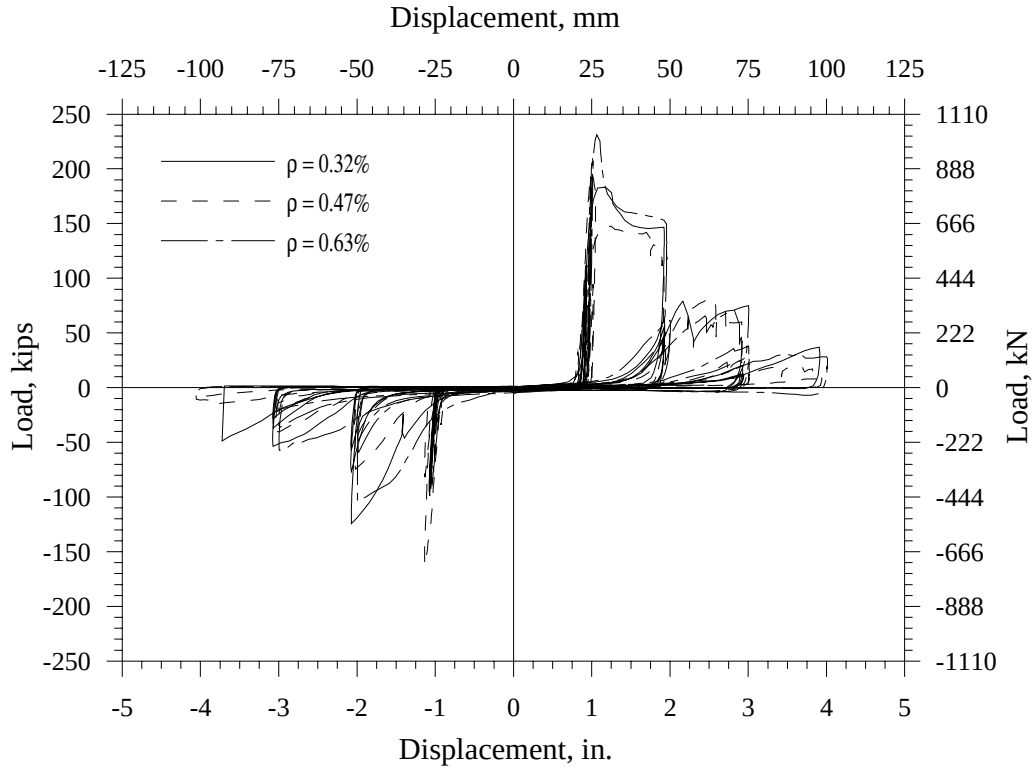

Figure 4.7 Load vs. Displacement – Varying Reinforcement Ratio

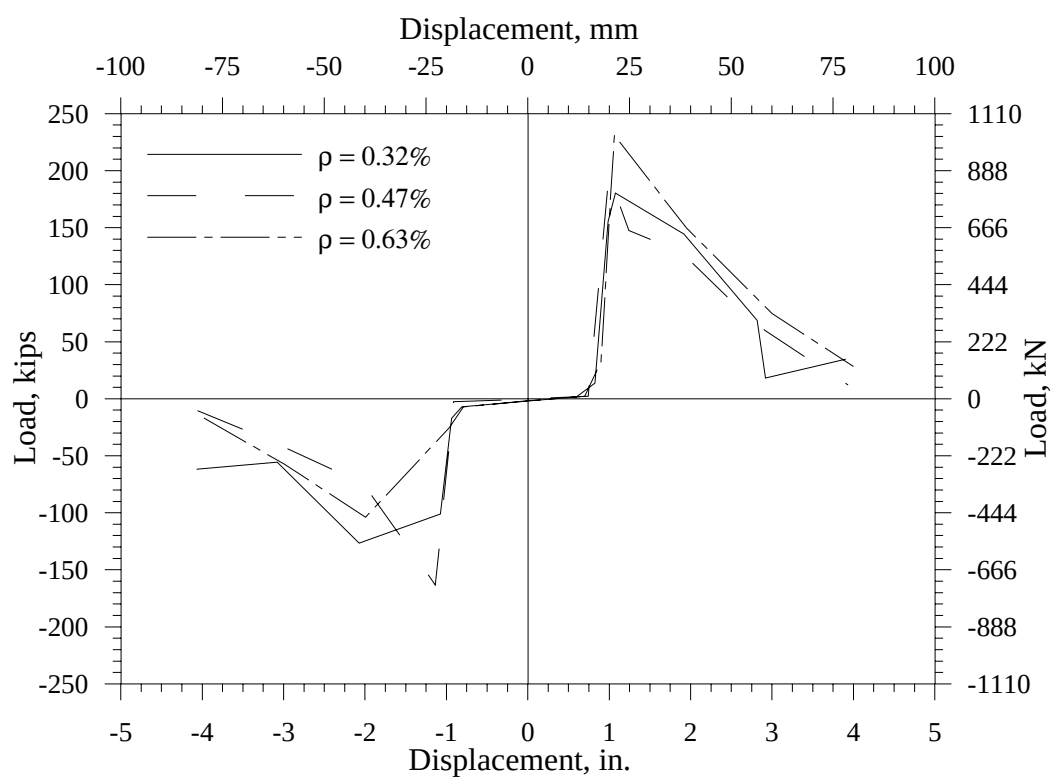

Figure 4.8 Load vs. Displacement Envelopes – Varying Reinforcement Ratio

4.1.2.1 Development of Strut-and-Tie Mechanism

All test units exhibited the same general behavioral characteristics as those observed during the first series of tests. The development of the strut-and-tie was apparent in each of the test units. All of the cracks observed during this series of tests could be classified as one of the three types of cracking for the first series. The interface crack was caused by the tension in the tie of the strut-and-tie mechanism. The horizontal cracks in sides of the shear keys resulted from development of the horizontal strut, and the inclined cracks in sides of the shear keys formed as a result of the inclined strut.

There was, however, variation in the behavior of the strut-and-tie mechanism of each test unit observed during the tests. Test Unit 2A, with a low aspect ratio, initially showed the development of the crack at the interface, as shown in Figure 4.9(a). This was accompanied by some minor horizontal cracks in the side of the shear key, resulting from the lower height of the key; the effective area of the horizontal strut was reduced as a result of this.

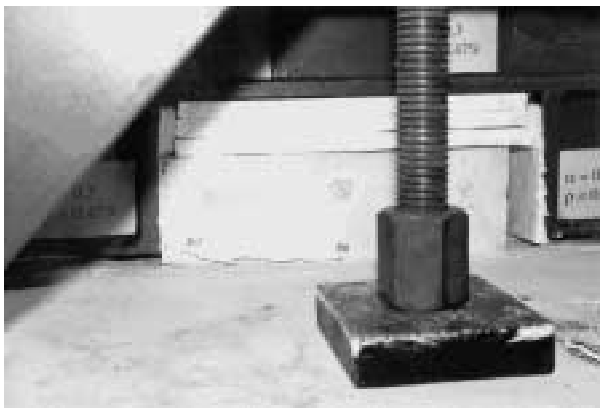

(a) Specimen 2A - Low aspect Ratio

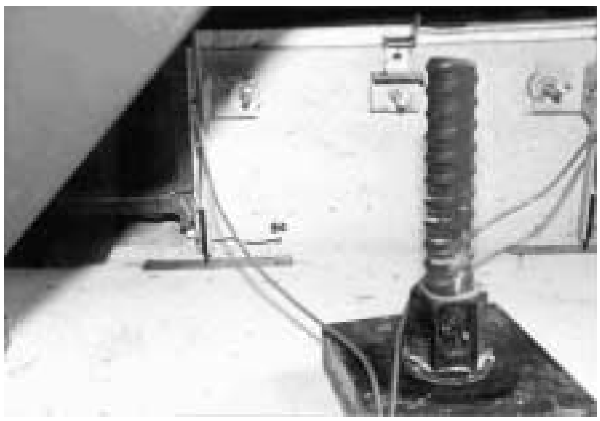

(b) Specimen 2B - High Aspect Ratio

(c) Specimen 2C - Low Reinf. Ratio

(d) Specimen 2D - High Reinf. Ratio

Figure 4.9 Test Observations at Onset of Cracking (LEVEL I) – Test Series II

At the peak load, there was localized failure of the concrete in bearing directly adjacent to the applied load, as shown in Figure 4.10(a). This was a result of the low height of the shear key causing higher bearing stresses than experienced by the other test units. This concrete local zone crushing in addition to the development of the crack at the interface, resulted in switching of the load transfer mechanism from that of a strut-and-tie to that of sliding shear friction. The failure occurred at a lower load level than was predicted by the strut-and-tie model.

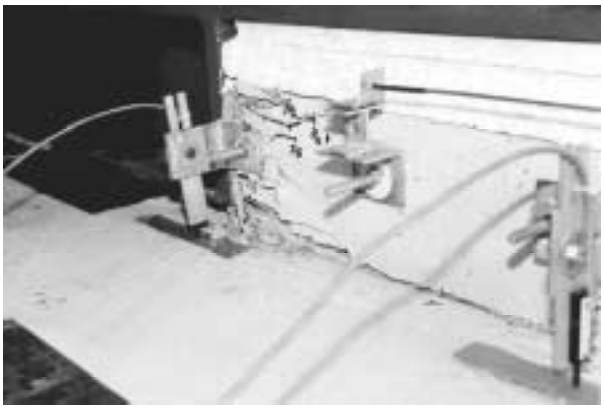

(a) Specimen 2A - Low aspect Ratio

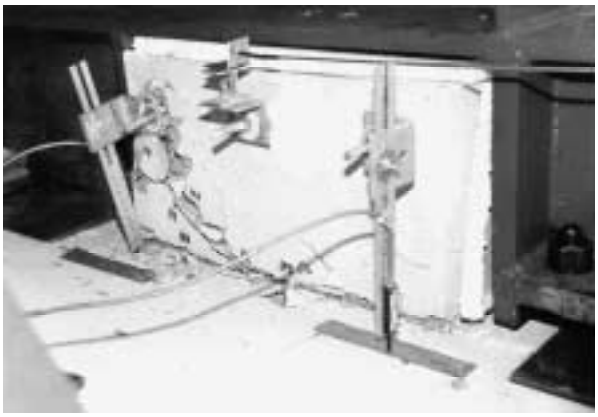

(b) Specimen 2B - High Aspect Ratio

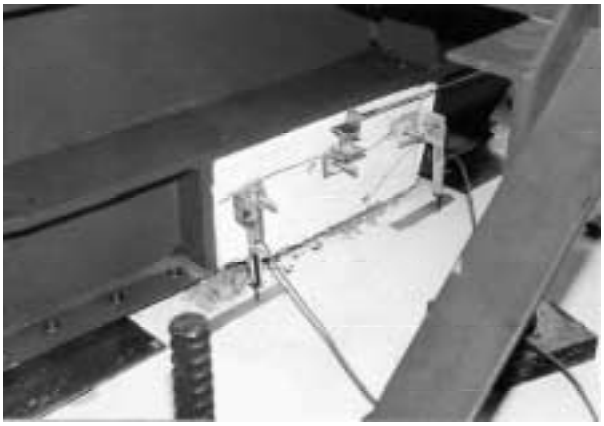

(c) Specimen 2C - Low Reinf. Ratio

(d) Specimen 2D - High Reinf. Ratio

Figure 4.10 Test Observations at Peak Load (LEVEL III) – Test Series II

Test Unit 2B, with the high aspect ratio, showed less cracking of the key itself, and showed more pronounced development of the crack at the interface, as shown in Figure 4.9(b). This was caused by the large angle of inclination producing a greater force in the tie. The relatively reduced cracking of the shear key itself was due to its larger size. This produced a larger effective strut area, and therefore a greater strut capacity. The failure of this test unit was characterized by a softening of the load vs. displacement curve as it neared the peak load, which was higher than that predicted by the strut-and-tie model. The peak load was reached when the

interface crack had propagated completely through the length of the key, as shown in Figure 4.10(b).

Test Unit 2C, with the low reinforcement ratio, showed very little cracking in the key itself, with nearly all crack development occurring at the interface, as shown in Figure 4.9(c). The reason for this is the low reinforcement ratio, which resulted in a tie of low capacity. Thus, formation of the crack at the interface was caused by the development of the tie. The weak tie also resulted in the strut having a high capacity relative to the tie, which restricted cracking in the shear key itself. The type of failure observed was characterized by very little crack development in the shear key itself, with substantial widening of the interface crack as the peak load was reached, as shown in Figure 4.10(c). The peak load was higher than that predicted by the strut-and-tie model.

Test Unit 2D, with the high reinforcement ratio, showed limited cracking at the interface, with considerable cracking in the sides of the key, as shown in Figure 4.9(d). This was caused by the weakness of the strut relative to the tie. Most of the cracking at the interface for this test unit resulted from the propagation of the inclined cracks. At the peak load there was a failure of the inclined portion of the strut. This was apparent by the substantial inclined crack development over the middle portion of the key, with the sides of the key bulging outward at the peak load. This was accompanied by the propagation of the cracks at the interface through the key, as shown in Figure 4.10(d). This occurred at a lower load level than that predicted using the strut-and-tie model since Eq. (2.10) is based on an assumption that failure would occur in the tension tie rather than in the compression strut.

Although there was a variation in the behavior of the strut-and-tie mechanisms, the peak load for each test unit was reached when the crack at the interface had propagated completely through the shear key-abutment interface. When this occurred, the load transfer mechanism switched from that of a strut-and-tie to shear friction. This resulted in a decrease in the capacity and stiffness of the shear key.

The effects of the higher aspect ratio and lower reinforcing ratio were to increase the ductility of the key at the peak load. This was caused by the increased development of the reinforcement forming the tie. The results of these tests show that regardless of the behavior of the strut-and-tie mechanism, the force required to develop this crack completely through the interface did not change significantly.

Because of the relatively high tie force in Units 2B and 2C, strains in the shear key reinforcement in Units 2B and 2C were relatively high (compare strains at locations A, B and C in Figure 3.17,

Figure 3.21 and Figure 3.13). This means that the actual stresses in the shear key reinforcement in Units 2b and 2C were considerably higher than the yield stress, f_y. Thus the strut-and-tie capacity of Units 2B and 2Cshould have been higher than the capacity calculated using Eq. (2.10); the calculated strut-and-tie capacity would have been closer to the experimental capacity if a steel stress higher than f_y was used in Eq. (2.1).

4.1.2.2 Development of Shear Friction Mechanism

After attaining the peak load, all test units exhibited a substantial loss in capacity, as the load transfer mechanism switched from that of a strut-and-tie to that of shear friction. This load was maintained as the displacement was increased to 2 in. (51 mm). The degradation under cyclic loading was, however, very similar in all the test units. Neither the aspect ratio nor the reinforcement ratio had affected the amount of degradation.

4.2 Development of Analytical Model

4.2.1 Calculation of Shear Key Capacity

4.2.1.1 Cracking Strength Concrete Approach For Deep Beams

The strut-and-tie model, which accurately predicted the capacity of the test units used in the first series of tests, did not accurately predict the capacity of the test units of the second series. The switch from a strut-and-tie mechanism to that of a sliding shear friction occurred when the crack at the interface had propagated through the entire length of the key. Neither the aspect ratio nor the reinforcement ratio considerably affected the load required to develop this crack.

Research on the shear strength of deep beams performed by Ramakrishnan et al. [22] have shown that the ultimate shear capacity may be predicted based on the cracking strength of the concrete and the dimensions of the beam. Their formula is:

$$V = \frac{\pi}{2} f_{sp}\, b\, d \qquad \textbf{(4.1)}$$

Where f_{sp} is the concrete cylinder splitting tensile strength and b and d are dimensions of the shear key-abutment interface. The π factor is a result of the circular cross section of the cylinder. Based on research by Kong et al. [23], this value may be related to f'_c by the following relation:

$$f_{sp} = 7.2\sqrt{f_c^{'}} \quad (psi) \;\; ; \; \left[= 0.60\sqrt{f_c^{'}} \quad (MPa) \right] \qquad \textbf{(4.2)}$$

Substituting Eq. (4.2) into (4.1) gives:

$$V_N = 11.3\sqrt{f_c^{'}} \quad (psi) \;;\; \left[= 0.94\sqrt{f_c^{'}} \quad (MPa) \right] \qquad \textbf{(4.3)}$$

According to this approach the capacity of the shear key was based only on the cracking strength of the concrete at the interface. The capacity of all of the test units was predicted within 15% using this method. Experimental and calculated capacities of the test units are given in Table 4.2. Figure 4.11 shows a comparison of the predicted and experimental results.

4.2.1.2 Sliding Shear Friction Model

This is the analytical approach currently under consideration for shear keys with aspect ratios less than 0.5 [2]. In all the tests, the experimental capacity was significantly greater than the calculated capacity. In the case of sacrificial elements, this is non-conservative, resulting in the probability that the capacity of the shear keys will exceed that of the piles. One of the principal objectives of shear key design is that they should perform as sacrificial elements or structural fuses; it means capacity of the shear keys should not exceed or be close to the shear capacity of the piles. It is noted that the calculated strength shown is nominal, and would be multiplied by a strength reduction factor, ϕ, of 0.85, which, again, is non-conservative for sacrificial members.

4.2.1.3 Strut-and-Tie Mechanism

This analytical method provided a realistic estimate for the capacity of the first series of tests. The second series showed, however, that the shear strength of the key is determined by the force required to develop a crack at the interface, which is only marginally affected by the aspect and reinforcing ratios.

4.2.1.4 Maximum Shear Stress of 800 psi (5.52 MPa)

This is the upper limit on the shear key capacity imposed by the Caltrans Specifications [2]. This value appears to be a reasonable estimate of the cracking strength of the concrete.

From Figure 4.11, it is clear that the most accurate method of calculating the capacity of a shear key is that based on the cracking strength of the concrete, given by Eq. (4.3). The experimental capacities can be used to verify the factor of 11.3 (or 0.94). The results are presented in Table 4.3. The average of these is 11.2 (or 0.93), which validates the use of the factor of 11.3 (or 0.94).

Table 4. 2 Experimental and Calculated Capacities

Test unit	Experimental Capacity		Shear * Friction		Strut-and-Tie*		Cracking Strength		Shear Stress of 800 psi	
	kip	(kN)	kip	(kN)	kip	(kN)	kip	(kN)	kip	(kN)
1A	210	(934)	116	(516)	208	(925)	206	(916)	224	(996)
1B	198	(881)	116	(516)	208	(925)	214	(952)	224	(996)
1C	220	(979)	116	(516)	208	(925)	225	(1001)	224	(996)
2A	200	(890)	116	(516)	277	(1232)	215	(956)	224	(996)
2B	214	(952)	116	(516)	166	(738)	212	(943)	224	(996)
2C	183	(814)	78	(347)	139	(618)	196	(872)	224	(996)
2D	235	(1045)	155	(690)	277	(1232)	206	(916)	224	(996)

* Yield strength of shear key reinforcement = 63 ksi (434 MPa) as determined from tensile tests.

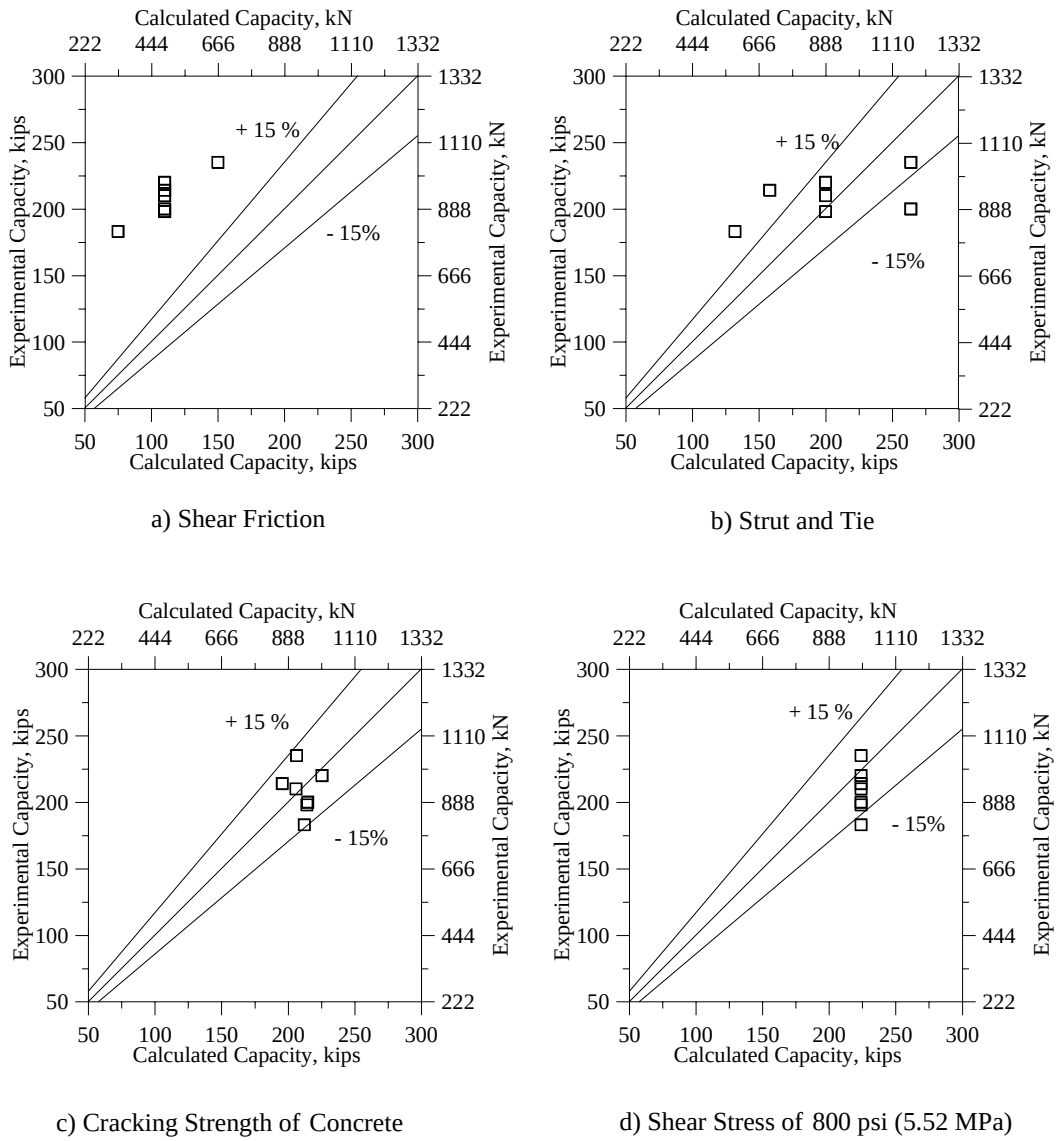

a) Shear Friction

b) Strut and Tie

c) Cracking Strength of Concrete

d) Shear Stress of 800 psi (5.52 MPa)

Figure 4.11 Comparison of Experimental and Calculated Capacities of Exterior Shear Keys

Table 4.3 Summary of Experimental $f'_c{}^{1/2}$ Factors

Test unit	f_c' (on testing day) psi	(MPa)	Experimental Capacity kips	(kN)	$f'_c{}^{1/2}$ factor kips	(kN)
1A	4230	(29.2)	210	(934)	11.5	(0.96)
1B	4570	(31.5)	198	(881)	10.5	(0.87)
1C	5070	(35.0)	220	(979)	11.0	(0.92)
2A	4600	(31.7)	200	(890)	10.5	(0.87)
2B	4490	(31.0)	214	(952)	11.4	(0.95)
2C	3820	(26.3)	183	(814)	10.6	(0.88)
2D	4250	(29.3)	235	(1045)	12.9	(1.07)

4.2.2 Discussion of Analytical Models

Figure 4.12 illustrates the comparison between the experimental results and the different analytical models that were used to characterize the capacity of all the test units. The vertical columns represent the analytical results, and the experimental peak and post-peak load levels are represented, respectively, by the horizontal solid and dashed lines.

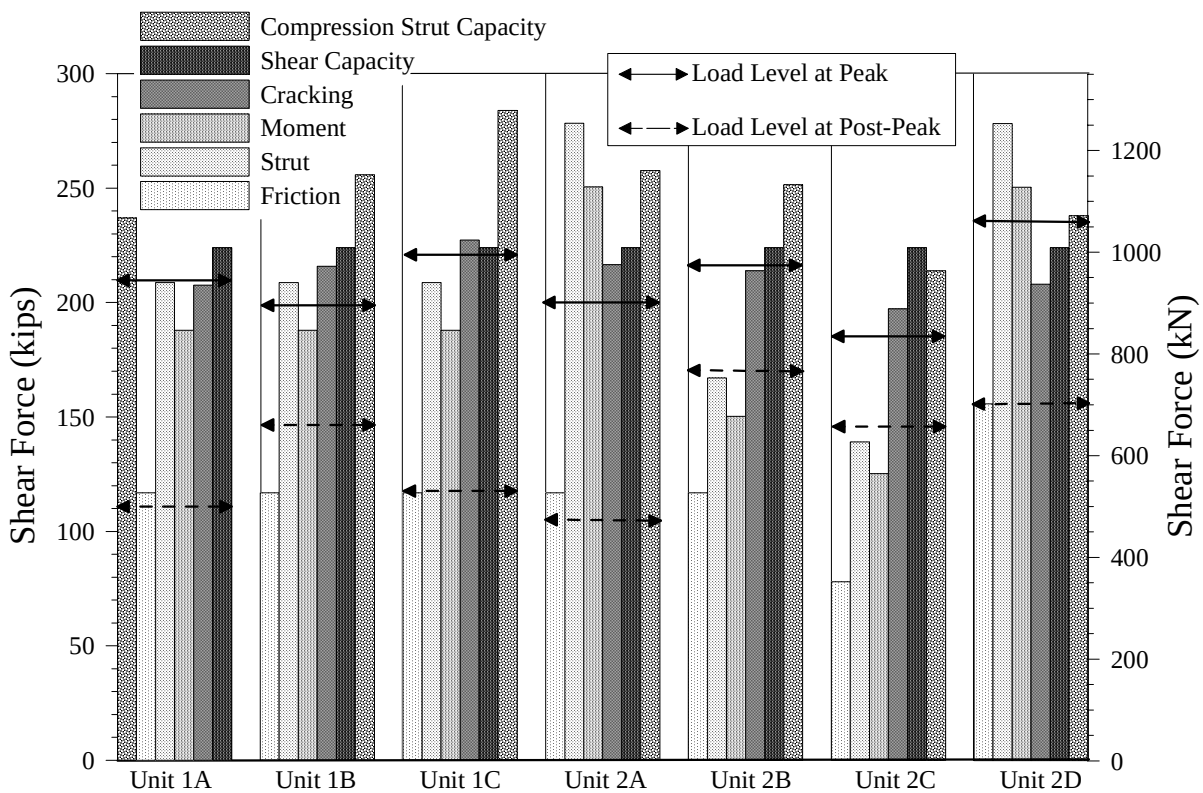

Figure 4.12 Comparison of Experimental Results versus Predicted Capacity

From Figure 4.12 it can be seen that for all of the test units the shear friction approach severely underestimated the peak load of the shear keys. This indicates that in its present form, current design methodologies under-predict the capacity of sacrificial interior shear keys and the seismic force input into the piles will be substantially higher than anticipated.

Unlike Series I test units, in all of Series II test units the strut-and-tie model did not accurately predict the magnitude of the peak loads recorded during testing. For Test Series II Specimens 2A, 2B and 2C, the observed peak loads were most accurately approximated by using the concrete cracking strength approach. For Specimen 2D, the observed peak load was most accurately approximated by using the capacity of the diagonal compression strut given by Eq. (2.4) (designated in Figure 4.12 as the compression strut capacity).

In most of the cases it can be seen that the post-peak capacity of the shear keys was best approximated by the sliding shear friction model. However, in cases where the strut-and-tie approach under-predicted the capacity of the shear key the initial drop in the lateral load was best characterized by the strut-and-tie model (Specimens 2B and 2C; see Figure 4.12).

In this research program a model was developed in order to estimate the maximum load carrying capacity and the post-peak load of sacrificial interior shear keys based on evaluation of the experimental results of all test units (i.e Test Series I and II), which is described next.

4.2.3 Sacrificial Shear Keys Peak Capacity

According to the test results, the following recommendations are made for the evaluation of the capacity of sacrificial interior shear keys with a single interface between the shear key and the abutment stem wall, reinforcement ratios between 0.32 percent and 0.63 percent, aspect ratios between 0.30 and 0.50, and width-to-depth ratio around 0.70.

The behavior of shear keys after closure of the gap and prior to reaching the peak capacity can be characterized by a strut-and-tie model. However because the peak load is reached when a horizontal crack fully propagates along the shear key-abutment interface, the peak capacity of the shear key is best estimated by the smallest value given by Eq. (4.3) and the following:

$$V_N < 800\ A_c\,(psi);\quad [5.52 A_c\,(MPa)] \qquad For: \rho < 0.60\% \qquad \textbf{(4.4a)}$$

And

$$V_{n,\max} = 0.2\ A_c\ f_c^{'} \qquad For: \rho \geq 0.60\% \qquad \textbf{(4.4b)}$$

The strength reduction factor, ϕ (=0.85), typically used in the design of reinforced concrete members, should not be used to further reduce the nominal capacity of sacrificial elements. The nominal capacity should instead be:

$$V_u = \phi^O\ V_{n,\max} \qquad \textbf{(4.5)}$$

Where ϕ^o is an over-strength factor equal to 1.30, which will ensure that there is no damage sustained by the piles. However, further experimental tests are required to validate the capacity of sacrificial interior shear keys with different interface and reinforcement areas.

4.2.4 Calculation of Force versus Displacement Envelopes

It is currently assumed in design that shear keys provide no further lateral resistance after their peak capacity has been reached. For this reason the columns are designed to provide full transverse support for the entire length of the bridge superstructure once the shear keys have failed. Test results show, however, that the shear keys maintained approximately 50% of their peak capacity within large levels of lateral displacement. The shear keys also had a residual capacity up to fracture of the shear reinforcement. In order to perform a detailed assessment of the seismic response of a bridge structure it is necessary to predict the performance of the interior shear keys to within large levels of lateral displacements. The seismic performance of the interior shear keys was achieved by estimating the equivalent stiffness and viscous damping of the shear keys after reaching the peak load. These two variables are particularly important when assessing the seismic response of a bridge structure.

The following procedure was developed for calculating the effective stiffness and effective damping of interior shear keys for a given displacement. This is done by first calculating the shape of the load versus displacement envelope for the peak load, which is reached during the first cycle at a given displacement, and the cyclic friction load, which is reached in the subsequent cycles. The envelopes for interior shear keys may be defined using the following points, as shown in Figure 4.13.

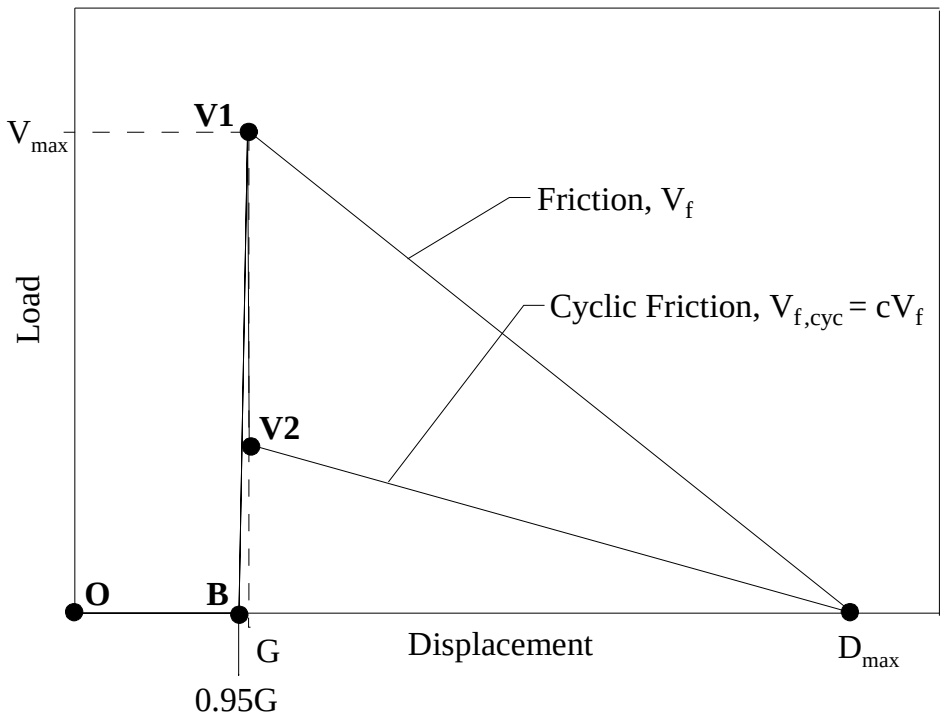

Figure 4.13 Load vs. Displacement Envelopes

i. Point O is the origin, with no load or displacement.

ii. Point B is reached when the expanded polystyrene has been completely compressed, with the loading frame making contact with the face of the shear key. This point has a negligible load at a displacement of 95% of the thickness of the expanded polystyrene.

iii. Point V1 defines the friction envelope up to the peak load. The maximum load carrying capacity is reached at this point, at which the crack at the interface has propagated completely through the section. The maximum load carrying capacity is best estimated by the smallest value given by Eq. (4.3) and Eq. (4.4). The displacement of the shear key is calculated by assuming a perfect rigid body, with the displacement resulting from the complete compression of the expanded polystyrene. The displacement at the peak load is then simply the gap width, G. After this level, the load transfer mechanism switches from a strut-and-tie to sliding shear friction.

iv. Point V2 defines the cyclic friction envelope, to which the shear key degrades as it is cycled. This amount of degradation is expressed by the variable c, which is a function of the aspect ratio and is determined using the following expression:

$$c = 1.5\,\alpha - 0.25 \qquad \textbf{(4.6)}$$

in which α is the aspect ratio of the shear key.

v. Point D_{max} is the point at which the friction capacity has degraded to essentially zero. The test units presented here all showed that this occurs at a displacement, D_{max}, of about 4 ½ in. (114 mm). The degradation comes from a number of sources, but the total degradation showed little variation. Based on these results, it appears that the D_{max}-value is not affected by the parameters investigated. Other parameters, such as the diameter of the reinforcing bars or the aggregate size, may affect this, but based on these tests a value of 4 ½ in. (114 mm) will be adopted in this model. The resulting envelopes are shown in Figure 4.14 for all units tested using a quasi-static loading protocol, superimposed on the corresponding load versus displacement curve.

4.2.5 Calculation of Effective Damping and Effective Stiffness

The load versus displacement curves for the test units show that the amount of degradation is a function of both the displacement and the number of cycles. The degradation can be assumed to be a function of the displacement for the first cycle, where the strength degrades to the value predicted by the force versus displacement envelope. Subsequent cycling at this displacement will produce further degradation to the value of the cyclic friction load envelope. For assessment purposes, the effective damping and effective stiffness should be calculated based on the cyclic friction envelope, to which the load versus displacement curve degrades after being cycled.

The equivalent viscous damping was calculated for the test units and is presented in Table 4.4. The average values of the calculated equivalent viscous damping of the test units subjected to quasi-static loading are plotted in Figure 4.15. Each data point in Figure 4.15 represents the average value of all test units for the equivalent viscous damping coefficient at the corresponding displacement level and loading cycle number. For calculation of the equivalent viscous damping values, the load-displacement envelopes were used to calculate the damping energy.

For assessment purposes, this damping should be assumed for the shear key. The damping at a given displacement, D, as shown in Figure 4.16, may then be calculated as [25]:

$$\zeta_{eq} = \frac{1}{4\pi}\frac{E_d}{E_s} \qquad \textbf{(4.7)}$$

Where E_d is the damping energy at D, calculated as the area contained within the hysteresis loops as shown in Figure 4.16 for one complete cycle:

$$E_d = V_{f,cyc}(D - G) \qquad \textbf{(4.8)}$$

Where $V_{f,cyc}$ is the cyclic friction load at D and G is the gap width. In Eq. (4.7), E_s is the elastic strain energy at D, calculated by:

$$E_s = V_{f,cyc} \frac{D}{2} \tag{4.9}$$

Substituting Eqs. (4.8) and (4.9) into Eq. (4.7) gives the following expression for the equivalent viscous damping for a given displacement, *D*:

$$\zeta_{eq} = \frac{1}{2\pi} \frac{(D-G)}{D} \tag{4.10}$$

The curve shown in Figure 4.15 represents the equivalent viscous damping versus shear key displacement according to Eq. (4.10). The figure indicates good correlation between the experimental equivalent viscous damping values obtained from Eq. (4.10) and the experimental ones. The effective stiffness, K_{eff}, at a displacement *D*, may then be calculated by:

$$K_{eff} = c\, V_n \frac{\left(D_{\max} - D\right)}{D\left(D_{\max} - G\right)} \tag{4.11}$$

Where D_{max} is the displacement at which the load versus displacement envelope degrades to zero and V_{max} is the peak load calculated by the smallest value given by Eq. (4.3) and Eq. (4.4). The value of c is given by Eq. (4.6).

Table 4.4 Experimental Equivalent Viscous Damping

Cycle Cyc x displ	Test unit 1B	Test unit 2A	Test unit 2B	Test unit 2C	Test unit 2D	Avg.
1 x 2 in. (51 mm)	16 %	21 %	14 %	14 %	17 %	16 %
2 x 2 in. (51 mm)	7%	11 %	6 %	5 %	7 %	7 %
3 x 2 in. (51 mm)	13%	7 %	5 %	5 %	7 %	7 %
1 x 3 in. (76 mm)	10 %	13 %	14 %	15 %	12 %	12 %
2 x 3 in. (76 mm)	11 %	11 %	10 %	8 %	10 %	10 %
3 x 3 in. (76 mm)	13 %	11 %	8 %	10 %	11 %	11 %
1 x 4 in. (102 mm)	9 %	10 %	10 %	10 %	14 %	11 %

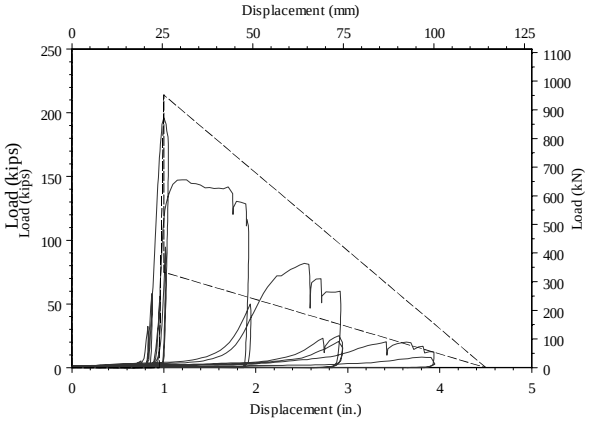

(a) Test Unit 1B

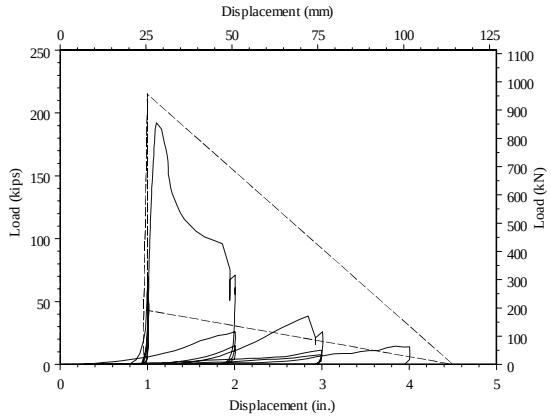

(b) Test Unit 2A

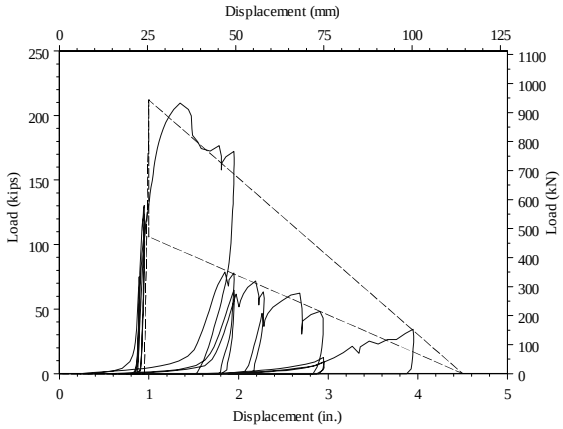

(c) Test Unit 2B

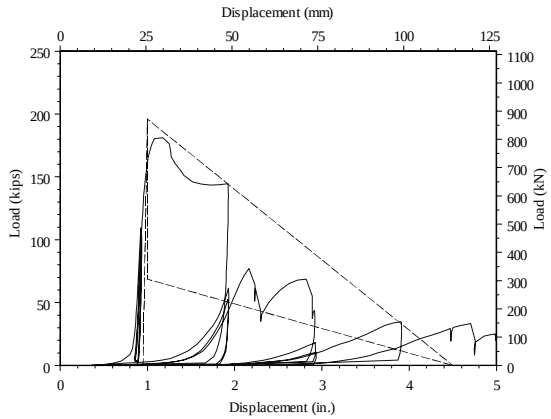

(d) Test Unit 2C

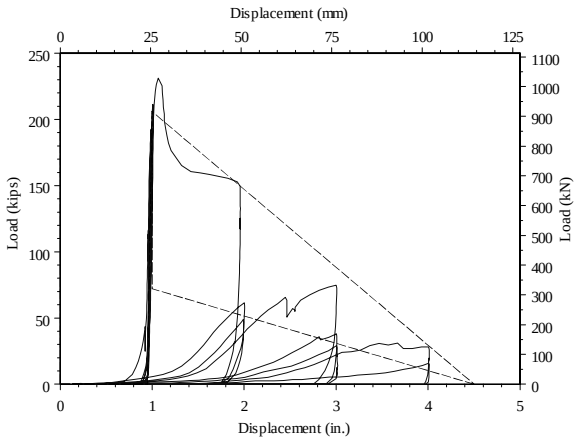

(e) Test Unit 2D

Figure 4.14 Calculated Load vs. Displacement Envelopes

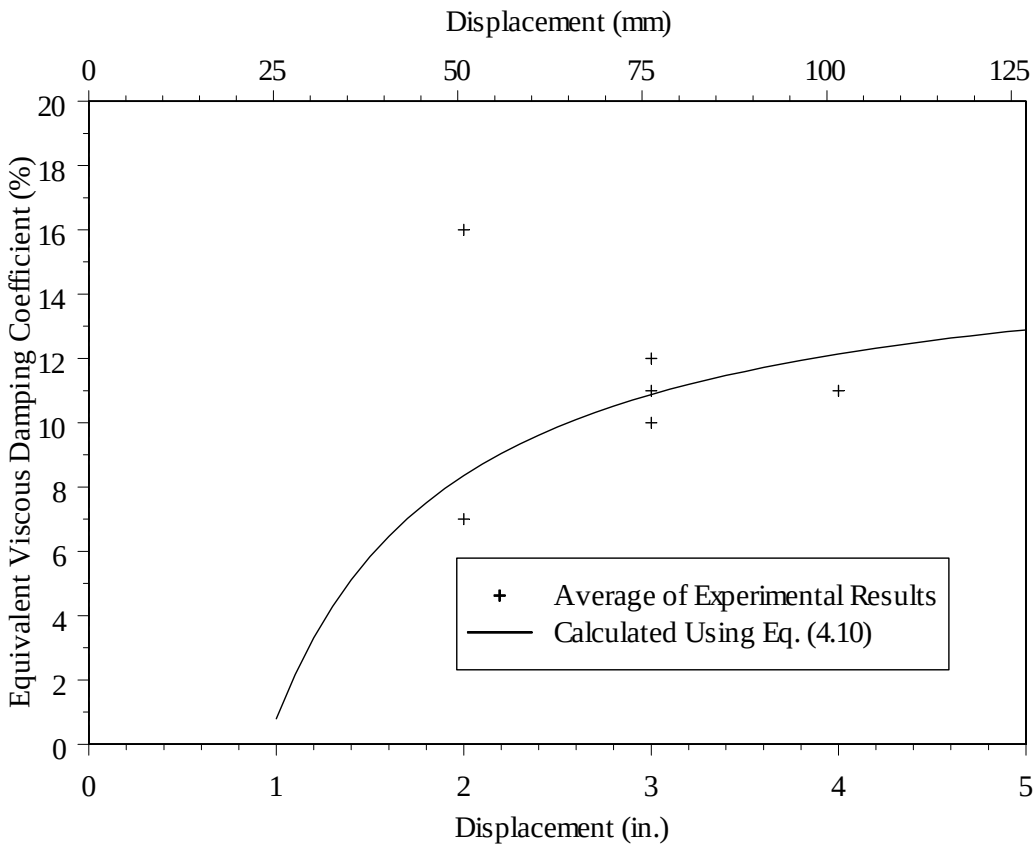

Figure 4.15 Experimental vs. Calculated Equivalent Viscous Damping

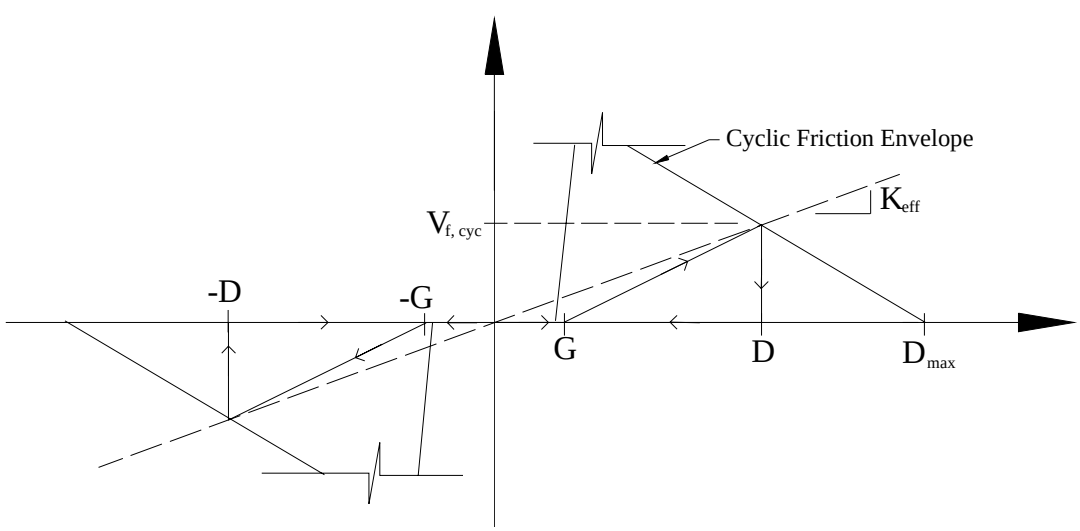

Figure 4.16 Cyclic Friction Hysteretic Behavior of Interior Shear Keys

5 EXPERIMENTAL PROGRAM OF SACRIFICIAL EXTERIOR SHEAR KEYS

Sacrificial exterior shear keys research phase is described in this chapter. The test units accurately reflected typical proportions of sacrificial exterior shear keys commonly used in bridge abutments.

5.1 Test Matrix

The sacrificial exterior shear key research program was divided in three test series. As shown in Table 5.1, Test Series I consisted of two test units, which were designed at a 2/5-scale with design details based on a prototype structure provided by Caltrans. The two test units from each series were built on the same foundation support. Test unit referenced as 1A was built without abutment walls, whereas unit referenced 1B included the abutment back wall and wing wall coupled together with the exterior shear key, as illustrated in Figure 5.1.

Table 5.1 Sacrificial Exterior Shear Keys Research Program Test Matrix

Test Series	Unit Designation	Abutment Wall	Predicted Failure Mode
I	1A	Yes	Shear
	1B	No	Shear
II	2A	No	Shear
	2B	No	Flexure-Shear
III	3A	No	Shear
	3B	No	Shear

Test Series II also consisted of two test units designed at a 2/5-scale and built on the same foundation support, as shown in Figure 5.2. The design of these test units was accomplished after testing of Units 1A and 1B. Test results obtained from Test Series I were used to improve the design of exterior shear keys. Test Unit 2A was a redesign of Unit 1A, and Unit 2B was designed to display a predominant flexure-shear response with the lateral load applied at the top of the key. Additional information will be provided in Section 5.3 while describing the design of the test units.

Test Series III consisted of two test units constructed on the same footing as in Series I and II. Series III test units were once again designed at a 2/5-scale. Figure 5.3 shows Series III test units and the position of load application. Series III units were a re-design of Test Unit 2A with the

difference that at the interface between the shear key and the abutment stem wall a bond breaker was applied to reduce the coefficient of friction. Based on the damage levels observed in the abutment wall of Unit 2A, it was decided to post-tension the abutment wall in test Series III. Additional information will be provided in Section 5.3.

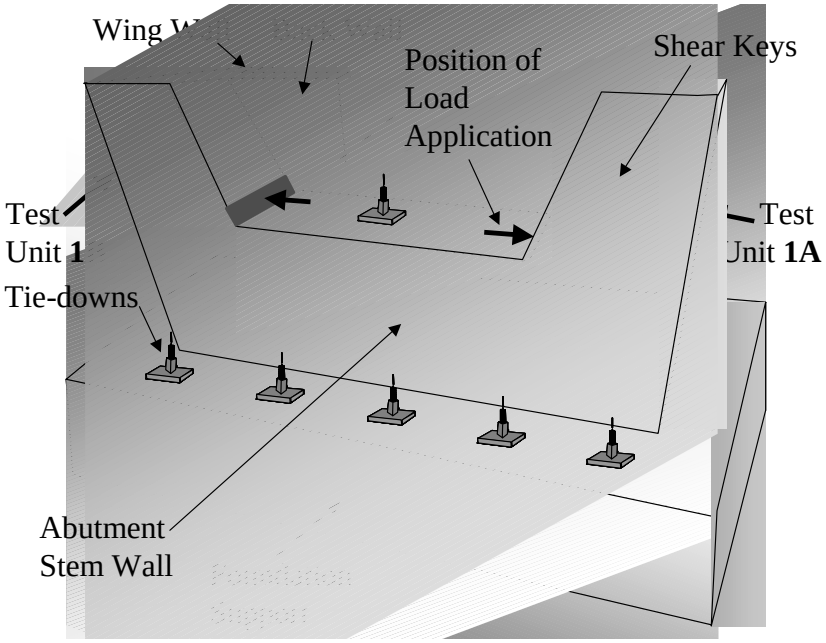

Figure 5.1 Test Units – Series I

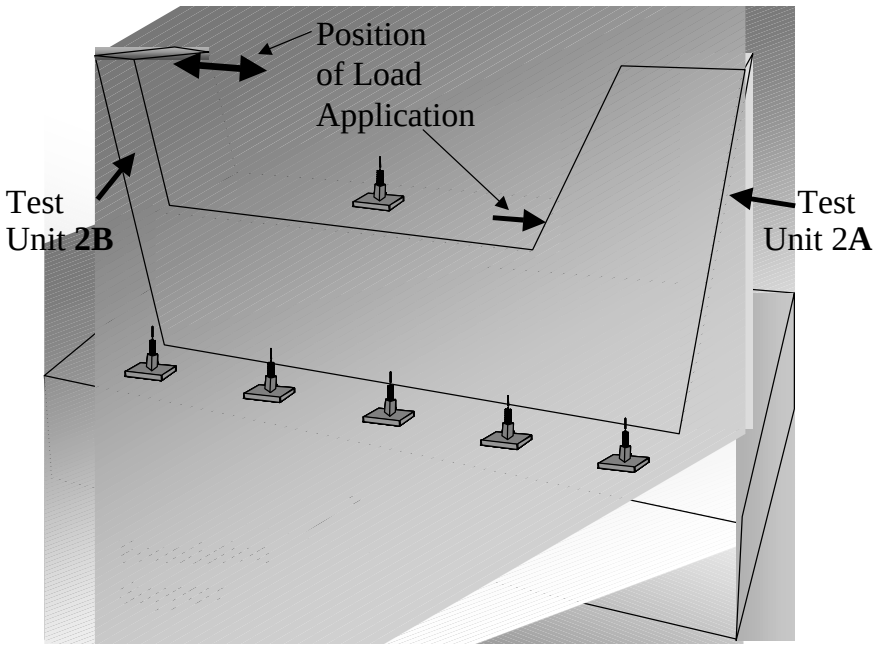

Figure 5.2 Test Units – Series II

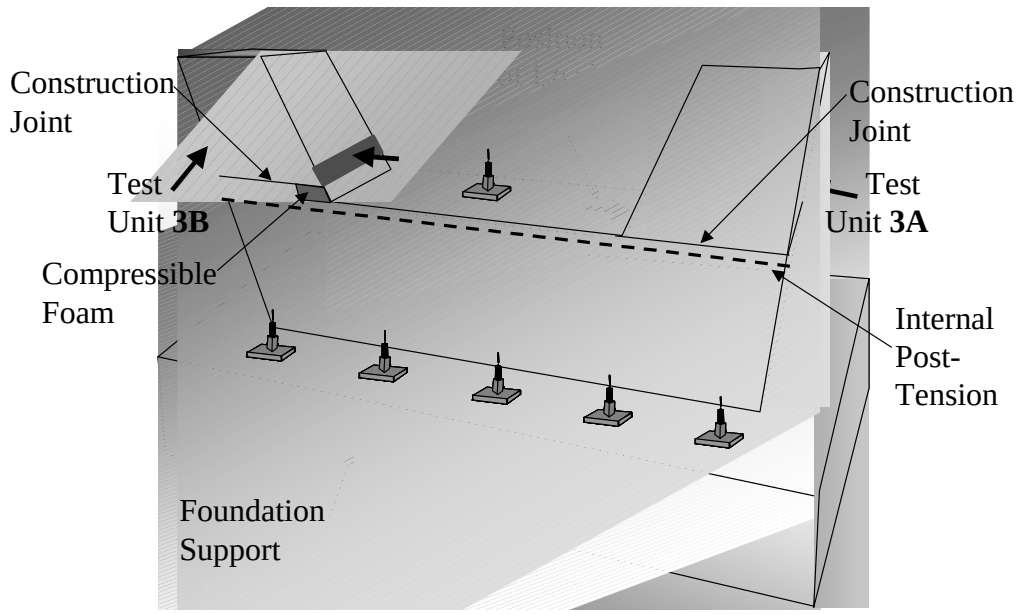

Figure 5.3 Test Units – Series III

5.2 Capacity Evaluation of Exterior Shear Keys

As for the interior shear keys, the capacity of the sacrificial exterior shear keys was evaluated based on the following models: (1) sliding shear friction model, (2) strut-and-tie analogy, and (3) moment-curvature analysis. These three models are described next.

5.2.1 Sliding Shear Friction Model

According to this model the capacity of the exterior shear keys, V_N, was based on:

$$V_N = \mu \left(A_{vf} f_{yf} + A_{vs} f_{ys} \right) \qquad \textbf{(5.1)}$$

Where μ is the coefficient of friction, taken as 1.4λ for concrete cast monolithically with λ = 1.0 for normal-weight concrete; A_{vf} and f_{yf} are, respectively, the area and the yield strength of the vertical shear reinforcement crossing the shear key-abutment stem wall interface. According to the Caltrans Design Specifications [2], the coefficient of friction is 1.0λ at the interface between two concrete elements cast on different days with a cold construction joint, such as in Units 2A, 3A and 3B. Also in Eq. (5.1) A_{vs} and f_{ys} are, respectively, the area and the yield strength of the vertical reinforcement on the sides of the abutment back and wing walls crossing the shear key-abutment stem wall interface.

As mentioned in Section 2.2.1 this model is based on the assumption that the shear key is cracked horizontally along its interface with the abutment stem wall, and V_N shall not exceed $0.2f'_cA_{cv}$ nor 800 A_{cv} (lb and in. units), regardless of the amount of reinforcement; where A_{cv} is the shear key-abutment contact interface area. The value of V_N is then multiplied by the strength reduction factor, ϕ (ϕ = 0.85).

5.2.2 Strut-and-Tie Analogous Model

Similar to the approach described in Section 2.2.2, the capacity of the designed exterior shear keys is calculated based on a response similar to a strut-and-tie behavior. According to this model the shear key capacity was calculated according to a strut-and-tie mechanism. The reinforcement is assumed to act as a tension member, or tie, with the concrete acting as compressive struts [12],[13].

Figure 5.4 schematically shows the diagonal concrete struts and the tie forces resisted by both horizontal and vertical reinforcement in the abutment stem wall. The figure shows a diagonal crack that develops in the abutment stem wall below the shear key. Based on experimental results, which will be presented in Chapter 6, this crack initiates at the shear key-abutment wall interface nearest the point of application of the lateral load. With further increase in the lateral load, the crack propagates diagonally downward until it reaches the base of the abutment wall, which is indicated as point A in Figure 5.4. The load is transferred from the shear key to the footing of the test unit by means of the diagonal compressive strut shown in Figure 5.4. The equations presented in this section were used to calculate the capacity of the exterior shear keys, and were developed based on equilibrium of the shear key along this diagonal crack. Using this model the capacity of the shear keys were:

$$V_N = V_C + V_S \qquad \textbf{(5.2)}$$

Where V_C and V_S are, respectively, the concrete and reinforcing steel contributions to the strength of the shear key. The concrete contribution, V_C, is given by:

$$V_C = \begin{cases} 2.4\sqrt{f_c^{'}}\, b\, h & (psi) \\ 0.2\sqrt{f_c^{'}}\, b\, h & (MPa) \end{cases} \qquad \textbf{(5.3)}$$

Where h is height of the abutment stem wall; b is width of the abutment stem wall and f_c' is the concrete compressive strength. For the test units of this experimental program, h = 30.5 in (775 mm); b = 16.75 in. (425 mm) and f_c' = 5,000 psi (34.5 MPa). This results in V_C = 87 kips (387 kN).

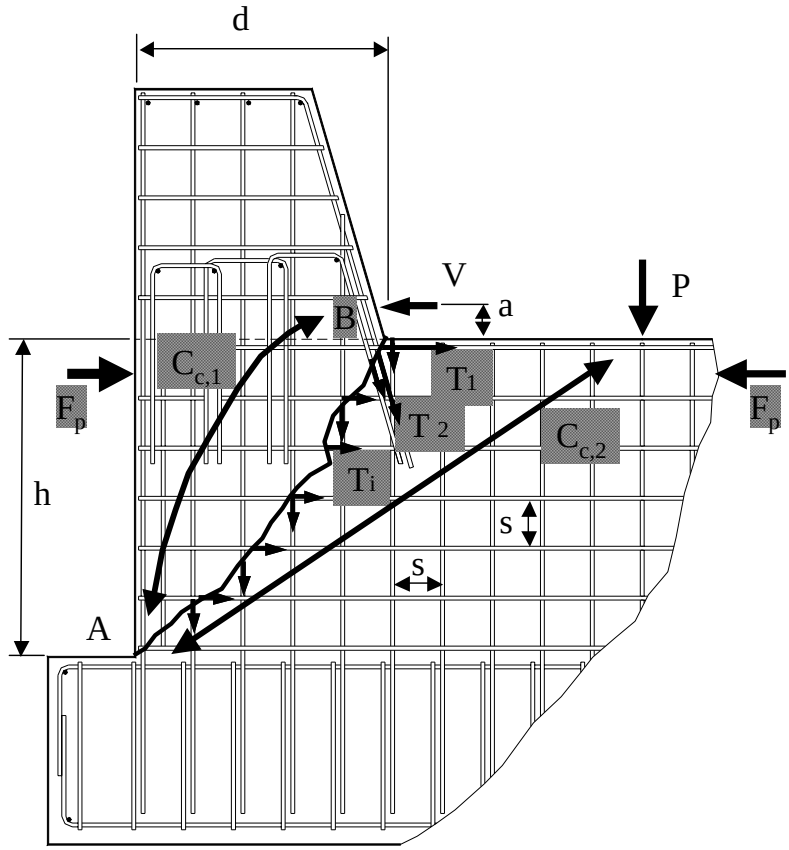

Figure 5.4 Exterior Shear Keys – Strut-and-Tie Analogous Model

The steel contribution to the capacity of the shear key, V_S, was obtained by equilibrium of the forces along the diagonal crack BA. The external forces are the applied lateral load, V, and the prestressing force, F_p, when the abutment wall is post-tensioned. Tensile forces in the reinforcing bars crossing the diagonal crack contribute to the steel resisting mechanism. The contribution of steel, V_S, is calculated by:

$$V_S = \left[F_p h_p + T_1 h + T_2 d + n_h T_{i,h} \frac{h^2}{2\,s} + n_v T_{i,v} \frac{d^2}{2\,s} \right] \left(\frac{1}{h+a} \right) \qquad \textbf{(5.4)}$$

Where $T_1 = A_{s,1}\ f_{y,1}$ is the force that can be developed by the tension tie, $T_2 = A_{s,2}\ f_{y,2}$ is the force that can be developed in the first row of steel bars crossing the shear key interface, n_h and n_v are the numbers of side faces with horizontal and vertical side reinforcement, (in Test Unit 1A, n_h and n_v is 2; in Unit 1B, n_h and n_v is 3; in Units 2A, 3A and 3B, n_h is 2 and n_v is 0), $T_{i,h} = A_{s,h}\ f_{y,h}$ and $T_{i,v} = A_{s,h}\ f_{y,v}$ are, respectively, the tensile forces on a single horizontal and vertical bar placed on the side faces of the abutment stem wall crossing the inclined crack, as shown in Figure 5.4. It is important to recognize that only the first line of shear reinforcement (i.e. T_2) is included in Eq. (5.4) because the remaining legs do not cross the inclined crack, and F_p is zero

when the abutment stem wall is not post-tensioned. In general $A_{s,h} = A_{s,v} = A_{s,s}$ and $f_{y,h} = f_{y,v} = f_{y,s}$; in this case Eq. (5.4) would be replaced by:

$$V_S = \left[F_p h_p + A_{s,1} f_{y,1} h + A_{s,2} f_{y,2} d + n_h \; A_{s,s} \; f_{y,s} \frac{h^2}{2\,s} + n_v \; A_{s,s} \; f_{y,s} \frac{d^2}{2\,s} \right] \left(\frac{1}{h+a} \right) \qquad \textbf{(5.5)}$$

Where $A_{s,1}$ is the total area of steel along the horizontal tension tie T_1 *(also known as hanger bars)*; $A_{s,2}$ is the total area of steel along T_2 (see Figure 5.4) and $A_{s,s}$ is the cross sectional area of the side reinforcement. For the test units of this experimental program, a = 4 in. (102 mm) and s = 4.75 in. (121 mm).

In this model it was assumed that the clamping force F_p is not adequate to prevent formation of the diagonal crack AB in Figure 5.4. In the redesign of Test Units 3A and 3B this post-tensioning force was designed with the main objective of preventing formation of this diagonal crack; in this case capacity of the shear key would be calculated using the shear friction model (Eq. (5.1)).

5.2.3 Moment-Curvature Analysis

For the exterior keys, this approach was only applicable to Test Unit 2B. In the moment-curvature analysis, the force equilibrium equations were written by equating the total compressive forces present in the concrete and reinforcing steel to the total tensile forces present in the reinforcing steel, given by [27]:

$$\sum C_C + \sum C_S^{'} = \sum T_S \qquad \textbf{(5.6)}$$

where at curvature, N, (see Figure 5.5), φC_c is the compression force in the concrete, φC_{si} ' is the compression force in the reinforcing steel, and φT_s is the tension force in the steel.

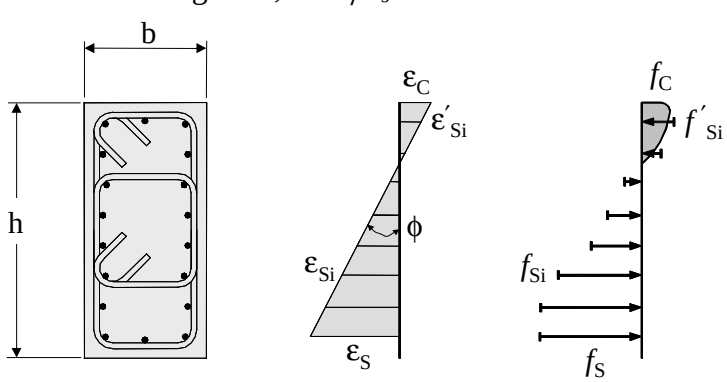

(a) Cross Section (b) Strain Diagram (c) Stress Diagram

Figure 5.5 Stress Block Design Parameters

The three models described in this chapter were used to calculate the capacity of the exterior shear keys. The calculated capacities are presented in Table 5.2. The reinforcement layout for all

the test units is described in the next sections. In calculating the shear keys capacity (see Table 5.2) a specified steel yield strength of 60 ksi (414 MPa) and concrete compressive strength of 5,000 psi (34.5 MPa) were assumed. The prestressing force of Units 3A and 3B was assumed to be 300 kips (1,335 kN).

Table 5.2 Calculated Capacity of Exterior Shear Key Test Units

Test Series	Test Unit	Vertical Steel Area Crossing Interface for Shear Friction		Steel Areas for Strut-and-Tie Model in.^{2} (mm^2)		V_N Shear Friction kips (kN) Eq. (5.1)	Strut-and-Tie Analogous Model kips (kN) Eq. (5.5)	
		No. of Bars	A_{vf} in.^{2} (mm^2)	$A_{s,1}$	$A_{s,2}$		V_S	V_N
I	1A	38 #3	4.18 (2697)	0.55 (355)	0.88 (568)	351 (1,561)	127 (565)	214 (952)
	1B	58 #3	6.38 (4,116)	0.55 (355)	0.88 (568)	536 (2,384)	190* (845)	277 (1,232)
II	2A	24 #3	2.64 (1,703)	0.66 (426)	0.44 (284)	158++ (703)	91** (405)	178 (792)
	2B	18 #5	5.58 (3,600)	1.32 (852)	-----	469 (2,086)	-----	68*** (303)
III	3A	8 #5	2.48 (1,600)	2.70 (1,742)	-----	149++ (663)	454+ (2,020)	541 (2,407)
	3B	8 #5	2.48 (1,600)	2.70 (1,742)	-----	149++ (663)	415+ (1,846)	502 (2,233)

* Contribution of vertical reinforcement in the abutment back wall and wing wall is included in calculation of V_S

** Because the side reinforcement is not continuous, V_S includes only the horizontal side reinforcement contribution term.

*** Capacity was obtained from a moment-curvature analysis.

+ Contribution of vertical reinforcement, A_{vf}, is considered in calculation of V_S.

++ Coefficient of friction, μ, is taken 1.0 λ (with λ = 1.0) because of the construction joint between the shear key and the abutment stem wall.

Analytical results presented in Table 5.2 indicate that for Units 1A and 1B, the calculated nominal shear key capacity, V_N, given by Eq. (5.2), which is based on the strut-and-tie analogous model, is considerably less than the sliding shear key capacity given by Eq. (5.1). This indicates that for these test units the inclined crack along the abutment stem wall (Figure 5.4) will dominate the performance of the shear key. Table 5.2 also indicates that failure of Unit 2B will occur by flexure rather than by sliding shear friction. If the abutment stem wall is post-tensioned, development of inclined cracks will not develop, because the post-tensioning force is adequate to prevent development of these cracks. Thus, for Units 3A and 3B seismic performance of the

shear keys will be dominated by sliding shear friction. The rational applied in the design of these test units (3A and 3B) was to minimize and localize damage in the abutment stem wall below the shear keys. These are two important aspects of shear key design because shear keys in the abutments act as structural fuses for protection of the abutment walls and piles, and post-earthquake repair is reduced if damage to the abutment wall is minimized and localized.

5.3 Overall Test Setup and Design of Test Units

The test setup was approximately the same for the three test series. The test setup was designed to realistically model the various bridge components that interact with an exterior shear key. As shown in Figure 5.6, the lateral load was applied to the key by a loading arm, which in turn was connected to the actuator. A hold-down frame was used to prevent any upward movement of the loading arm, which in a typical bridge represents the bridge end diaphragm.

Figure 5.6 Overall Test Setup for Exterior Shear keys

5.3.1 Design of the Test Units – Test Series I

Each specimen consisted of two exterior shear key test units designed at a 2/5-scale. Series I test units conformed to existing Caltrans abutment as-built bridge design details. One shear key was built without the abutment walls and was designated as Test Unit 1A, whereas the other shear key was designated as Test Unit 2B and was built with the abutment back and wing walls

coupled together with the exterior shear key, as illustrated in Figure 5.7 and Figure 5.8. Direct comparison between the lateral response of these two shear keys will be presented in Chapter 7.

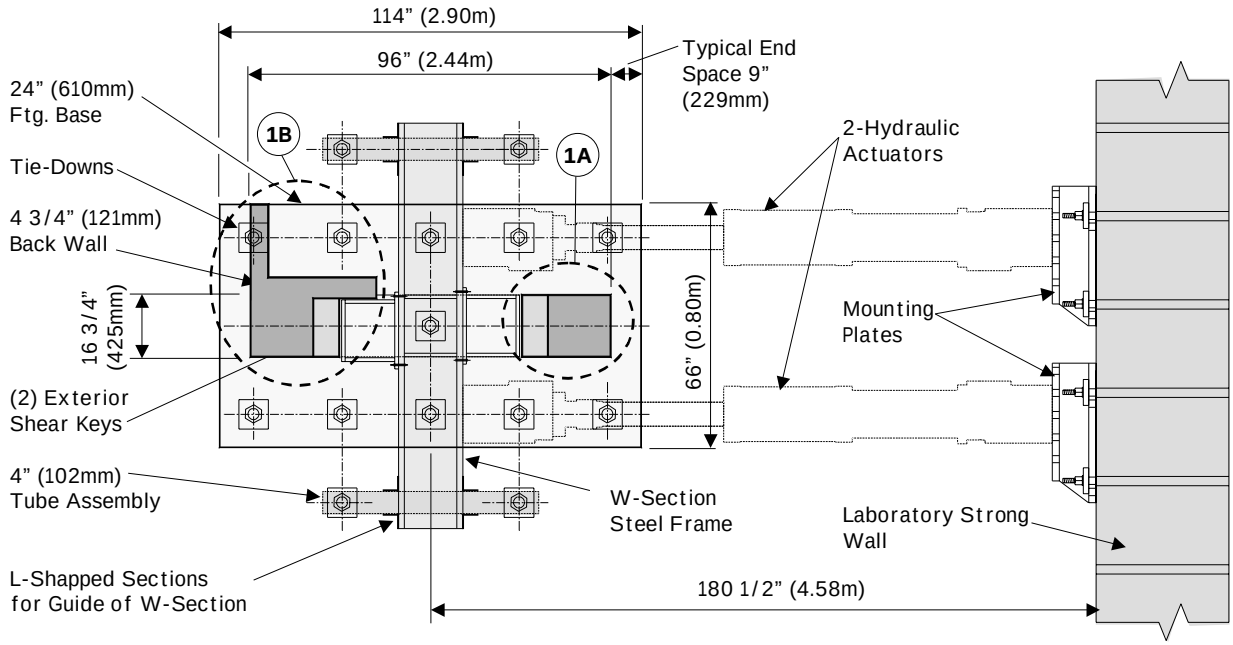

Figure 5.7 Plan View of the Test Setup of Exterior Shear Keys – Test Series I

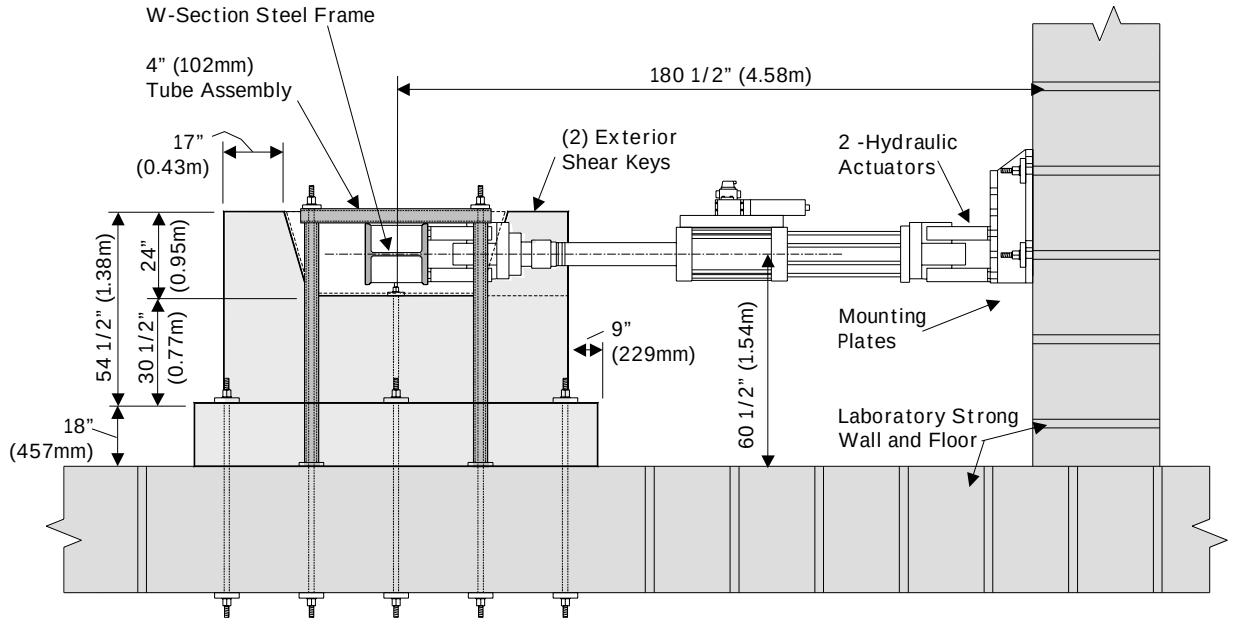

Figure 5.8 Elevation View of the Test Setup of Exterior Shear Keys – Test Series I

The simulated lateral load was applied to the test units, as seen in Figure 5.8, by means of two servo-controlled hydraulic actuators connected to a steel-loading frame. In order to support and

restrain the loading frame from any undesirable motions such as twisting and rising, two support steel frames were used, one at each end of the loading frame.

The foundation block was post-tensioned to the strong floor by using ten tie-down bars placed on the sides of the shear keys and one central tie-down bar to the top of the stem wall. Each of these high-strength bars was stressed to a force of 150 kips (667 kN); thus, a fixed condition was established between the footing and the laboratory strong floor. A typical bridge superstructure is supported transversely by exterior shear keys and the superstructure sits over square steel bearing pads, spaced along the abutment stem wall. A single tie-down high-strength bar (see Figure 5.8) was utilized at the middle of the test specimen to generate a downward force on the abutment stem wall of 150 kips (667 kN). This was to duplicate the vertical load corresponding to the tributary weight of the bridge superstructure at one of the bearing pads adjacent to the exterior keys.

5.3.1.1 Reinforcement Layout

As previously described, Series I test units conformed to existing Caltrans abutment as-built bridge design details. The steel reinforcement arrangement was scaled down to match a commonly used abutment design that was provided by Caltrans (see Figure 5.9 and Figure 5.10).

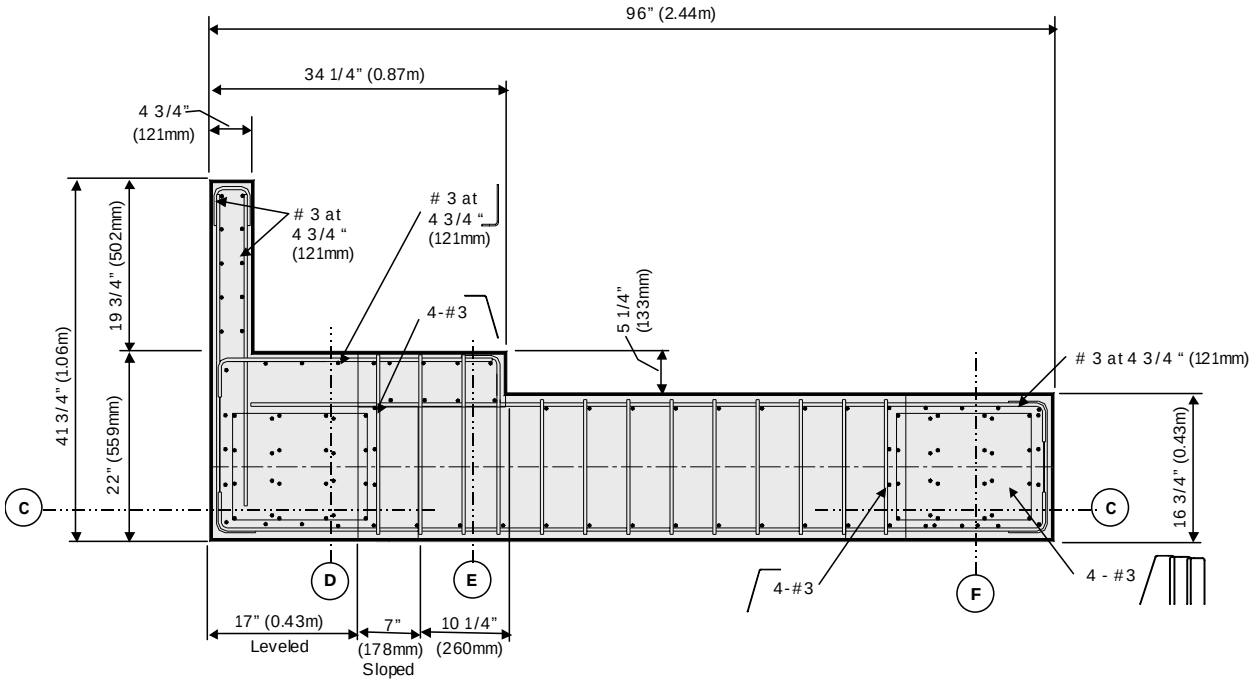

Figure 5.9 Plan View of the Reinforcement Layout – Test Series I

In Series I, the U-shaped shear reinforcement consisted of 4 rows each of 6- #3 bars. In addition, the horizontal reinforcement at the top level of the stem wall, which is often defined as the

tension tie [2], consisted of a single layer of 5-#3 bars, conforming to the minimum requirements specified by Caltrans. The horizontal and vertical reinforcement on the sides of the shear keys consisted of #3 bars at 4.75 in. (121 mm) on centers. For Test Unit 1B, the shear key and the abutment walls were coupled together internally with #3 bars at 4.75 in. (121 mm) on centers matching an integral as-built abutment wall. Figure 5.9 to Figure 5.13 show reinforcement details at different cross sections of the test specimen.

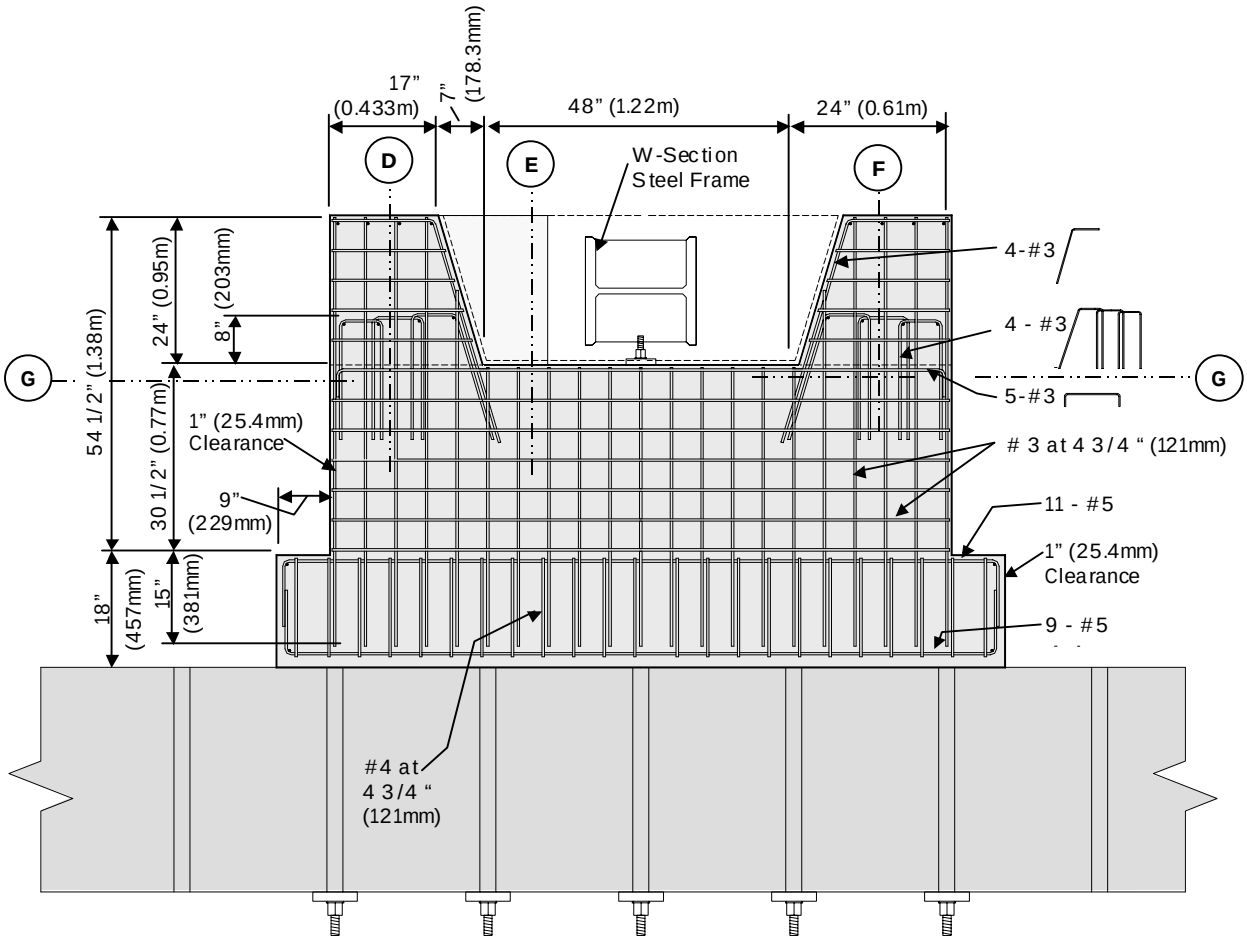

Figure 5.10 Elevation View of the Reinforcement Layout (Section C-C) –Test Series I

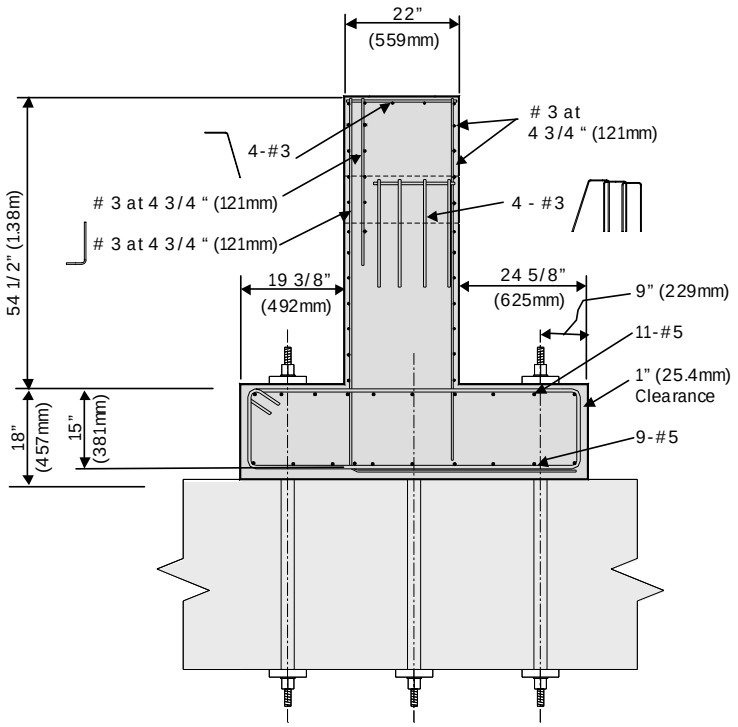

Figure 5.11 Reinforcement Layout (Section D-D) –Test Series I

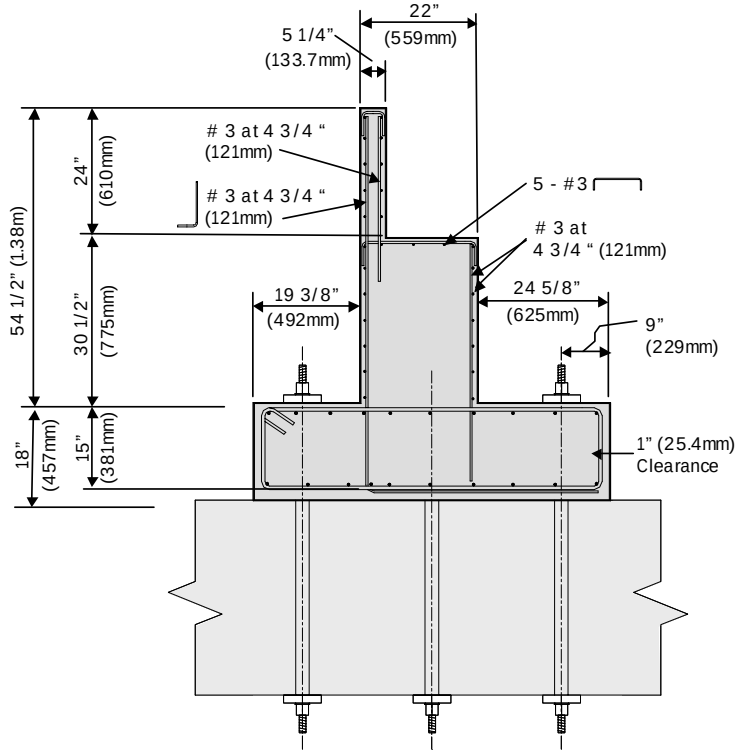

Figure 5.12 Reinforcement Layout (Section E-E) –Test Series I

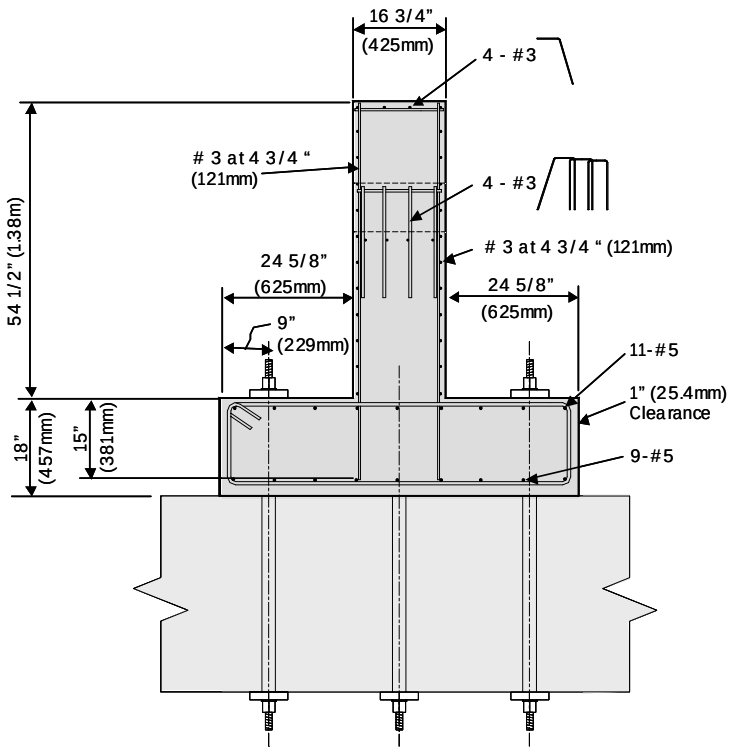

Figure 5.13 Reinforcement Layout (Section F-F) – Test Series I

5.3.2 Design of Test Units – Test Series II

As in Test Series I, Test Series II consisted also of two test units designed at a 2/5-scale. Test Unit 2A was a redesign of Test Unit 1A, and Test Unit 2B was designed to display a predominant flexure-shear response with the lateral load applied at the top of the key (see Figure 5.2). The test setup for Series II units was the same as the test setup for the Series I test units and is shown in Figure 5.14 and Figure 5.15.

The two test units of Series II were designed following testing of Test Series I units. As will be shown in Chapter 6, Test Unit 1A experienced severe damage in the abutment stem wall below the shear key. The applied lateral load, V, was transferred to the footing of the test unit through a diagonal concrete compression strut and resulted in the diagonal crack shown in Figure 5.4. The severe damage to the abutment stem wall of Unit 1A leads to difficult post-earthquake repair, and reconstruction of the abutment stem wall would be likely in this case.

The test units of Series II were constructed in three stages. The footing was constructed in the first stage followed by construction of the abutment stem wall and the flexural key of Test Unit 2B in the second stage. The top surface of the abutment stem wall was smoothly finished.

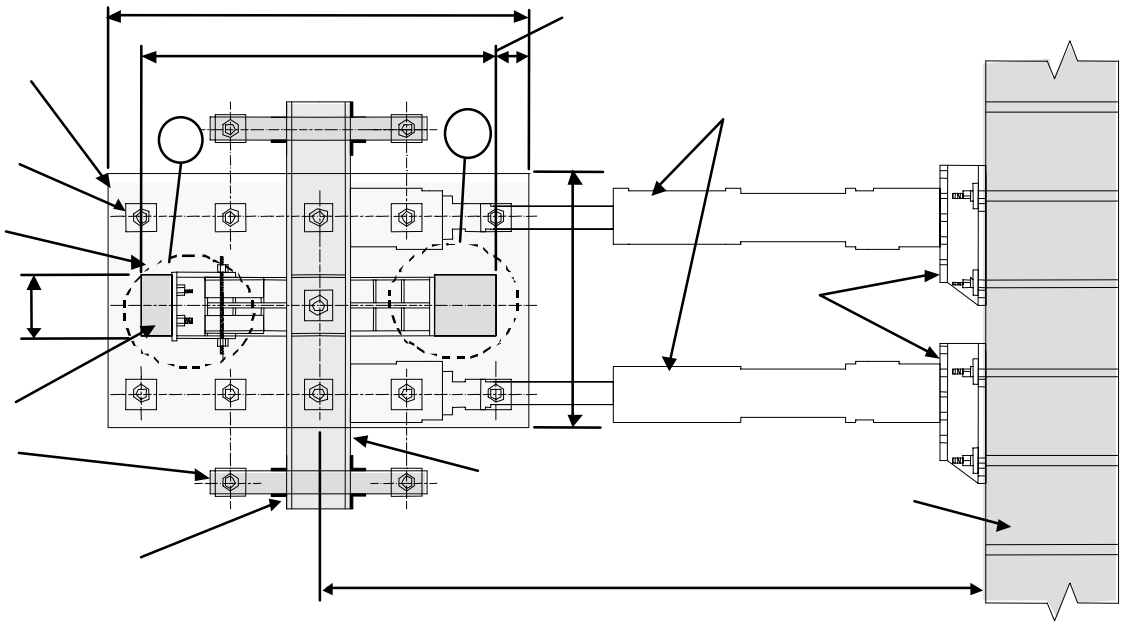

Figure 5.14 Plan View of the Test Setup of Exterior Shear Keys – Test Series II

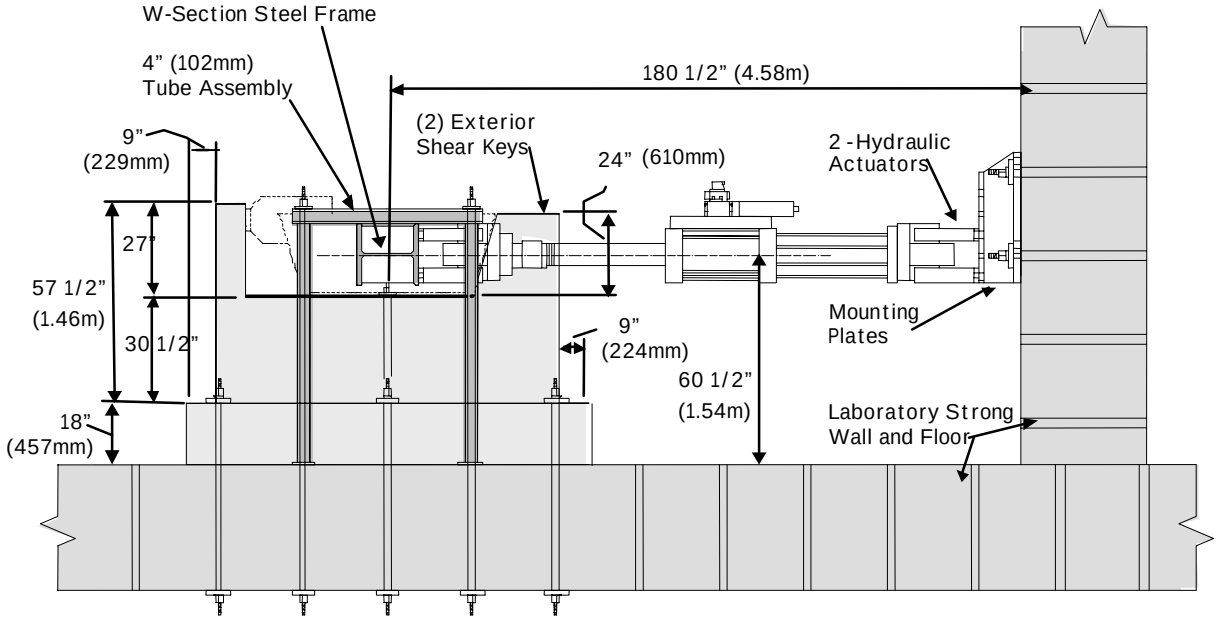

Figure 5.15 Elevation View of the Test Setup of Exterior Shear Keys – Test Series II

Hydraulic oil was placed on the top surface of the abutment wall; this was followed by construction of the shear key of Unit 2A. In the third construction stage, the shear key of Test Unit 2A was cast against the smooth finished surface of the abutment wall. The objective of

smooth finishing of the abutment stem wall and use of the hydraulic oil was to create a construction joint between the shear key and the abutment. It was sought that with the construction joint, the response of the shear key would be ductile and the damage will occur by sliding shear friction between the shear key and the abutment wall, which will reduce damage in the abutment wall and facilitate any required post-earthquake repair without difficulty.

5.3.2.1 Reinforcement Layout

Test Unit 2A was a redesign of Unit 1A with the variable being the detail at the interface between the shear key and the abutment stem wall. Plan view of reinforcement of the shear keys and the abutment stem wall is shown in Figure 5.16.

The shear key was connected to the abutment wall by 24-#3 vertical reinforcing bars arranged in four rows, whereas the vertical reinforcement of the abutment wall stopped below the shear key-abutment stem wall interface, as shown in Figure 5.17 and Figure 5.18. The horizontal tensile tie reinforcement (to resist force T_1 in Figure 5.4) consisted of 6-#3 bars, as shown in Figure 5.16. Other reinforcement details are shown in Figure 5.19 to Figure 5.21.

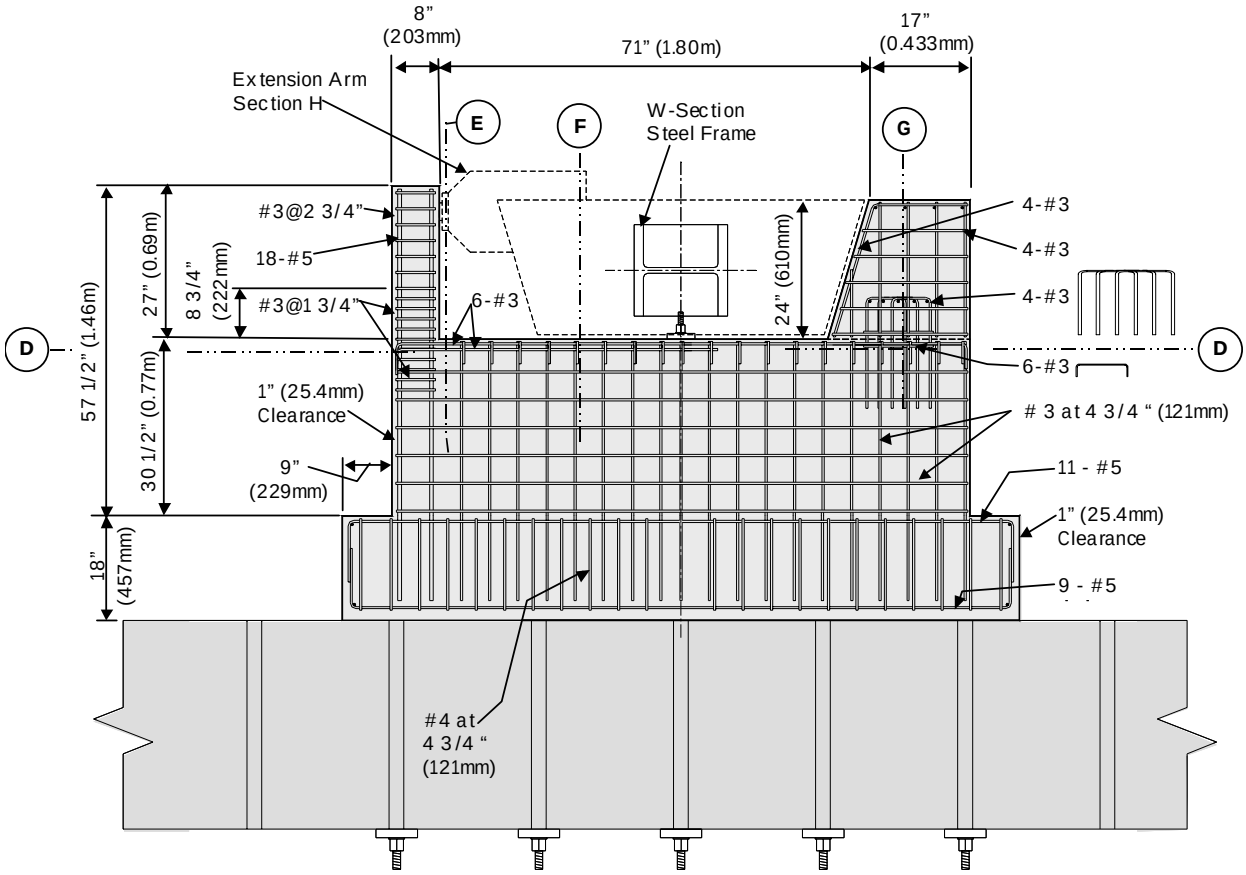

Figure 5.16 Elevation View of the Reinforcement Layout (Section C-C) – Test Series II

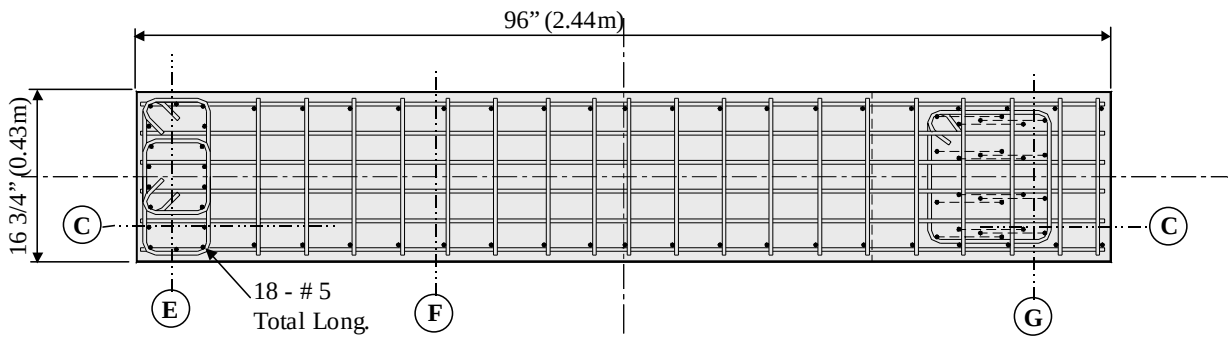

Figure 5.17 Plan View of the Reinforcement Layout – Test Series II

As mentioned earlier, Unit 2B was designed to display a predominant flexure-shear response. The flexural key of Unit 2B was monolithically constructed with the abutment stem wall. Vertical reinforcement of the flexural key consisted of 18-#5 bars as shown in Figure 5.17 and Figure 5.18. The depth of the shear key was reduced from 24 in. (610 mm) in Units 1A, 1B and 2A to 8 in. (203 mm) in Unit 2B so that the flexural key of Unit 2B would display a flexural response. For the same reason, the lateral load was applied at the top of the flexural key, as shown in Figure 5.2. In order to prevent buckling of the longitudinal reinforcement, provide adequate confinement to the section core where a plastic hinge is expected to form, and prevent shear failure, the flexural key was transversely reinforced with #3 closed stirrups, as shown in Figure 5.17 and Figure 5.18. Reinforcement of the horizontal tie of the abutment stem wall (tie resisting the force T_1 in Figure 5.4) was also increased to 12-#3 bars to control cracking of the abutment stem wall.

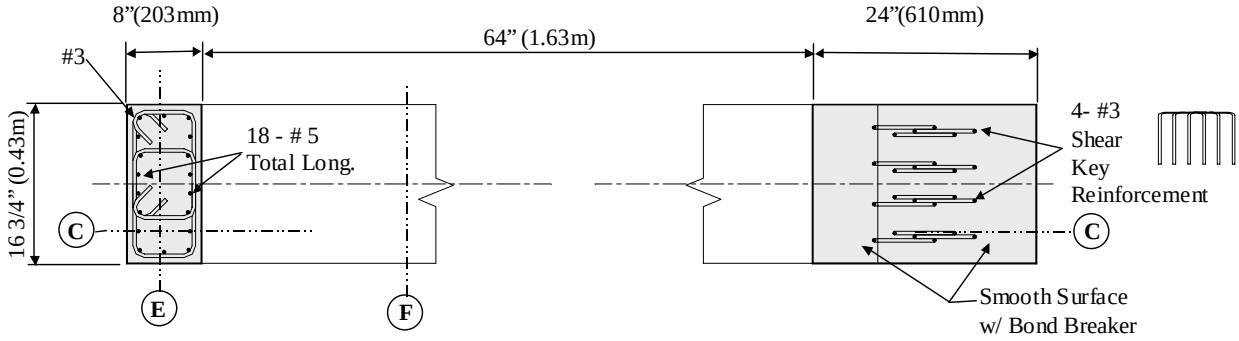

Figure 5.18 Reinforcement Layout (Section D-D) – Test Series II

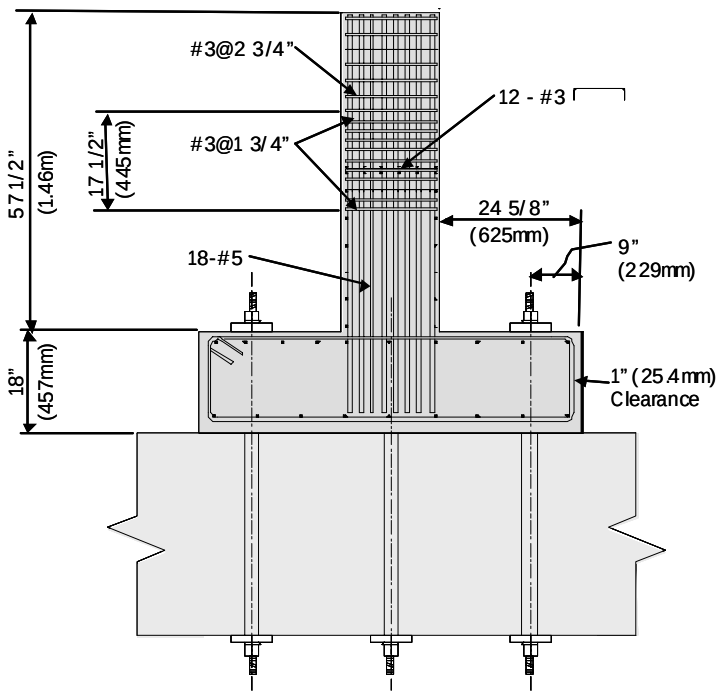

Figure 5.19 Reinforcement Layout (Section E-E) –Test Series II

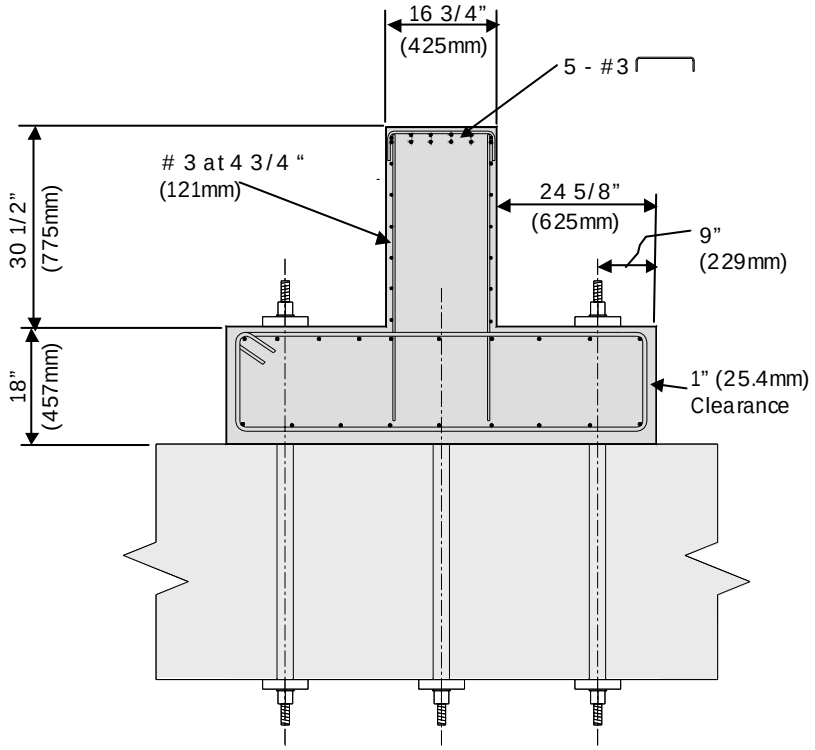

Figure 5.20 Reinforcement Layout (Section F-F) – Test Series II

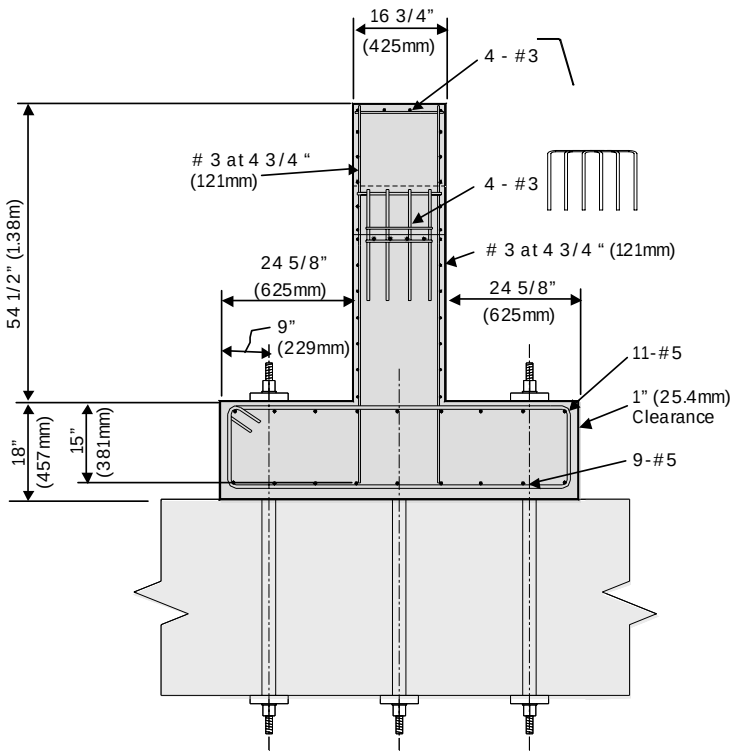

Figure 5.21 Reinforcement Layout (Section G-G) – Test Series II

As for Units 1A and 1B, the lateral load, V, was applied at the bottom end of the shear key of Test Unit 2A. However, the lateral load was applied in Unit 2B at the top of the sacrificial key (see Figure 5.2) so that the key would display a predominant ductile flexural response. The steel loading arm was modified to facilitate loading at top of the key of Unit 2B. A steel bracket consisting of two side plates were attached to the loading arm by high-strength bolts. The bracket was welded to a steel plate; this steel plate was connected to the top of the key by means of threaded rods, which were installed in the formwork before concrete casting of the key. Details of the loading fixtures for Test Unit 2B are shown in Figure 5.22.

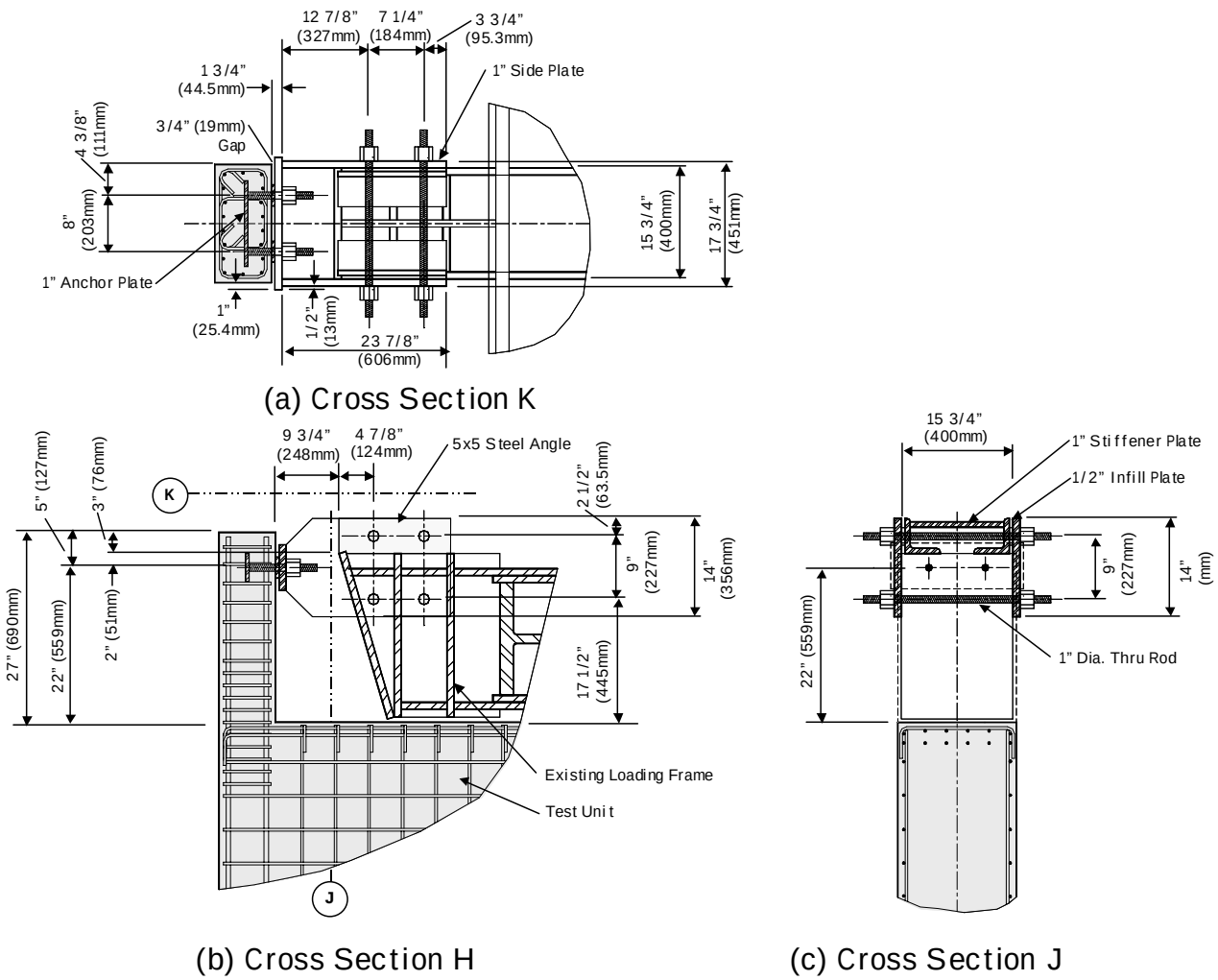

Figure 5.22 Details of Loading Arm of Test Unit 2B

5.3.3 Design of Test Units – Test Series III

As it will be shown in Chapter 6, the cold construction joint between the shear key and the abutment stem wall in Unit 2A was useful in improving the ductility of the shear key, but significant damage of the abutment stem wall could not be prevented. It is expected that damage of the abutment stem wall could be controlled by increasing the amount of tension tie reinforcement (hanger bars) in the abutment stem wall. However provision of excessive amount of hanger bars would not prevent diagonal cracking in the abutment stem wall (shown in Fig. 5.4). This diagonal crack could be avoided only by post-tensioning of the abutment stem wall. As before, Test Series III consisted also of two test units, which were a redesign of Test Unit 2A. The same area of vertical reinforcement between the shear key and the abutment stem wall were also used in Units 3A and 3B. Figure 5.23 and Figure 5.24 show the concrete dimensions of Test Units 3A and 3B. The abutment stem wall was post-tensioned in the transverse direction, with

respect to the longitudinal axis of the superstructure, by means of two 1 3/8 in. (35 mm) diameter high-strength bars, which were placed inside 2 in. (50.8 mm) PVC ducts (see Figure 5.23).

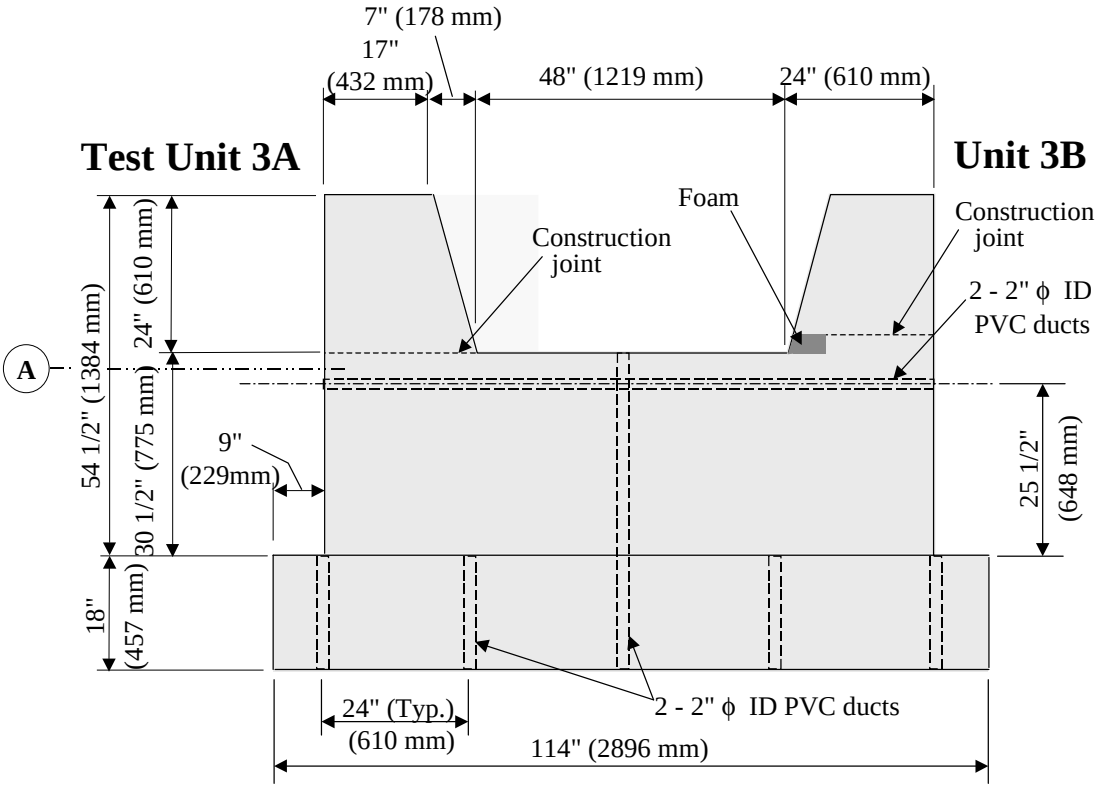

Figure 5.23 Concrete Dimensions of Test Series III Units – Elevation View

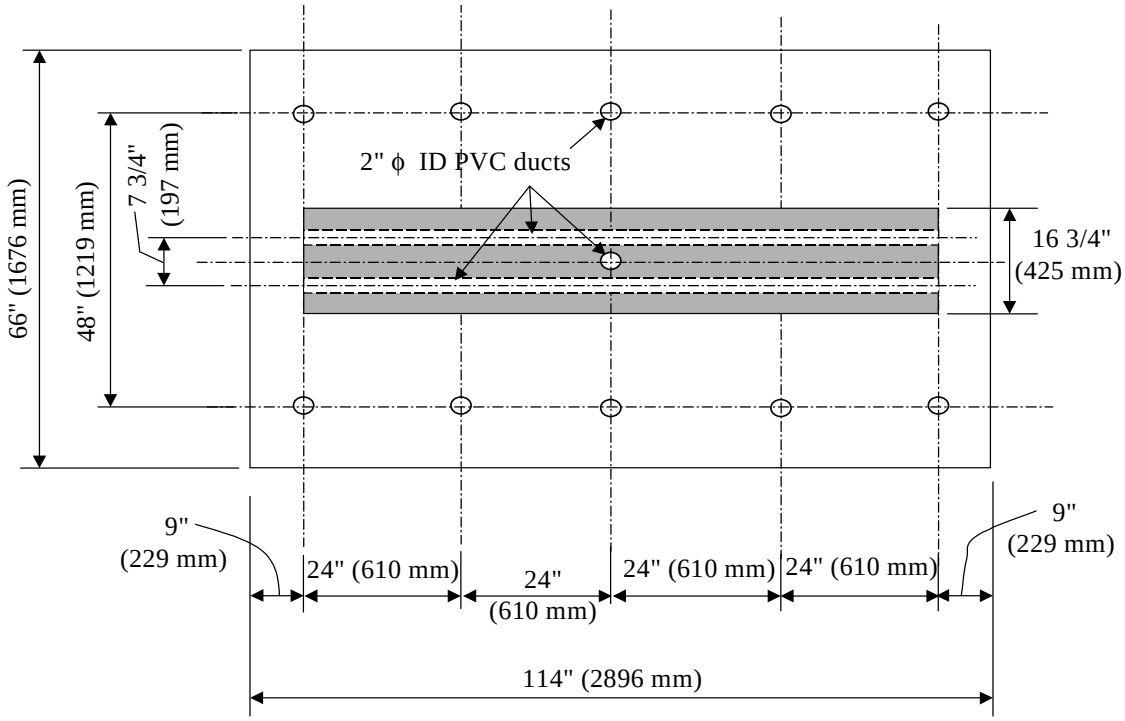

Figure 5.24 Concrete Dimensions of Test Series III Abutment Stem Wall – Plan View

It should be mentioned that the PVC ducts were not grouted, which means that internal unbonded bars achieved post-tensioning of the abutment stem wall. The post-tensioning force, *Fp*, was chosen to be equal to the highest expected lateral load on the shear key; this was estimated using Eq. (4.3) based on the concrete cracking strength assuming that the exterior key would fail in a similar way to the interior keys presented earlier. Assuming concrete compressive strength of 5,000 psi (34.5 MPa), the prestressing force, P, should be about 320 kips (1,423 kN). As for Unit 2A, in the shear keys of Units 3A and 3B a cold construction joint was provided between the shear key and the abutment stem wall interface.

Construction was completed in three stages. The footing was constructed in the first stage followed by construction of the abutment stem wall, in the second stage. The top surface of the abutment stem wall was smoothly finished. Hydraulic oil, intended to be a bond breaker, was placed on the top surface of the abutment stem wall before placement of the reinforcement cage and formwork of the shear key Units 3A and 3B. Location of the cold construction joints between the shear keys and the abutment stem wall is indicated in Figure 5.23 by the horizontal dashed lines.

A protrusion in the abutment stem wall of Unit 3B was provided in order to move the sliding failure plane farther away from the top surface of the stem wall (see Figure 5.23). The shear key-abutment stem wall interface in Unit 3B was 3 inches (76 mm) higher than the top surface of the abutment stem wall. Styrofoam was placed at the toe of the shear key and across its full width in Unit 3B as shown in Figure 5.23. The purpose of this detail was to create a weak plane along the shear key-abutment wall interface; thus a horizontal crack would develop along the interface and to have a sliding shear failure between the shear key and the abutment wall rather than diagonal cracking of the abutment stem wall (Figure 5.4).

5.3.3.1 Reinforcement Layout

In each of Units 3A and 3B, the shear key was connected to the abutment wall by means of 8-#5 headed bars with a total area of 2.48 in.^{2} (1600 mm^2). These reinforcing bars will be referred to throughout this report as the shear key reinforcement. The shear key reinforcement of Units 3A and 3B is comparable to that of Unit 2A, which had 24-#3 bars with a total area of 2.64 in.^{2} (1703 mm^2). The shear key reinforcement was placed in the formwork before concrete casting of the abutment stem wall. Fewer bars were used in Units 3A and 3B to facilitate easy smooth finishing of the abutment stem wall at the location of the shear keys, which were constructed in the third stage.

The shear key reinforcement as well as the high-strength bars used for post-tensioning of the abutment wall are shown schematically in Figure 5.25 for Units 3A and 3B. The figure shows that each of the shear key reinforcing bars in Unit 3B was spliced at the location of shear key-abutment wall interface by means of a mechanical coupler. The design objective is to design the sacrificial shear keys as structural fuses. With post-tensioning, damage could be minimized to the abutment wall and the failure would occur by sliding of the shear keys. If severe damage occurs during an earthquake, the shear keys can be demolished and new ones constructed on the repairable abutment wall. The purpose of the couplers is to facilitate easy removal of the damaged shear key reinforcement and installation of new bars with threaded ends inside the couplers followed by construction of the new shear key.

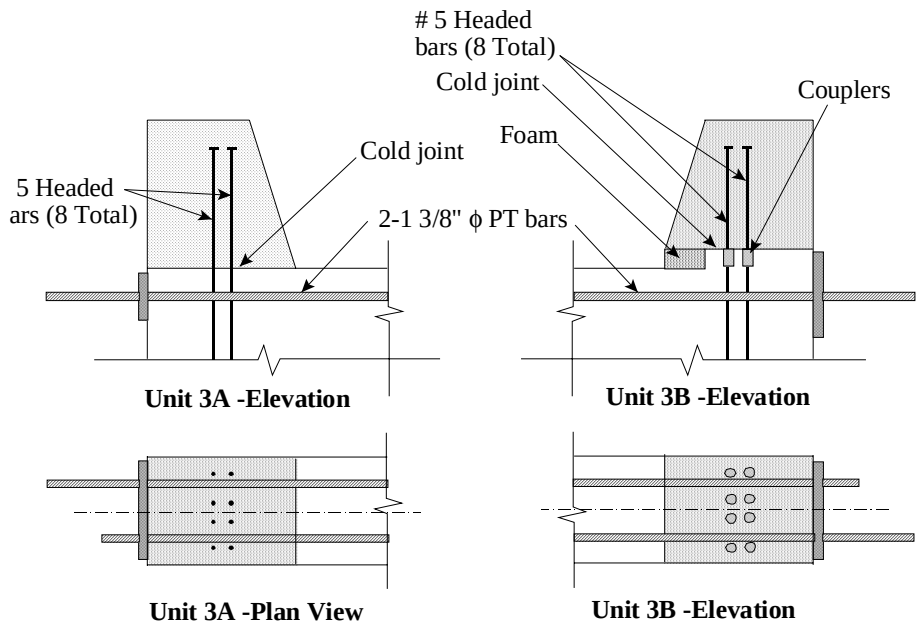

Figure 5.25 Schematic Drawing of the Shear Key Reinforcement of Units 3A and 3B

Figure 5.26 to Figure 5.32 show the reinforcement details of Test Series III units. Abutment wall reinforcement of Series III units was the same as for Unit 2A except for the horizontal tie reinforcement (to resist force T_1 in Figure 5.4), which were increased to 8-#5 bars to control any cracking that could develop in the abutment wall. Also, additional 8-#5 headed vertical bars were placed in the abutment wall below the shear key toe of Units 3A and 3B (bars designated as VW in Figure 5.32). Linear elastic finite element analyses and a strut-and-tie model indicated relatively high vertical tensile force in the abutment wall below the shear key toe; thus the above mentioned 8-#5 headed bars were placed to resist these tensile forces and to control possible cracks in the abutment wall.

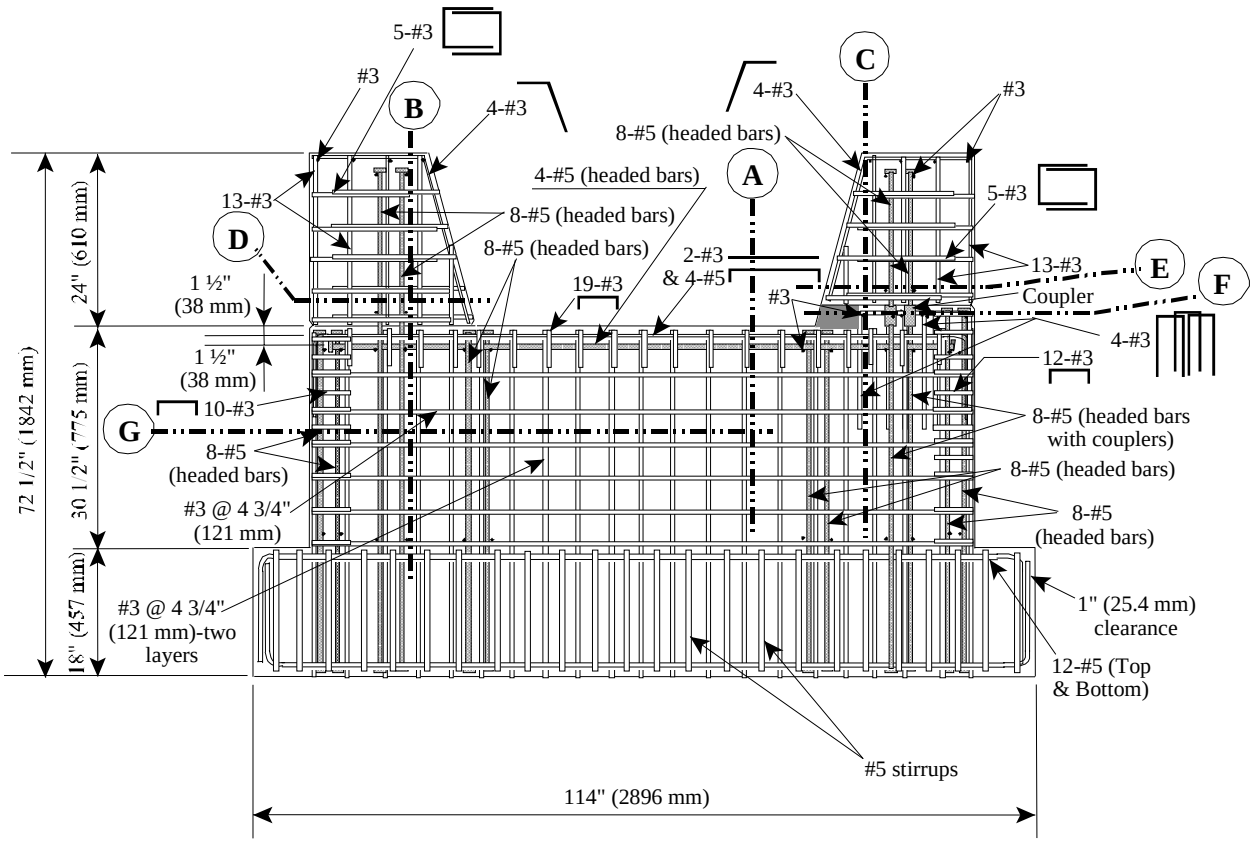

Figure 5.26 Elevation View of the Reinforcement Layout – Test Series III

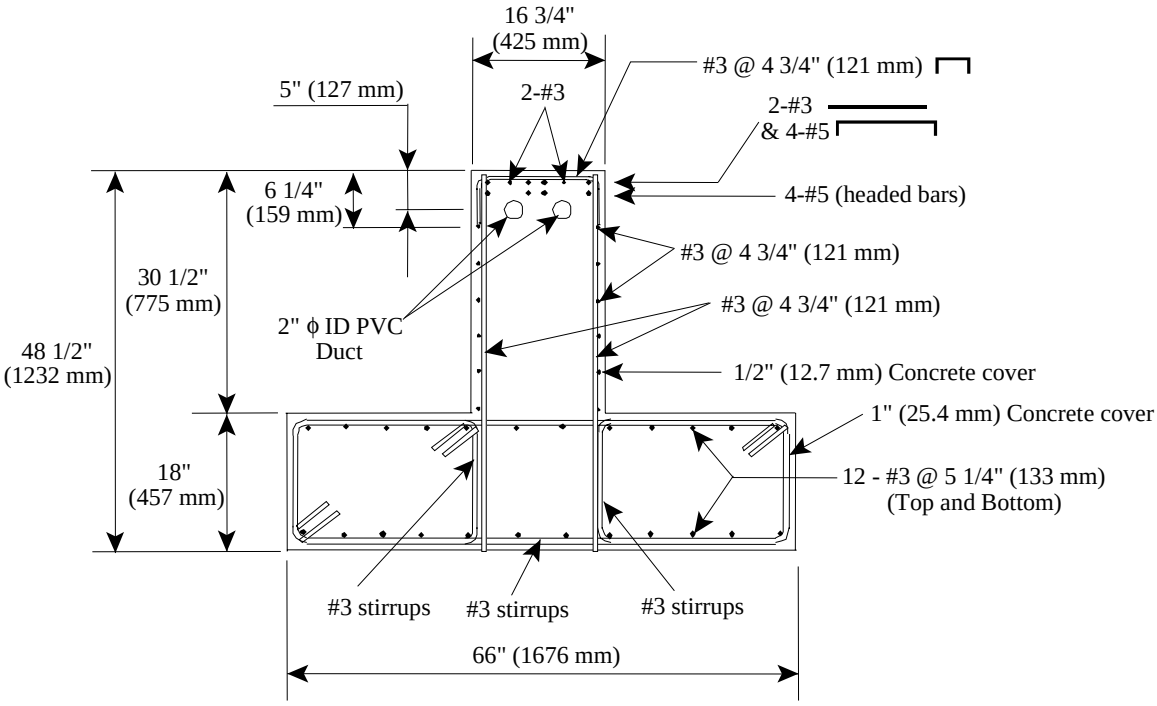

Figure 5.27 Reinforcement Layout (Section A-A) – Test Series III

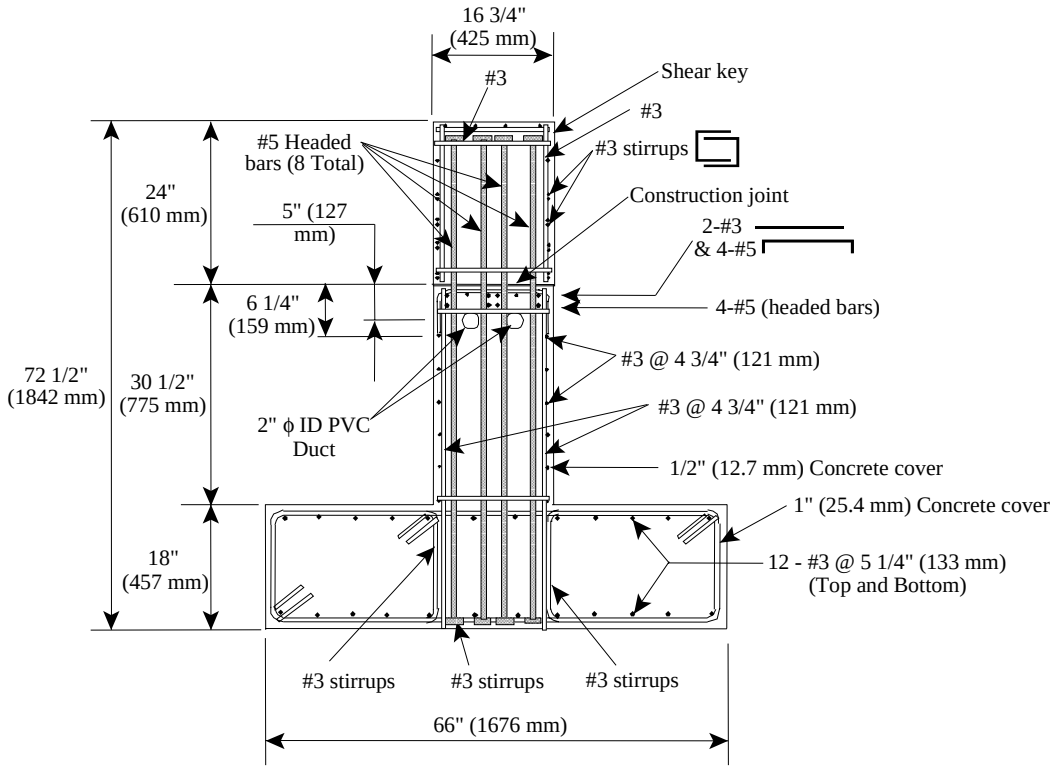

Figure 5.28 Reinforcement Layout (Section B-B) –Test Series III

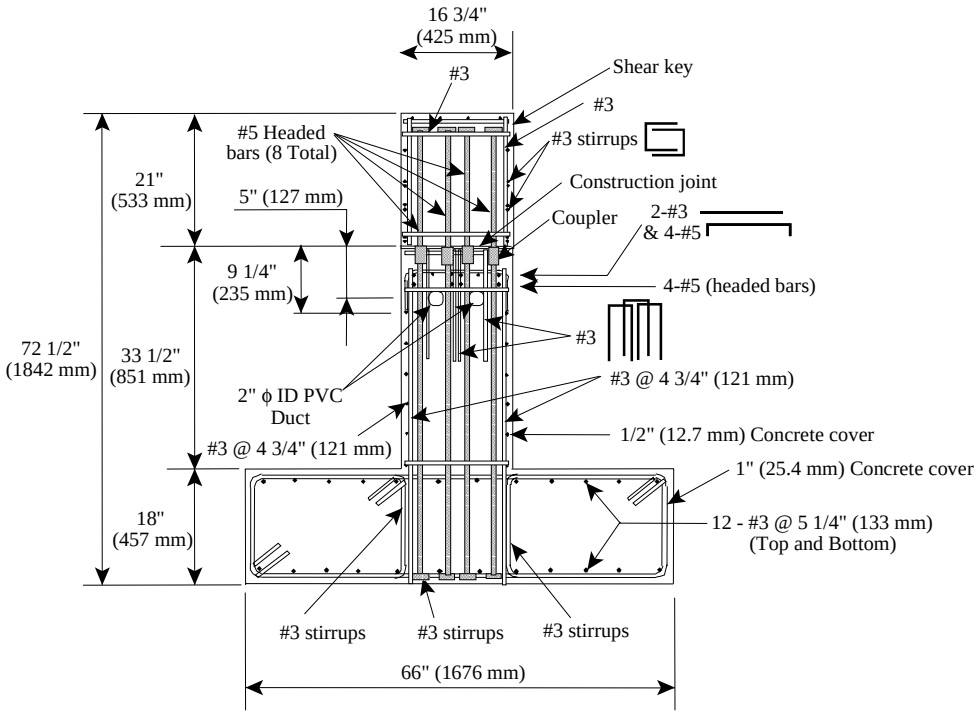

Figure 5.29 Reinforcement Layout (Section C-C) – Test Series III

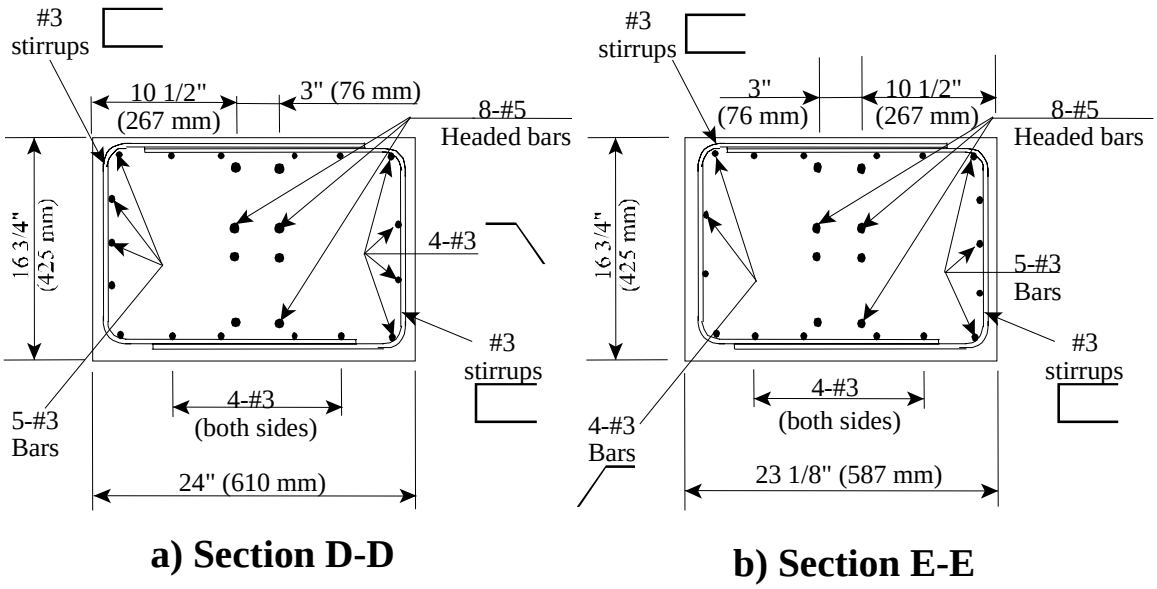

a) Section D-D **b) Section E-E**

Figure 5.30 Layout of Vertical Reinforcement of the Shear Keys – Test Series III

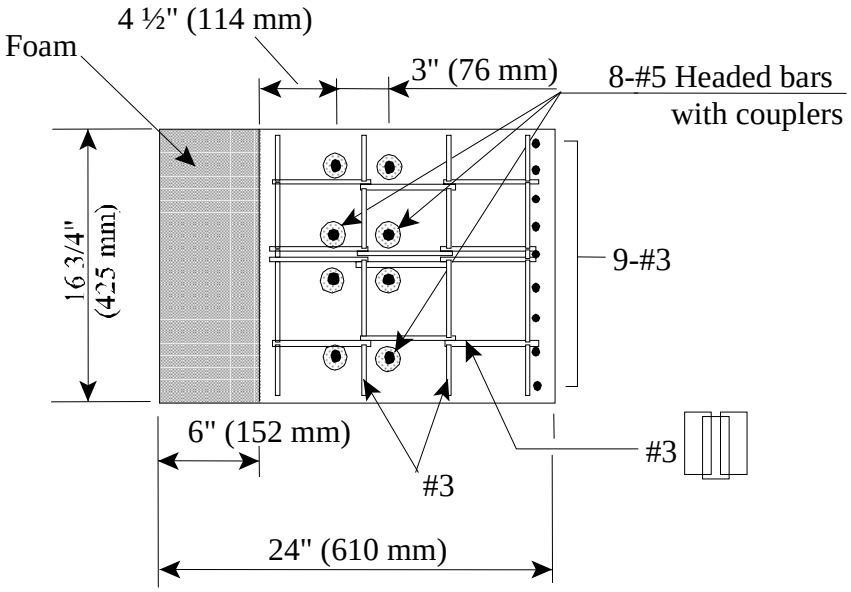

(3 inches below the construction joint)

Figure 5.31 Reinforcement Layout (Section F-F) – Test Series III

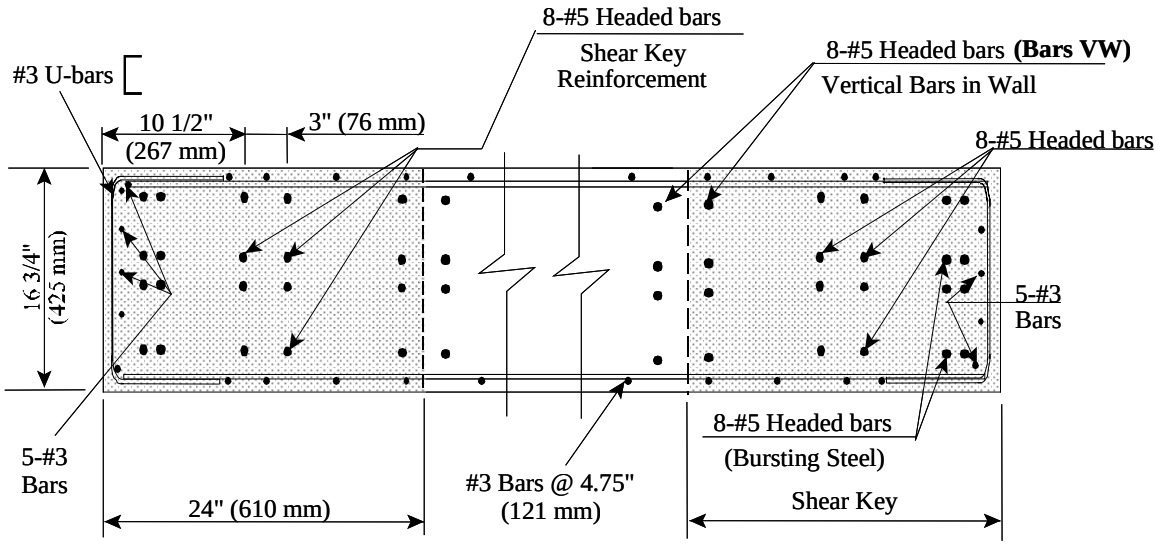

Figure 5.32 Reinforcement Layout (Section G-G) – Test Series III

5.4 Instrumentation of the Test Units

Instrumentation used for testing of the exterior shear keys is described in this section. Electrical resistance strain gages were used to record strains in the reinforcement, linear potentiometers were used to record displacements and rotations of the shear keys, and load cells were used to record the post-tensioning force in the high-strength bars in Units 3A and 3B. This section presents a summary of the instrumentation setup.

5.4.1 Test Series I

Both strain gages and displacement transducers were essential instruments during the testing of the shear key abutment. Strain gages were implemented in the rebar areas subjected to potential high strains, whereas displacement measurements were placed at locations of high displacement or to monitor undesirable movements of the test unit.

5.4.1.1 Strain Gages

A concentration of strain gages along the legs of the U-shaped shear reinforcement in each of the two shear keys can be viewed in Figure 5.33. Due to the fact that there were some uncertainties on how the wall would influence the capacity of the shear key, several strain gages were applied in strategic locations in both the back wall and wing wall of the test unit. Locations of wall rebar strain gages are shown in Figure 5.34. In addition to the shear reinforcement gages, strain gages were also positioned along two of the five tension tie bars (see Figure 5.35).

5.4.1.2 Displacement Transducers

Displacement measuring devices were utilized in both shear key tests. For both keys, displacements were recorded along the centerline of the key at the top and the interface levels, as illustrated in Figure 5.36. In addition, two more devices were installed to measure the movement of the wing wall. Labels of potentiometers are given in Figure 5.37.

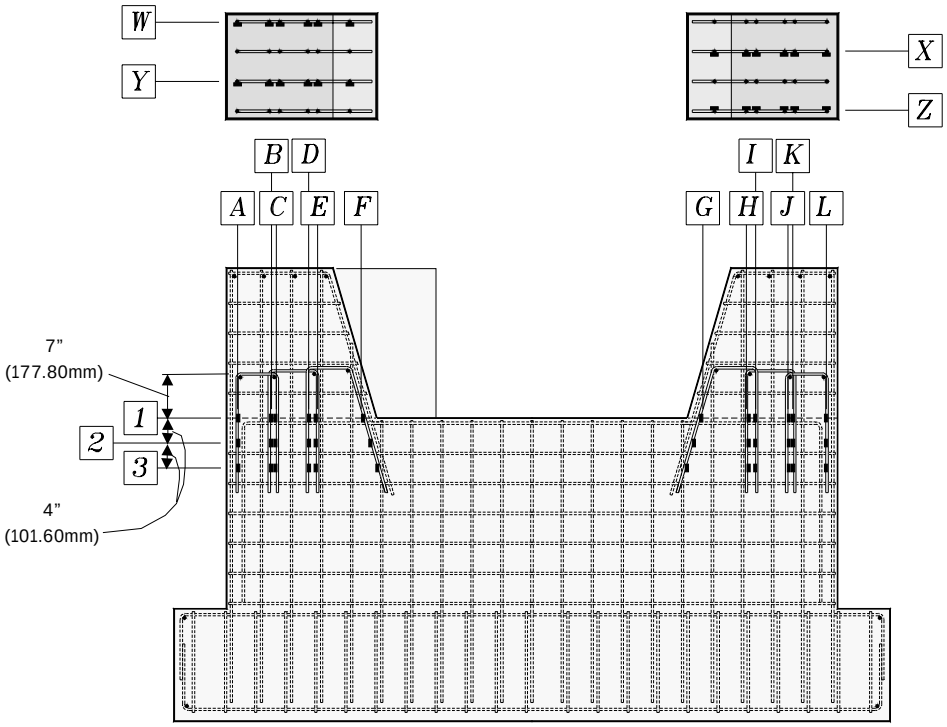

Figure 5.33 Locations of Strain Gages in Shear Key Reinforcement – Test Series I

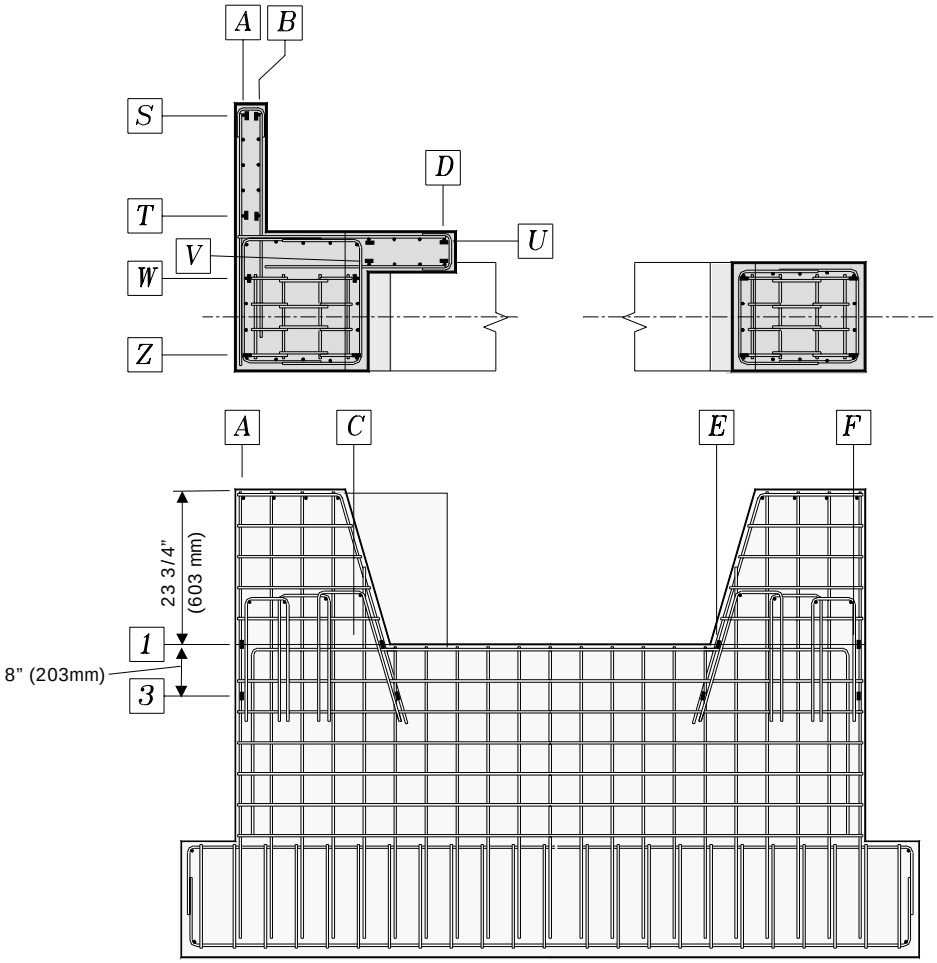

Figure 5.34 Locations of Strain Gages in Vertical Bars of Wing Wall and Back Wall – Test Series I

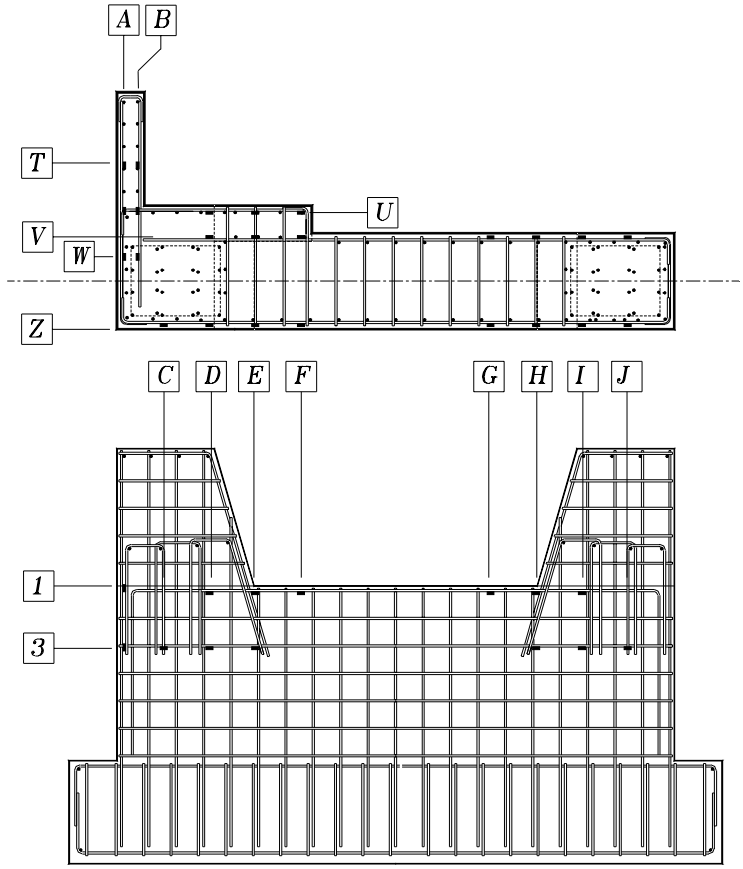

Figure 5.35 Locations of Strain Gages in Horizontal Reinforcement of the Abutment Stem Wall – Test Series I

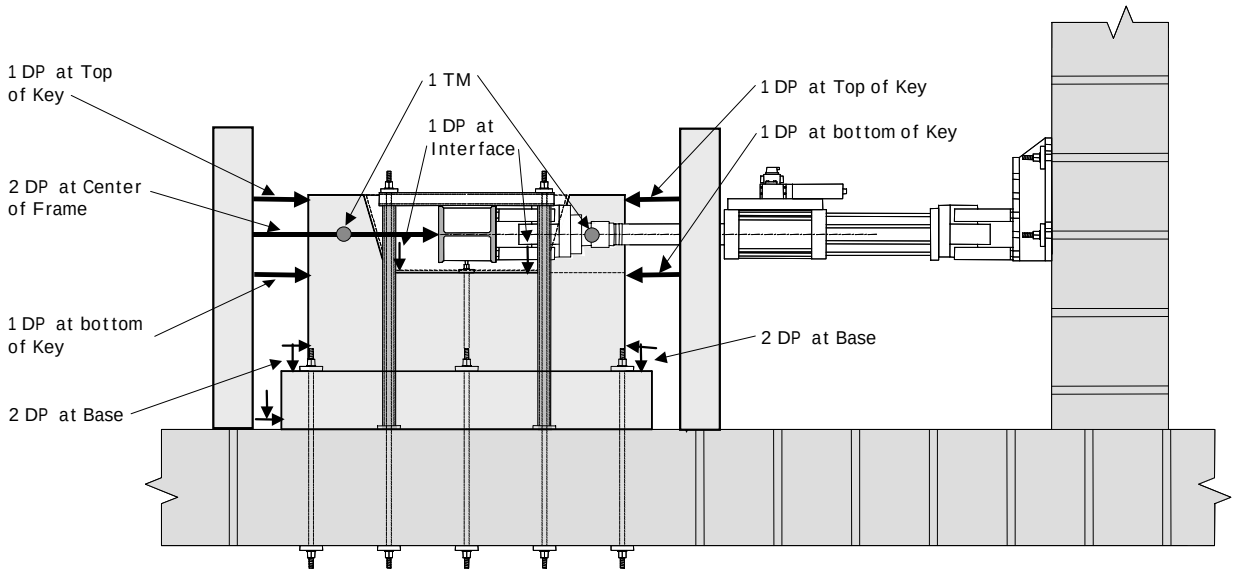

Figure 5.36 Layout of Displacement Transducers – Test Series I

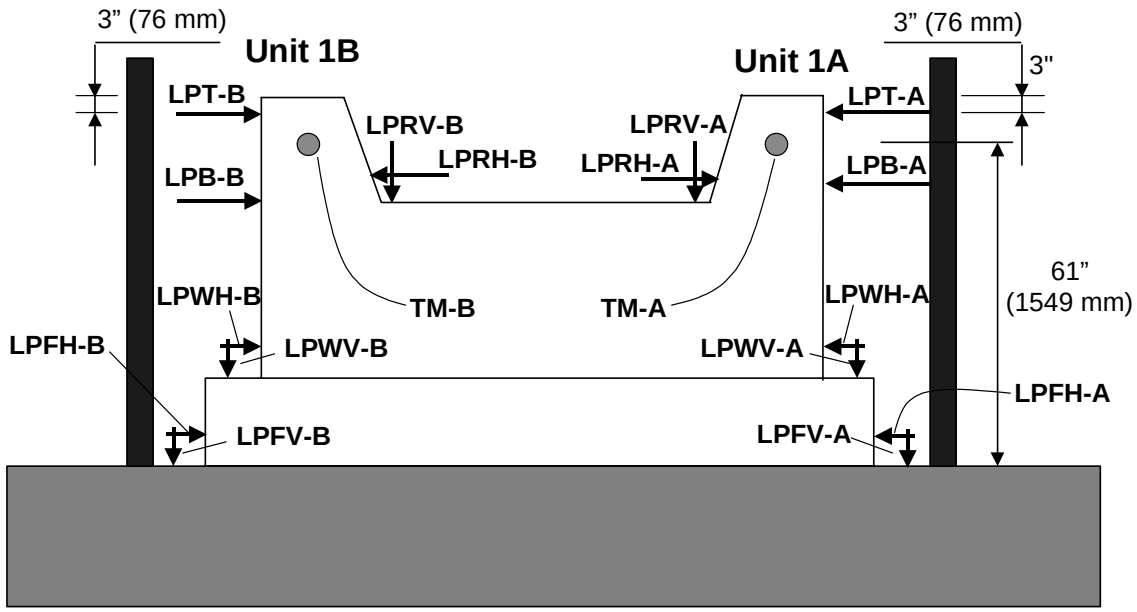

Figure 5.37 Labels of Displacement Transducers – Test Series I

5.4.2 Test Series II

5.4.2.1 Strain Gages

As for Units 1A and 1B, several strain gages were placed on the legs of the U-shaped shear reinforcement in the shear key of Test Unit 2A. Electrical resistance strain gages were also placed along the vertical reinforcing bars of the flexural key of Test Unit 2B; these strain gages were concentrated around the location of the sacrificial flexural key-abutment stem wall interface, in which the plastic hinge was expected to occur. Strain gages were also placed on the horizontal tie reinforcement (tie to resist tensile force T_1 in Figure 5.4). Locations of strain gages will be shown in Chapter 6 in presentation of the experimental results.

5.4.2.2 Displacement Transducers

Displacement measuring devices were utilized in Units 2A and 2B. For both keys, displacements were recorded along the centerline of the key at the top and the interface levels, as illustrated in Figure 5.38.

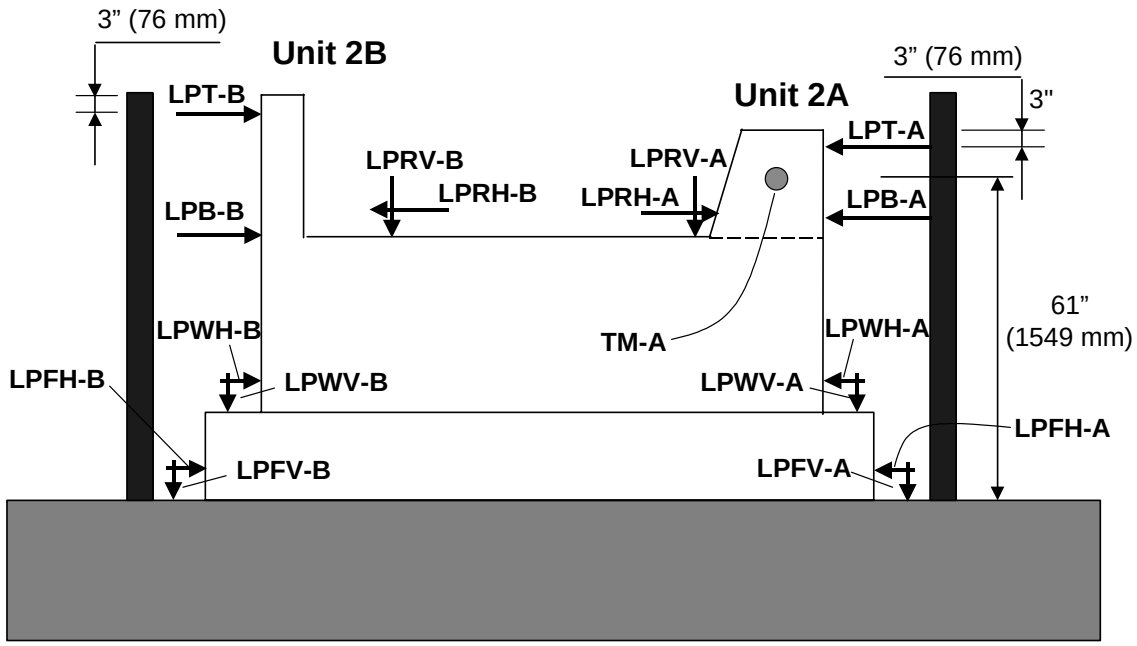

Figure 5.38 Labels of Displacement Transducers – Test Series II

5.4.3 Test Series III

5.4.3.1 Strain Gages

Several electrical resistance strain gages were placed on the legs of the shear key vertical reinforcement (the 8-#5 headed bars; see Figure 5.25) in the shear keys of Test Units 3A and 3B. Strain gages were also placed on the horizontal tie reinforcement (tie to resist tensile force T_1 in Figure 5.4). In addition, strain gages were also placed on the vertical 8-#5 headed bars placed in the wall below the shear key toe (bars designated as VW in Figure 5.32). Locations of strain gages will be shown in Chapter 6 in presentation of the experimental results.

5.4.3.2 Displacement Transducers

Displacement measuring devices were utilized in Units 3A and 3B. For both keys, displacements were recorded along the centerline of the key at the top and the interface levels, as illustrated in Figure 5.39.

5.4.3.3 Load Cells

Each of the two high-strength bars used for post-tensioning of the abutment wall was provided with a load cell to monitor the prestressing force before and throughout the test.

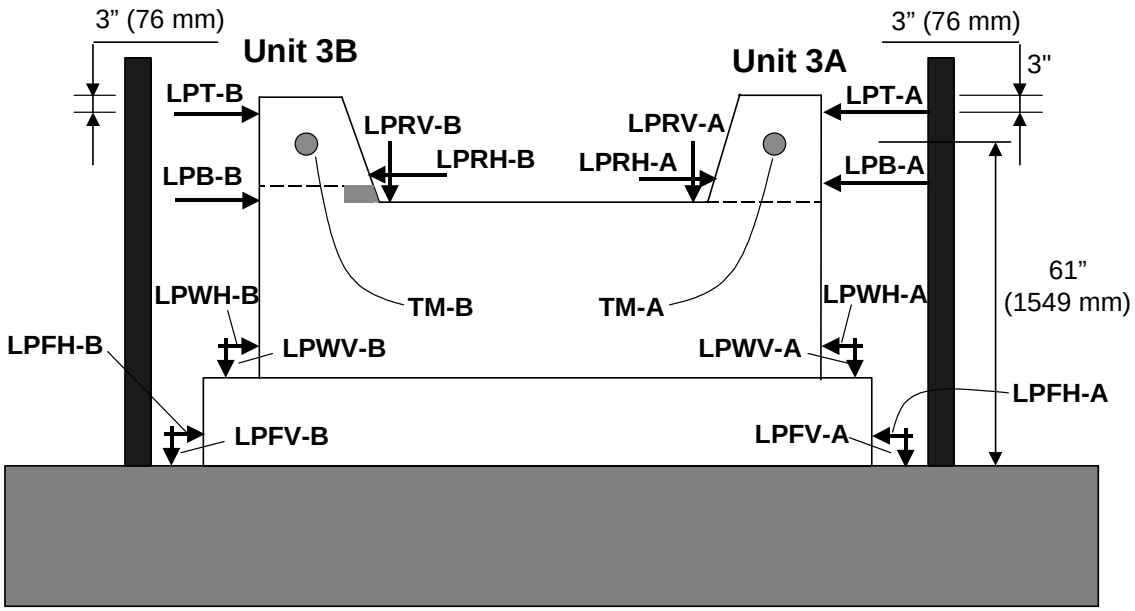

Figure 5.39 Labels of Displacement Transducers – Test Series III

5.5 Loading Protocol

5.5.1 Test Series I

Test Unit 1A was initially loaded in force control to 50 kips (222 kN) and 100 kips (445 kN) followed by unloading. The next target was a 150 kips (667 kN) lateral load or the displacement at which the test unit began to exhibit initial signs of post yielding. At a load of approximately 135 kips (601 kN) and a displacement of 0.4 inches (10 mm), the horizontal load remained approximately constant and testing was paused. The loading protocol was then switched to displacement control. Once in displacement control testing continued and the unit was cycled three times at the displacement of 0.4 inches (10 mm).

The test unit was then displaced to 1.27 in. (32 mm). Three cycles were supposed to be performed at this displacement level but without going to zero load the actuators were inadvertently displaced to 2.60 in. (66 mm). Testing proceeded, and three complete cycles were completed at this displacement level. Finally, the test unit was displaced to 4.4 in. (112 mm) at which point the lateral load carrying capacity of the test unit was negligible and testing was stopped at this level. Test Unit 2B, which included the abutment wing wall and back wall, was subjected to the same loading protocol as for Unit 2A, so that a direct comparison of the response of Units 1A and 1B can be made. The loading protocol for Units 1A and 1B is shown in Figure 5.40.

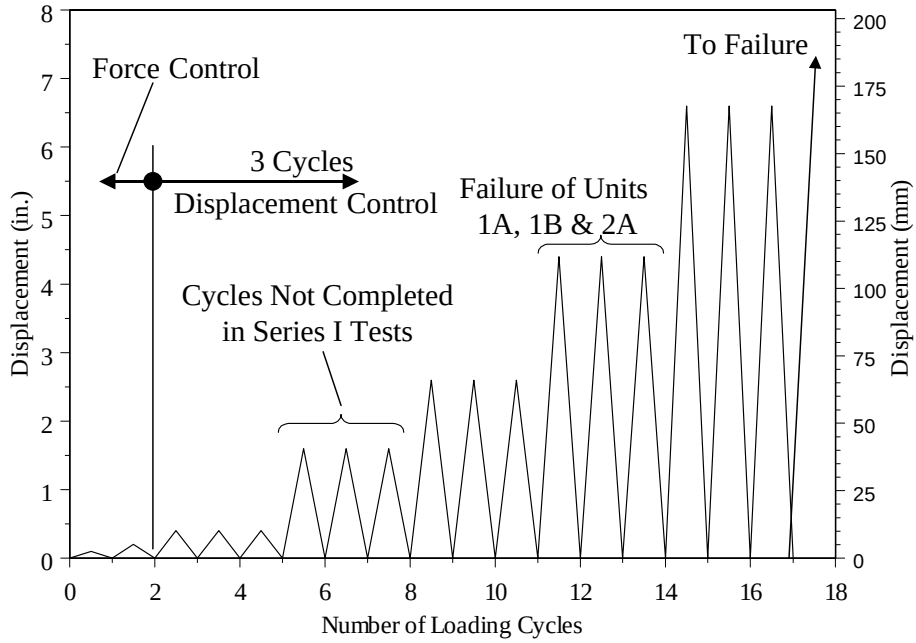

Figure 5.40 Loading Protocol of Test Series I, Series III and Test Unit 2A

5.5.2 Test Series II

5.5.2.1 Test Unit 2A

Loading protocol for Test Unit 2A was similar to that of Test Series I units and is shown in Figure 5.40.

5.5.2.2 Test Unit 2B

Test Unit 2B was subjected to fully reversed cyclic loading up to failure. The test unit was initially loaded in force control at increasing fully reversed lateral load levels with increment of 11 kips (49 kN). One fully reversed loading cycle was performed at each load level until a total load of 44 kips (196 kN) was reached. After this level, the testing procedure was switched to displacement control and the test unit was subjected to 0.5 in. (13 mm) lateral displacement at top of the flexural key, which corresponded to ductility level 1.0. Three fully reversed displacement cycles were performed. The test unit was then subjected to fully reversed cyclic displacements with increasing amplitudes up to failure. The applied displacements corresponded to ductility levels of 1.5, 2, 3, 4, 6 and 8. Three cycles were performed at each displacement, or ductility level. The loading protocol of Unit 2B is shown in Figure 5.41; the figure also shows the positive sign convention for the applied lateral load and displacement (positive in the push direction).

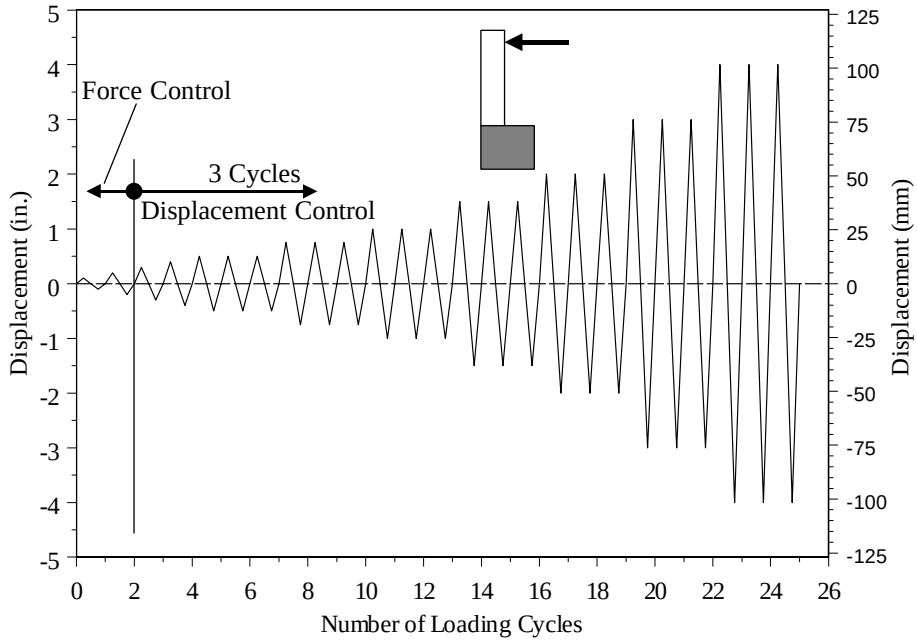

Figure 5.41 Loading Protocol of Test Unit 2B

5.5.3 Test Series III

The loading protocol for Units 3A and 3b was similar to that of Series I units and is shown in Figure 5.40.

5.6 Material Properties

As in the construction of the interior shear keys, the concrete used in the construction of the exterior shear keys was specified to have a minimum 28-day compressive strength of f'_c = 3,250 psi (22.4 MPa). The concrete had a maximum aggregate size of ½ in. (13mm). Test cylinders were cast with the specimens and tested at 28 days and on the day of testing. The concrete used in construction of Test Series III units had a minimum 28-day compressive strength of 5,000 psi (34.5 MPa).

The reinforcement used in construction of the exterior shear key test units was Grade 60 deformed mild steel bars. Tensile tests were performed on three 36 in. (914 mm) bars to determine their tensile strength properties.

5.6.1 Test Series I

Standard compression cylinder tests were performed to determine the 28-day strength as well as the day-of-testing strength of the concrete. The concrete cylinders test results on day-of-testing are given in Table 5.3.

The yield strength for the #3 bars used in the construction of the two test units was 65 ksi (448 MPa) and the ultimate strength was 98 ksi (676 MPa).

Table 5.3 Concrete Properties – Test Series I

Test Unit Designation	Day-of-Test Strength psi (MPa)
1A	4,960 (34.2)
1B	4,870 (33.6)

5.6.2 Test Series II

Standard compression cylinder tests were performed to determine the 28-day strength as well as the day-of-testing strength of the concrete. The concrete cylinders test results on day-of-testing are given in Table 5.4.

The yield strength for the #3 bars used in the construction of the abutment stem wall and the shear key reinforcement of Unit 2A was 84 ksi (579 MPa) and the ultimate strength was 124 ksi (855 MPa). The yield strength of the #5 bars used in the vertical reinforcing bars of the flexural key in Unit 2B was 65 ksi (448 MPa) and the ultimate strength was 105 ksi (724 MPa).

Table 5.4 Concrete Properties – Test Series II

Test Unit Designation	Day-of-Test Strength psi (MPa)
2A	3,110 (21.4)
2B	4,710 (32.5)

5.6.3 Test Series III

Standard compression cylinder tests were used to determine the 28-day strength as well as the day-of-testing strength of the concrete. The concrete cylinders test results on day-of-testing are given in Table 5.5.

The yield strength for the #3 bars used in the construction of the abutment stem wall was 79 ksi (545 MPa) and the ultimate strength was 119 ksi (821 MPa). The yield strength of the #5 bars used in the shear key vertical reinforcement (headed bars) of Test Units 3A and 3B was 72 ksi (497 MPa) and the ultimate strength was 99 ksi (683 MPa).

Table 5.5 Concrete Properties – Test Series III

Test Unit Designation	Day-of-Test Strength psi (MPa)
3A	5,630 (38.8)
3B	5,630 (38.8)

6 EXPERIMENTAL RESULTS OF SACRIFICIAL EXTERIOR SHEAR KEYS

This chapter describes test observations recorded during lateral load testing of the sacrificial exterior shear key test units and summarizes the experimental results.

6.1 Test Unit 1A

The loading protocol of this test unit was described in Section 5.5.1 (see Figure 5.40).

6.1.1 General Test Observations

General test observations recorded during testing (i.e. force and displacement controlled cycles) are summarized in this section and relevant damage levels are presented in Figure 6.1. The testing procedure was stopped at different load levels in order to assess damage in the test unit. Following is a summarized description of damage levels observed during testing.

Level I: Onset of cracking occurred at a horizontal load of 76 kips (338 kN). This limit state was defined by a single crack that was formed at the interface between the shear key inclined face and the abutment stem wall close to the point of application of the lateral load (see Figure 6.1b). The crack inclination angle was measured at about 56° with respect to the horizontal direction. Extension of this crack was pointed towards the stem wall toe, which matches with the angle of inclination depicted in Figure 5.4. In addition, it is important to recognize that this crack intersected only the first line of shear key reinforcement. This suggests that other lines of shear key reinforcement did not contribute to the shear key load resistance.

Level II: On the cycle prior to peak loading an increase in the number of inclined cracks was observed, as shown in Figure 6.1c. These cracks propagated towards the stem wall toe and along the stem wall length. The widths of these cracks were fairly small indicating that shear stresses were transferred across these cracks, and expressed as the concrete contribution term to the shear resisting mechanism defined in Eq. (5.3).

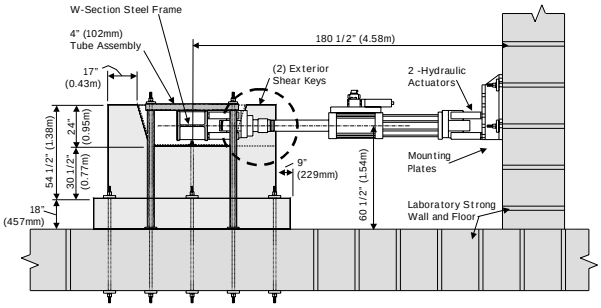

(a) Test Unit Layout

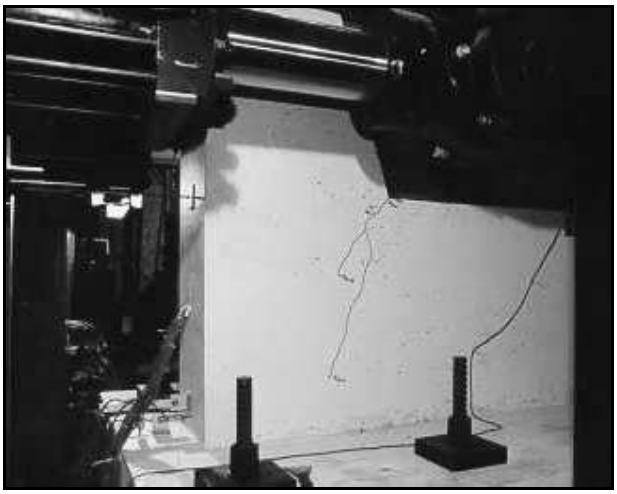

(b) *Level I*

(c) *Level II*

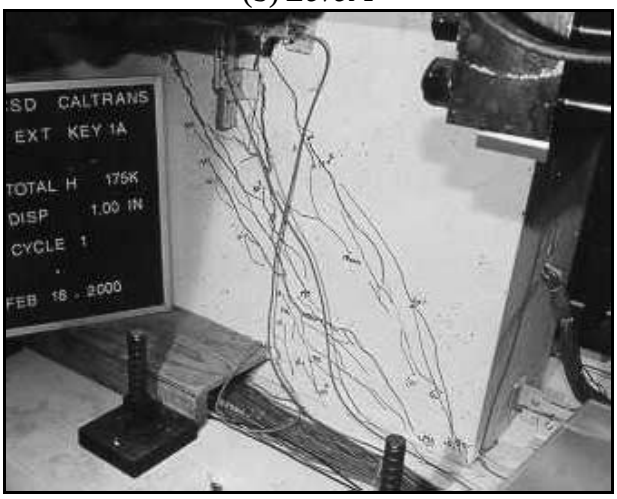

(d) *Level III*

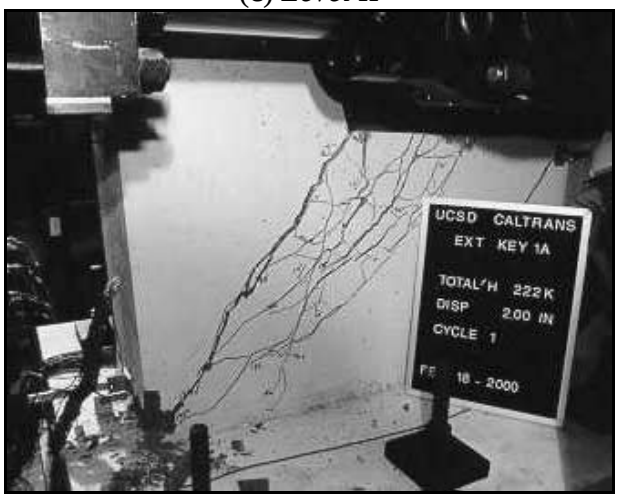

(e) *Level IV*

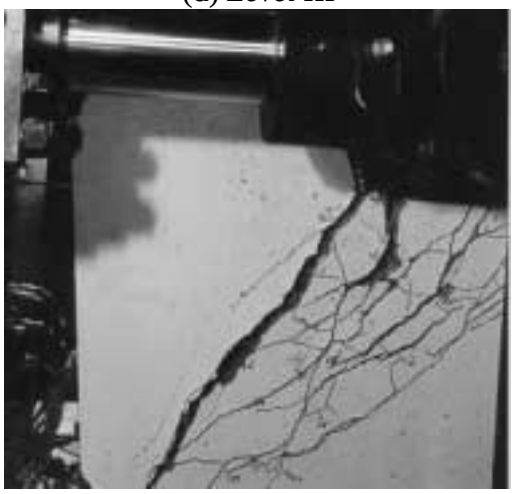

(f) *Level V*

Figure 6.1 Observations at Relevant Limit States of Test Unit 1A

Level III: Immediately after reaching the peak lateral load, a significant drop in the lateral load was recorded. The recorded peak horizontal load was 222 kips (988 kN). This damage level was characterized by a significant opening of the inclined cracks, but no spalling of the cover concrete was observed either in the diagonal compression strut or in the compression toe of the stem wall, as shown in Figure 6.1d. This suggests that the significant drop in the lateral load was a consequence of the reduction of the concrete contribution to the shear resisting mechanism.

Level IV: After peak load, the lateral load stabilized for approximately 0.5 in. (13 mm) of lateral displacement. This relatively stable lateral load was about 130 kips (578 kN). This value is very close to the computed steel contribution term given by Eq. (5.5). After this level onset of spalling of the cover concrete at the compression toe was observed (see Figure 6.1e).

Level V: During the final stages of testing an additional reduction in the lateral load was observed. Considerable amount of rotation of the shear key was observed characterized by significant opening of the inclined cracks, and spalling of the cover concrete along the compression strut and compression toe. These observations were accompanied by reduction in the shear key strength. The test was stopped at 4.40 in (112 mm) of lateral displacement after large number of reinforcing bars fractured. The load at the maximum registered displacement was 50 kips (222 kN). Damage at the end of the testing procedure is shown in Figure 6.1f.

6.1.2 Lateral Load vs. Displacement Curve

Observations described in the previous section are depicted in Figure 6.2 as they occurred during testing. Figure 6.2 shows the measured lateral load versus the lateral displacement response of Test Unit 1A along with the computed concrete contribution, V_C, and steel contribution, V_S, to the total shear key capacity, V_N. Response of the test unit shows that the achieved maximum lateral load is within the computed values.

The resulting load displacement curve shows a hysteretic response, which exhibited limited energy absorption potential after the first cycle at each displacement level. Based on the analytical models described in Section 5.2 and Table 5.2, the peak load of 222 kips (988 kN) was best correlated using the strut-and-tie analogous model (Eq. (5.2)). In Chapter 8, a hysteretic model is described using the main features observed in Figure 6.1. The main observations in Figure 6.2 are:

1. A significant reduction in stiffness was observed following the propagation of inclined cracks along the stem wall.

2. After cracking, the capacity of the exterior shear key is best represented by a strut-and-tie analogous mechanism (Section 5.2.2) with significant contribution from shear friction transferred across the inclined cracked faces. The crack opening width was fairly small up to the peak lateral load, indicating considerable transfer of shearing forces by shear friction along the cracks.

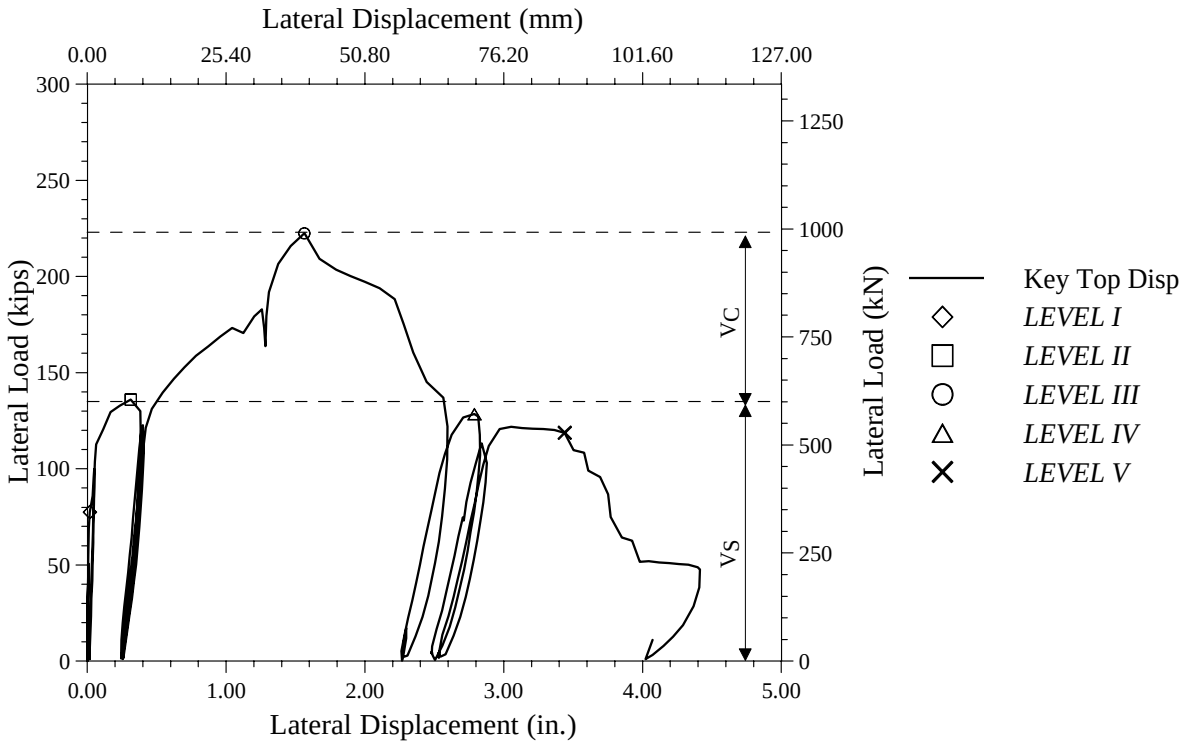

Figure 6.2 Load-Deformation Response of Test Unit 1A

3. A significant decrease in the shear capacity was observed after the peak lateral load. This decrease matched with the concrete component V_C, calculated according to Eq. (5.3). The crack width was rather large after the peak lateral load was achieved. This indicates a decrease in the shear friction transfer capacity across the cracks.

4. An additional decrease in the capacity of the shear key was observed after spalling of the cover concrete in the diagonal compression strut and toe, followed by fracture of a large number of reinforcing bars crossing the cracks interface.

6.1.3 Shear Key Reinforcement Strain Profiles

Observations recorded during testing indicate that the inclined cracks along the abutment stem wall intersected only with the first line of shear key reinforcement, represented in Figure 6.3 as strain gages G. The horizontal strain profiles presented in Figure 6.3 for the shear key

reinforcement indicate that only the first line of shear key reinforcement could develop its yield strength whereas the strain values at positions H to L were nearly zero.

Strain values at position G are higher in Line 1 than in Line 3 (see Figure 6.3b). Line 1 represents the uppermost strain gauges near the shear key-abutment stem wall interface. Based on the values recorded in the strain gauges G at Lines 1 and 3 it is clear that the first line of shear key reinforcement has yielded at the peak load. The contribution of this line of reinforcement to the capacity of the shear key is incorporated in the third term of Eq. (5.5).

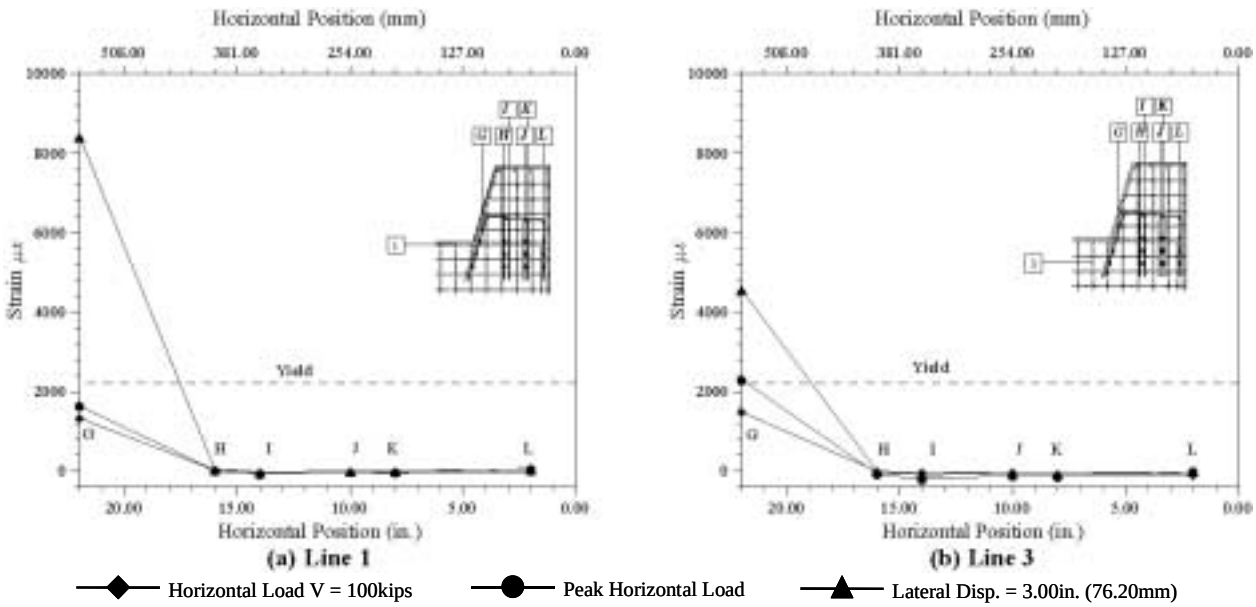

Figure 6.3 Horizontal Profiles of Strains in Shear Key Reinforcement of Unit 1A

6.1.4 Horizontal Reinforcement Strain Profiles

Figure 6.4 shows the horizontal profiles of strains recorded in the horizontal reinforcement of the abutment stem wall (tension tie). Figure 6.4a indicates the high tensile strain levels reached in these horizontal reinforcing bars at the intersection of the shear key inclined side and the abutment wall. These high strains agree with the crack pattern, which indicates significant cracking in the abutment stem wall at the toe of the shear key (see Figure 6.1f). Stem wall horizontal reinforcing bars located farther below the shear key also yielded as evidenced by the strain profiles shown in Figure 6.4b; yielding of these bars occurred as a result of the significantly wide diagonal cracks which initiated at the shear key-abutment wall interface and propagated towards the abutment wall toe.

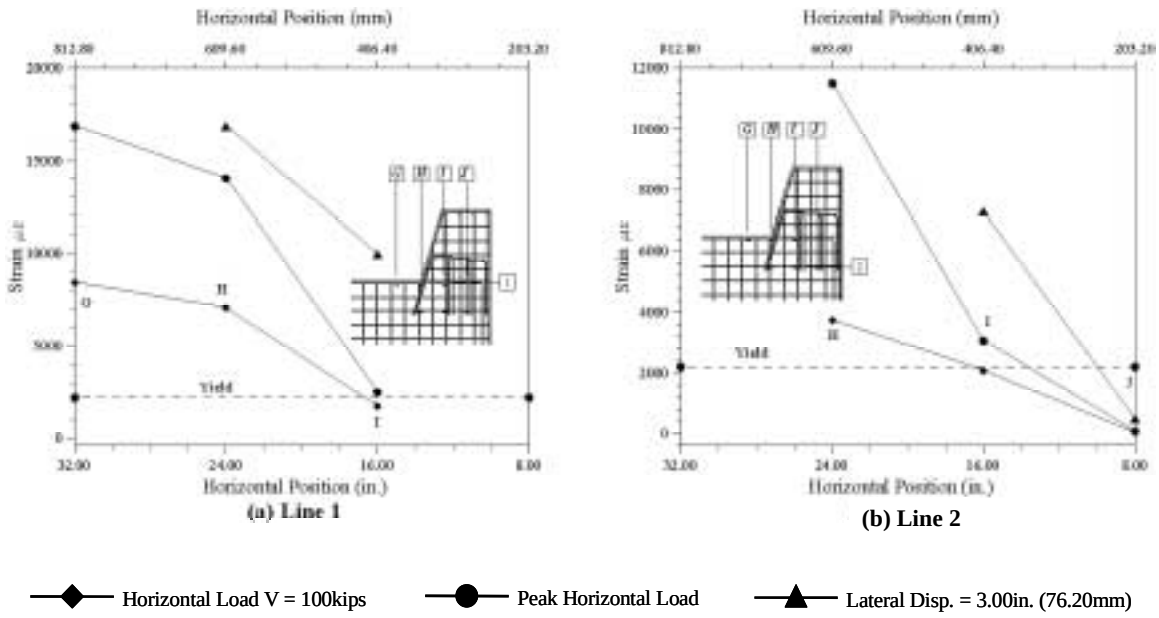

Figure 6.4 Horizontal Profiles of Strains in Horizontal Side Reinforcement of Unit 1A

6.1.5 Vertical Reinforcement Strain Profiles

Figure 6.5 shows the vertical profiles of strains in the vertical side reinforcing bars of the abutment stem wall. Figure 6.5a shows very low strains in the vertical bars nearest the end of the abutment stem wall (Line F). However the reinforcing bars nearest the inner side (sloped side) of the shear key experienced very high strains (see Figure 6.5b) due to severe crack opening in the abutment stem wall at its intersection with the inner side of the shear key.

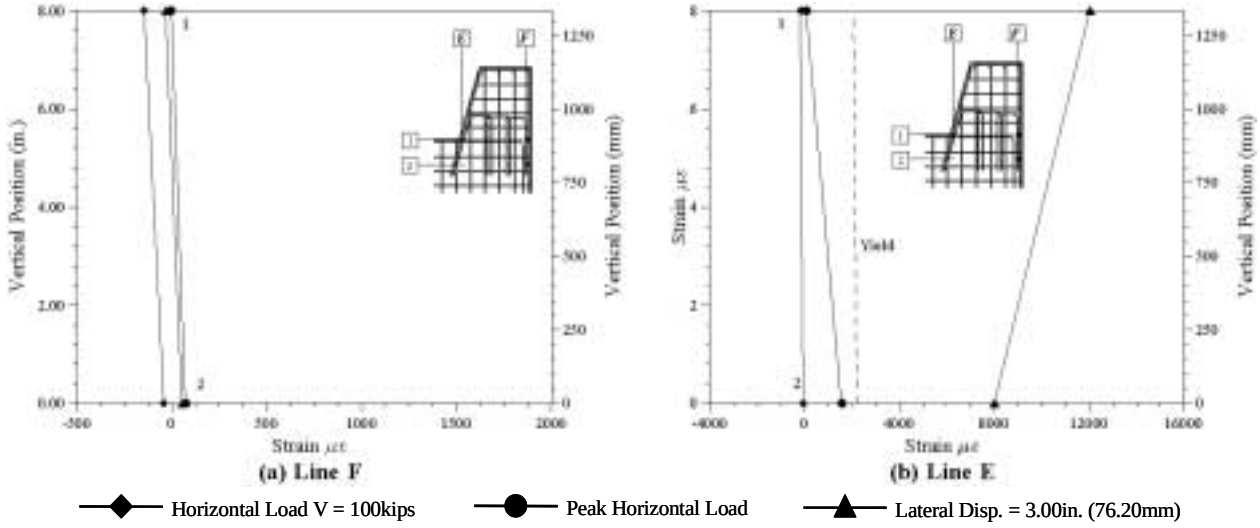

Figure 6.5 Vertical Profiles of Strains in Vertical Bars of the Abutment Wall of Unit 1A

6.2 Test Unit 1B

The load sequence of this test unit matched the sequence used in testing of Unit 1A in order to determine the influence of the back and wing wall contribution to the shear key capacity. The loading protocol of Unit 1B is shown in Figure 5.40.

6.2.1 General Test Observations

General test observations recorded during testing of Test Unit 1B are summarized in this section and relevant damage levels are presented in Figure 6.6. As before, the testing procedure was stopped at different load levels in order to assess the damage to the test units. Following is a description of damage levels observed during testing of Unit 1B. These damage levels were very similar to those registered for Test Unit 1A, indicating a similar force transfer mechanism.

Level I: Onset of cracking occurred at the horizontal load of approximately 100 kips (445 kN). This value was higher than that recorded in Test Unit 1A, which indicates that the back and wing walls contributed to the cracking strength of the test unit. As before, this limit state was defined by a single crack, as shown in Figure 6.6b, which intersected only the first line of shear key reinforcement.

Level II: Prior to peak load an increase in the number of inclined cracks was observed, as shown in Figure 6.6c. Widths of these cracks were fairly small indicating that high shear stresses were transferred across these cracks.

Level III: Immediately after reaching the peak lateral load a significant drop in the lateral load was recorded. The recorded peak horizontal load was 285 kips (1,268 kN). This damage level was characterized by a significant opening of the inclined cracks, but no spalling of the cover concrete was observed, as shown in Figure 6.6d.

Level IV: As in Test Unit 1A, after peak load, the lateral load stabilized for approximately 0.5 in (13 mm) of lateral displacement. The lateral load at the post peak load level was 200 kips (890 kN). This value was very close to the computed steel contribution term given by Eq. (5.5). After this level onset of spalling of the cover concrete at the compression toe was observed (see Figure 6.6e).

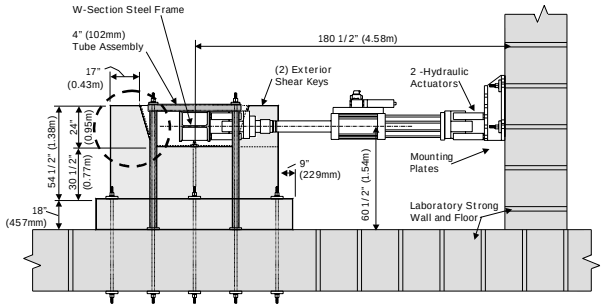

(a) Test Unit Layout

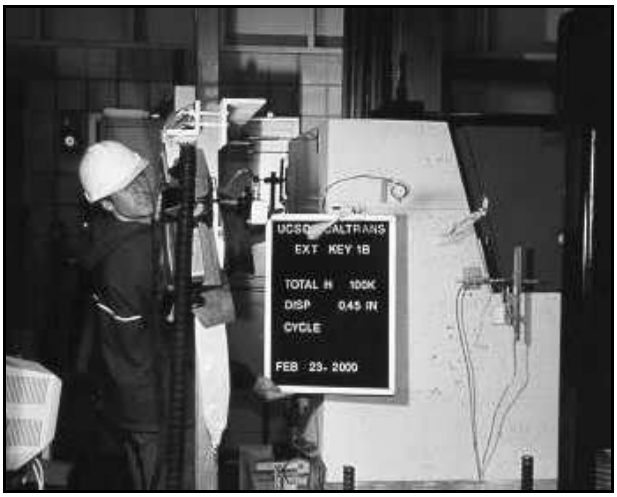

(b) *Level I*

(c) *Level II*

(d) *Level III*

(e) *Level IV*

(f) *Level V*

Figure 6.6 Observations at Relevant Limit States of Test Unit 1B

Level V: During the final stages of testing an additional reduction in the lateral load was observed, which can be characterized by significant opening of the inclined cracks, and spalling of the cover concrete. The test was also stopped at 4.40 in (112 mm) of lateral displacement after large number of reinforcing bars fractured. The load at the maximum displacement was 100 kips (445 kN). Damage at the end of the testing is shown in Figure 6.6f.

6.2.2 Lateral Load vs. Displacement Curve

Observations described in the previous section are depicted in Figure 6.7 as they occurred during testing. Figure 6.7 shows the measured lateral load versus the lateral displacement response of Test Unit 1B along with the computed concrete contribution, V_C, and steel contribution, V_S, to the total shear key capacity, V_N. Response of the test unit shows that the achieved maximum lateral load was within the computed values.

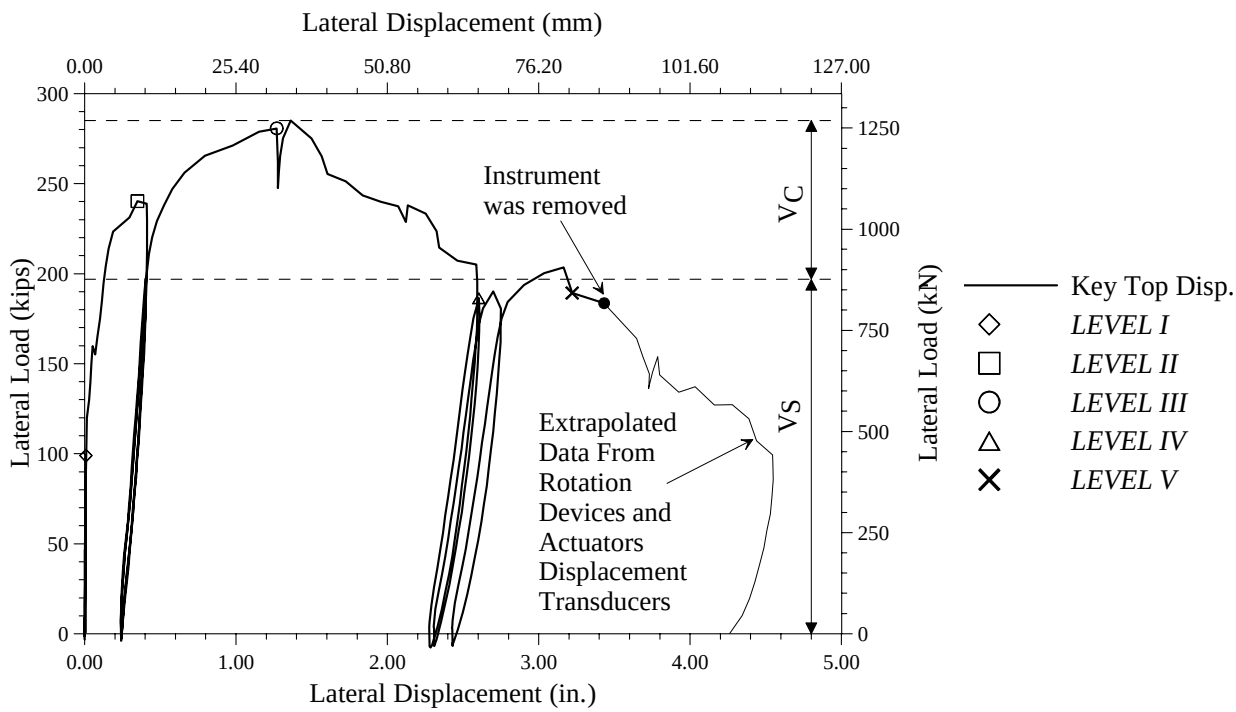

Figure 6.7 Load Deformation Response of Test Unit 1B

The resulting load displacement curve shows a hysteretic response, which exhibited limited energy absorption potential after the first cycle at each displacement level. Based on the analytical models described in Section 5.2 and Table 5.2, the peak load of 285 kips (1,268 kN) was best represented with the strut-and-tie analogous model. The main observations in Figure 6.7 are:

1. A significant reduction in stiffness was observed following the propagation of inclined cracks along the abutment stem wall.

2. After cracking, the capacity of the exterior shear key is best represented by a strut-and-tie analogous mechanism (Section 5.2.2) with significant contribution from shear transferred across the inclined cracked faces. Widths of cracks were fairly small up to the peak lateral load, indicating possibility of good shear friction transfer across the cracks.

3. A significant decrease in the shear capacity was observed after the peak lateral load. This decrease matched with the concrete component V_c, calculated according to Eq. (5.3). The crack width was rather large after the peak lateral load was achieved. This indicates a decrease in the shear friction transfer capacity across the cracks.

4. An additional decrease in the capacity of the key was observed after spalling of the cover concrete in the diagonal compression strut and toe, followed by fracture of a large number of reinforcing bars crossing the diagonal cracks.

6.2.3 Shear Key Reinforcement Strain Profiles

Observations recorded during testing indicate that the inclined cracks along the abutment stem wall intersected only with the first line of shear key reinforcement, represented in Figure 6.8 as strain gauges F. The horizontal strain profiles presented in Figure 6.8 for the shear key reinforcement, indicate that only the first line of shear key reinforcement could develop its yield strength whereas the strain values at positions A to E were nearly zero.

Strain values at position F are higher in Line 1 than in Line 3 (see Figure 6.8b). Line 1 represents the uppermost strain gauges near the shear key-abutment stem wall interface. Based on the values recorded in the strain gauges F at Lines 1 and 3 it is clear that the first line of shear key reinforcement has yielded at the peak load. The contribution of this line of reinforcement to the capacity of the shear key is incorporated in the third term of Eq. (5.5).

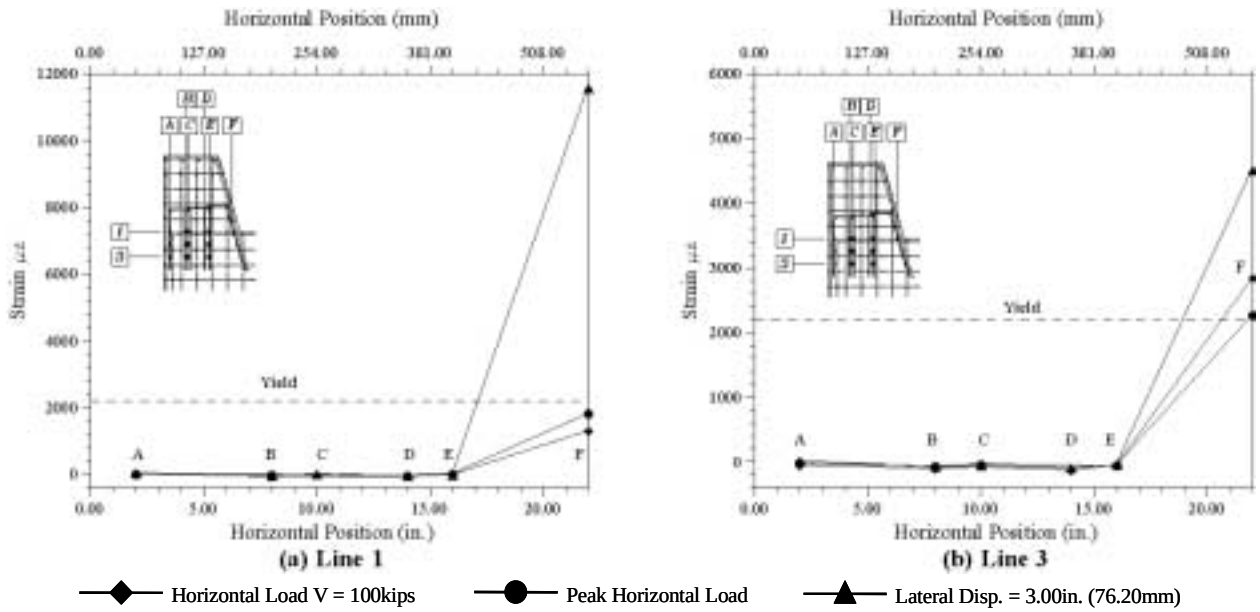

Figure 6.8 Horizontal Profiles of Strains in Shear Key Reinforcement of Unit 1B

6.2.4 Horizontal Reinforcement Strain Profiles

Figure 6.9 shows the horizontal profiles of strains recorded in the horizontal reinforcement of the abutment stem wall. Figure 6.9a indicates the high tensile strain levels reached in these horizontal reinforcing bars at the intersection of the shear key inclined side and the abutment wall. These high strains agree with the crack pattern, which indicates significant cracking in the abutment stem wall at the toe of the shear key (see Figure 6.6f). Horizontal stem wall reinforcing bars located further below the shear key also yielded as evidenced by the strain profiles shown in Figure 6.9b; yielding of these bars occurred as a result of the significantly wide diagonal cracks which initiated at the shear key-abutment wall interface and propagated towards the abutment wall toe.

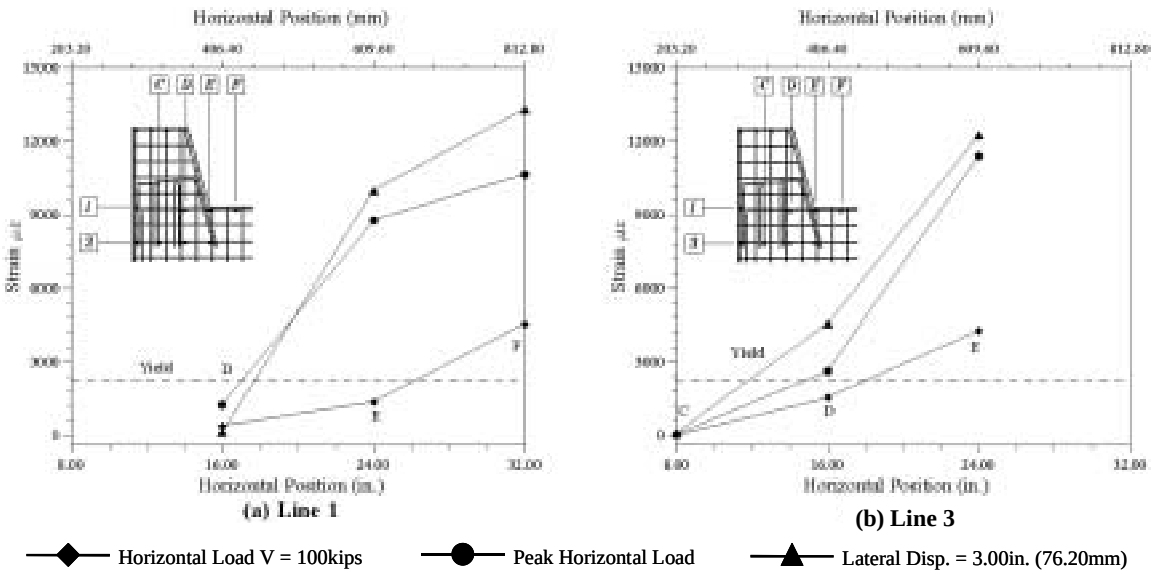

Figure 6.9 Horizontal Profiles of Strains in Horizontal Side Reinforcement of Unit 1B

6.2.5 Vertical Reinforcement Strain Profiles

Figure 6.10 shows the vertical profiles of the vertical side reinforcing bars of the abutment back wall and wing wall. Figure 6.10a shows very low strains in the vertical bars nearest the end of the abutment wall (Line A). However the reinforcing bars nearest the inner side of the abutment back wall experienced very high strains (see Figure 6.10b) due to severe crack opening in the abutment wall at its interface with the shear key.

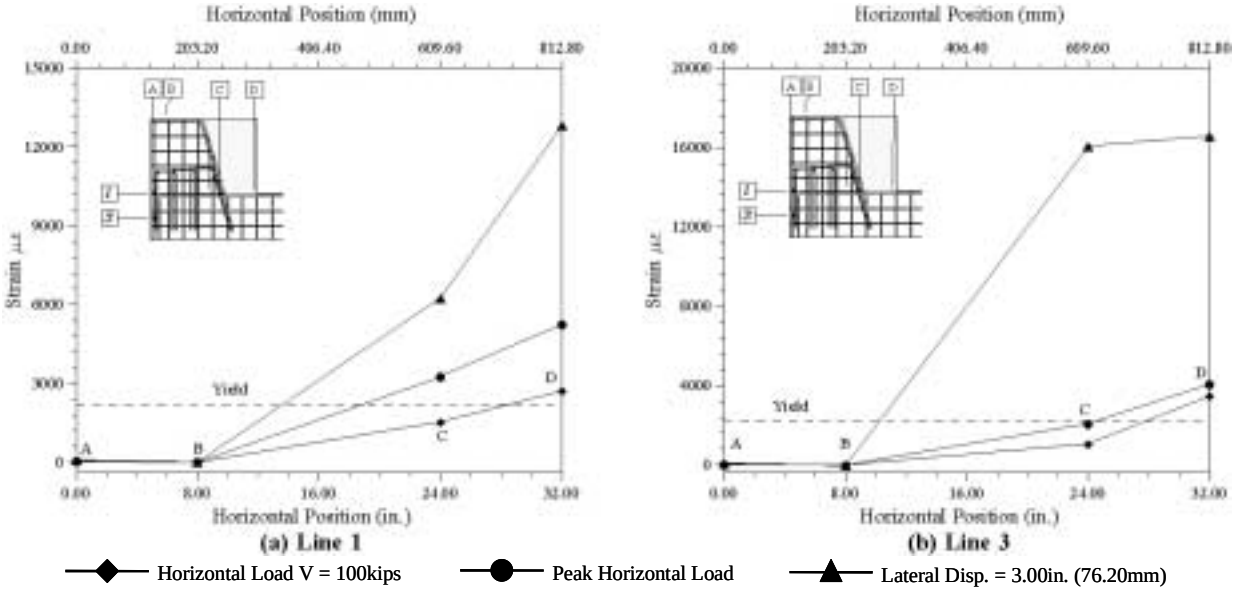

Figure 6.10 Horizontal Profiles of Strains in Vertical Reinforcement of Abutment Back Wall and Wing Wall of Test Unit 1B

6.3 Test Unit 2A

The loading protocol of Unit 2A is shown in Figure 5.40.

6.3.1 General Test Observations

General test observations recorded during testing of Test Unit 2A are summarized in this section and relevant damage levels are presented in Figure 6.11. As mentioned before, Test Unit 2A was a redesign of Unit 1A. Following is a description of damage levels observed during testing of Unit 2A. These damage levels were very similar to those observed for Test Unit 1A, indicating a similar force transfer mechanism.

Level I: Onset of cracking occurred at the horizontal load of approximately 100 kips (445 kN). This value was higher than that recorded in Test Unit 1A. As mentioned in Chapter 5, there was a cold construction joint between the abutment stem wall and the sacrificial shear key. The initial crack occurred at the shear key-abutment wall interface. This horizontal crack initiated at the intersection of the inclined side of the shear key and the abutment stem wall (see Figure 6.11b). This crack propagated along the interface until its intersection with the first row of shear key vertical reinforcement. This was followed by deviation of the crack into the abutment stem wall and the crack propagated downward at an angle towards the abutment stem wall toe.

Level II: Prior to peak load an increase in the number of inclined cracks was observed, as shown in Figure 6.11c. Widths of these cracks were fairly small indicating that high shear stresses were transferred across these cracks.

Level III: Concrete crushing was observed at this level at the toe of the abutment stem wall. The inclined cracks in the abutment stem wall also widened at this damage level. However unlike Units 1A and 1B, there was no drop in the lateral load capacity after the maximum load carrying capacity was reached. This indicates the effect of the cold construction joint between the abutment wall and the shear key in enhancement of ductility of the sacrificial exterior shear keys. The maximum lateral load carrying capacity was about 158 kips (703 kN). Figure 6.11d shows the shear key at this damage level.

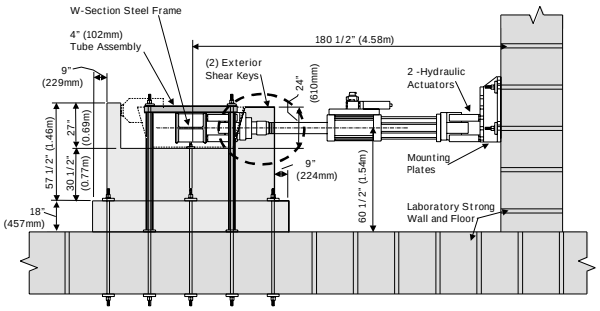

(a) Test Unit Layout

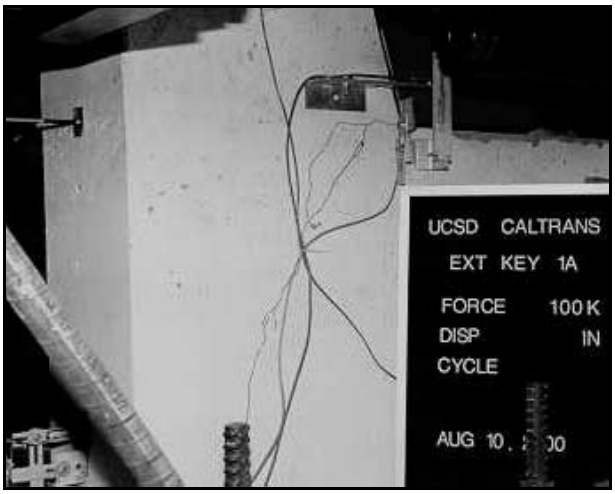

(b) *Level I*

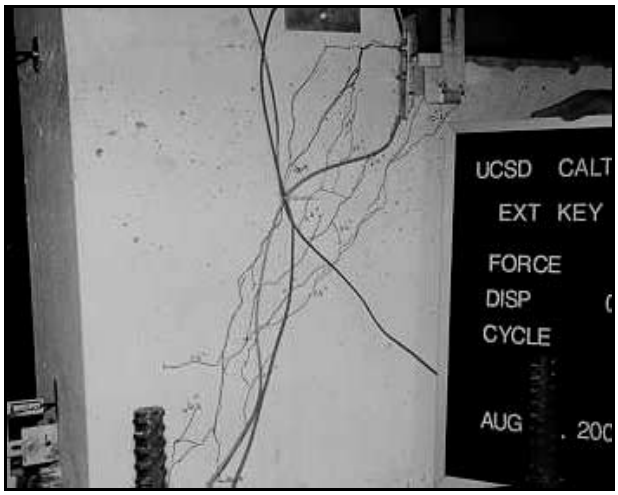

(c) *Level II*

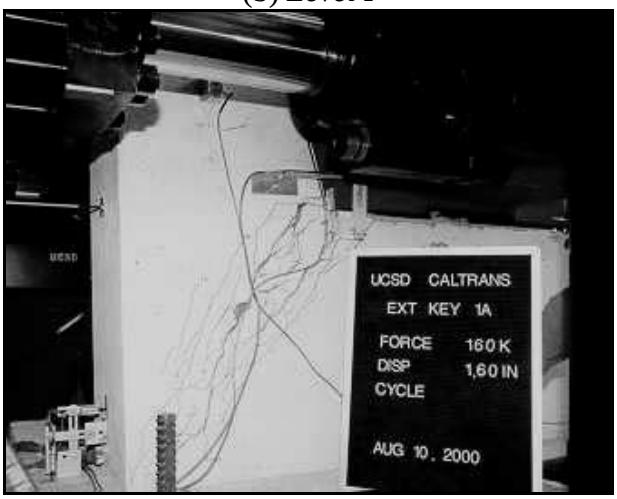

(d) *Level III*

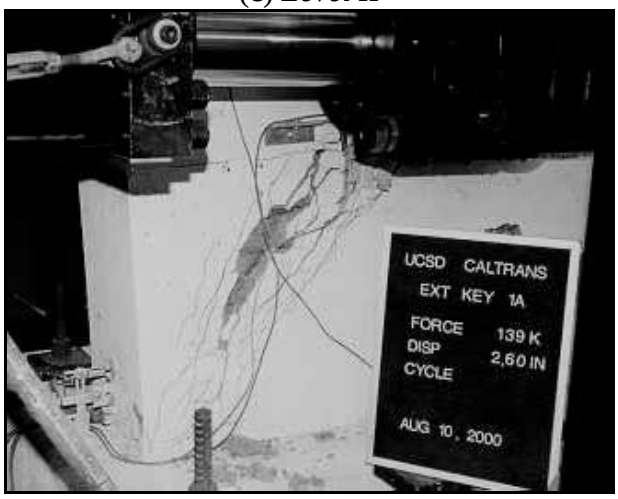

(e) *Level IV*

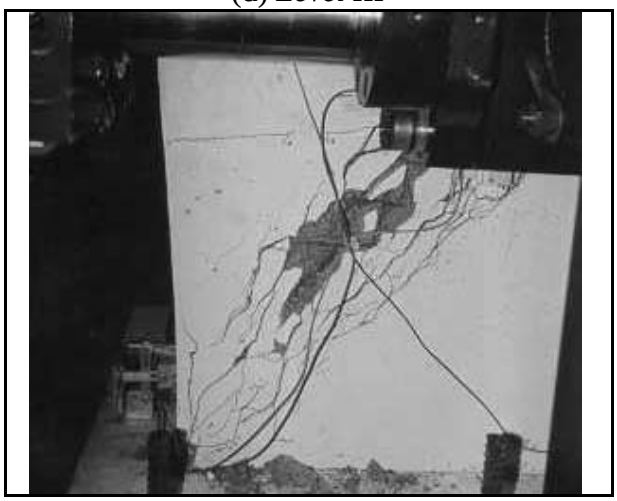

(f) *Level V*

Figure 6.11 Observations at Relevant Limit States of Test Unit 2A

Level IV: After the maximum capacity was reached, the lateral load was maintained at relatively constant value up to about 2.6 in. (66 mm). At this damage level, the initial horizontal crack propagated along the full area of the shear key-abutment interface. Also, concrete spalling occurred on the sides of the abutment wall below the shear key as shown in Figure 6.11e, resulting in exposure of side reinforcement of the abutment wall. The inclined cracks in the abutment wall widened significantly and the lateral load capacity started to drop with increased lateral displacements. This indicates that the increase in the amount of tension tie steel was not adequate to prevent formation of the diagonal crack.

Level V: During the final stages of testing an additional reduction in the lateral load was observed, which can be characterized by significant opening of the inclined cracks, and significant spalling of the concrete on the sides and toe of the abutment stem wall. The test was stopped at 4.40 in. (112 mm) of lateral displacement. The load at the maximum displacement was about 40 kips (178 kN). Damage at the end of the testing is shown in Figure 6.11f.

6.3.2 Lateral Load vs. Displacement Curve

Observations described in the previous section are depicted in Figure 6.12 as they occurred during testing. Figure 6.12 shows the measured lateral load versus the lateral displacement response of Test Unit 2A along with the computed concrete contribution, V_C, and steel contribution, V_S, to the total shear key capacity, V_N. Response of the test unit shows that the achieved maximum lateral load is less than the computed values. The calculated capacity was about 195 kips (867 kN) compared to an experimental value of about 158 kips (703 kN). The concrete contribution, V_c could be overestimated by Eq. (5.3) because of presence of the cold construction joint between the shear key and the abutment wall.

The resulting load displacement curve shows a hysteretic response, which exhibited limited energy absorption potential after the first cycle at each displacement level. The main observations in Figure 6.12 are:

1. A significant reduction in stiffness was observed following the propagation of inclined cracks along the abutment stem wall.

2. After cracking, the capacity of the exterior shear key is best represented by the strut-and-tie analogous mechanism (Section 5.2.2).

3. The maximum load carrying capacity was maintained at a relatively constant value with increasing displacements, which indicates the relative enhancement of shear keys ductility when

there is a cold construction joint between the shear key and the abutment stem wall. Degradation of the shear key capacity occurred at higher displacement levels.

4. An additional decrease in the capacity of the key was observed after spalling of the cover concrete in the diagonal compression strut and toe.

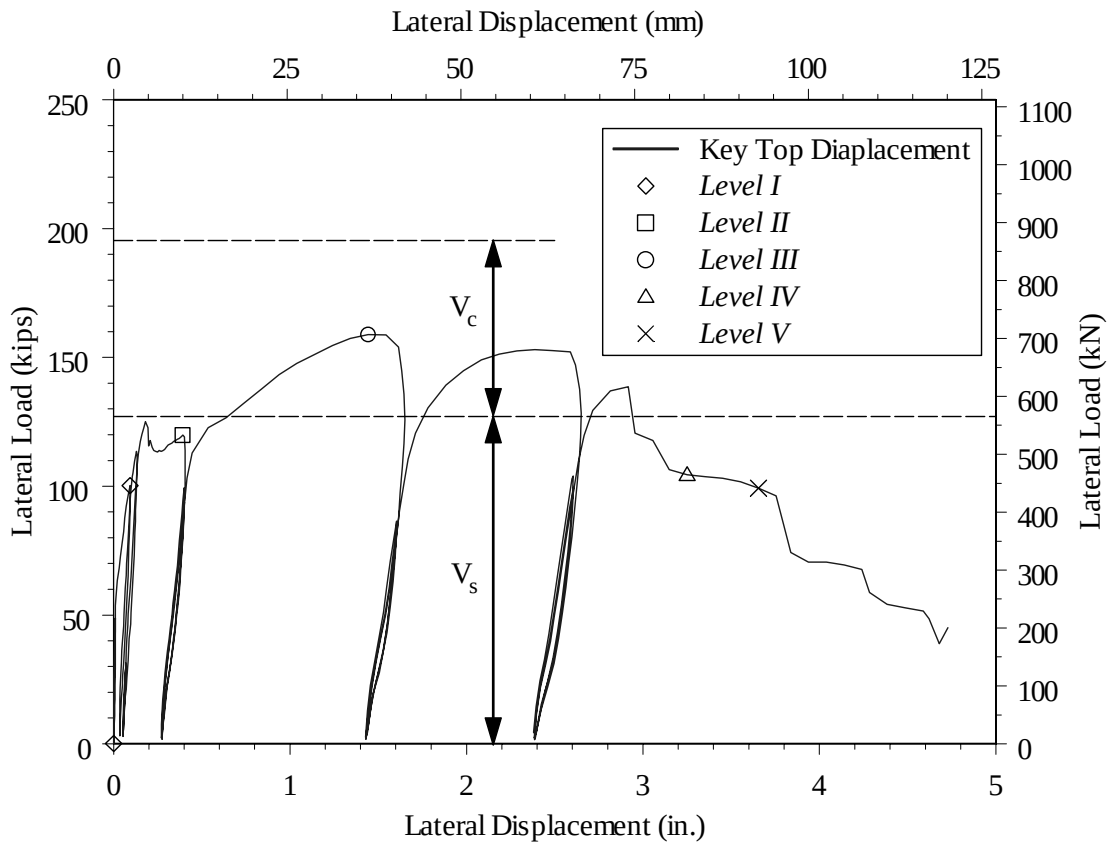

Figure 6.12 Load Deformation Response of Test Unit 2A

6.3.3 Shear Key Reinforcement Strain Profiles

Figure 6.13 to Figure 6.15 show the horizontal profiles of strains in the shear key vertical reinforcement. The three figures show the strain profiles at the level of the shear key-abutment wall interface, as well as at 4 in. (102 mm) and 8 in. (203 mm) below the interface. The figures show the low strains in all vertical bars except those in the first row (Line F), which indicates that only the first row of shear key reinforcement nearest the point of load application developed its yield strength. The figures also indicate that the first row of shear key reinforcing bars yielded

below the interface level as the diagonal crack propagated in the abutment wall towards the abutment wall toe.

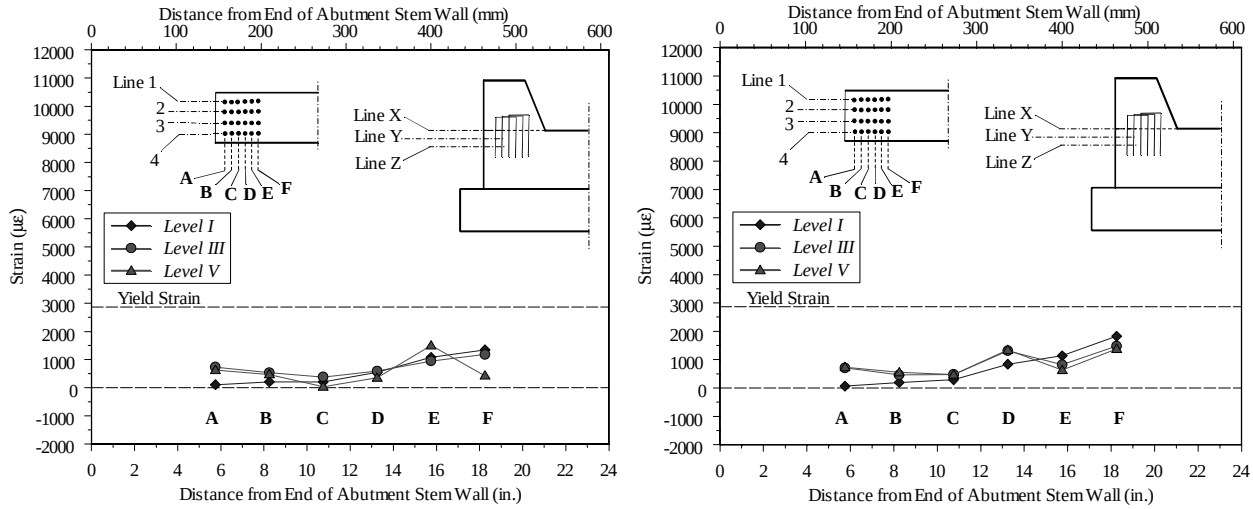

a) Line 1-X b) Line 4-X

Figure 6.13 Horizontal Profiles of Strains in Shear Key Reinforcement of Unit 2A (at Level of Shear Key-Abutment Wall Interface)

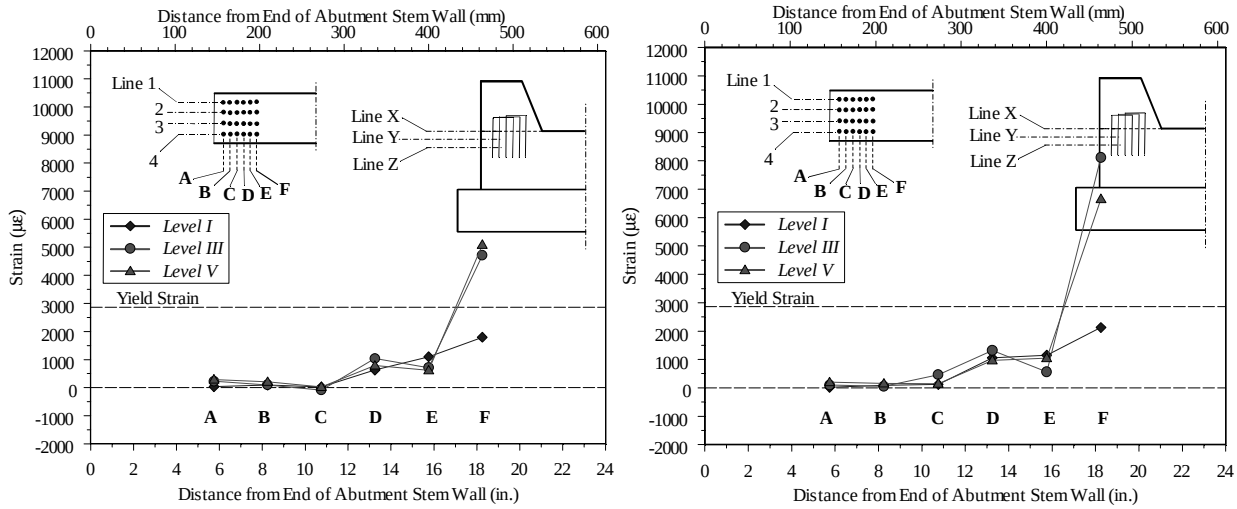

a) Line 1-Y b) Line 4-Y

Figure 6.14 Horizontal Profiles of Strains in Shear Key Reinforcement of Unit 2A (at 4 inches Below the Shear Key-Abutment Wall Interface)

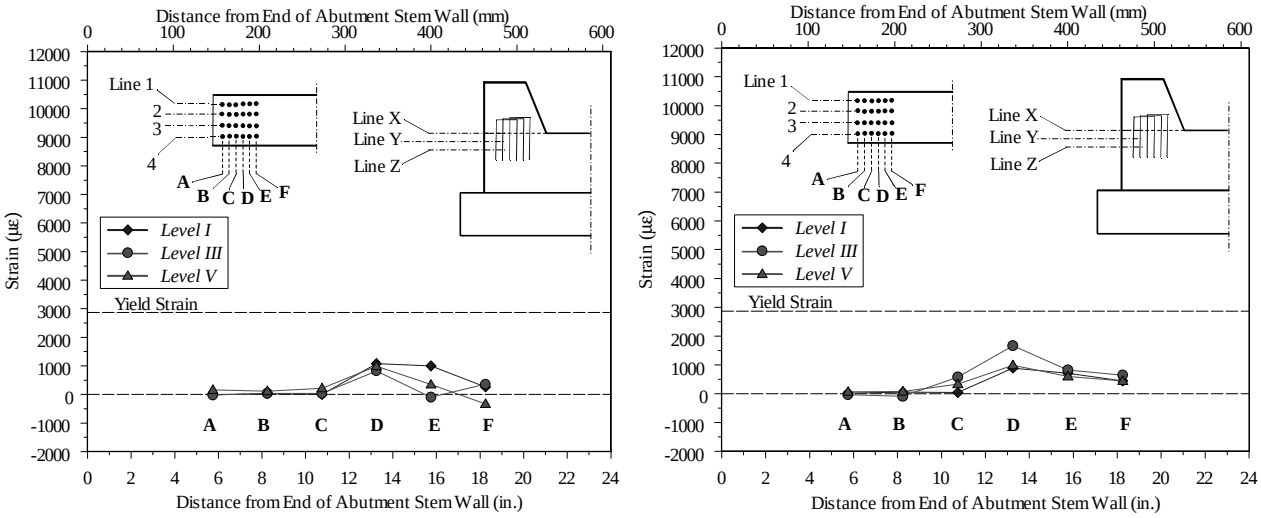

a) Line 1-Z b) Line 4-Z

Figure 6.15 Horizontal Profiles of Strains in Shear Key Reinforcement of Unit 2A (at 8 inches Below the Shear Key-Abutment Wall Interface)

6.3.4 Horizontal Reinforcement Strain Profiles

Figure 6.16 shows the horizontal profiles of strains in the horizontal reinforcement nearest to the top surface of the abutment stem wall (tension tie, or hanger bars). The figure shows the excessive inelastic strains in those bars in the area below the shear key (Lines B to F in Figure 6.16). These high inelastic strains resulted from the significant cracks that occurred in the abutment stem wall below the shear key (see Figure 6.11f).

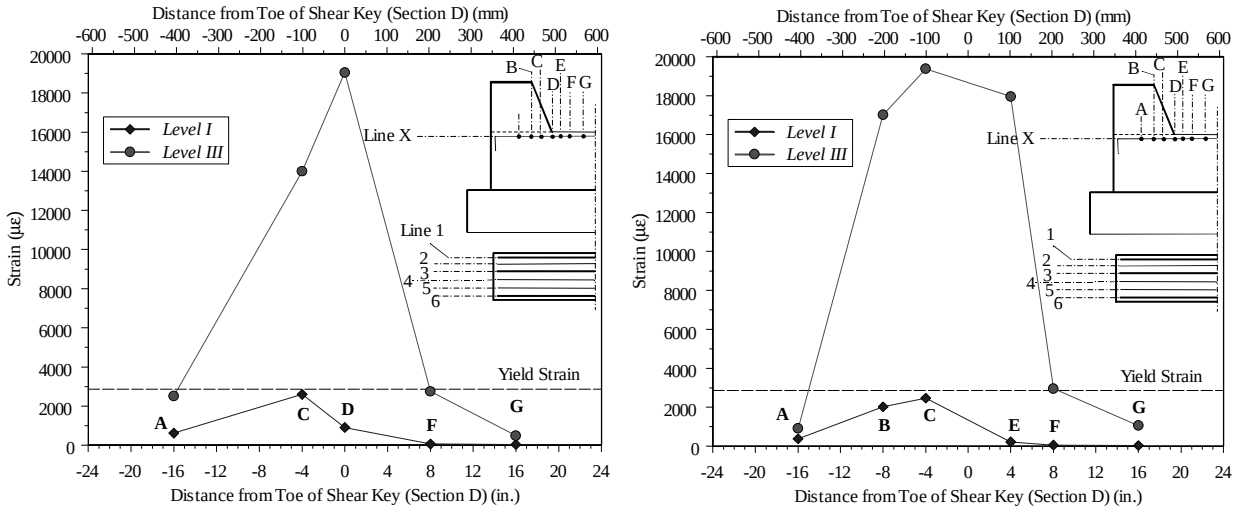

a) Line 1 b) Line 4

Figure 6.16 Horizontal Profiles of Strains in Horizontal Side Reinforcement of Unit 2A

6.4 Test Unit 2B

Unit 2B had a flexural key and was subjected to fully reversed cyclic loading. The loading protocol of Unit 2B is shown in Figure 5.41.

6.4.1 General Test Observations

General test observations recorded during testing of Unit 2B are summarized in this section and relevant damage levels are presented in Figure 6.17. Following is a description of damage levels observed during testing of Unit 2B.

Level I: Onset of cracking occurred at a horizontal load of approximately 11 kips (49 kN). The initial crack occurred at the flexural key-abutment wall interface. This horizontal crack initiated at the intersection of the vertical side of the flexural key and the abutment stem wall (see Figure 6.17b). This was followed by development of other horizontal cracks along the height of the flexural key.

Level II: The vertical reinforcing bars of the flexural key reached yielding at this load level. In addition, increase in the number of horizontal cracks was observed in the flexural key prior to peak load, and some of the earlier horizontal cracks and new cracks extended diagonally in abutment wall below the flexural key. Widths of cracks in the abutment wall were fairly small, which most likely would not require repair after an earthquake. Cracking pattern of the flexural key at Level II is shown in Figure 6.17c.

Level III: Concrete spalling was observed at this load level under both loading directions. More diagonal cracks developed and existing cracks widened. The maximum load carrying capacity was reached at this level. However unlike Units 1A and 1B, there was no drop in the lateral load capacity after the maximum load carrying capacity was reached. The maximum lateral load carrying capacity was about 60 kips (267 kN). Figure 6.17d shows the shear key at this damage level. The test unit reached a ductility of 3.0 at this damage level.

Level IV: After the maximum capacity was reached, the lateral load was maintained at relatively constant value with increased lateral displacements. The crack that initially developed at the intersection of the inner vertical side of the flexural key with the abutment stem wall widened significantly at this stage. Also major concrete spalling was observed, indicating formation of the plastic hinge at the joint between the flexural key and the abutment stem wall. The flexural key showed very ductile performance, as it will be shown in the next section. Figure 6.17e shows the flexural key at this damage level. The ductility reached at this damage level was 4.0.

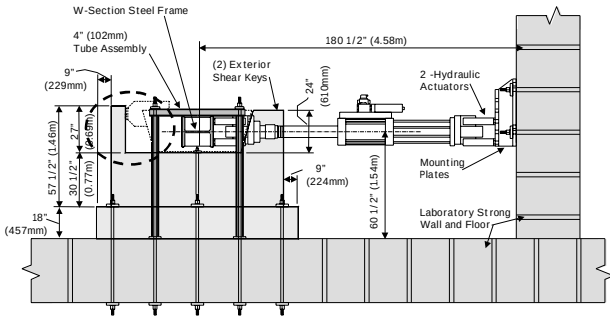

(a) Test Unit Layout

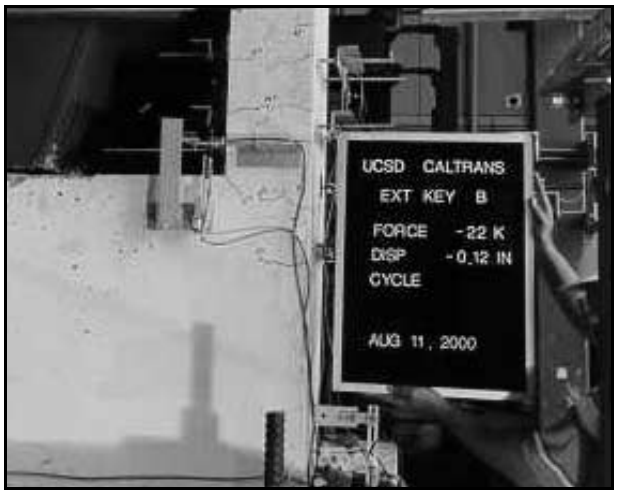

(b) *Level I*

(c) *Level II*

(d) *Level III*

(e) *Level IV*

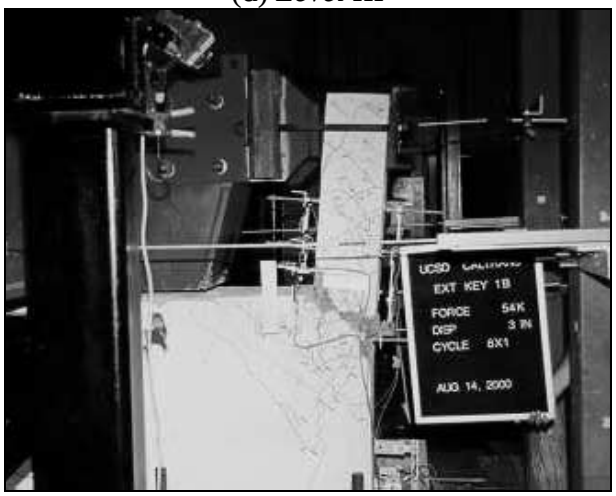

(f) *Level V*

Figure 6.17 Observation at Relevant Limit States of Test Unit 2B

Level V: The test unit reached a displacement ductility of 8.0 with minor loss in the load carrying capacity. A horizontal tension tie developed in the abutment stem wall below the flexural key as evidenced from the strain gage readings. This horizontal tension tie consisted of 12-#3 horizontal bars that had 90-degree hooks at their ends. The bars reached excessive inelastic strains and the end of the 90-degree hooks opened, which resulted in further loss of the load carrying capacity. The test was terminated at this stage. Damage at the end of the testing is shown in Figure 6.11f.

6.4.2 Lateral Load vs. Displacement Curve

Observations described in the previous section are depicted in Figure 6.18 as they occurred during testing. Figure 6.18 shows the measured lateral load versus the lateral displacement response of Test Unit 2B. The horizontal dashed line represents the load level at onset of yielding of the vertical reinforcing bars of the flexural key, V_y. Displacement ductility values corresponding to different lateral displacement levels are also shown in Figure 6.18. Figure 6.18 clearly indicates the significant ductile performance of the flexural key. The test unit reached a displacement ductility factor of 8.0 before the 90-degree hooks of the abutment wall horizontal reinforcement opened and the test was terminated. Figure 6.18 also indicates the significant energy absorption capability of flexural keys.

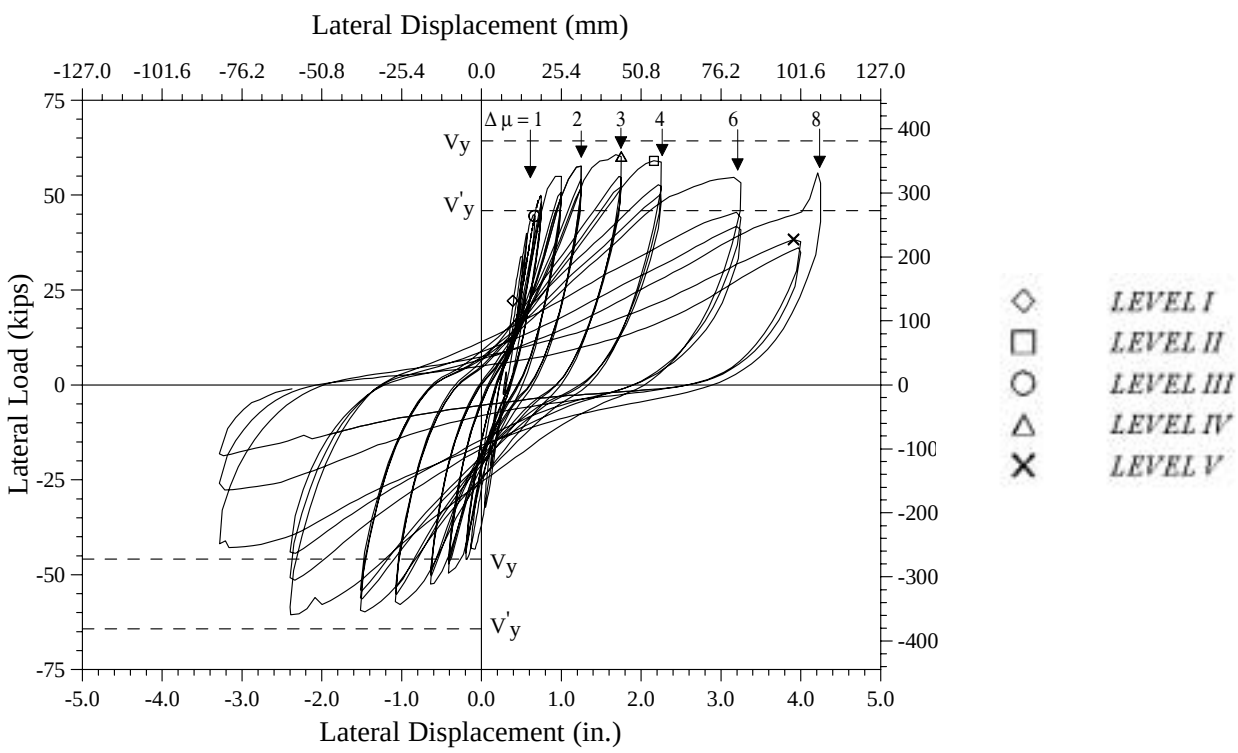

Figure 6.18 Load Deformation Response of Test Unit 2B

6.4.3 Strain Profiles in Vertical Bars of the Flexural Key

Figure 6.19 shows the vertical profiles of strains in the flexural key vertical reinforcement under lateral loading in both directions. Gauges 4 are located at the level of interface between the flexural key and the abutment stem wall. Excessive yielding of the flexural key bars is clear in Figure 6.19. This was expected due to plastic hinge formation at the bottom end of the flexural key.

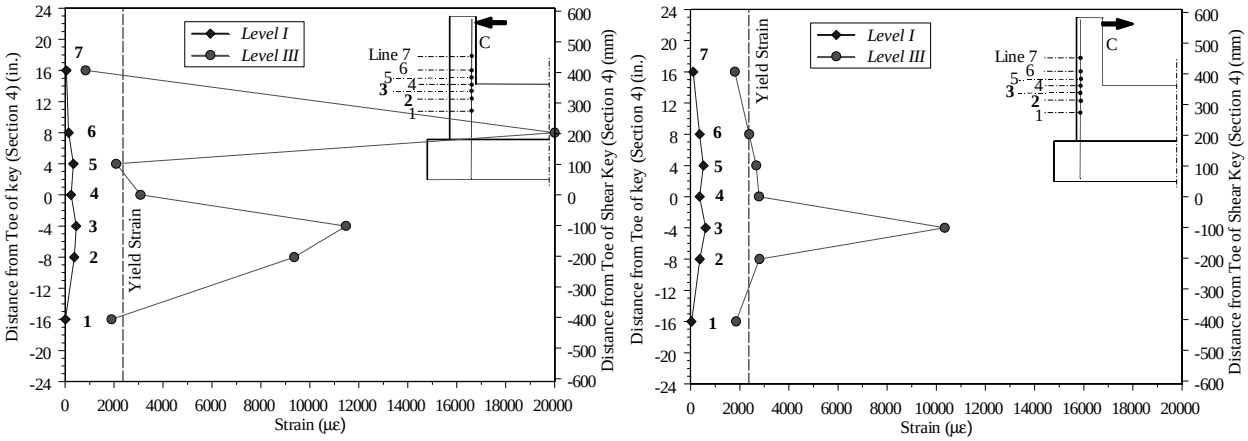

a) Bars Nearest to the Key Inner Side b) Bars Nearest to the Key Outer Side

Figure 6.19 Vertical Profiles of Strains in Flexural Key Reinforcement of Unit 2B

6.4.4 Horizontal Strain Profiles in the Side Reinforcement of the Abutment Wall

Figure 6.20 shows the horizontal profiles of strains in the horizontal reinforcing bars nearest the top surface of the abutment stem wall (tension tie, or hanger bars). The figure indicates the strains in bars 4X and 6X are higher than strains in other bars. The highest strains were recorded near the intersection between the inner vertical side of the flexural key and the abutment stem wall (Section B in Figure 6.20).

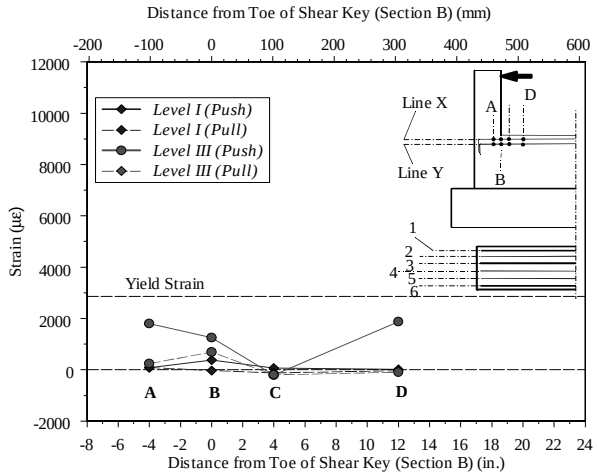

a) Reinforcing Bar #1X

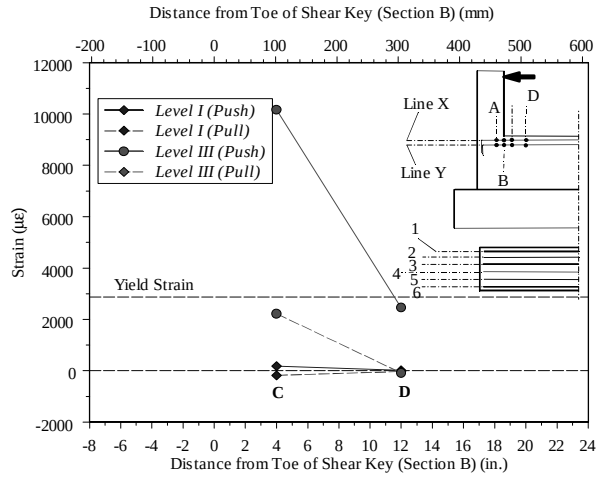

b) Reinforcing Bar #4X

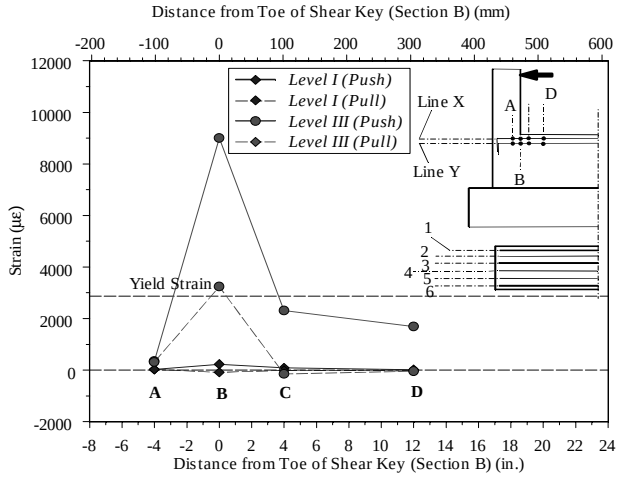

c) Reinforcing Bar #6X

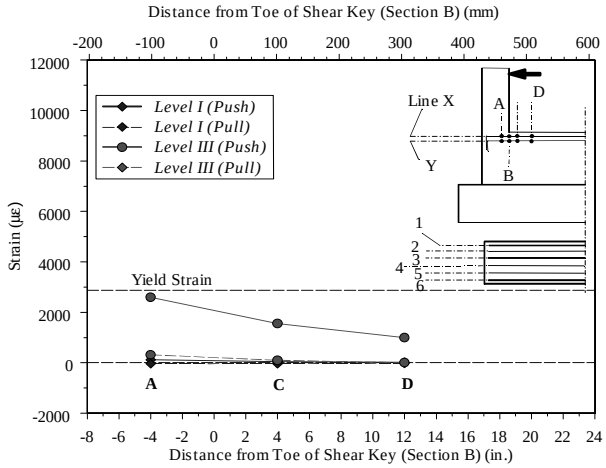

d) Reinforcing Bar #1Y

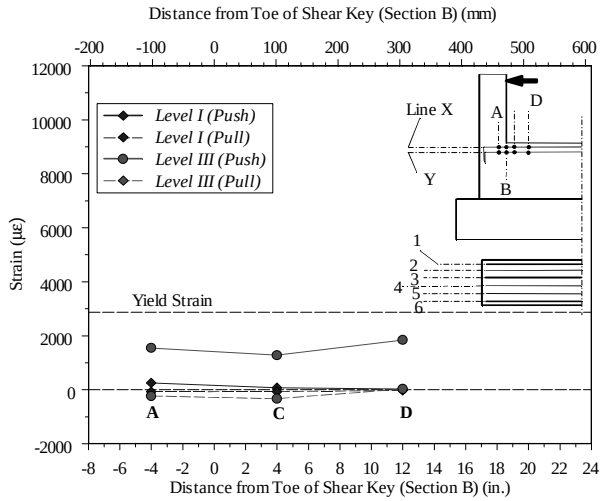

e) Reinforcing Bar #4Y

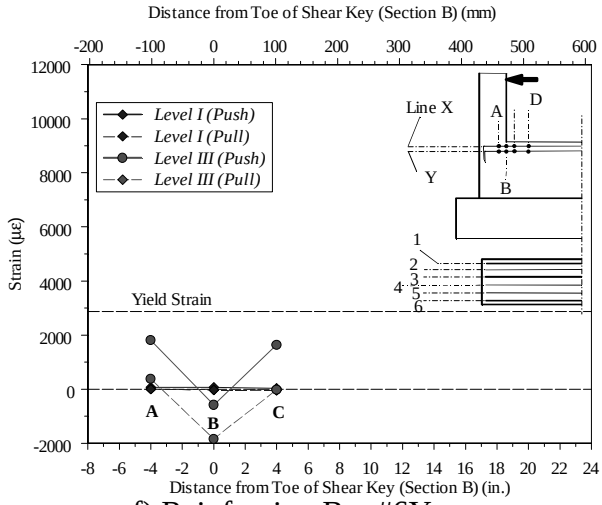

f) Reinforcing Bar #6Y

Figure 6.20 Horizontal Strain Profiles in Abutment Horizontal Reinforcement in Unit 2B

6.5 Test Unit 3A

The loading protocol of Unit 3A was the same as for Units 1A, 1B and 2A and is shown in Figure 5.40.

6.5.1 General Test Observations

General test observations recorded during testing of Unit 3A are summarized in this section and relevant damage levels are presented in Figure 6.21. As mentioned before, Test Unit 3A was a redesign of Unit 2A. Following is a description of damage levels observed during testing of Unit 3A.

Level I: Onset of cracking occurred at the horizontal load of approximately 50 kips (222 kN). As mentioned in Chapter 5, there was a cold construction joint between the abutment stem wall and the sacrificial shear key. The initial crack occurred at the shear key-abutment wall interface. This horizontal crack initiated at the intersection of the inclined side of the shear key and the abutment stem wall (see Figure 6.21b). The cracking load was relatively low because of the cold construction joint between the shear key and the abutment stem wall. This crack propagated along the interface. At higher load levels, the crack propagated completely at the interface.

Level II: The shear key vertical reinforcement (8-#5 headed bars) yielded at this level. Horizontal sliding was observed between the shear key and the abutment stem wall. Also, hairline cracks developed in the shear key at the location of load application. Figure 6.21c shows the shear key at this damage level.

Level III: Horizontal sliding of the shear key was observed as the lateral displacement was increased. Cracks developed in the abutment stem wall, but the widths of these cracks were very small and they extended for no more than 8 in. (203 mm) below the shear key-abutment wall interface. There were also signs of local minor spalling of the concrete cover in the abutment stem wall just below the shear key-abutment interface. Observations recorded during testing clearly show that the lateral load was transferred from the shear key to the abutment wall by a sliding shear mechanism.

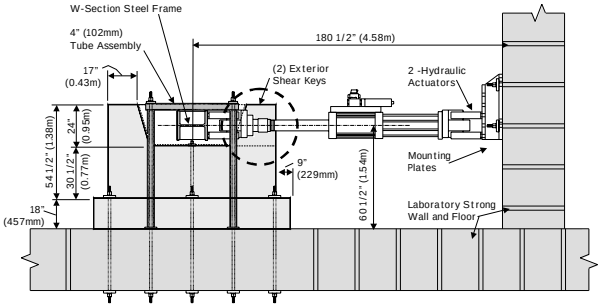

(a) Test Unit Layout

(b) *Level I*

(c) *Level II*

(d) *Level III*

(e) *Level IV*

(f) *Level V*

Figure 6.21 Observations at Relevant Limit States of Test Unit 3A

The maximum lateral load carrying capacity was about 267 kips (1,188 kN). At the maximum load carrying capacity, four of the eight shear key reinforcement (total of 8-#5 bars; see Figure 5.25) fractured as they reached their ultimate tensile strength. The shear key reinforcement bars that fractured were those located between the two prestressing high-strength bars (see Figure 5.25). Because of less confinement of the exterior shear key reinforcement bars, which were closer to the sides of the abutment, they had the ability to displace horizontally and bend inside the abutment stem wall and, as a result, these bars did not rupture. Figure 6.21d shows the test unit at this damage level.

Level IV: Just after the maximum capacity was reached, the lateral load dropped significantly as a result of rupturing of some of the shear key vertical reinforcement. Despite this significant load drop, the remaining shear key vertical reinforcing bars could sustain significant load carrying capacity up to high displacement levels. The lateral load was transferred from the shear key to the abutment stem wall through a sliding shear friction mechanism. Figure 6.21e shows the shear key and the abutment wall at this damage level. Sliding of the shear key with respect to the abutment stem wall can be clearly seen in the figure.

Level V: Despite rupture of some of the shear key reinforcing bars at damage Level IV, significant residual shear capacity was sustained up to lateral displacements of about 7 in. (178 mm). At this level (damage Level V), the remaining shear key vertical reinforcing bars reached their ultimate tensile strength and started to rupture. The test was terminated at about 8.5 in. (216 mm) when all of the shear key reinforcing bars failed and all of the load carrying capacity was lost. Figure 6.21f shows the test unit at damage Level V, just before failure of the remaining shear key reinforcement.

6.5.2 Lateral Load vs. Displacement Curve

Observations described in the previous section are depicted in Figure 6.22 as they occurred during testing. Figure 6.22 shows the measured lateral load versus the lateral displacement response of Test Unit 3A along with the computed shear key capacity, V_N, which is represented by the horizontal dashed line in the figure. The capacity was calculated using the Caltrans equation for shear friction, Eq. (5.1). According to Caltrans Specifications, a coefficient of friction of 0.60 was used in Eq. (5.1) since the interface between the shear key and the abutment stem wall was not intentionally roughened. Figure 6.22 shows that the Caltrans shear friction model severely underestimates the shear key capacity. The capacity according to Eq. (5.1) was about 107 kips (476 kN) compared to an experimental value of about 267 kips (1,188 kN).

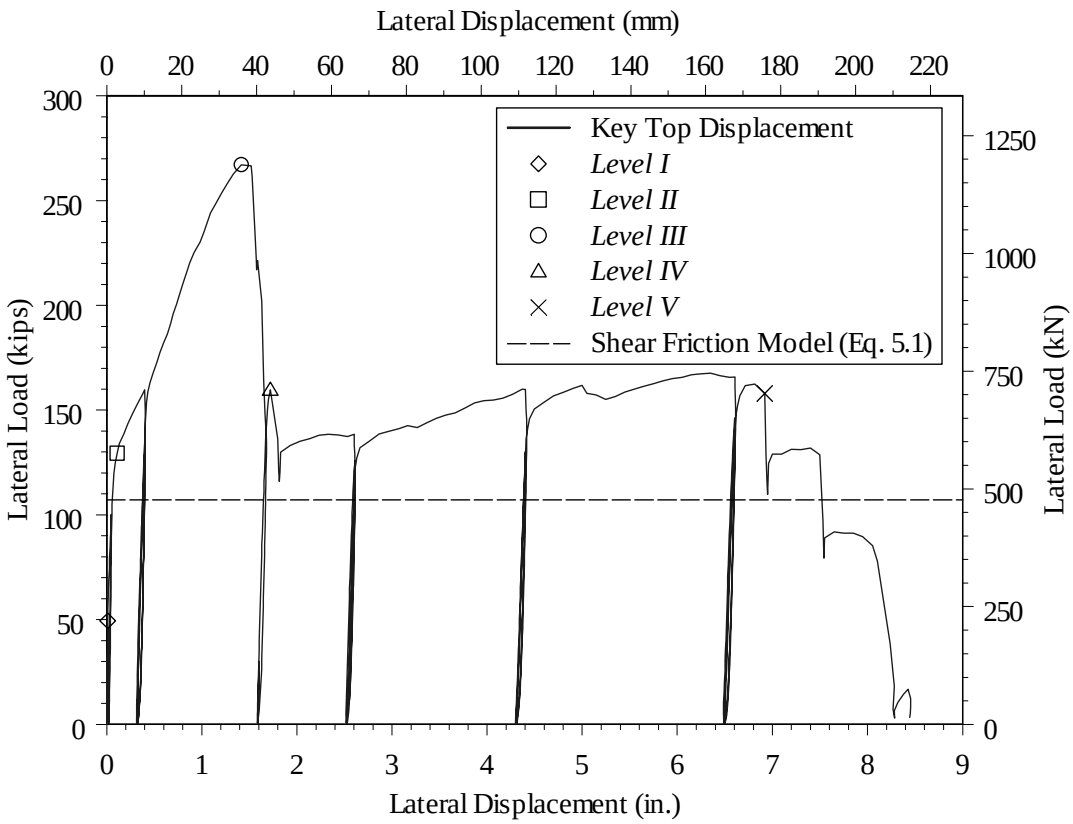

Figure 6.22 Load Deformation Response of Test Unit 3A

The resulting load displacement curve shows a hysteretic response, which exhibited limited energy absorption potential after the first cycle at each displacement level. The main observations in Figure 6.22 are:

1. A significant reduction in stiffness was observed following yielding of the shear key vertical reinforcing bars (Level II).

2. The predominant horizontal crack occurred along the interface between the shear key and the abutment stem wall. The lateral load was transferred from the shear key to the abutment wall through a sliding shear friction mechanism. Thus, the capacity of the shear key should be estimated based on the shear friction model (Section 5.2.1) after appropriate modifications.

3. When the maximum load carrying capacity was reached, the four interior vertical headed bars that connected the shear key to the abutment failed, resulting in a significant drop in the load at about 1.4 in. (36 mm) displacement. These interior bars were subjected to high tensile stresses combined with severe bar dowel action deformation as the shear key was sliding with respect to

the abutment wall. These bars were confined with the surrounding concrete, thus they could not be displaced or bent inside the abutment wall. The exterior bars were relatively close to the sides of the abutment wall. Because of the less concrete confinement around the exterior bars, they could displace and bend inside the abutment wall with increasing applied displacements on the shear key. These bars developed their full strength and the test unit had a significant residual capacity. In this phase of the test, the shearing force was transferred between the shear key and the abutment stem wall through a sliding shear friction mechanism up to high displacement levels before the shear key exterior vertical reinforcement fractured in tension. Figure 6.23 shows the top surface of the abutment wall after removal of the sacrificial shear key, indicating also the minimum damage in the abutment wall. The four interior bars that failed when the maximum load carrying capacity was reached are shown in Figure 6.23. Figure 6.23 also shows the exterior vertical bars, which had the ability to displace and bend inside the abutment stem wall because of softening of the concrete cover.

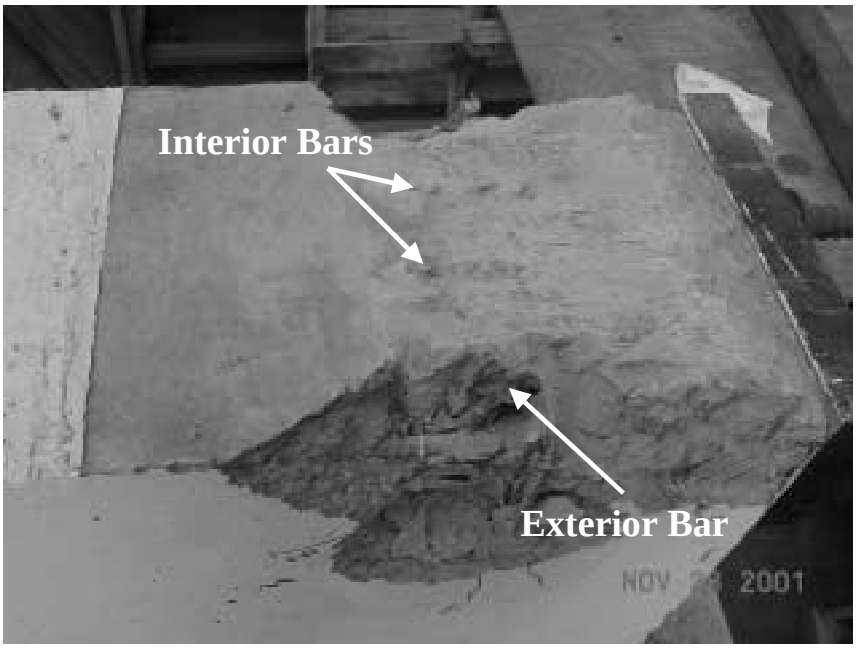

Figure 6.23 Top Surface of the Abutment Stem Wall After Removal of the Shear Key of Test Unit 3A

6.5.3 Shear Key Reinforcement Strain Profiles

Figure 6.24 shows the horizontal profiles of strains in the shear key vertical reinforcement (#5 headed bars). The strain profiles are shown at three different lines (Line X, Y and Z), which were at the level of shear key-abutment wall interface, at 4 in. (102 mm) and 8 in. (203 mm) below the interface, respectively. The figure shows that the entire shear key reinforcing bars developed their yield strength. Figure 6.24c and Figure 6.24d also show that the strains recorded at Lines

2Y and 2Z at Level V were lower than the strains measured in the same locations at Level III. This reduction in strains resulted from rupture of these bars at Level III.

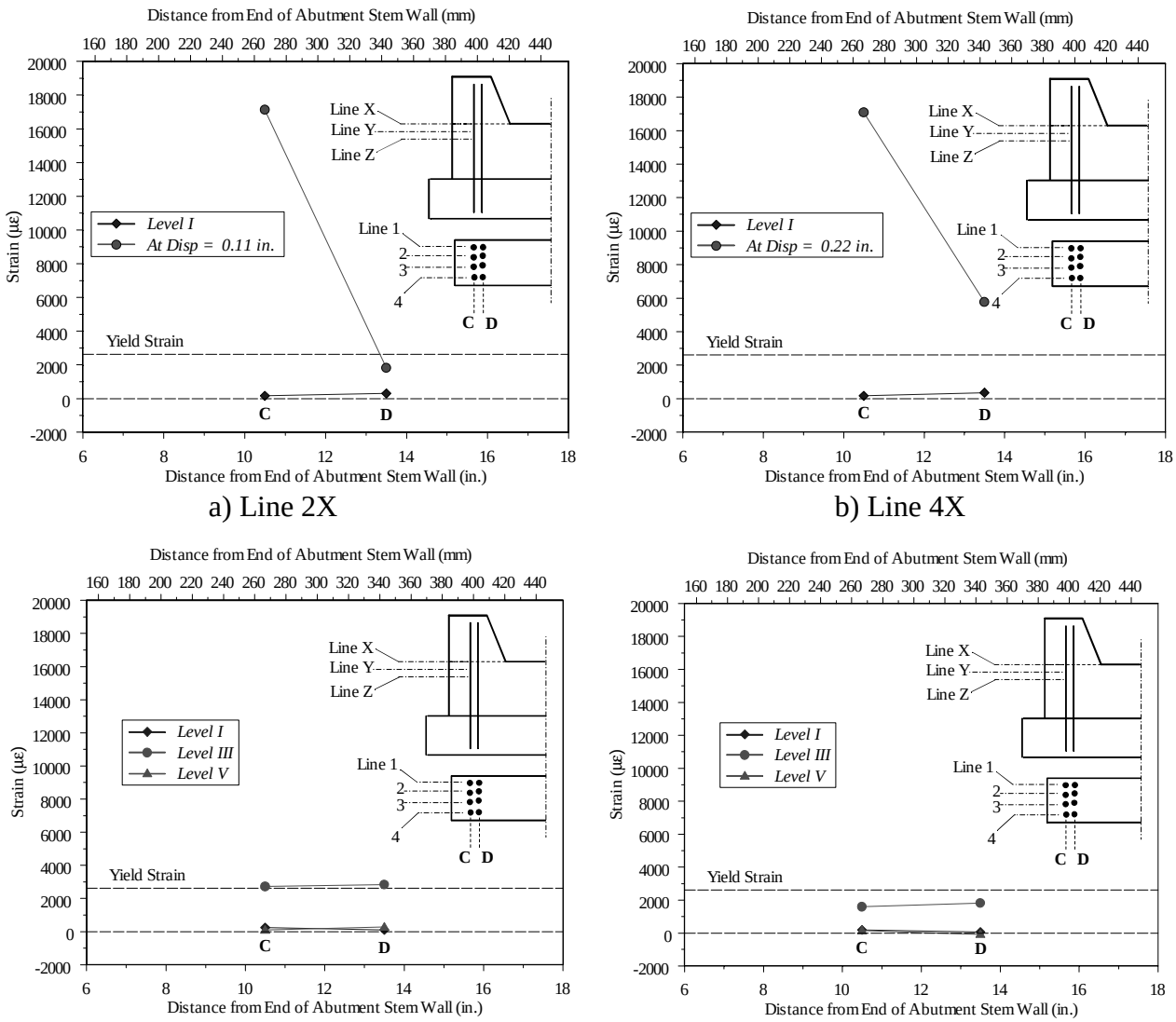

a) Line 2X b) Line 4X

c) Line 2Y d) Line 2Z

Figure 6.24 Horizontal Profiles of Strains in Shear Key Vertical Reinforcement of Test Unit 3A

6.5.4 Strains in Side Vertical Reinforcement in the Abutment Wall

As mentioned before, additional 8-#5 headed bars were placed in the abutment stem wall below the shear key toe (bars VW in Figure 5.32). Strains were recorded at these bars to investigate if these bars are necessary as was indicated by a developed strut-and-tie model. Figure 6.25 shows the recorded strains in one of these bars. The figure shows that the maximum strain was about

200 μs, which indicates that provision of these additional headed bars, below the shear key-abutment wall interface, is not necessary.

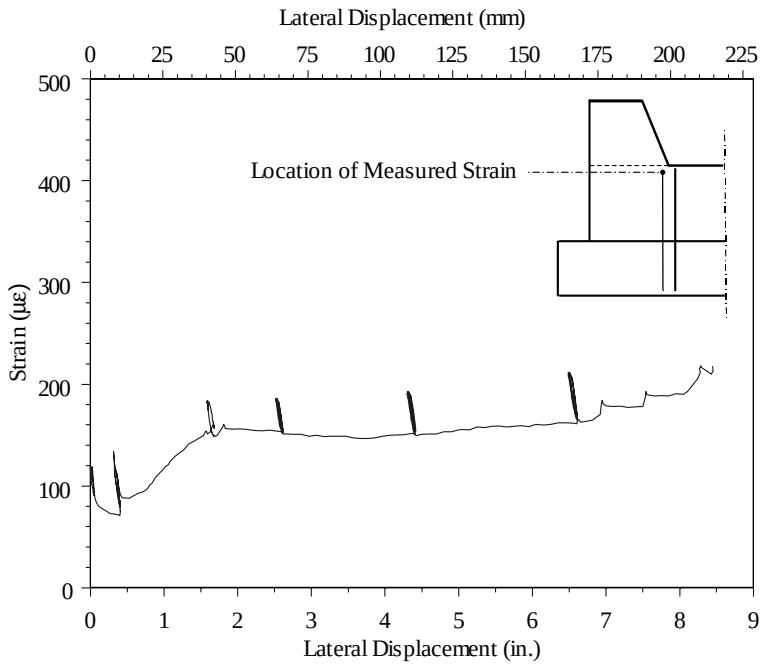

Figure 6.25 Strain in Side Vertical Reinforcement of the Abutment Stem Wall in Unit 3A

6.5.5 Horizontal Reinforcement Strain Profiles

Figure 6.26 and Figure 6.27 show the horizontal profiles of strains in the horizontal reinforcement nearest to the top surface of the abutment stem wall (tension tie, or hanger bars).

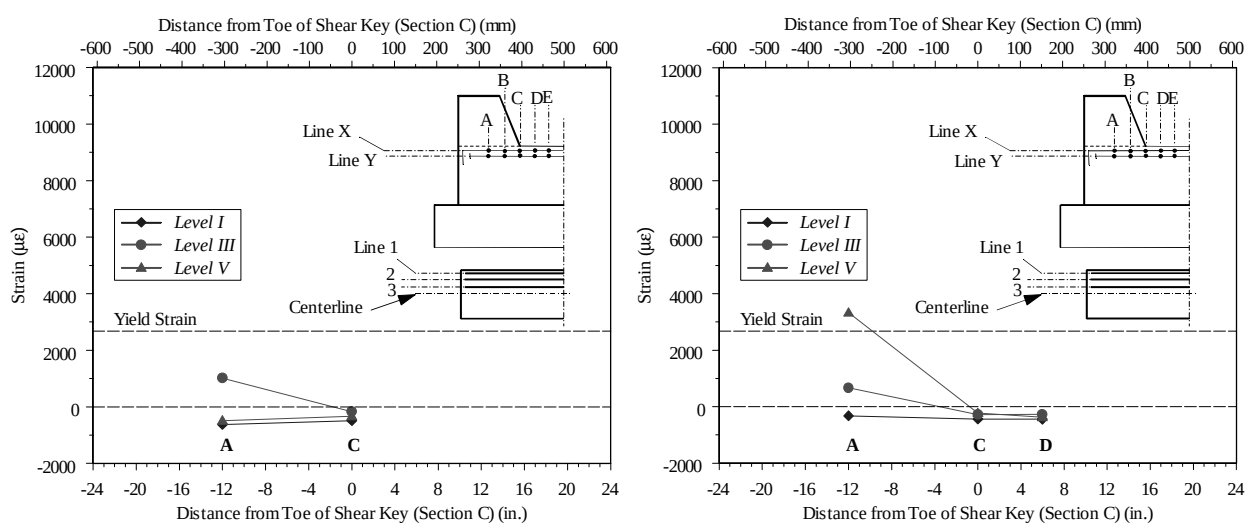

a) Line 1X b) Line 1Y

Figure 6.26 Horizontal Profiles of Strains in Horizontal Reinforcement of the Abutment Wall in Unit 3A (#3 bars)

Figure 6.26 shows the strain profiles for the #3 bars (Lines 1X and 1Y), whereas Figure 6.27 shows the strain profiles for the #5 bars (Lines 2X, 2Y, 3X and 3Y). Except for Gage A in Line 1Y, the strains recorded at other locations were well below the yield strain as a result of minimal damage of the abutment stem wall. Most of the recorded strains were compressive as a result of post-tensioning of the abutment stem wall.

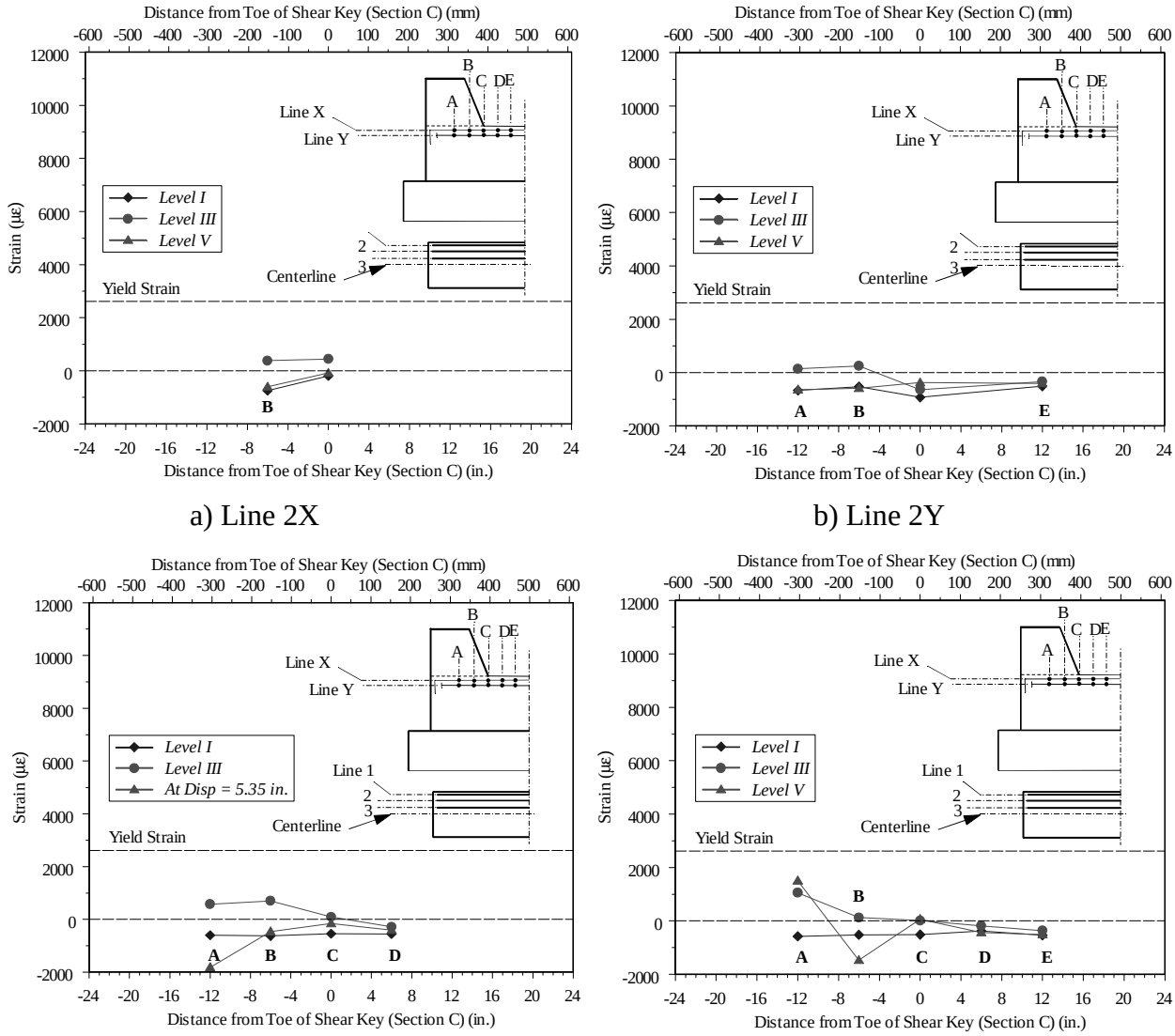

a) Line 2X

b) Line 2Y

c) Line 3X

d) Line 3Y

Figure 6.27 Horizontal Profiles of Strains in Horizontal Reinforcement of the Abutment Wall in Unit 3A (#5 bars)

6.5.6 Variation of Prestressing Force in the Abutment

As mentioned earlier in Chapter 5, load cells were used to monitor variation of the post-tensioning force before and during testing of Units 3A and 3B. Figure 6.28 shows the variation of the force in the high-strength bars, used for the post-tensioning of the abutments, with increased lateral displacement of the shear key Unit 3A. The prestressing force just before testing was about 313 kips (1,392 kN). The force in the prestressing steel increased with increased values of the applied load until it reached about 322 kips (1,432 kN) when the maximum load carrying capacity was reached. Because the abutment post-tensioning was internal unbonded (PVC ducts of the high-strength bars were not grouted), the increase in the prestressing steel force was about 3 percent only. Also, after testing the prestressing force was about 311 kips (1,383 kN) which was almost equal to its initial value before the test (see Figure 6.28). These observations indicate that post-tensioning of the abutment wall with internal unbonded tendons or prestressing bars may have more advantages over post-tensioning with internally bonded tendons or prestressing bars.

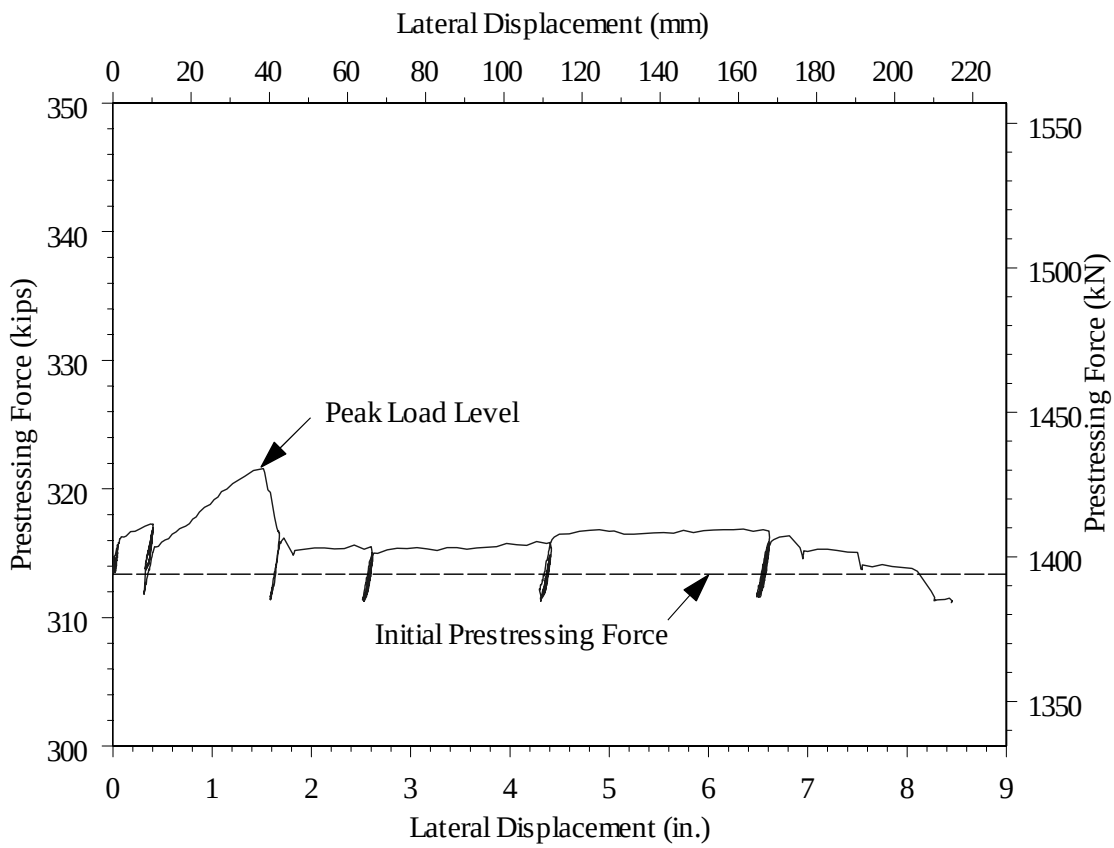

Figure 6.28 Variation of Prestressing Force in the Abutment Stem Wall During Testing of Unit 3A

6.6 Test Unit 3B

The loading protocol of Unit 3B is the same as for Units 1A, 1B, 2A and 3A and is shown in Figure 5.40.

6.6.1 General Test Observations

Behavior of Unit 3B was similar to that of Unit 3A. General test observations recorded during testing of Unit 3B are summarized in this section and relevant damage levels are presented in Figure 6.29. As mentioned before, Test Unit 3B was a redesign of Unit 2A. Following is a description of damage levels observed during testing of Unit 3B.

Level I: As in Unit 3A, onset of cracking occurred at a horizontal load of approximately 50 kips (222 kN). There was a protrusion in the abutment stem wall of Unit 3B of 3 in. (76 mm) above the top surface of the abutment wall in Unit 3A. Also, a block of foam was placed at the shear key toe (see Figure 5.23). Again, there was a cold construction joint between the abutment stem wall and the sacrificial shear key. The purpose of the cold construction joint and the foam block was to create a weak surface between the shear key and the abutment, thus a horizontal crack would occur along the shear key-abutment wall interface and sliding shear mechanism would be activated. The initial crack occurred at the shear key-abutment wall interface as desired (see Figure 6.29b). The cracking load was relatively low because of the cold construction joint between the shear key and the abutment stem wall. This crack propagated along the interface. At higher load levels, the crack propagated completely at the shear key-abutment wall interface.

Level II: The shear key vertical reinforcement (8-#5 headed bars) yielded at this level. Horizontal sliding was observed between the shear key and the abutment stem wall. Also, hairline cracks developed on the shear key at the location of load application and in the abutment stem wall. Figure 6.21c shows the shear key at this damage level.

Level III: Horizontal sliding of the shear key was observed as the lateral displacement was increased. Cracks developed in the abutment stem wall, but the widths of these cracks were very small and they extended for no more than 11 in. (279 mm) below the shear key-abutment wall interface. There were also signs of local minor spalling of the concrete cover in the abutment stem wall just below the shear key-abutment interface. It was obvious that the lateral load was transferred from the shear key to the abutment wall by a sliding shear mechanism.

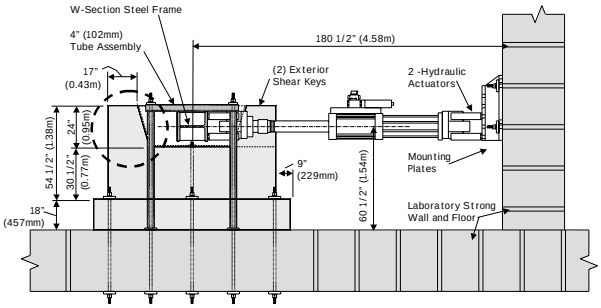

(a) Test Unit Layout

(b) *Level I*

(c) *Level II*

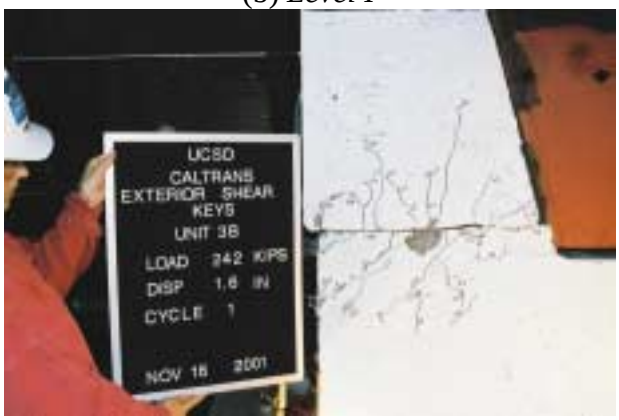

(d) *Level III*

(e) *Level IV*

(f) *Just Before End of the Test*

Figure 6.29 Observations at Relevant Limit States of Test Unit 3B

The maximum lateral load carrying capacity was about 239 kips (1,063 kN). Just after the maximum load carrying capacity was reached, four of the eight shear key reinforcement bars (total of 8-#5 bars; see Figure 5.25) fractured as they reached their ultimate tensile strength. As in Unit 3A, the shear key reinforcement bars that fractured were those placed between the two

prestressing high-strength bars (see Figure 5.25). Because of less concrete confinement around the exterior shear key reinforcement bars, which were closer to the sides of the abutment, they had the ability to displace horizontally and they did not rupture. Figure 6.29d shows the test unit at this damage level.

Level IV: Just after the maximum capacity was reached the lateral load dropped by approximately 50%, due to rupture of 50% of the shear key vertical reinforcement. Despite this significant load drop, the remaining shear key vertical reinforcing bars could sustain significant residual load carrying capacity up to high displacement levels. The lateral load was transferred from the shear key to the abutment stem wall through a sliding shear friction mechanism. Figure 6.29e shows the shear key and the abutment wall at this damage level. Sliding of the shear key with respect to the abutment stem wall can be clearly seen in the figure.

Just Before End of the Test: Despite rupture of some of the shear key reinforcing bars at damage Level III, significant residual shear capacity was sustained up to lateral displacements of 6 in. (152 mm). The test was terminated when the steel loading arm began touching the protrusion of the abutment stem wall. Thus, Damage Level V was not reached during this test. Figure 6.29f shows Unit 3B just before end of the test.

6.6.2 Lateral Load vs. Displacement Curve

Observations described in the previous section are depicted in Figure 6.30 as they occurred during testing. Figure 6.30 shows the measured lateral load versus the lateral displacement response of Test Unit 3B along with the computed shear key capacity, V_N, which is represented by the horizontal dashed line in the figure. The capacity was calculated using the Caltrans equation for shear friction, Eq. (5.1). According to Caltrans Specifications, a coefficient of friction of 0.60 was used in Eq. (5.1) since the interface between the shear key and the abutment stem wall was not intentionally roughened. Figure 6.30 shows that the Caltrans shear friction model severely underestimates the shear key capacity. The capacity according to Eq. (5.1) was about 107 kips (476 kN) compared to an experimental value of about 239 kips (1,063 kN).

The resulting load displacement curve shows a hysteretic response, which exhibited limited energy absorption potential after the first cycle at each displacement level. The main observations in Figure 6.30 are:

1. A significant reduction in stiffness was observed following yielding of the shear key vertical reinforcing bars (Level II).

2. The predominant crack occurred along the interface between the shear key and the abutment stem wall. The lateral load was transferred from the shear key to the abutment wall through a sliding shear friction mechanism. Thus, the capacity of the shear key should be estimated based on the shear friction model (Section 5.2.1) after appropriate modifications.

3. When the maximum load carrying capacity was reached, the four interior vertical headed bars that connected the shear key to the abutment failed, which resulted in the significant drop in the load at about 1.4 in. (36 mm). These interior bars were subjected to high tensile stresses combined with severe bar dowel action deformation as the shear key was sliding with respect to the abutment wall. These bars were confined with the surrounding concrete, thus they could not be displaced or bent inside the abutment wall. The exterior bars were relatively close to the sides of the abutment wall. Because of the less concrete confinement around the exterior bars, they could displace horizontally and bend inside the abutment wall with increasing applied displacements on the shear key. These bars developed their full strength and the test unit had a significant residual capacity. The sliding shear friction mechanism was still capable of carrying the load up to a high displacement level before termination of the test.

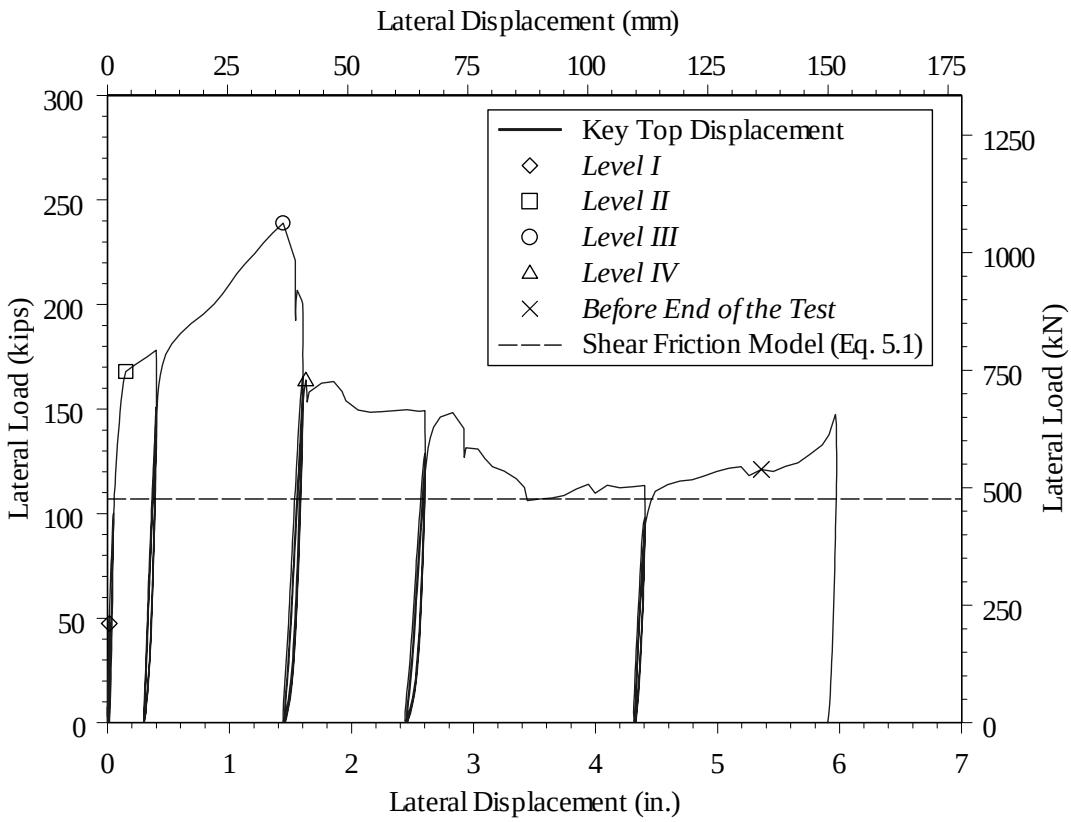

Figure 6.30 Load Deformation Response of Test Unit 3B

6.6.3 Shear Key Reinforcement Strain Profiles

Figure 6.31 shows the horizontal profiles of strains in the shear key vertical reinforcement (#5 headed bars). The strain profiles are shown at four different lines (Lines V, X, Y and Z) which were at the level of shear key-abutment wall interface, below the mechanical coupler (see Figure 5.25 for location of couplers), at 4 in. (102 mm) and 8 in. (203 mm) below the interface, respectively. The figure shows that the shear key vertical reinforcing bars developed their yield strength.

6.6.4 Horizontal Reinforcement Strain Profiles

Figure 6.32 and Figure 6.33 show the horizontal profiles of strains in the horizontal reinforcement nearest to the top surface of the abutment stem wall. Figure 6.32 shows the strain profiles for the #3 bars (Lines 1X and 1Y), whereas Figure 6.33 shows the strain profiles for the #5 bars (Lines 2X, 2Y and 3X). The figure shows that the recorded strains were significantly below the yield strain as a result of minimal damage of the abutment stem wall. Most of the recorded strains were compressive as a result of post-tensioning of the abutment stem wall.

6.6.5 Variation of Prestressing Force in the Abutment

As mentioned earlier in Chapter 5, electrical load cells were used to monitor variation of the post-tensioning force before and during testing of Units 3A and 3B. Figure 6.34 shows the variation of the force in the high-strength bars, used for abutment post-tensioning, with increased lateral displacement of the shear key of Unit 3B. The prestressing force just before testing was about 312 kips (1,388 kN). The force in the prestressing steel increased with increased values of the applied load until it reached about 322 kips (1,432 kN) when the maximum load carrying capacity was reached. Because the abutment post-tensioning was internal unbonded (PVC ducts of the high-strength bars were not grouted), the increase in the prestressing steel force was about 3 percent only. Also, after testing the prestressing force was not reduced below its initial value before the test (see Figure 6.34). These observations indicate that post-tensioning of the abutment wall with internal unbonded tendons or prestressing bars may have more advantages over post-tensioning with internally bonded tendons or prestressing bars.

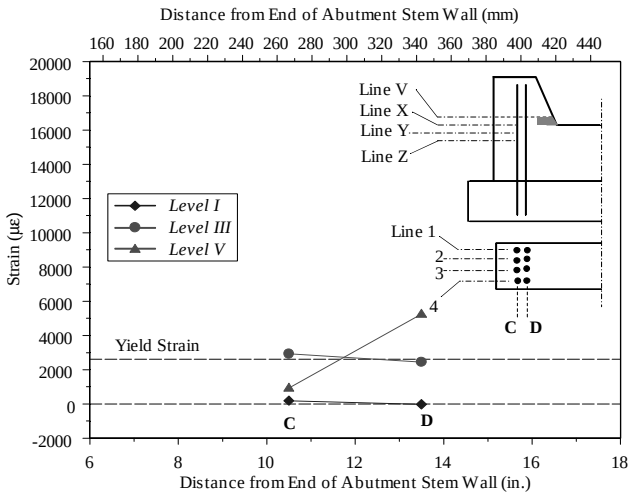

a) Line 1V

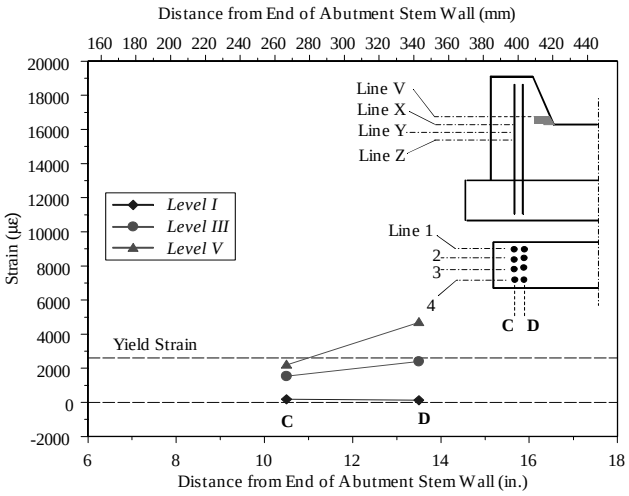

b) Line 4V

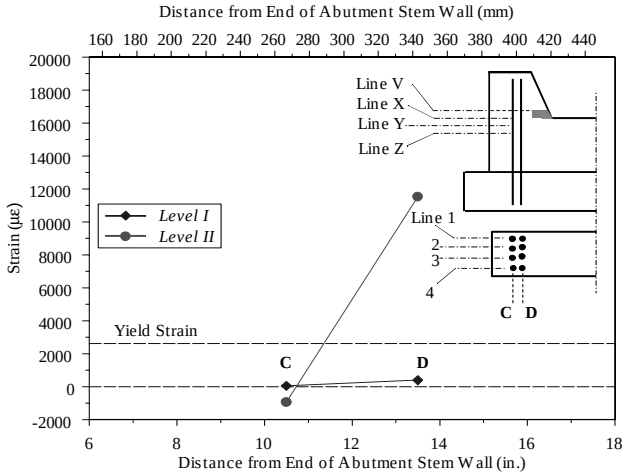

c) Line 2X

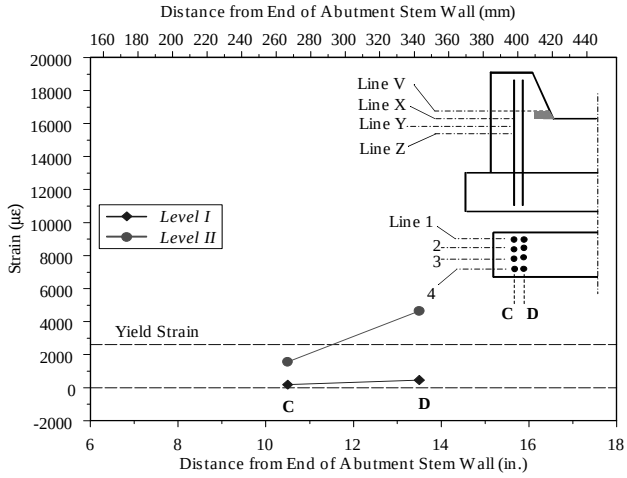

d) Line 1Y

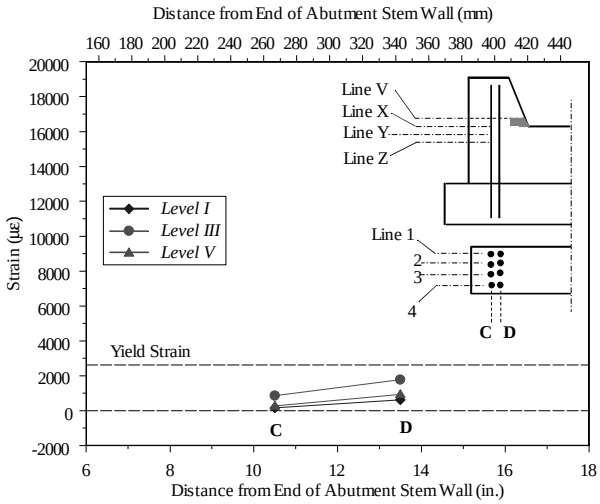

e) Line 2Z

Figure 6.31 Horizontal Profiles of Strains in Shear Key Vertical Reinforcement of Unit 3B

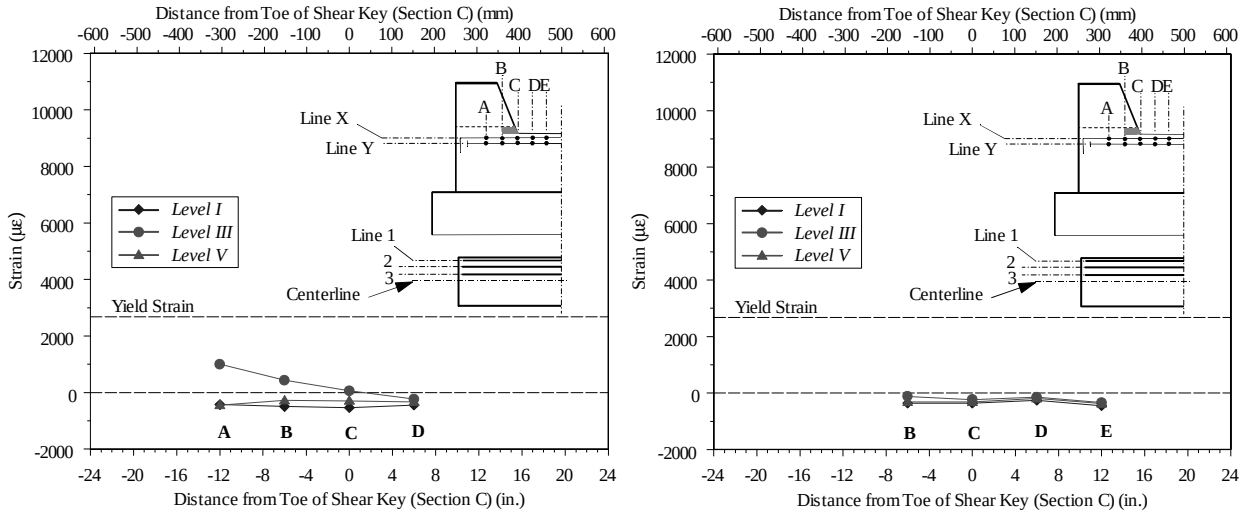

a) Line 1X b) Line 1Y

Figure 6.32 Horizontal Profiles of Strains in Horizontal Reinforcement of the Abutment Wall in Unit 3B (#3 bars)

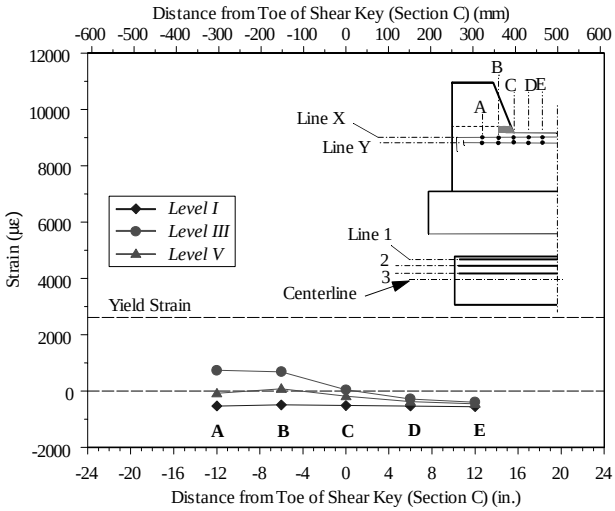

a) Line 2X

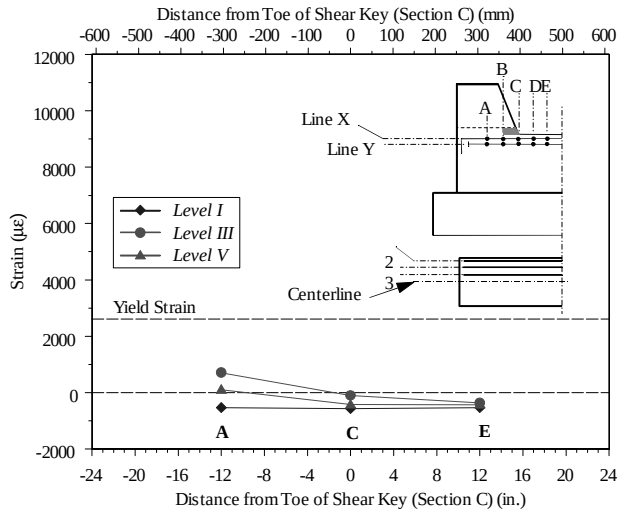

b) Line 2Y

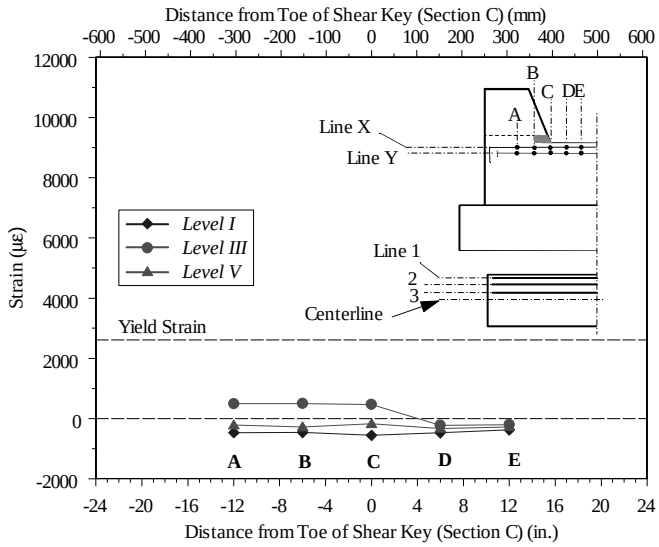

c) Line 3X

Figure 6.33 Horizontal Profiles of Strains in Horizontal Reinforcement of the Abutment Wall in Unit 3B (#5 bars)

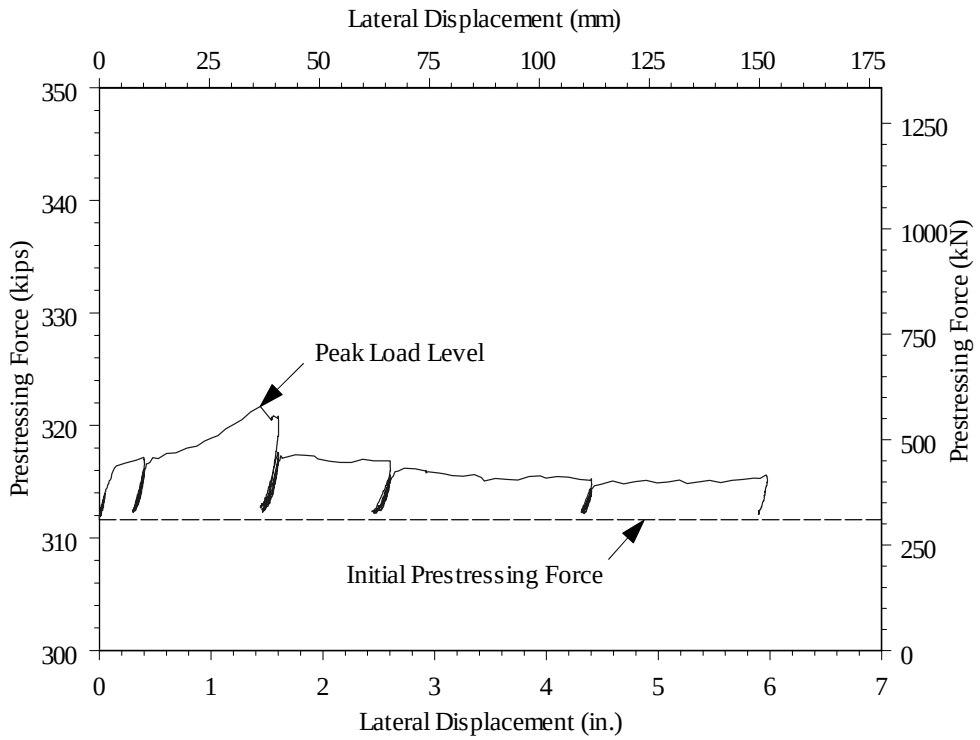

Figure 6.34 Variation of Prestressing Force in the Abutment Stem Wall During Testing of Unit 3B

7 DISCUSSION OF EXPERIMENTAL RESULTS OF SACRIFICIAL EXTERIOR SHEAR KEYS

The experimental results presented in Chapter 6 are discussed in this chapter. As discussed earlier in Chapter 1, sacrificial shear keys should be designed such that their shear capacity does not exceed 75% of the shear capacity of the piles plus one of the wing-walls. Sacrificial shear keys should perform as structural fuses during earthquake events. It is desirable that failure during an earthquake would occur in the sacrificial shear keys with minimum and repairable damage in the abutments. Major damage of the abutment is not desirable as it makes post-earthquake repair difficult and may require reconstruction of the abutment. If failure occurs in the shear keys, they can be removed after the earthquake, and if necessary new shear keys may be constructed on the repairable abutment wall. The major objective of this experimental program was to investigate the seismic performance of sacrificial exterior shear keys with the main intent in reducing and localizing damage in the abutment walls. Test results have shown that these objectives may be readily achieved by providing: (1) cold construction joints between the shear key and the abutment, (2) keys with flexural dominated response, and (3) post-tensioning of the abutment stem wall. These conditions were investigated in this research program and evaluation of these design details is described in this chapter.

7.1 Comparison of Cracking Patterns at Different Damage Levels

The cracking patterns for the sacrificial exterior keys tested in this research work are compared in this section at different damage levels. Since the cracking patterns for Units 1A and 1B were very similar, only the cracking pattern for Unit 1B is included in this discussion. Figure 7.1 to Figure 7.4 show the cracking patterns for the different shear keys at damage Level II to Level V, respectively.

Level II: Figure 7.1 shows the diagonal cracks that occurred in the abutment stem wall at Level I. As mentioned in Chapter 6 onset of cracking occurred at this level. For Test Units 1A, 1B and 2A a crack was clearly visible at the intersection of the inner inclined side of the shear key and the top surface of the abutment stem wall. In Test Units 1A and 1B, this crack propagated in the downward direction in the abutment stem wall at an angle towards the abutment stem wall's toe. In Test Unit 2A, the initial crack occurred at the shear key-abutment wall interface and it propagated horizontally along the shear key-abutment stem wall interface until its intersection with the first row of the shear key vertical reinforcement. This was followed by propagation of the crack along the abutment wall towards the base of the abutment. This was followed by

occurrence of other diagonal cracks in the abutment wall. Comparison of Figure 7.1a and Figure 7.1b shows that most of the diagonal cracks in Unit 2A occurred below the shear key, whereas in Unit 1B with monolithic construction of the shear key with the abutment walls, diagonal cracks extended farther away from the shear key and inside the abutment stem wall. Figure 7.1c and Figure 7.1d show that with abutment post-tensioning a major horizontal crack occurred at the shear key-abutment stem wall interface with minor cracks in the abutment stem wall below the shear key.

(a) Test Unit 1B

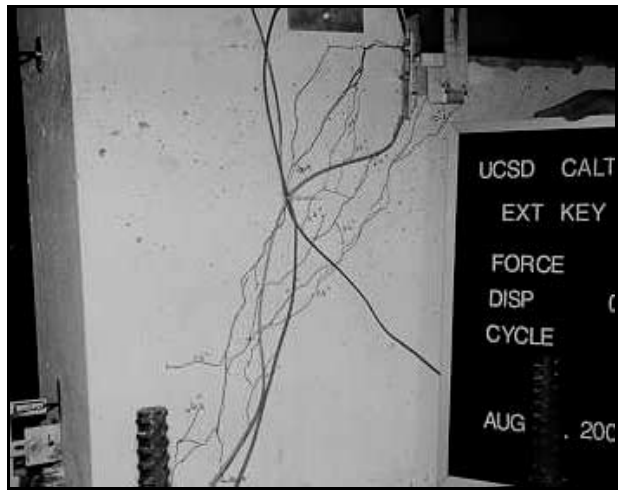

(b) Test Unit 2A

(c) Test Unit 3A

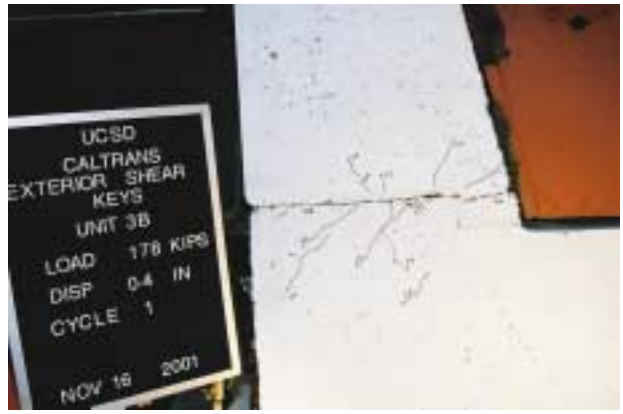

(d) Test Unit 3B

Figure 7.1 Cracking Patterns at Level II

Level III: Figure 7.2 shows the cracking patterns for different test units at damage Level III. Figure 7.2a to Figure 7.2b show the diagonal cracks in the abutment reflecting the formation of a compressive strut between the point of load application to the toe of the abutment stem wall (see Figure 5.4). If the abutment wall is post-tensioned with adequate clamping force, the failure mode shown in Figure 5.4 can be prevented. Post-tensioning of the abutment in Units 3A and 3B

prevented formation of these diagonal cracks in the abutment stem wall. Damage of the abutment wall was minimal in Units 3A and 3B and was localized in the shear key-abutment interface zone (see Figure 7.2c and Figure 7.2d). Minor spalling of the concrete cover of the abutment wall just below the shear key was observed in Units 3A and 3B at this displacement level.

(a) Test Unit 1B

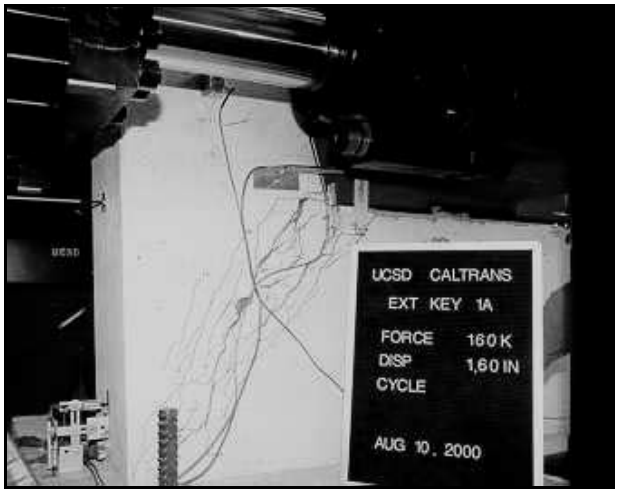

(b) Test Unit 2A

(c) Test Unit 3A

(d) Test Unit 3B

Figure 7.2 Cracking Patterns at Level III

Level IV: The diagonal cracks in the abutment of Units 1A, 1B and 2A widened significantly with increased shear key displacements as seen at Level IV for Units 1B and 2A in Figure 7.3a and Figure 7.3b, respectively. However, post-tensioning kept the abutment wall undamaged in Units 3A and 3B with only some minor concrete cover spalling in a limited zone below the shear key-abutment interface. It is clear in Figure 7.3c and Figure 7.3d that the lateral load was transferred from the shear keys to the abutment by sliding shear friction rather than by formation

of diagonal compressive struts in the abutment walls; which means that the strut-and-tie analogous model shown in Figure 5.4 was not applicable for Units 3A and 3B. This will be discussed further in Section 7.5.

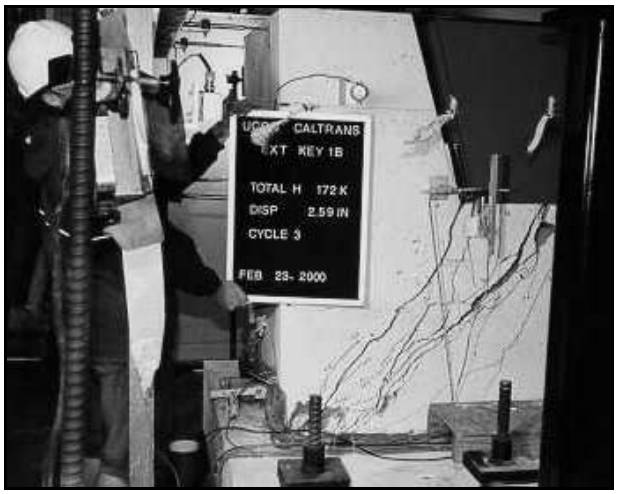

(a) Test Unit 1B

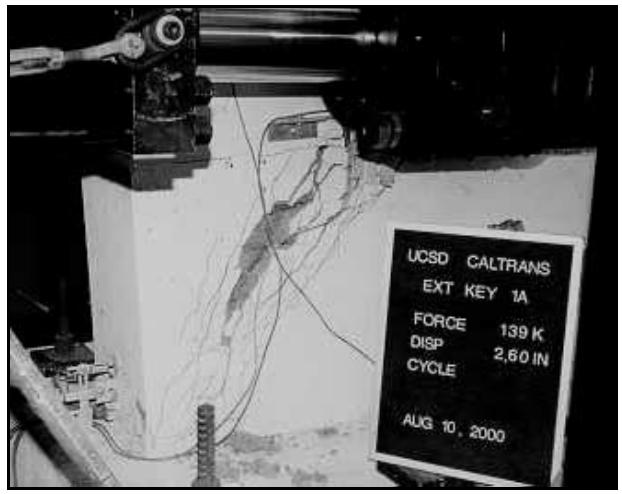

(b) Test Unit 2A

(c) Test Unit 3A

(d) Test Unit 3B

Figure 7.3 Cracking Patterns at Level IV

Level V: Testing of Units 1A, 1B and 2A was terminated at 4.4 in. (112 mm) displacement. Figure 7.4a and Figure 7.4c show Units 1A and 2A, respectively, at damage Level V. The abutment walls of Units 1B, 2A, and similarly Unit 1A, suffered significant damage that hampers easy post-earthquake repair of these abutments (see Figure 7.4a to Figure 7.4c). On the other hand, damage of post-tensioned abutments is minimal and is restricted to spalling of concrete cover in a local zone below the shear key-abutment interface. Comparison of Figure 7.4e and Figure 7.4f with Figure 7.4a to Figure 7.4c clearly shows the effect of post-tensioning in reduction of damage to the abutment walls.

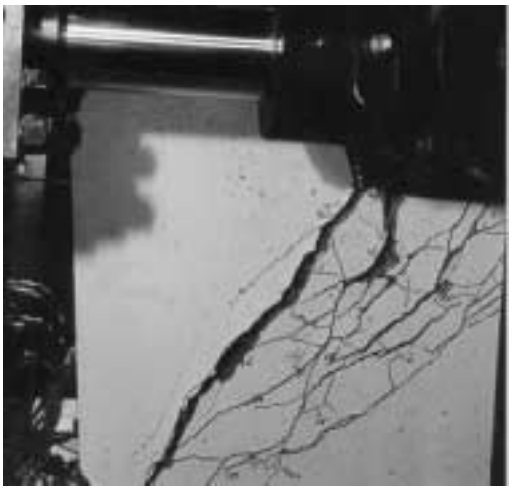

(a) Test Unit 1A

(b) Test Unit 1B

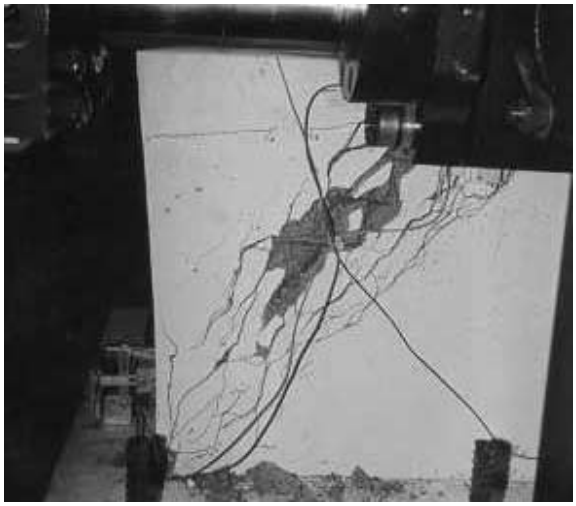

(c) Test Unit 2A

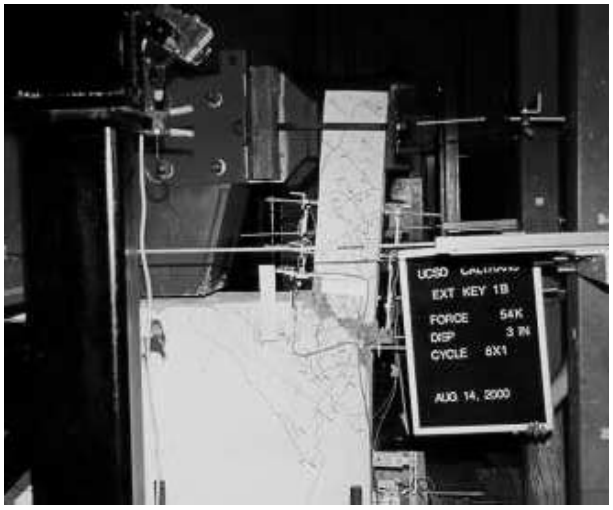

(d) Test Unit 2B

(e) Test Unit 3A

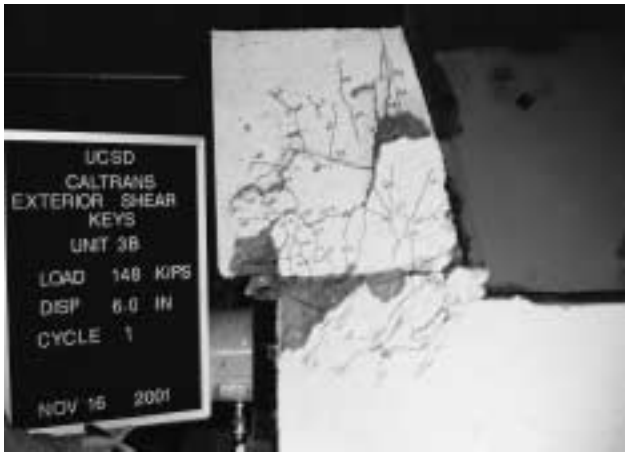

(f) Test Unit 3B

Figure 7.4 Cracking Patterns at End of Testing

Cracking patterns of all exterior shear key test units are shown in Figure 7.4. Figure 7.4a and Figure 7.4b show Test Units 1A and 1B, respectively, at the end of testing. It can be seen from these figures that significant damage occurred to the abutment stem wall rather than in the sacrificial shear key. This means that the shear keys did not perform as structural fuses in Units 1A and 1B. Figure 7.4c shows that failure of Unit 2A occurred in the abutment wall rather than in the shear key. Again, the shear key did not perform as a structural fuse. Diagonal cracking of the abutment wall was prevented by post-tensioning of the abutment stem wall of Units 3A and 3B. Thus, failure of Units 3A and 3B occurred by sliding of the shear key with respect to the abutment stem wall. The damage of the abutment wall was minimal, which means that the abutment can be easily repaired after earthquake occurrence. Figure 7.4e and Figure 7.4f show Units 3A and 3B, respectively at the end of testing. The figures show the sliding failure of the shear keys, which indicates that the shear keys performed as structural fuses in these test units as desired.

The flexural key of Test Unit 2B showed a predominant flexural behavior as intended. A plastic hinge was formed in the flexural key at its interface with the abutment stem wall. This failure was local with insignificant damage of the abutment stem wall (see Figure 7.4d), which indicates that the flexural key of Unit 2B performed as a structural fuse.

7.2 Maximum Load Carrying Capacity

The maximum load carrying capacities of the sacrificial exterior shear keys tested in this experimental program are given in Table 7.1 as well as their modes of failure.

Table 7.1 Loads and Modes of Failure of Sacrificial Exterior Shear Key Test Units

Test Series	Test Unit	Day-of-Test Concrete Strength, f_c' Psi (MPa)	Experimental Failure Load, V_{test} kips (kN)	Mode of Failure
I	1A	4,960 (34.2)	222 (988)	Diagonal cracking in abutment
	1B	4,870 (33.6)	285 (1,268)	Diagonal cracking in abutment
II	2A	3,110 (21.4)	159 (707)	Diagonal cracking in abutment
	2B	4,710 (32.5)	60 (267)	Plastic hinge in flexural key
III	3A	5,630 (38.8)	267 (1,188)	Sliding of shear key
	3B	5,630 (38.8)	239 (1,063)	Sliding of shear key

It can be seen from Table 7.1 that the capacity of Test Unit 1B was higher than the capacity of Unit 1A. It should be remembered that the abutment back wall and wing wall were modeled in Test Unit 1B; the abutment back wall and wing wall contributed to the capacity of the Unit 1B. Test Units 2A, 3A and 3B had cold construction joints between the shear key and the abutment stem wall. The shear key in each of these three units was attached to the abutment stem wall only by vertical reinforcing bars with a total area, A_{vf}.

The shear key vertical reinforcing bars consisted of 24-#3 bars in Unit 2A and of 8-#5 bars in Units 3A and 3B. The total area of the shear key reinforcement, A_{vf}, was comparable in Units 2A, 3A and 3B as can be seen in Table 5.2. The only difference among these test units was post-tensioning of the abutment stem wall in Units 3A and 3B. Table 7.1 shows that the capacities of Units 3A and 3B were much higher than that of Unit 2A. Figure 7.4c shows that failure of Unit 2A occurred in the abutment stem wall rather than in the shear key. Diagonal cracking of the abutment wall was prevented by post-tensioning of the abutment stem wall of Units 3A and 3B. Thus, failure of Units 3A and 3B occurred by sliding of the shear key with respect to the abutment stem wall.

The flexural key of Test Unit 2B showed a predominant flexural behavior as intended. A plastic hinge was formed in the flexural key at its interface with the abutment stem wall. It should be mentioned that the load carrying capacity of the flexural key is much less than capacity of the other test units as shown in Table 7.1.

7.3 Post-Peak Performance

It may be assumed in design that sacrificial shear keys do not provide any further support for the bridge superstructure once they reach their maximum load carrying capacities. This design assumption was investigated in this experimental research and the results can be discussed with the aid of Figure 7.5 and Figure 7.6. Figure 7.5 shows the load versus lateral displacement at top of the shear keys of Units 1A, 1B, 2A, 3A and 3B. The load versus lateral displacement at top of the flexural key of Unit 2B is shown in Figure 7.6; the figure also shows values of the displacement ductility corresponding to different key displacements. It should be mentioned that the potentiometer measuring the displacement at top of the shear key in Unit 1B was removed at about 3.4 in. (86 mm) but the test unit was loaded up to 4.4 in. (112 mm) key top displacement. Figure 7.5 shows the load versus deformation curve for Unit 1B until the potentiometer was removed.

Figure 7.5 shows the relatively high stiffness of all shear keys until the onset of yielding, followed by significant reduction in stiffness. Once Units 1A and 1B reached their maximum load carrying capacities, the applied load dropped significantly and both tests were terminated at about 4.4 in. (112 mm) lateral displacement when some of the reinforcing bars in the abutment wall fractured. Test Unit 2A with the cold construction joint between the shear key and the abutment wall showed a more ductile performance than Units 1A and 1B. Figure 7.5 shows that Unit 2A reached its maximum load carrying capacity at about 1.4 in. (36 mm). Test Unit 2A could undergo lateral displacement up to about 2.6 in. (66 mm) with almost no drop in the transferred load. Under higher displacement, there was significant deterioration of the shear key's capacity in Test Unit 2A and the test was terminated at about 4.6 in. (117 mm) displacement. The load carrying capacity of the shear key at the end of the test was only about 40 kips (178 kN).

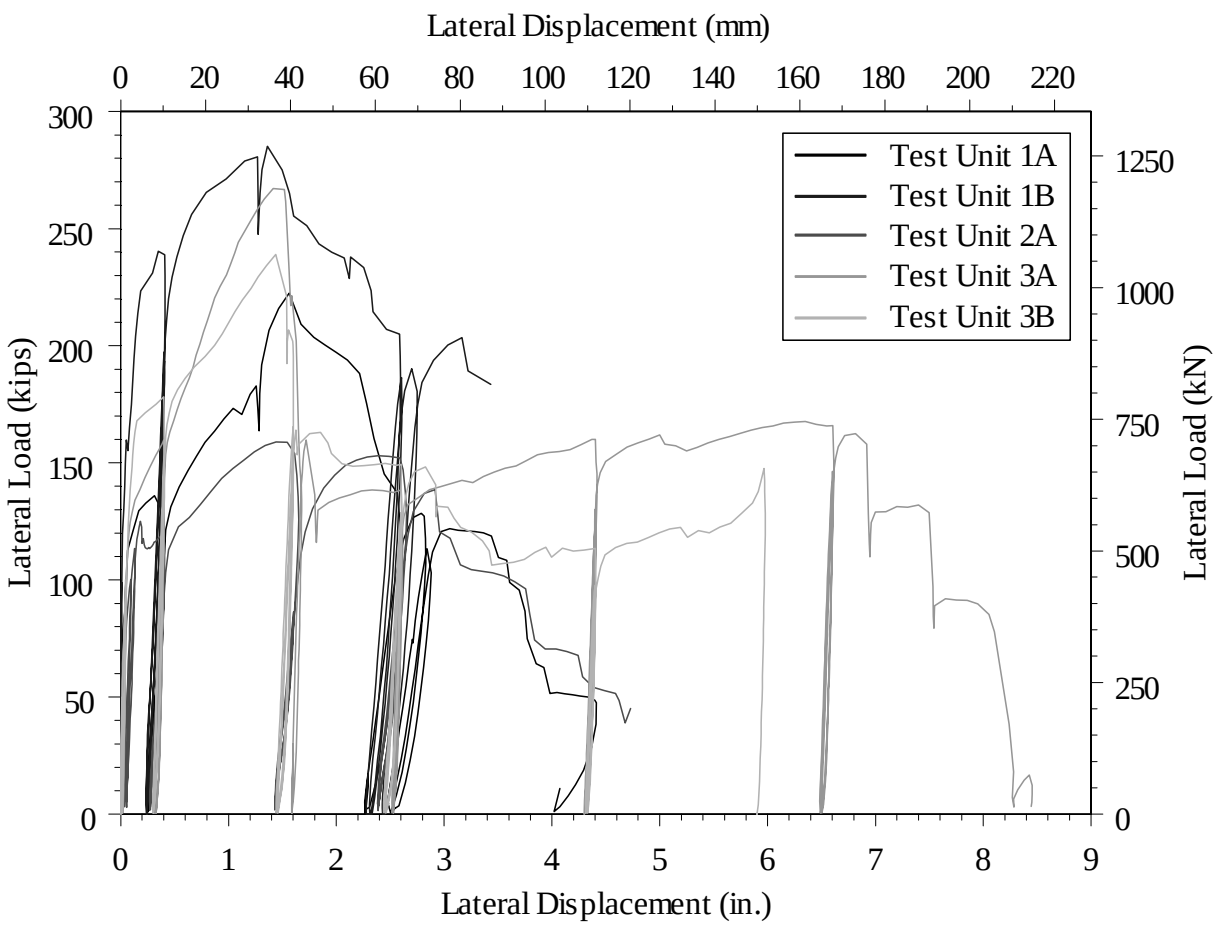

Figure 7.5 Load versus Deformation for Exterior Shear Key Test Units

Test Units 3A and 3B reached their maximum load carrying capacities at about 1.4 in. (36 mm) displacement. A drastic drop occurred in capacities of these two test units once they reached their

peak loads. As mentioned earlier, this sudden drop in the load carrying capacity resulted from fracture of some of the shear key reinforcement bars. Because the remaining shear key reinforcing bars did not fracture, both Units 3A and 3B had significant residual shear key capacity.

The residual capacity of both units could be sustained up to significantly higher displacement levels as seen in Figure 7.5. As previously described testing of Unit 3B was terminated at 6 in. (152 mm) displacement when the steel loading arm started to contact the protrusion of the abutment stem wall below the shear key-abutment wall interface. The curves shown in Figure 7.5 for Units 3A and 3B indicate that with post-tensioning of the abutment stem wall, the shear keys could provide significant transverse support to bridge superstructures up to very high transverse displacement levels. The ability of the shear keys to support the bridge superstructure in the post-peak range should not be ignored as it can significantly affect the overall performance of the bridge system.

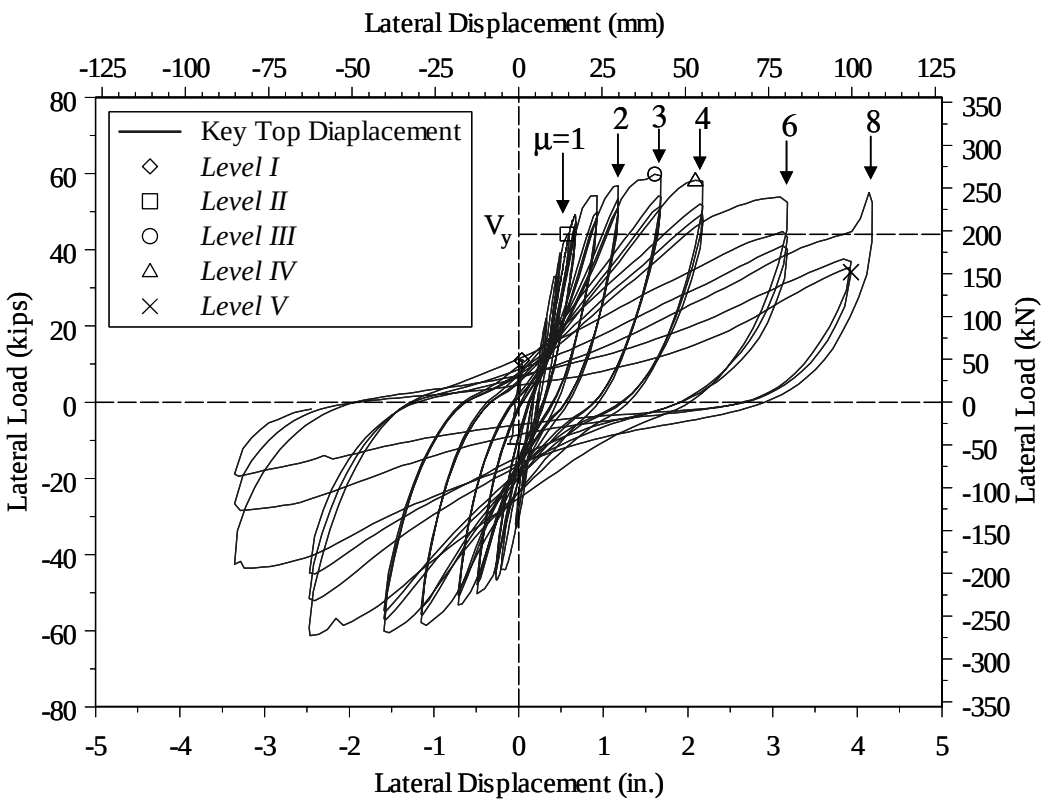

Figure 7.6 Load-Deformation Response of Unit 2B with Flexural Key

Figure 7.6 clearly demonstrates the dominant flexural performance of Test Unit 2B, with significant ductility capacity. The test was terminated when the 90-degree hooks of the

horizontal reinforcement nearest to the top surface of the abutment stem wall opened. The flexural key could have been subjected to higher displacements if seismic hooks were used for these reinforcing bars. The assumption that shear keys do not provide any transverse support to the superstructure in the post-peak range is clearly not correct for flexural keys, and an evaluation should be performed in order to investigate which of the shear keys investigated in this research program would lead to a better seismic performance of the bridge structure.

7.4 Post-Earthquake Repair

The possibility of post-earthquake repair of sacrificial shear keys-abutment systems is one of the important issues that need to be addressed in bridge design. Figure 7.4a and Figure 7.4b show Test Units 1A and 1B, respectively. In Units 1A and 1B, the shear key was monolithically constructed with the abutment wall. Severe damage occurred in the abutment wall in both test units and the sacrificial shear keys did not perform as structural fuses. This suggests that if the sacrificial shear keys are constructed monolithically with non-prestressed abutments, post-earthquake repair will be difficult and it may be necessary to re-build the damaged abutment.

Use of cold construction joint between the abutment and the shear key in Unit 2A could not prevent damage to the abutment wall as can be seen in Figure 7.4c. Again, the shear key in Unit 2A did not perform as a structural fuse and the abutment may have to be re-built if post-earthquake repair is required. Damage of the abutment wall can be reduced by increasing the amount of tension tie reinforcement (hanger bars) in the abutment stem wall; hanger bars are the reinforcing bars that carry the tensile force T_1 shown in Figure 5.4.However damage of the abutment stem wall may not be prevented even if the abutment is provided by excessive amount of hanger bars. An effective way to prevent formation of cracks and subsequently to minimize damage in the abutments is to post-tension the abutment wall. Post-tensioning of the abutment is more efficient since increasing the amount of tension tie reinforcement (hanger bars) alone may not prevent occurrence of diagonal cracks in the abutment wall.

The experimental results of Units 3A and 3B indicate that post-tensioning is an efficient solution to minimize the damage in the abutment walls. Figure 7.4e and Figure 7.4f show that post-tensioning prevented occurrence of diagonal cracks in the abutment stem-wall and the load was transferred to the abutment by a sliding shear friction mechanism. Thus the shear keys performed as sacrificial elements, or structural fuses, to protect the abutment and the piles.

The exterior shear key of Unit 3A was dismantled after end of testing, and Figure 7.7 shows the abutment stem wall after removal of the shear key. Figure 7.7a shows that spalling of the

concrete cover of the abutment wall occurred only in a localized region below the shear key-abutment interface. Figure 7.7b shows a close-up view of the top surface of the abutment stem wall at location of the interface with the shear key. The shear key failed by sliding shear as can be seen in Figure 7.4e. Despite the high forces and high displacements that Unit 3A could undergo, the top surface of the abutment wall remained in a good condition except for fracture of the vertical headed bars that connected the shear key to the abutment wall.

(a) Abutment wall

(b) Close-up view of the abutment wall surface

Figure 7.7 Abutment Stem Wall of Test Unit 3A after Removal of the Exterior Shear Key

In case of post-earthquake repair of post-tensioned abutments similar to Unit 3A, minimum repair is needed with new vertical reinforcing bars re-installed to connect the abutment wall with the new sacrificial shear key. These new vertical bars may be installed by drilling vertical holes in the abutment wall to accommodate the new bars followed by grouting of these holes. An alternative simpler approach is by providing mechanical couplers.

Figure 6.23 (or Figure 7.7b) shows four interior vertical headed bars, which fractured at the shear key-abutment wall interface. These four bars were well confined by the surrounding concrete and the two prestressing bars. Thus, these interior bars did not have the ability to displace as the shear key was sliding against the abutment wall. These vertical bars could have mechanical couplers at their end and flushed with the abutment top surface at the interface with the shear key. Vertical bars with threaded ends can be installed inside the couplers. Thus, the couplers provide mechanical splices between the vertical reinforcing bars inside the abutment wall and the vertical bars inside the shear keys. Splicing the shear key vertical reinforcement with mechanical couplers was adopted in Test Unit 3B (see Figure 5.25).

As shown earlier, the performance of Test Unit 3B was similar to that of Unit 3A. Thus, the use of mechanical couplers to splice the shear key vertical reinforcing bars of Unit 3B did not have adverse effects on the performance of Test Unit 3B. As mentioned earlier, testing of Unit 3B was

terminated when the steel loading arm started to contact with the protrusion of the abutment stem wall. Half of the shear key reinforcing bars had not yet fractured by the end of the test, and these bars were bent significantly, as observed in Figure 7.8a. The threaded end of the bar was inside one of the couplers shown in Figure 7.8b. The figure shows that despite the significant displacements that Unit 3B underwent, the couplers were still in a very good condition such that the bar shown in Figure 7.8a could be removed and re-installed in the couplers. Easy removal of these bars in the damaged shear keys and easy installation of new bars with threaded ends into the undamaged couplers provide an easy alternative for post-earthquake repair of sacrificial shear keys. However couplers in the shear reinforcement bars, which fractured at the maximum load carrying capacity level, were damaged and not re-usable. This indicates that couplers would be protected from damage and can be re-usable if fracture of the shear key reinforcement is avoided.

(a) One of the shear key reinforcing bars

(b) Close-up view of the couplers

Figure 7.8 Shear Key Reinforcement with Mechanical Couplers in Test Unit 3B

7.5 Analytical Models for Sacrificial Exterior Shear Keys

Two models were presented in Chapter 5 to evaluate the capacity of sacrificial exterior shear keys. These models are briefly described below for convenience.

7.5.1 Sliding Shear Friction Model

The first model is currently under consideration for the Caltrans Design Specifications [2], which assumes that the lateral force is transferred from the shear key to the abutment stem wall through a shear friction mechanism. This model was described in Section 5.2.1. Capacity of the shear key was given by:

$$V_N = \mu \left(A_{vf} f_{yf} + A_{vs} f_{ys} \right) \qquad \textbf{(7.1)}$$

According to the Caltrans Design Specifications [2], the coefficient of friction = 0.6λ at the interface between two concrete elements with a cold construction joint and when the concrete surfaces are not intentionally roughened, such as in Units 2A, 3A and 3B. Also in Eq. (7.1) A_{vs} and f_{ys} are, respectively, the area and the yield strength of the vertical reinforcement on the sides of the abutment back wall and wing wall that cross the shear key-abutment stem wall interface. The value of V_N calculated using Eq. (7.1) and the coefficient of friction values specified by Caltrans [2] is denoted by $V_{N,Calt}$.

7.5.2 Strut-and-Tie Analogous Model Type I

Section 5.2.2 described a strut-and-tie analogous model that can be used in prediction of the shear key capacity. In this model, it is assumed that the lateral load is transferred to the footing by a diagonal compressive strut that forms in the abutment stem wall between the point of application of the load and the toe of the abutment wall. The dominant crack in this case will be a diagonal one in the abutment stem wall. This model is schematically shown in Figure 5.4, but it is also shown here in Figure 7.9 for convenience.

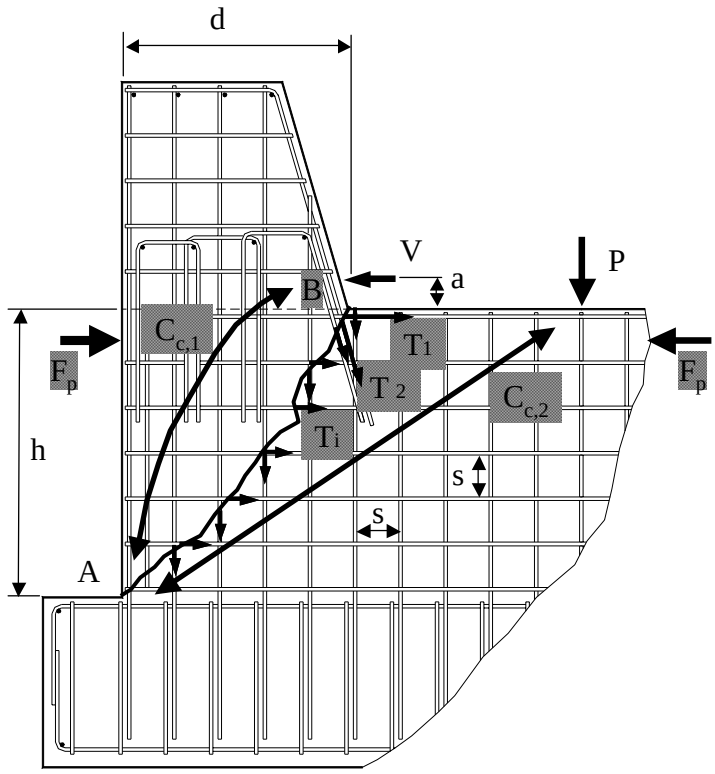

Figure 7.9 Strut-and-Tie Analogous Model Type I

The strut-and-tie model shown in Figure 7.9 is referred to throughout this Section as Model I. It should be mentioned that this model may be applicable only if the abutment stem wall is not

post-tensioned or if the prestressing force of the abutment stem wall is small such that the diagonal crack AB dominates the response of the shear key. In this case the shear key capacity is given by Eq. (5.2) to (5.5).

Test Units 1A and 1B, displayed a load transfer mechanism similar to that given by Model Type I (see Figure 7.9). The dominant diagonal crack shown in Figure 7.9 can be seen in Figure 7.4a and Figure 7.4b for Test Units 1A and 1B, respectively. The capacity of test Units 1A and 1B can be calculated by this model using Eqs. (5.2), (5.3) and (5.5), with $F_P = 0.0$ in Eq. (5.5).

7.5.3 Strut-and-Tie Analogous Model Type II

Model II is similar to Model I, but should be applicable for sacrificial shear keys in which a cold construction joint exists between the shear key and the abutment stem wall, such as in Unit 2A. It was noticed during testing of Unit 2A that the initial crack occurred at the interface between the shear key and the abutment wall. Because of the construction joint, this propagated along the interface until it intersected with the first row of shear key reinforcement. This was followed by deviation of the crack inside the abutment stem wall, as shown in Figure 7.10.

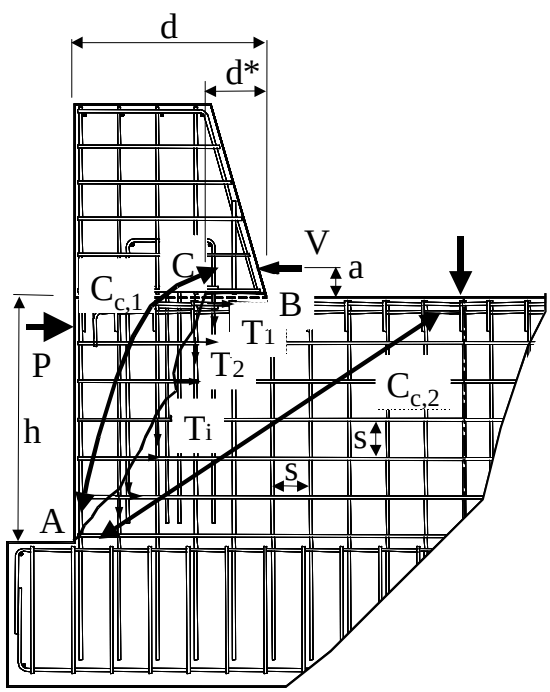

Figure 7.10 Strut-and-Tie Analogous Model Type II

The capacity of the shear key was also calculated using Eq. (5.2), (5.3) and (7.2) or (7.3). Equations (7.2) and (7.3) replace Eqs. (5.4) and (5.5) used in Model I. The major difference is ignoring the last term inside the brackets, which represents contribution of the vertical side

reinforcement of the abutment wall to the capacity of the shear key. The contribution of the abutment wall side vertical reinforcement is ignored in Model II because the vertical side reinforcing bars are not continuous and they stop below the shear key-abutment wall interface. The terms given in Eqs. (7.1), (7.2) and (7.3) were defined in Section 5.2.2.

$$V_s = \left[F_p h_p + T_1 h + T_2 (d - d^*) + n_h T_{i,h} \frac{h^2}{2\,s} \right] \left(\frac{1}{h + a} \right) \qquad \textbf{(7.2)}$$

and

$$V_s = \left[F_p h_p + A_{s,1} f_{y,1} h + A_{s,2} f_{y,2} (d - d^*) + n_h A_{s,s} f_{y,s} \frac{h^2}{2\,s} \right] \left(\frac{1}{h + a} \right) \qquad \textbf{(7.3)}$$

This model is applicable if the abutment wall is not post-tensioning or if the prestressing force, F_p is relatively small. The shear key capacity of Unit 2A can be calculated by Eqs. (5.2), (5.3), and (7.3).

7.5.4 Strut-and-Tie Analogous Model Type III

The third model is applicable only when the abutment stem wall is post-tensioned with sufficient force that prevents the diagonal cracking inside the abutment stem wall. The load transfer mechanism for Model III is schematically shown in Figure 7.11. The figure shows that the load is transferred to the abutment at the location of the prestressing force, F_p, by a diagonal compressive strut inside the shear key. The diagonal compressive strut is in equilibrium with the vertical tie represented by the vertical reinforcement connecting the shear key to the abutment.

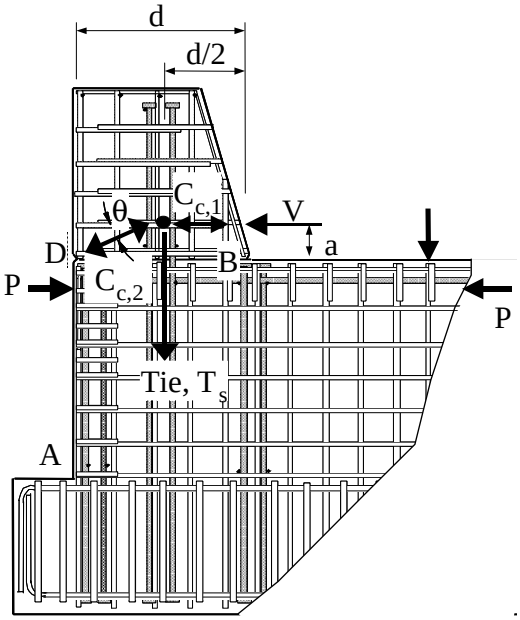

Figure 7.11 Strut-and-Tie Analogous Model Type III

Utilizing this mechanism, the total capacity of the shear key is given by:

$$V_N = A_{vf} \; f_{yv} \cot\theta \qquad \textbf{(7.4)}$$

Where A_{vf} and f_{yv} are the area and yield strength of the shear key vertical reinforcement and θ is the angle of the compressive strut as shown in Figure 7.11. This model is applicable only for assessment of shear keys similar to those of Test Units 3A and 3B.

7.5.5 Moment-Curvature Analysis

Flexural keys, such as the one used in Unit 2B, have a predominant flexural behavior. Capacity of flexural keys can be predicted by conventional methods of flexural capacity calculation or, more accurately, using a moment-curvature analysis as described in Section 5.2.3.

The experimental values of maximum load carrying capacity of all the exterior key test units as well as the capacities calculated using the above mentioned analytical models are presented in Table 7.2. Moment-curvature analysis was used to predict the failure load of the flexural key of Unit 2B; the predicted failure load was about 68 kips (303 kN) compared to the experimental failure load of 60 kips (267 kN).

Table 7.2 Experimental and Calculated Maximum Load Carrying Capacities of Exterior Sacrificial Shear Keys

Test Series	Test Unit	f_c' psi (MPa)	V_{Test} kips (kN)	V_{nCalt} kips (kN)	$V_{n\ Strut\text{-}and\text{-}Tie}$ kips (kN)			$V_{n\ SF}$ kips (kN)	$V_{n\ Calc}$ kips (kN)	$\frac{V_{n\ Calc}}{V_{Test}}$
					I	II	III			
(1)	(2)	(3)	(4)	(5)	(6)	(7)	(8)	(9)	(10)	(11)
I	1A	4,960 (34.2)	222 (988)	380 (1690)	223 (992)	-----	-----	-----	223 (992)	1.00
	1B	4,870 (33.6)	285 (1268)	581 (2585)	291 (1294)	-----	-----	-----	291 (1294)	1.02
II	2A	3,110 (21.4)	159 (707)	133 (592)	-----	189 (841)	-----	-----	189 (841)	1.19
III	3A	5,630 (38.8)	267 (1188)	107 (476)	-----	595 (2647)	536 (2384)	246 (1094)	246 (1094)	0.92
	3B	5,630 (38.8)	239 (1063)	107 (476)	-----	552 (2456)	536 (2384)	246 (1094)	246 (1094)	1.03

In Table 7.2, f_c' is the concrete compressive strength determined on day-of-test; V_{Test} is the experimental maximum load carrying capacity; V_{nCalt} is the capacity calculated using the shear friction model Eq. (7.1) using a coefficient of friction of 1.4 for Units 1A and 1B and 0.6 for Units 2A, 3A and 3B according to Caltrans Design Specifications [2] and $V_{n\ Strut\text{-}and\text{-}Tie}$ is calculated using the above mentioned strut-and-tie models.

Model I was used in calculation of the capacity of Units 1A and 1B. Model II was used for Units 2A, 3A and 3B, whereas Model III was used for Units 3A and 3B only. Comparison of the values in Columns 4 and 5 of Table 7.2 indicates that the current Caltrans shear friction model severely underestimates the capacity of shear keys which fail by sliding shear (Units 3A and 3B). The shear key reinforcement bars in Units 3A and 3B reached their ultimate tensile strength of 99 ksi (683 MPa). Using the experimental failure loads and the ultimate tensile strength f_{uv} of the shear key reinforcement in Eq. (7.1), the coefficients of friction as determined for Units 3A and 3B are 1.09 and 0.97, respectively. This indicates that the coefficient of friction adopted in the Caltrans Design Specifications is very conservative and results in significant underestimation of the capacity of shear keys. This means that if the current Caltrans shear friction model is used in design of sacrificial exterior shear keys with construction joint between the post-tensioned abutment stem wall and the shear keys, higher forces will be transferred to the abutment and the piles than anticipated in design. Piles may be overloaded and may suffer damage in this case.

The tests performed in this research work are not sufficient to suggest modifications to the current Caltrans shear friction model. However, $V_{n\ SF}$ in Table 7.2 is calculated using Eq. (7.1), but with using $\mu = 1.0$ (instead of 0.6) and the ultimate tensile strength, f_{uv} (instead of the yield strength). Values of the calculated capacity of Units 3A and 3B, which actually failed by sliding shear, are given in Column 9 of Table 7.2. The designer may use the strut-and-tie models and the shear friction model to determine an upper bound in the estimation of the capacity of sacrificial shear keys.

The calculated capacity, $V_{n\ Calc}$ is the lowest of the values given in Columns 6 through 9 of Table 7.2. The calculated capacity is in close agreement with the experimental values as can be seen from the last column in Table 7.2. Further research work is needed to modify the current shear friction model for design of sacrificial shear keys.

8 ANALYTICAL MODELS OF EXTERIOR SHEAR KEYS

The load vs. displacement curves for Test Units 1A, 1B and 2A are shown in Figure 8.1, and their envelopes in Figure 8.2. These figures indicate strong similarities amongst the three test units. Observation of these figures suggests five distinctive branches. In the first branch, the initial stiffness of the test units was approximately the same up to damage Level I, which corresponds to cracking of the shear keys at the interface between the shear keys' sloped surface and the abutment stem wall. The next branch that can be visualized is the ascending branch up to the peak load and is defined in terms of damage Level III. This branch may be represented between damage Levels II and III. The third branch can be characterized as the descending curve between damage Levels III and IV. The fourth branch is depicted by a flat curve between Levels IV and V, and finally, the fifth branch is the descending branch beyond Level V. A detailed description of these damage levels is presented next.

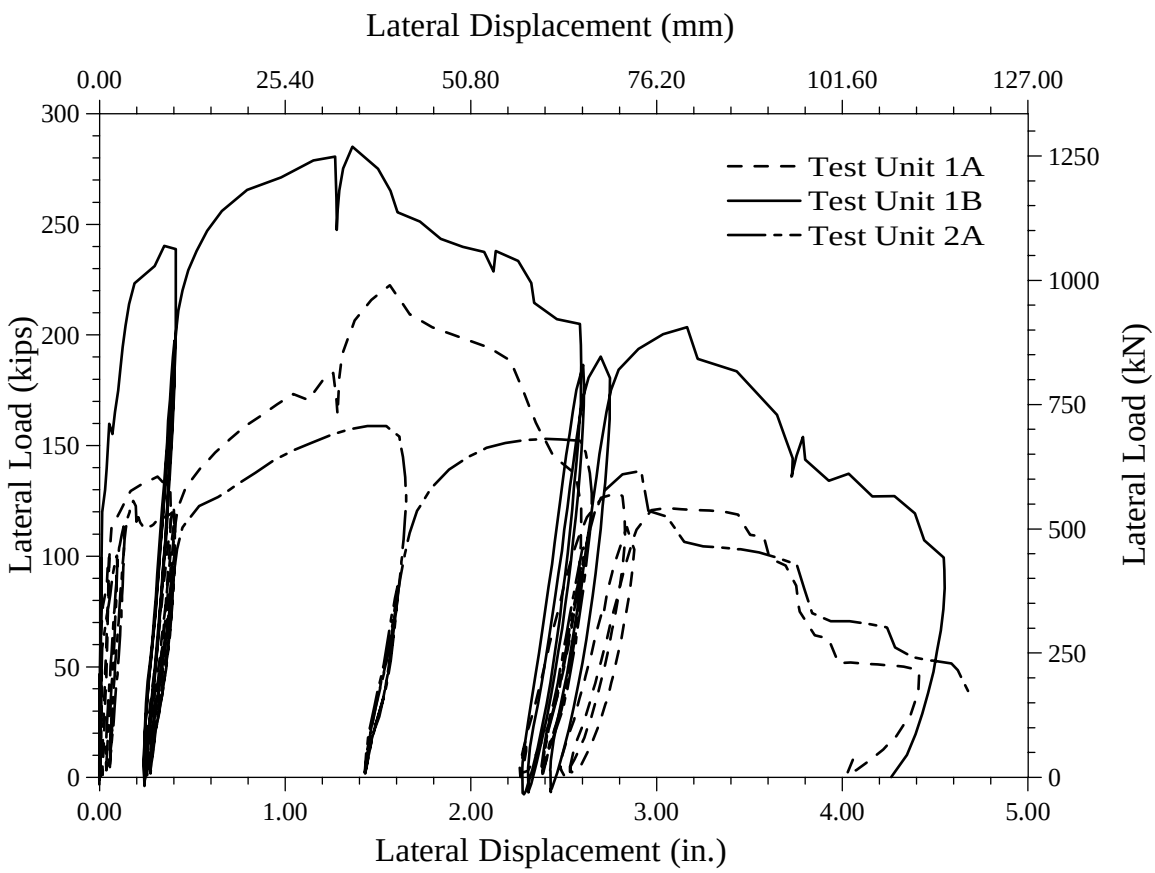

Figure 8.1 Load vs. Displacement – Exterior Shear Keys

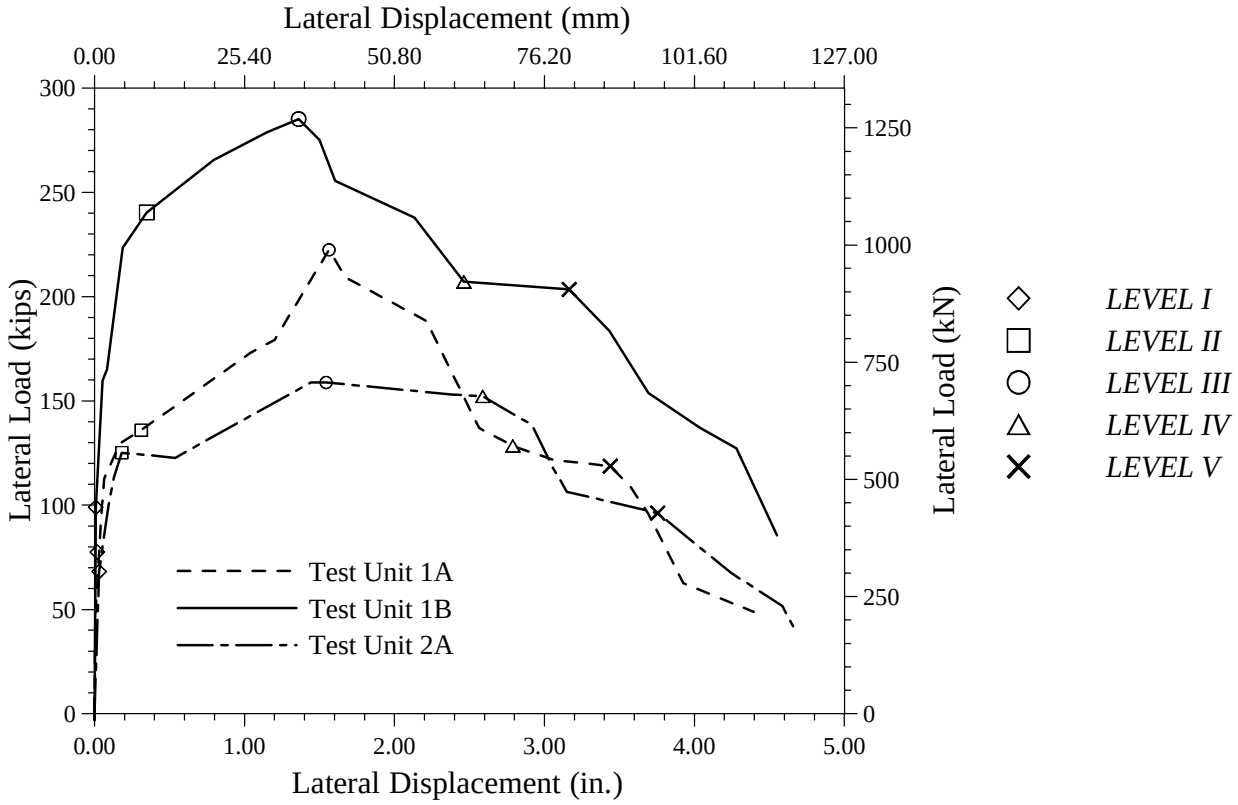

Figure 8.2 Envelope of Load vs. Displacement Curves

8.1 Development of Strut-and-Tie Mechanism and Hysteretic Model

Figure 8.3 shows an idealized load versus displacement envelope for the sacrificial exterior shear keys defined as Test Units 1A, 1B, and 2A. This idealized hysteretic model was expressed in terms of two models, which correspond to the concrete and steel components, as shown in Figure 8.4 and Figure 8.5, respectively.

The concrete component model was defined as an idealized elasto-plastic model as shown in Figure 8.4(a), but with a strength loss model as depicted in Figure 8.4(b). The strength loss model was implemented in order to describe the reduction in the concrete component due to loss of the aggregate interlock beyond the peak load.

The steel component model was also defined as an idealized elasto-plastic model as shown in Figure 8.5 (a), and with a strength loss model as depicted in Figure 8.5 (b). As before, the strength loss model was implemented in order to describe the reduction of the steel component due to fracture of the reinforcement that crosses the cracking zone. Description of these models and analytical values in terms of the five damage levels is presented next.

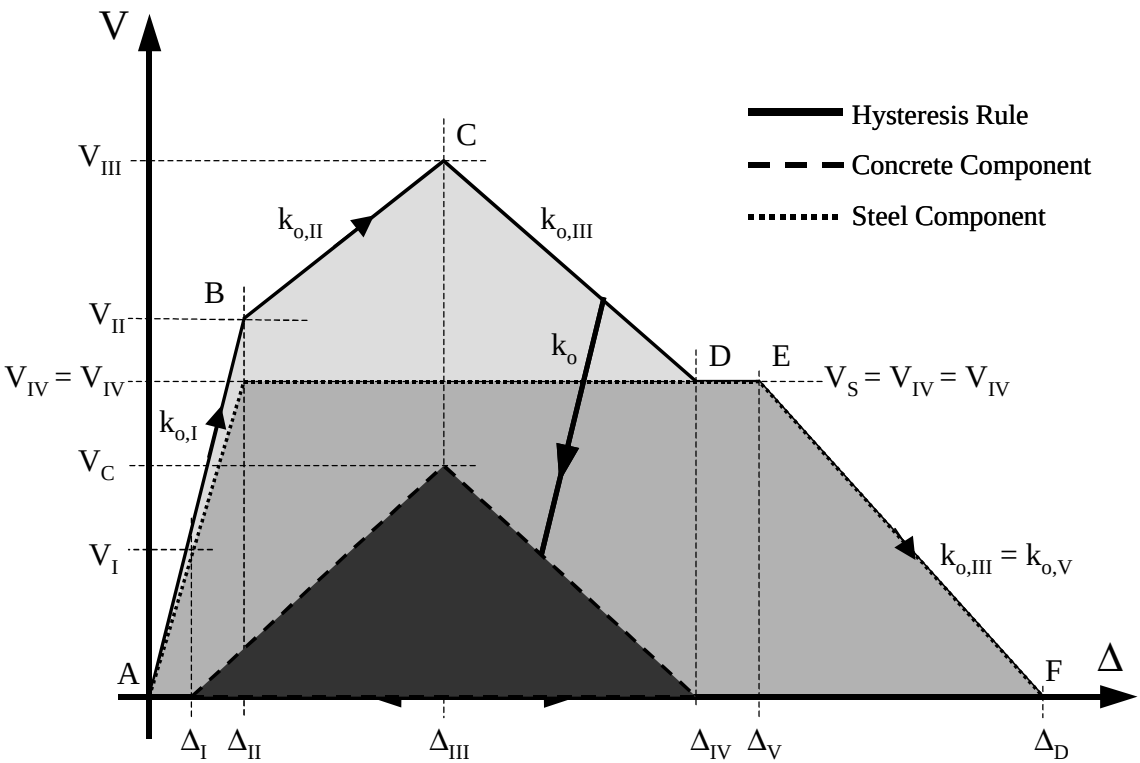

Figure 8.3 Hysteresis Rule for Exterior Shear Keys

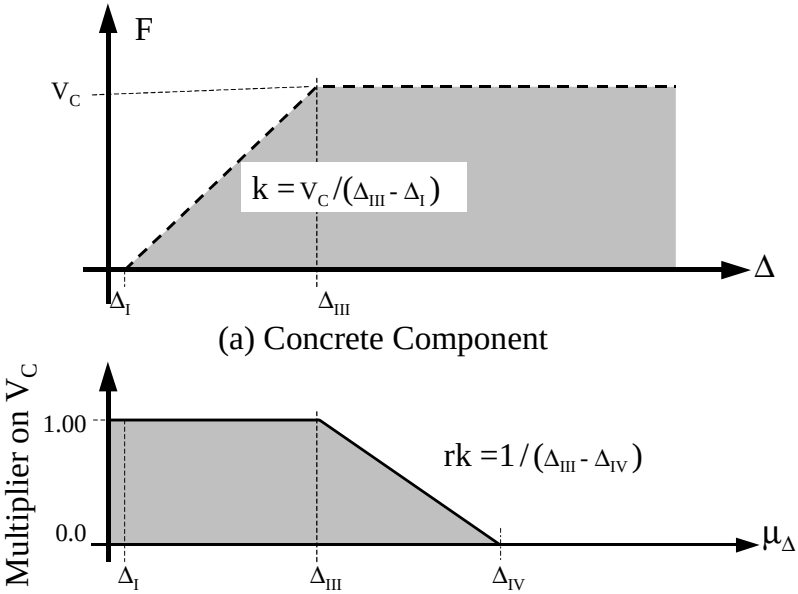

(a) Concrete Component

(b) Concrete Strength Reduction Variation

Figure 8.4 Concrete Component Model

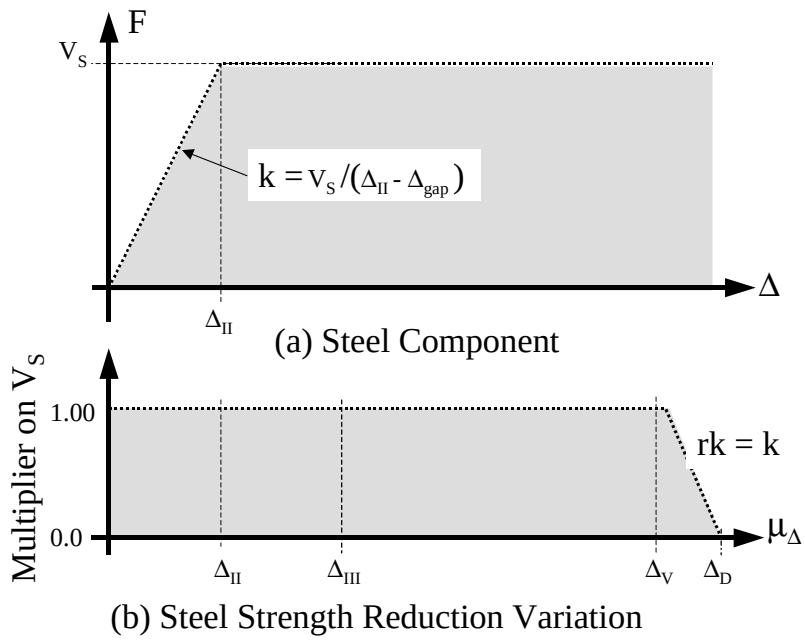

Figure 8.5 Steel Component Model

8.1.1 LEVEL I

This damage level was characterized by onset of cracking at the shear key-abutment stem wall interface. Lateral load at this level was computed based on principal tensile stresses in this region. Based on a finite element analysis it is clear from Figure 8.6(a) that shear stresses that develop at the level of the stem wall vary linearly from zero at the exterior wall face to the maximum shear stress at the intersection with the shear key.

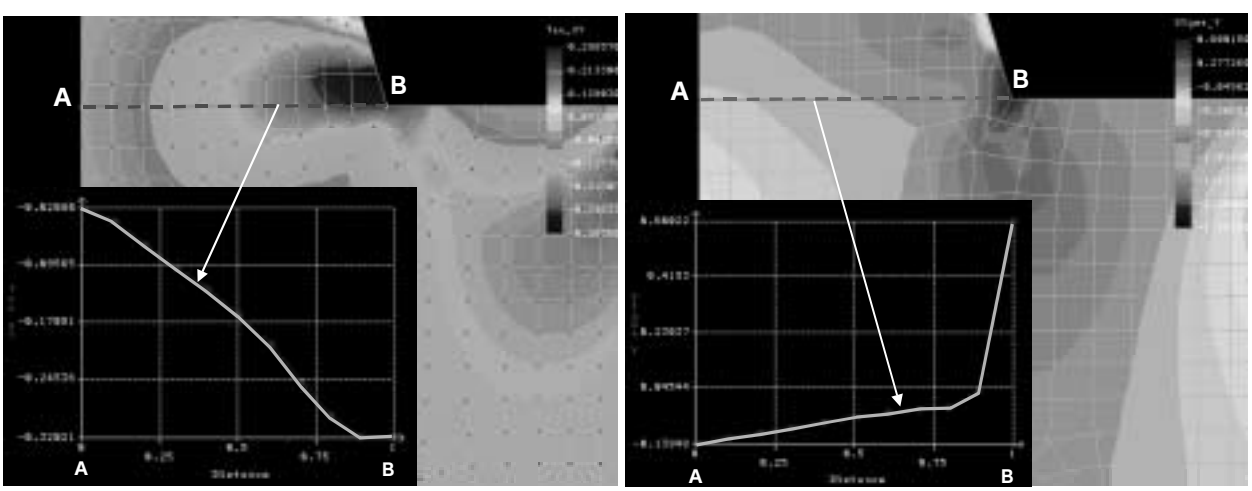

(a) Shear Stresses **(b)** Normal Stresses

Figure 8.6 Finite Element Analysis Results

In the vicinity of the applied load the shear stresses were computed as follows:

$$v_{xy} = \frac{2V}{bd} \qquad \textbf{(8.1)}$$

Similarly from Figure 8.6(b) it can be seen that the normal stresses also vary linearly at the level of the stem wall according to the flexural theory, expressed as follows:

$$f_y = \frac{6\,Va}{bd^2} \qquad \textbf{(8.2)}$$

Where *a* is the distance from the top of the stem wall to center of application of the lateral load, V (see Figure 5.4). According to the principal stresses the following relation is obtained:

$$f_t^{'} = \frac{f_y}{2} + \sqrt{\frac{f_y^2}{4} + v_{xy}^2} \qquad \textbf{(8.3)}$$

Assuming that $f_t^{'} = 7.5\sqrt{f_c^{'}}$ for shear keys cast monolithically with the stem wall and substituting Eqs. (8.1) and (8.2) into Eq. (8.3) one obtains:

$$7.5\sqrt{f_c^{'}} = \frac{3Va}{bd^2} + \sqrt{\frac{9V^2a^2}{b^2d^4} + \frac{4V^2}{b^2d^2}} \qquad \textbf{(8.4)}$$

Assuming that *a=kd*, the shear force required to cause cracking is:

$$V_{cr} = \frac{7.5\sqrt{f_c^{'}}bd}{3k + \sqrt{9k^2 + 4}} \qquad \textbf{(8.5)}$$

Table 8.1 Experimental vs. Theoretical Loads - Level I

Test Unit	Section Properties in. (mm)	Experimental kips (kN)	Theoretical - Eq. (8.5) kips (kN)
1A[1]	b=16.75 in. (425 mm) d=24 in. (610 mm) k=0.167	78 (347)	82 (365)
1B[1]	b=22 in. (559 mm) d=24 in. (610 mm) k=0.167	99 (440)	107 (476)
2A[2]	b=16.75 in. (425 mm) d=24 in. (610 mm) k=0.167	68 (302)	66 (294)

[1] Shear keys were cast monolithically with the stem walls and footing, use $f_t^{'} = 7.5\sqrt{f_c^{'}}$.

[2] Shear keys were cast after casting of the stem wall, use $f_t^{'} = 6.0\sqrt{f_c^{'}}$

8.1.2 LEVEL II

This level corresponds to onset of yielding of the shear key reinforcement and corresponds to point B in Figure 8.3. Lateral load at this damage level was computed according to the strut-and-tie analogous model presented in Section 5.2.2. The lateral load at yielding was given by Eq. (5.4), and an additional term to account for the concrete component as:

$$V_{II} = V_S + V_C \frac{\Delta_{II}}{\Delta_{III}} \qquad \textbf{(8.6)}$$

Where V_c is the concrete component to the shear resisting mechanism and is given by Eq. (5.3), and Δ_{II} and Δ_{III} are the shear keys top displacement at damage Levels II and III. The shear key top displacement was computed as:

$$\Delta_{II} = \sqrt{2}\varepsilon_y (L_d + L_a) \frac{(h+d)}{\sqrt{h^2 + d^2}} \qquad \textbf{(8.7)}$$

Where L_d is the reinforcement development length given by:

$$L_d = \frac{d_b f_y}{25\sqrt{f_c^{'}}} \qquad [psi, in] \qquad \textbf{(8.8)}$$

and L_a is the cracked region as shown in Figure 8.7 and based on observed test observations this value is approximately the width of the stem wall, *b*. In Eq. (8.7) the term $\sqrt{2}$ is implemented because the reinforcement crosses the crack at approximately 45°. The geometric ratio $(h+d)/\sqrt{h^2+d^2}$ in Eq. (8.7) was derived based on the assumption that the shear keys deform as a rigid body with the center of rotation at the base of the stem wall near the compression zone identified as point A in Figure 8.7. Using test results it can be shown that the shear key deforms primarily as a rigid body. This is illustrated next. In Figure 8.8 the crack width opening, Δ_{crack}, was obtained as follows:

$$\Delta_{crack} = \sqrt{\Delta_{HORIZ}^2 + \Delta_{VERT}^2} \qquad \textbf{(8.9)}$$

Where Δ_{HORIZ} and Δ_{VERT} are, respectively, the recorded horizontal and vertical components, as shown in Figure 8.8(b). Next, using the crack width obtained by Eq. (8.9) and the rigid body analogy the shear key top displacement was computed. Figure 8.9 shows the shear key load-top displacement envelope and the computed shear key top displacement, which was obtained in terms of the crack width opening as:

$$\Delta_{TOP} = \Delta_{crack} \frac{(h+d)}{\sqrt{h^2 + d^2}} \qquad \textbf{(8.10)}$$

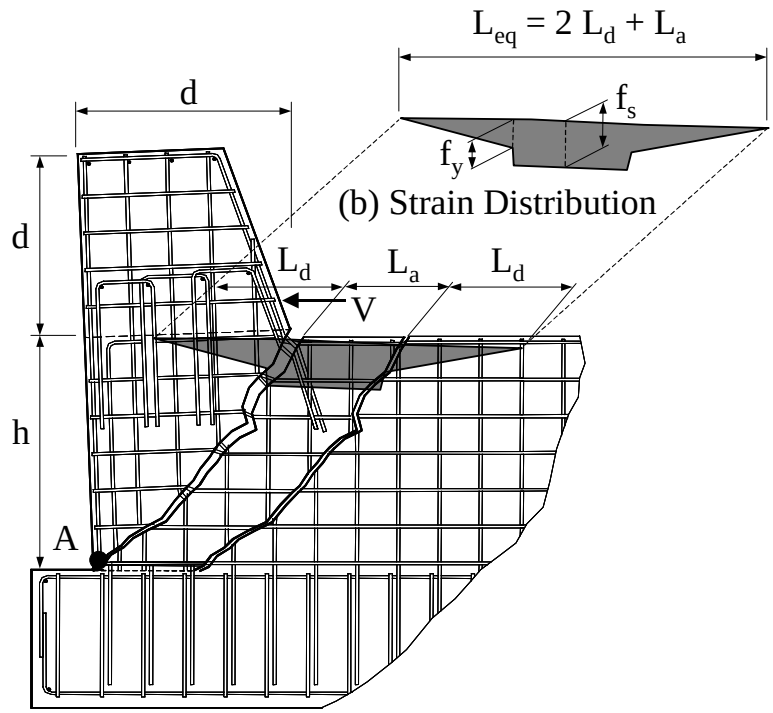

(a) Shear Key Deformed Shape

Figure 8.7 Shear Keys Response Mechanism

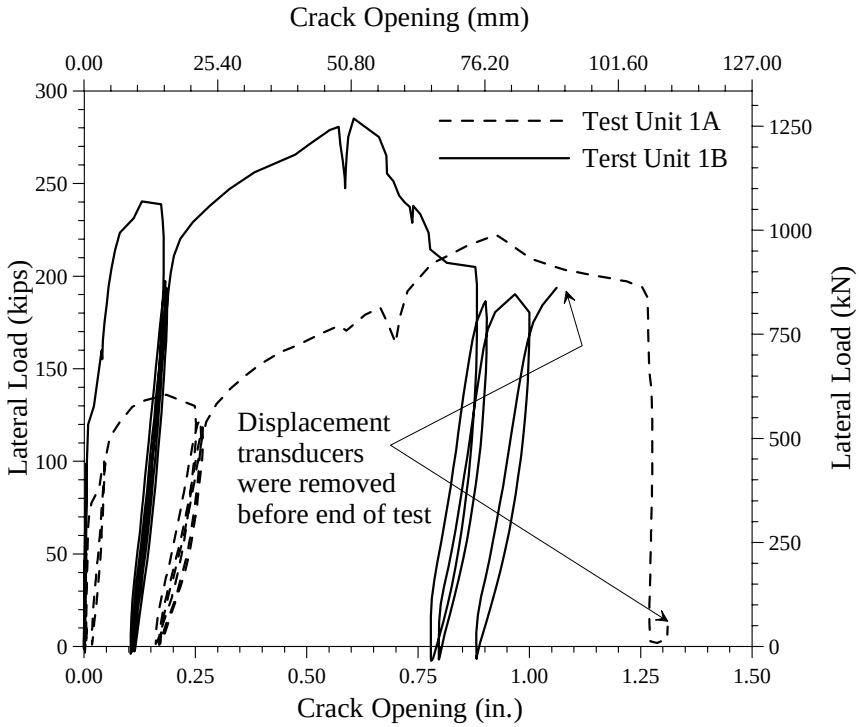

(a) Test Results

(b) General Observations

Figure 8.8 Crack Width Opening at Interface with Shear Key

Results shown in Figure 8.9 show a good agreement between the computed top displacement from the crack width opening measurement and the top displacement measured directly from the LVDT instrument. This indicates that the deformation of the shear key may thus be represented as that of a rigid body.

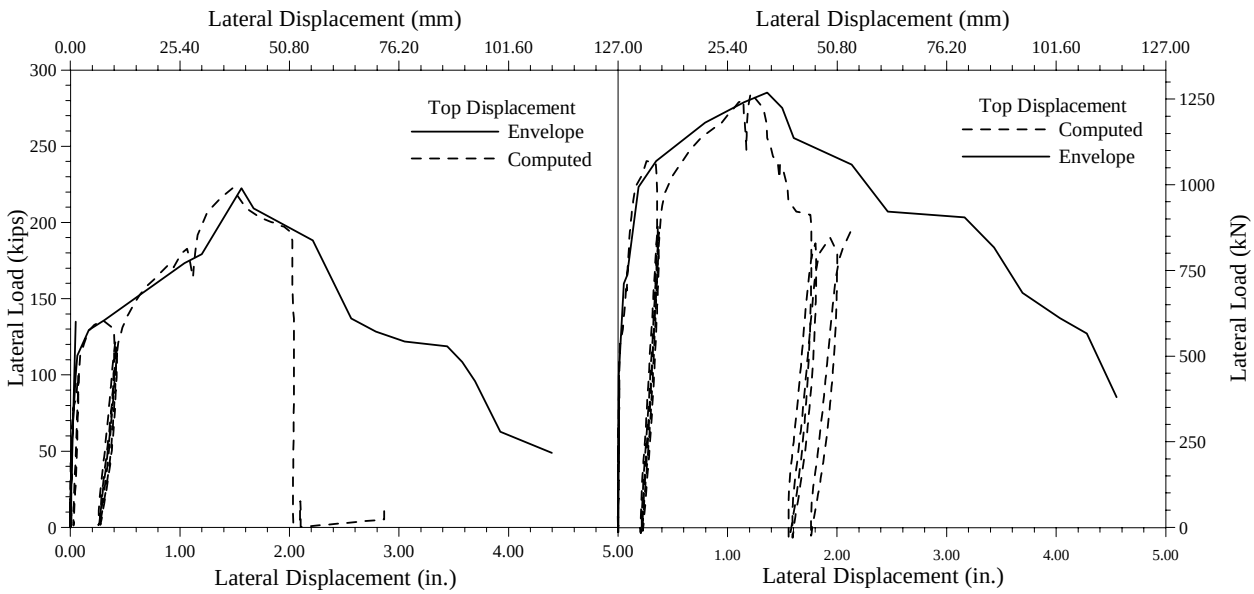

(a) Test Unit 1A **(b)** Test Unit 1B

Figure 8.9 Top Displacement

Table 8.2 Experimental versus Theoretical Loads and Displacements- Level II

Test Unit	Lateral Load Experimental kips (kN)	Lateral Disp. Experimental in. (mm)	Lateral Load Theoretical (Eq. 8.6) kips (kN)	Lateral Disp Theoretical (Eq. 8.7) in. (mm)
1A	136 (605)	0.31 (7.9)	145 (645)	0.14 (3.6)
1B	240 (1,068)	0.35 (8.9)	209 (930)	0.16 (4.1)
2A	125 (556)	0.18 (4.6)	89 (396)	0.14 (3.6)

8.1.3 LEVEL III

This level corresponds to the peak load and corresponds to point C in Figure 8.3. At this level increase in the crack width opening at the shear key stem wall interface leads to reduction of the concrete contribution to the shear resisting mechanism. The peak lateral load was given by Eq.

(5.2), and the shear key top displacement was computed by assuming that all the rebars that cross the cracked zone have reached yielding. Thus:

$$\Delta_{III} = \sqrt{2}\varepsilon_y (L_d + L_a)\frac{(h+d)}{s} \qquad \textbf{(8.11)}$$

Where s is the reinforcement spacing in the stem wall. The variable s in the denominator of Eq. (8.11) is different from the denominator in Eq. (8.7) ($\sqrt{h^2+d^2}$) because the crack width is taken at the reinforcement near the stem wall compression toe.

Table 8.3 Experimental vs. Theoretical Loads and Displacements - Level III

Test Unit	Lateral Load Experimental kips (kN)	Lateral Disp. Experimental in. (mm)	Lateral Load Theoretical (Eq. 5.2) kips (kN)	Lateral Disp. Theoretical (Eq. 8.11) in. (mm)
1A	222 (988)	1.5 (38.1)	223 (992)	1.2 (30.5)
1B	285 (1,268)	1.3 (33.0)	291 (1,294)	1.2 (30.5)
2A	159 (707)	1.5 (38.1)	189 (841)	1.2 (30.5)

8.1.4 LEVEL IV

At this level full reduction in the concrete contribution to the shear resisting mechanism is expected, and the shear key capacity is equal to the steel contribution to the shear resisting mechanism. This damage level corresponds to point D in Figure 8.3. Because of lack of research data to justify the crack width and steel strain to produce the full reduction in the concrete shear resisting mechanism the crack width and steel strain to produce this reduction was back calculated from the experimental results by assuming rigid body deformation and using the top displacement data. In this way the crack width and steel strain were computed using Eqs. (8.12) and Eq. (8.13) as follows:

$$\Delta_{crack} = \Delta_{TOP}\frac{\sqrt{h^2+d^2}}{(h+d)} \qquad \textbf{(8.12)}$$

Computing the crack width at the reinforcement near the compression toe (i.e. point A in Figure 8.7) the following relation for the steel strain near the compression toe is derived:

$$\varepsilon_{s,IV} = \Delta_{TOP}\frac{s}{\sqrt{2}\,(h+d)(L_d + L_a)} \qquad \textbf{(8.13)}$$

Table 8.4 Experimental vs. Theoretical Displacements - Level IV

Test Unit	Lateral Disp. Experimental in. (mm)	Steel Strain (Eq. 8.13)	Lateral Disp. Theoretical (Eq. 8.14) in. (mm)
1A	2.5 (63.5)	0.0049	2.5 (63.5)
1B	2.6 (66.0)	0.0045	3.1 (78.7)
2A	2.8 (71.1)	0.0055	2.5 (63.5)

Investigation of these values indicate that full degradation of the concrete contribution to the shear resisting mechanism is likely to occur at a steel strain of approximately 0.005 in all of the test units. Thus, theoretically top deflection at Level IV may be computed as:

$$\Delta_{TOP} = \sqrt{2}\varepsilon_{0.005}(L_d + L_a)\frac{(h+d)}{s} \qquad \textbf{(8.14)}$$

8.1.5 LEVEL V

At this level fracture of the reinforcement crossing the cracking zone is initiated and corresponds to point E in Figure 8.3. As before, the steel strain in the reinforcement near the compression toe at onset of fracture of the reinforcement near the shear key stem wall interface is computed as:

$$\varepsilon_{s,A} = \Delta_{TOP}\frac{s}{\sqrt{2}\,(h+d)(L_d + L_a)} \qquad \textbf{(8.15)}$$

Investigation of these values indicate that $\varepsilon_{s,A}$ occurs at a steel strain of approximately 0.007in/in in all of the test units. Thus, for this value the steel strain at onset of fracture of the longitudinal reinforcement near the shear key stem wall interface is computed as:

$$\varepsilon_{s,V} = \varepsilon_{0.007}\frac{\sqrt{h^2 + d^2}}{s} \qquad \textbf{(8.16)}$$

With h = 30.5 in. (775 mm), d = 24 in. (610 mm) and s = 4.75 in. (121 mm), Eq. (8.16) indicates that fracture of the reinforcement initiates at approximately a steel strain of 0.06, which is consistent with the steel strain that becomes critical for onset of low-cycle fatigue. Thus, theoretically the top deflection at Level V may be computed as:

$$\Delta_{TOP} = \sqrt{2}\varepsilon_{0.007}(L_d + L_a)\frac{(h+d)}{s} \qquad \textbf{(8.17)}$$

Table 8.5 Experimental vs. Theoretical Displacements - Level V

Test Unit	Lateral Disp. Experimental in. (mm)	Steel Strain (Eq. 8.15)	Lateral Disp. Theoretical (Eq. 8.17) in. (mm)
1A	3.4 (86.4)	0.0070	3.4 (86.4)
1B	3.2 (81.3)	0.0060	3.7 (94.0)
2A	3.8 (96.5)	0.0075	3.4 (86.4)

8.2 Time History Analysis

A nonlinear time history analysis was performed using the simulated ground motion presented in Figure 8.10 and the hysteretic model presented in Figure 8.3 to Figure 8.5, in order to correlate the experimental results to the hysteretic model. The software program used to perform the nonlinear time history analysis was the program *Ruaumoko* [28]. Results presented in Figure 8.11 show a good correlation between the hysteretic model results and the experimental results.

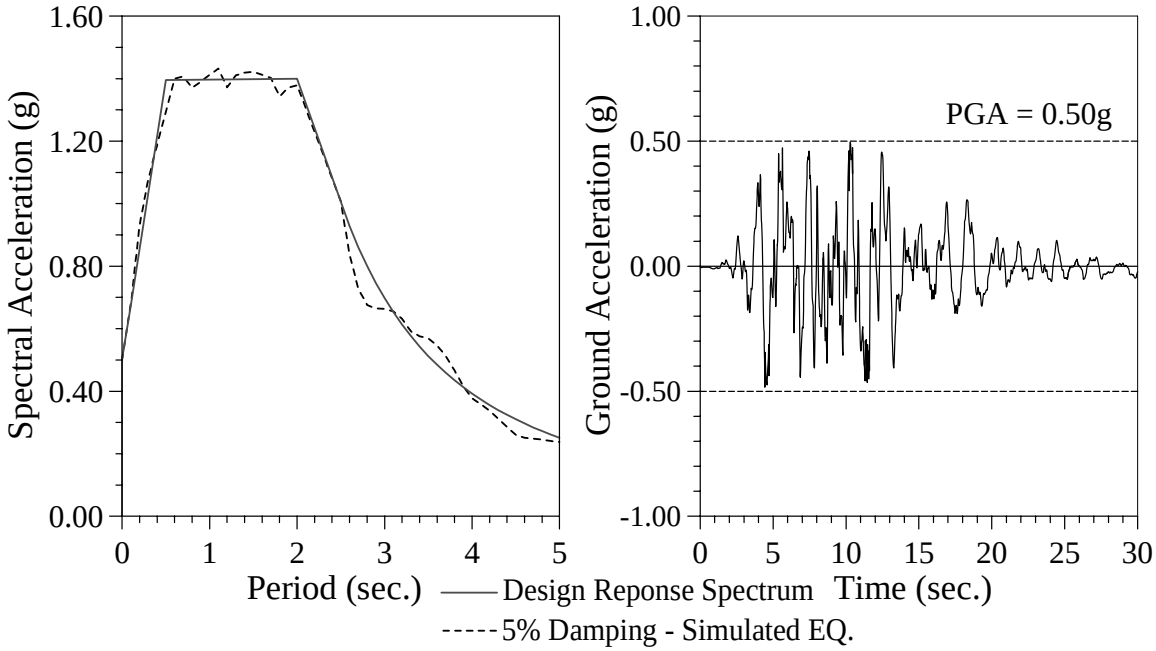

Figure 8.10 Simulated Ground Motion

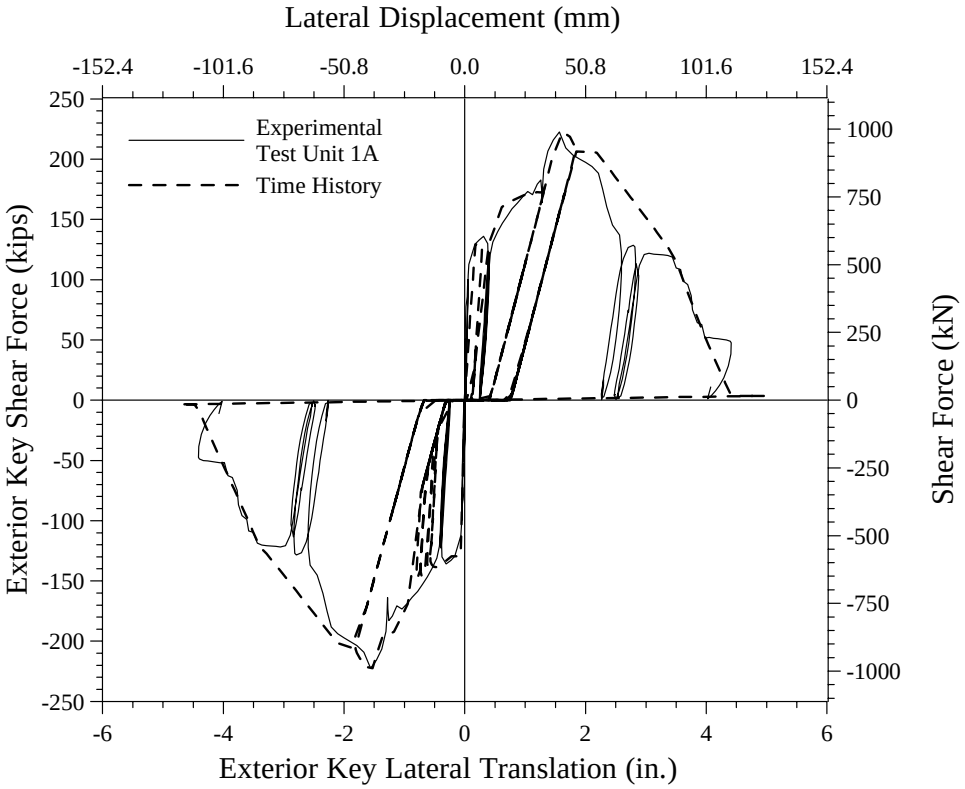

Figure 8.11 Experimental vs. Time History Results of Exterior Shear Keys

9 CONLUSIONS AND RECOMMENDATIONS

This report presents the results of an experimental program that was developed and conducted at the University of California-San Diego (UCSD) to study the seismic response of interior and exterior sacrificial shear keys. The experimental program consisted of seven interior shear keys and six exterior shear keys experiments. Variables investigated during testing of the interior keys were: (1) loading protocol (monotonic, quasi-static reversed cyclic, and dynamic reversed cyclic), (2) geometric aspect ratio of the shear key, and (3) shear key reinforcement ratio. The term shear key reinforcement refers to the vertical mild reinforcing bars, which connect the shear key to the abutment stem wall. Variables investigated during testing of the exterior keys were: (1) inclusion of back and wing walls, (2) adoption of different key details such as use of sacrificial flexural keys and use of construction joints between the abutment stem wall and the shear keys, and (3) post-tensioning of the abutment stem wall. These experiments provided useful results to develop analytical models that will serve to evaluate the capacity of shear keys as well as their post-peak performance under cyclic loads. The conclusions of this research are presented in Sections 9.1 and 9.2 for interior and exterior sacrificial shear keys, respectively. Recommendations for future research are given in Section 9.3.

9.1 Interior Sacrificial Shear Keys

Based on the research presented in this report, the response of interior sacrificial shear keys can be characterized by several regions. The first region had no load or stiffness, during which the response was controlled by the properties of the expanded polystyrene used to fill the gap between the shear key and the bridge superstructure.

The next region was dominated by a strut-and-tie mechanism, which transferred the applied load to the abutment. High strength and stiffness characterized this region, with the shear key remaining essentially rigid. This response was maintained under cyclic loading until the load reached its peak value. This value was most accurately calculated based on the cracking strength of the concrete. After the horizontal crack propagated completely through the shear key-abutment stem wall interface the response of the shear key switch to a sliding shear friction mechanism. The vertical reinforcing bars of the shear key provided clamping forces between the shear key and the abutment stem wall. A high coefficient of friction was provided by aggregate interlock.

As the load was cycled, the strength and stiffness degraded rapidly. Degradation of the aggregate interlock reduced the coefficient of friction. Concrete spalling on the sides of the shear key exposed the outer lines of reinforcing bars, thus reducing the clamping forces. The clamping forces were further reduced by fracture of the shear key reinforcement. Although the contribution of each of these sources varied among different test units, the total degradation was found to decrease linearly from the peak load.

Test Series I experimental results showed that the regions discussed above are not affected by the history or rate of the applied load. Experimental results showed essentially the same response under monotonic, quasi-static reversed cyclic and dynamic reversed cyclic loading protocols in terms of the peak load and degradation under cyclic loading.

Results of the second test series showed that the aspect ratio and reinforcement ratio have little effect on response of interior shear keys. All test units showed the same qualities and magnitudes of response. The aspect ratio does, however, affect the degradation of the cyclic friction load and observed damage levels. Less degradation of the friction load under cyclic loading was observed for Test Unit 2B with a higher aspect ratio.

From the information presented, the following recommendations are made for the design of interior sacrificial shear keys with a single interface between the shear keys and the abutment, shear key reinforcement ratios between 0.32% and 0.63%, shear key aspect ratios between 0.3 and 0.5, and shear key width-to-depth ration around 0.7:

1. The method under consideration for the Caltrans Design Specifications [2], which calculates the capacity of shear keys with aspect ratios less then 0.5 based on shear friction, does not accurately predict the actual shear key capacity. This method assumes that the shear key section is cracked throughout the shear key-abutment interface. Development of this crack requires a much higher load than that calculated using the shear friction model. For sacrificial elements, this results in non-conservative designs. With shear keys designed to have a peak capacity of 75% of the shear capacity of the piles, use of the shear friction model to estimate the load carrying capacities of shear keys will result in the likelihood that the piles will be damaged before the failure of the shear keys.

2. Behavior of the shear keys after gap closure and prior to reaching its peak capacity is best described by a strut-and-tie mechanism. Although the load is transferred through a strut-and-tie mechanism, failure occurs when the crack at the interface has propagated completely through the

section. The parameters investigated did not considerably affect the force required to develop this crack.

3. The actual capacity is mainly influenced by the cracking strength of the concrete. Calculating the capacity based on this alone was found to be the most accurate procedure for the test units. It should be kept in mind that the test units in this research were built at a reduced scale with respect to the prototype structure. The scale effect on capacity of the tested shear keys was not investigated in this research. Based on the experimental results, it is recommended that the nominal capacity of shear keys be calculated by the smallest value given by Eq. (4.3) and Eq. (4.4). Further experimental tests are required to investigate the capacity of sacrificial interior shear keys with different details and dimensions of the shear key-abutment interface (including cold construction joints between the shear keys and the abutment) and different ratios of shear key reinforcement.

4. The strength reduction factor of 0.85, typically used for concrete members, should not be used to further reduce the nominal capacity of sacrificial shear keys. The nominal capacity should instead be multiplied by an over-strength factor, ϕ^o, of 1.30 to provide a realistic estimate of the maximum shear key capacity. This will ensure that there is no damage sustained by the piles.

5. The assumption that shear keys do not provide additional transverse support for the superstructure after their failure is conservative. The experimental results show that there is a substantial loss in both the strength and stiffness of shear keys after reaching their peak load. The amount of degradation will depend to a certain extent on the stiffness of the columns, which will affect the amount of displacement experienced at the abutments. For assessment purposes, a more realistic method of characterizing shear key response after reaching the peak load was developed. The effective stiffness and effective damping characterize the response. Effective stiffness and effective damping are calculated after cyclic degradation. The effective damping is calculated using Eq. (4.10) and the effective stiffness using Eq. (4.11).

9.2 Exterior Sacrificial Shear Keys

As mentioned earlier, sacrificial shear keys should perform as structural fuses to protect the abutment and the piles from damage during earthquake events. The exterior shear key test units tested in this research program adopted different details such as use of construction joints between the shear key and the abutment, use of flexural keys and post-tensioning of the abutment stem wall. The major objectives of these experiments were to investigate the load transfer mechanisms in these shear keys and whether they perform as structural fuses.

All of the tested shear key units had initial high stiffness until onset of yielding of the mild steel reinforcement. However the load transfer mechanism varied among different test units. When the shear keys are constructed monolithically with the abutment wall, sliding shear does not occur between the shear key and the abutment. The lateral load is transferred from the shear key to the abutment through a diagonal compressive strut that develops from the point of load application to the toe of the abutment stem wall (see Figure 7.9). The shear keys did not perform as structural fuses and the abutment stem wall was severely damaged (see Figure 7.4a and Figure 7.4b), which makes post-earthquake repair extremely difficult.

The abutment wall and the shear key were constructed on two different days in Unit 2A. Because of the construction joint between the shear key and the abutment wall, a crack was initiated at the shear key-abutment stem wall interface and propagated in the horizontal direction until it intersected the first row of shear key vertical reinforcement. This was followed by propagation of this crack in the abutment wall towards the wall's toe (see Figure 7.4c). The abutment stem wall experienced severe damage in this case. A strut-and-tie model was the best to characterize the performance of this test unit (see Figure 7.10).

Use of flexural key was successful in terms of ductility and damage control. The flexural key of Test Unit 2B was able to undergo high displacements without considerable loss in the load carrying capacity. The key had a predominant flexural performance and a plastic hinge formed at the interface between the flexural key and the abutment stem wall (see Figure 7.4d). It is reasonable to expect that damage to the abutment wall is minor when flexural keys are used (see Figure 7.4d).

The most efficient way to minimize damage to abutments is by post-tensioning of the abutment stem wall. Adequate post-tensioning will prevent occurrence of diagonal cracks in the abutment wall as for the case of Units 3A and 3B. With abutment post-tensioning and use of cold construction joints between the shear keys and the abutment wall, the load is transferred from the shear keys to the abutment through a sliding shear friction mechanism. Failure occurs by sliding of the shear keys above the abutment rather than by failure of the abutment stem wall. Thus, the shear keys would perform as structural fuses as intended in design.

The following can be concluded from the experimental research on exterior sacrificial shear keys:

1. The method under consideration for the Caltrans Design Specifications [2], which calculates the capacity of shear keys based on shear friction, does not accurately predict the actual shear key capacity. Use of the shear friction model with the current values of the coefficient of friction given in the Caltrans Design Specifications [2] will severely underestimate the shear key capacity. For sacrificial elements, this results in non-conservative design. With shear keys designed to have a peak capacity of 75% of the shear capacity of the piles, use of the shear friction model to estimate the load carrying capacities of shear keys will result in the likelihood that the piles will be damaged before failure of the shear keys.

2. Maximum load carrying capacity of exterior shear keys built monolithically with the abutment should be estimated based on a strut-and-tie model, which is schematically shown in Figure 7.9. The nominal capacity of exterior shear keys may be estimated using Eqs. (5.2) to (5.5).

3. Maximum load carrying capacity of exterior shear keys, which are built on a construction joint with the abutment, should be estimated based on the strut-and-tie model that is schematically shown in Figure 7.10. The shear key capacity may be estimated by Eqs. (5.2), (5.3) and (7.2) or (7.3).

4. Maximum load carrying capacity of exterior shear keys, which are built on a construction joint and with post-tensioned abutment stem walls, may be estimated based on the strut-and-tie model that is schematically shown in Figure 7.11. The capacity may also be estimated using the sliding shear friction model. In Eq. (7.1) of the shear friction model, the ultimate tensile strength of the shear key reinforcement should be used instead of the specified yield strength. Based on the experimental results of Units 3A and 3B, the coefficient of friction should be increased by an over-strength factor of about 1.8.

5. The strength reduction factor of 0.85, typically used for concrete members, should not be used to further reduce the nominal capacity of sacrificial exterior shear keys.

6. Flexural keys have significantly higher ductility and energy absorption capabilities and damage is localized over a small region at the flexural key-abutment wall interface.

7. It is recommended to have cold construction joints between the abutment stem wall and the shear keys. The abutment stem wall should also be post-tensioned. The prestressing force of the abutment stem wall may be estimated by the smallest value given by using Eq. (4.3) and Eq. (4.4). Sacrificial shear keys that incorporate these details were shown to be capable of performing as structural fuse elements.

8. Post-tensioned abutments with construction joints between the abutment wall and the shear keys can be easily repaired after an earthquake.

9. The assumption that exterior shear keys do not provide additional transverse support for the superstructure after their failure is conservative. If the shear keys are built monolithically with the abutment, the experimental results show that there is a substantial loss in both the strength and stiffness of shear keys after reaching their peak load. Use of construction joints between the shear keys and the abutment can improve their ductility. Flexural keys have significant ductility and can undergo high displacements without loss in the load carrying capacity. Post-tensioned abutments with construction joints between the shear keys and the abutment walls can undergo substantial lateral displacements with significant load carrying capacity.

9.3 Recommendations for Future Research

Exterior shear keys should be used for future construction because they are easier to repair, especially if the abutment is post-tensioned. The following is recommended for future research:

1. Experiments on full-scale test units should be performed to examine any effects caused by the scaling of the test units.

2. Experiments should be performed on interior shear keys with different dimensions than the ones tested in this research. The analytical models given in Chapter 4 to estimate the load carrying capacity of interior shear keys are based on the tests performed in this research work. Applicability of these analytical models to interior shear keys with wider range of variables should be investigated before making definitive design recommendations.

3. Experiments should be performed on interior shear keys with construction joints between the abutment seat and the shear keys.

4. More experiments with post-tensioned abutments with sacrificial exterior shear keys should be performed to collect sufficient data to modify the current sliding shear friction model. The test variables should include the amount of shear key vertical reinforcement, use of mechanical couplers for the shear key reinforcement and variation of the prestressing force of the abutment.

5. More experiments should also be performed on exterior shear keys with different amounts of tension tie reinforcement (hanger bars) in the abutment stem wall. The hanger bars represent the current Caltrans' policy for design of shear keys in bridge abutments.

6. Experiments on shear keys-abutment-pile systems should be performed to investigate the overall seismic response of bridge abutment systems.

7. Seismic assessment of straight and curved bridge structures with either a single, two or multiple spans should be performed in order to estimate the optimum design for exterior shear keys. In this seismic assessment nonlinear hysteretic models such as those described in Section 8.2 may be used.

10 REFERENCES

[1] Caltrans, *Bridge Memo to Designers Manual*, *California Department of Transportation*, Section 5, 1993.

[2] Caltrans, *Bridge Design Specifications*, California Department of Transportation, 1993.

[3] Kaneko, Y.; Connor, J. J.; Thanassis, T. C.; and Leung, C., "Shear Keys: Fracture Mechanics Approach for Failure of Concrete Shear Key: I Theory", *Journal of Engineering Mechanics*, V. 4, 1993, pp. 681-699.

[4] Kaneko, Y.; Connor, J. J.; Thanassis, T. C.; and Leung, C., "Shear Keys: Fracture Mechanics Approach for Failure of Concrete Shear Key: II Verification", *Journal of Engineering Mechanics*, V. 4, 1993, pp. 700-719.

[5] Cholewicki, A., "Loadbearing Capacity and Deformability of Vertical Joints in Structural Walls of Large Panel Buildings", *Building Science*, V. 6, 1971, pp. 163-184.

[6] Watkins, J.; and Liu, K. L. W., "A Finite Element study of the Short Beam Test Specimen under Mode II Loading", *International Journal of Cem. Compos. Lightweight Concrete*, V. 7, No. 1, pp. 39-47.

[7] Zielinski, Zenon A., "Tests on Shear Capacity of Reinforced Concrete" *Journal of Structural Engineering*, Nov., 1995, pp. 1660-1666.

[8] Hagberg, T., "Design of Concrete Brackets: On the Application of the Truss Analogy", *ACI Journal*, V. 80, No. 1, 1983, pp. 3 -12.

[9] Kriz, L. B.; and Raths, C. H., "Connections in Precast Concrete Structures – Strength of Corbels", *PCI Journal*, V. 10, No. 1, 1965, pp. 16-61.

[10] Somerville, G., "The Behavior and Design of Reinforced Concrete Corbels", *Shear in Reinforced Concrete, American Concrete Institute Special Publication SP-42*, 1974, pp. 477-502.

[11] Mattock, A. H.; Chen, K. C.; and Soonswang, K., “The Behavior of Reinforced Concrete Corbels”, *PCI Journal*, V. 21, No. 3, 1976, pp. 18-42.

[12] Schlaich, J.; Schafer, K.; and Jennewein, M., “Toward a Consistent Design of Structural Concrete”, *PCI Journal*, V. 32, No. 3, 1987, pp. 74-150.

[13] Schlaich, J.; and Schafer, K., “Design and detailing of Structural Concrete Using Strut and Tie Models”, *The Structural Engineer*, V. 69, No. 6, 1991, 13 pp.

[14] Mattock, A. H.; and Hawkins, N. M., “Shear Transfer in Reinforced Concrete – Recent Research”, *ACI Journal, Proceedings*, V. 66, No. 2, 1969, pp. 119-128.

[15] ACI-ASCE Committee 426,“The Shear Strength of Reinforced Concrete Members”, *Proceedings ASCE, Journal of the Structural Division*, V. 99, No. ST6, pp. 1148-1157.

[16] Rogowsky, D. M.; MacGregor, J. G.; and Ong, S. Y., “Tests of Reinforced Concrete Deep Beams”, *ACI Journal*, V. 83, No. 4, 1986, pp. 614-623.

[17] Rogowsky, D. M.; MacGregor, J. G., “The Design of Reinforced Concrete Deep Beams”, *Concrete International: Design and Construction*, V. 8, No. 8, 1986, pp. 49-58.

[18] de Paiva, H. A. Rawdon; and Seiss, C. P., “Strength and Behavior of Deep beams in Shear”, *Proceedings, ASCE*, V. 91, ST5, 1965, pp. 19-41.

[19] Manuel, R. F.; Slight, B. W.; and Suter, G. T., “Deep Beam Behavior Affected by Length and Shear Span Variations”, *ACI Journal*, V. 79, No. 3, 1971, pp. 954-958.

[20] Smith, K.N.; and Vantsiotis, A.S., “Shear Strength of Deep Beams”, *ACI Journal*, V. 65, No. 2, 1968, pp. 201-213.

[21] Mau, S. T.; and Hsu, T. T. C., “Formula for the Shear Strength of Deep Beams” *ACI Structural Journal*, V. 86, No. 5, 1989, pp. 516-523.

[22] Ramakrishnan, V.; and Ananthanarayana, Y., “Ultimate Strength of Deep Beams in Shear”, *ACI Journal*, V. 65, No. 2, 1968, pp. 87-98.

[23] Kong, F.-K.; Robins, P. J.; and Cole, D. F., “Web Reinforcement Effects on Deep Beams”, *ACI Journal*, V. 67, No. 12, 1970, pp.1010-1017.

[24] Harper, K., “Shear Key Design”, Working Paper, 1993, pp. 1-2.

[25] Priestley, M. J. N., Seible, F., Calvi, M., *Seismic Design and Retrofit of Bridges*, John Wiley & Sons, Inc., New York, September 1995, 672 pp.

[26] Hose, Y. D., Silva, P. F., Seible, F., *Performance Evaluation of Concrete Bridge Components and Systems under Simulated Seismic Loads*, *EERI Earthquake Spectra*, Vol. 16, No. 2, May 2000, pp. 413-442.

[27] King, D.J., Priestley, M.J.N., Park, R., *Computer Program for Concrete Column Design*, Department of Civil Engineering, University of Canterbury Christchurch, New Zealand, Report No. 86-12, May 1986.

[28] Carr, A.J., *Ruaumoko Inelastic Analysis Program*, University of Canterbury, Christchurch, New Zealand, 2000.